



University
of Glasgow

Stortz, Johannes Felix (2020) *A conditional CRISPR/Cas9 system gives novel insights into actin dynamics in Toxoplasma gondii*. PhD thesis.

<http://theses.gla.ac.uk/77880/>

Copyright and moral rights for this work are retained by the author

A copy can be downloaded for personal non-commercial research or study, without prior permission or charge

This work cannot be reproduced or quoted extensively from without first obtaining permission in writing from the author

The content must not be changed in any way or sold commercially in any format or medium without the formal permission of the author

When referring to this work, full bibliographic details including the author, title, awarding institution and date of the thesis must be given

Enlighten: Theses

<https://theses.gla.ac.uk/>
research-enlighten@glasgow.ac.uk

**A conditional CRISPR/Cas9 system
gives novel insights into actin
dynamics in *Toxoplasma gondii***

By

Johannes Felix Stortz
B.Sc., M.Sc.

Submitted in fulfilment of the requirements for the
Degree of Doctor of Philosophy

School of Life Sciences
College of Medical, Veterinary & Life Science
Institute of Infection, Immunity & Inflammation
University of Glasgow

Abstract

Actin is a highly abundant structural protein in eukaryotes that is critical for several cellular processes. In the apicomplexan parasite *Toxoplasma gondii*, actin is critical for the completion of the lytic cycle and, thus, parasite survival. Only recently, actin structures were visualised in *Toxoplasma* by exploiting actin-chromobodies, revealing an extensive actin network within the parasitophorous vacuole (PV) (Periz et al. 2017). This network consists of intravacuolar filamentous structures that connect individual parasites within the PV. In addition, parasites possess a cytosolic actin centre (cAC) anterior to the nucleus.

The study presented here aimed at exploiting actin visualisation to investigate actin dynamics in unprecedented detail *in vivo*. For this purpose, I established a conditional CRISPR/Cas9 that allows for rapid and efficient gene disruption in *Toxoplasma*. Combining this system with the actin-chromobody technology granted detailed insights into the actin dynamics in intracellular parasites. I identified the actin depolymerisation factor (*TgADF*) as an important factor in the disassembly of the intravacuolar F-actin filaments prior to parasite egress from the host cell. Furthermore, this study revealed *TgFormin2* to be critical for maintaining the cAC. Since cAC loss severely impaired actin distribution and peripheral actin flow in intracellular parasites, I concluded that *TgFormin2* represents a major key player in mediating proper actin dynamics. *TgFormin2* also appeared to be important for apicoplast inheritance and positioning.

In summary, data presented in this thesis significantly contribute to the understanding of actin dynamics in *Toxoplasma*. Further insights into apicomplexan actin dynamics will be gained by exploiting the conditional CRISPR/Cas9 technology for phenotypic screening approaches.

Table of Contents

Abstract.....	2
Table of Contents	3
List of Tables.....	7
List of Figures	8
List of Supplement Material.....	11
Table of copyright permissions	12
Acknowledgements.....	13
Author's Declaration	14
Publications arising from this work and collaborations	16
Conference Proceedings.....	16
Definitions/abbreviations	17
1 Introduction.....	21
1.1 Taxonomie.....	21
1.2 Health Impact of apicomplexan parasites	22
1.3 The life cycle of <i>Toxoplasma</i>	22
1.3.1 Definitive host - sexual replication	23
1.3.2 Environmental stage	24
1.3.3 Intermediate host - asexual lytic cycle.....	25
1.4 The asexual lytic cycle of <i>Toxoplasma</i> tachyzoites: a closer look	25
1.4.1 Tachyzoite structure	25
1.4.1.1 The apicoplast.....	29
1.4.2 Gliding motility	31
1.4.3 Invasion	35
1.4.4 Asexual replication	38
1.4.5 Egress.....	39
1.5 Molecular Tools to dissect <i>Toxoplasma</i> biology	42
1.5.1 The type II CRISPR/Cas9 system.....	43
1.6 Actin in eukaryotes.....	47
1.6.1 Structure of actin monomers and filaments	47
1.6.2 Function of Actin binding proteins (ABPs)	50
1.6.2.1 Actin treadmilling.....	50
1.6.2.2 Actin nucleation	52
1.7 Actin in <i>Toxoplasma</i>	56
1.7.1 Actin binding proteins (ABPs) in <i>Toxoplasma</i>	60
1.8 Aims of this study.....	63

2	Materials and Methods.....	65
2.1	Equipment	65
2.2	Computer Software.....	66
2.3	Consumables, biological and chemical reagents.....	66
2.4	Kits.....	67
2.5	Buffers, solutions and media.....	68
2.6	Antibodies	69
2.7	Oligonucleotides	70
2.8	Plasmids.....	71
2.9	Cell strains.....	72
2.9.1	Bacteria strains and mammalian cell lines.....	72
2.9.2	<i>Toxoplasma</i> strains	72
2.10	Microbiology Methods.....	74
2.10.1	Liquid cultures and cryopreservation stocks of <i>E. coli</i>	74
2.10.2	Transformation of chemically competent <i>E. coli</i>	74
2.11	Molecular Biology Methods.....	74
2.11.1	Polymerase Chain Reaction (PCR)	74
2.11.2	Agarose Gel Electrophoresis (AGE)	75
2.11.3	DNA restriction	75
2.11.4	DNA purification.....	76
2.11.5	DNA ligation.....	76
2.11.6	Isolation of plasmid DNA from <i>E.coli</i>	76
2.11.7	Alcohol precipitation of plasmid DNA for <i>Toxoplasma</i> transfections 77	
2.11.8	Isolation of genomic DNA (gDNA) from <i>Toxoplasma</i>	77
2.11.9	Sub-cloning of the split-Cas9 plasmids.....	78
2.11.10	Sub-cloning of gRNA plasmids	79
2.11.11	DNA sequencing	79
2.12	Biochemistry Methods	80
2.12.1	Indirect Immunofluorescence Analysis (IFA)	80
2.13	Cell Culture	81
2.13.1	Culturing host cells (HFFs) and <i>Toxoplasma</i>	81
2.13.2	Cryopreservation of <i>Toxoplasma</i>	81
2.13.3	Stable and transient transfections of <i>Toxoplasma</i>	81
2.13.4	Generation of the parental split-Cas9 (sCas9) strain	82
2.13.5	Generation of sCas9-sgRNA strains	83
2.13.6	Generation of RHsCas9-CbEmerald strain	83
2.13.7	Serial dilution of transfected <i>Toxoplasma</i> parasites.....	83
2.13.8	Induction of the split-Cas9 or DiCre system in <i>Toxoplasma</i>	84

2.13.9	Egress Assay	85
2.14	Microscopy	85
2.14.1	Light microscopy	85
2.14.2	Time-lapse video microscopy for <i>Toxoplasma</i>	86
2.15	Bioinformatics	86
2.15.1	Design of gRNAs for <i>Toxoplasma</i>	86
2.15.2	Kymograph analysis	88
2.15.3	Skeletonization analysis	88
3	Establishment of a novel conditional CRISPR/Cas9 system for reliable gene disruption in <i>Toxoplasma</i>	89
3.1	Proof of Principle I: Targeting <i>Tggap40</i> with split-Cas9	91
3.2	Proof of Principle II: Targeting <i>Tgsag1</i> with split-Cas9	96
3.3	Investigating the effect of split-Cas9 activation on <i>Toxoplasma</i> I: <i>TgSAG1</i> complementation studies	98
3.4	Investigating the effect of split-Cas9 activation on <i>Toxoplasma</i> II: Disruption of <i>Tgsag1</i> in RH vs RH Δ ku80 parasites	103
3.5	A case study: Disruption of <i>TgMec17</i> -mediated tubulin acetylation via the split-Cas9 and DiCre systems	104
3.6	Summary and conclusions	109
4	Combining the split-Cas9 and actin-chromobody technology to investigate actin distribution and dynamics in <i>Toxoplasma</i>	112
4.1	Disruption of <i>Tgactin1</i> and <i>Tgadf</i> with the split-Cas9 system	113
4.2	Investigating the impact of <i>Tgadf</i> disruption on actin filament dynamics	118
4.2.1	Analysis of egress behaviour in conditional sCas9 mutants	118
4.2.2	Impact of <i>Tgadf</i> disruption on filament disassembly upon egress ..	121
4.3	Re-defining intracellular actin distribution and dynamics	125
4.4	Summary and conclusions	132
5	Investigating the role of <i>TgFormin2</i> within the intracellular actin network	135
5.1	Localisation and function of <i>TgFormin2</i> within the actin network of intracellular <i>Toxoplasma</i>	136
5.2	Confirmation of <i>TgFormin2</i> function with the DiCre system	144
5.3	The role of the apicoplast in maintenance of actin dynamics	152
5.4	The effect of the cytosolic actin centre on overall actin dynamics in intracellular <i>Toxoplasma</i>	154
5.5	Summary, conclusions and on-going work	160
6	Discussion	164
6.1	Application of CRISPR/Cas9 strategies in <i>Toxoplasma</i>	165
6.2	Actin dynamics in <i>Toxoplasma</i>	171
6.3	<i>In vivo</i> Functions of Formins in <i>Toxoplasma</i>	174

6.4	<i>In vivo</i> Functions of TgADF in <i>Toxoplasma</i>	177
6.5	Outlook on TgProfilin function and concluding remarks.....	179
7	Appendix	181
8	Bibliography.....	190

List of Tables

Table 0-1: Table of copyright permissions	12
Table 1-1: Depiction of selected actin binding proteins (ABPs) found in apicomplexan and eukaryotic genomes	60
Table 2-1: Equipment	65
Table 2-2: Computer software	66
Table 2-3: Biological and Chemical reagents.....	66
Table 2-4: Kits	67
Table 2-5: Buffers for DNA analysis.....	68
Table 2-6: Buffers and media for bacterial culture	68
Table 2-7: Buffers and media for <i>Toxoplasma</i> and mammalian cell culture	68
Table 2-8: Antibodies	69
Table 2-9: Oligonucleotides	70
Table 2-10: Plasmids.....	71
Table 2-11: Bacteria strains	72
Table 2-12: Mammalian cells	72
Table 2-13: <i>Toxoplasma</i> strains	72
Table 3-1: Phenotypic characterisation of the lines RHsCas9-sag1-3 clone1 and 2	98
Table 3-2: Phenotypic characterisation of the lines RHsCas9-mec17-2 and RHsCas9-mec17-3.....	107
Table 3-3: Prerequisites for DNA damage to occur in <i>Toxoplasma</i> upon split-Cas9 activation	109

List of Figures

Figure 1-1: The life cycle of <i>Toxoplasma gondii</i>	23
Figure 1-2: The Lytic cycle of <i>Toxoplasma</i>	26
Figure 1-3: Schematic of the <i>Toxoplasma</i> tachyzoite ultrastructure	27
Figure 1-4: Gliding motility in <i>Toxoplasma</i> tachyzoites	32
Figure 1-5: Cartoon depicting the involvement of the retrograde membrane flow (fountain-flow model) in <i>Toxoplasma</i> motility	35
Figure 1-6: The type II CRISPR/Cas9 system in prokaryotes	44
Figure 1-7: Schematic of the sgRNA-mediated gene specificity of the type II CRISPR/Cas9 system	46
Figure 1-8: Actin treadmilling in eukaryotes	49
Figure 1-9: The three types of actin nucleation factors in eukaryotes	53
Figure 1-10: Schematic of the actin network in <i>Toxoplasma</i>	63
Figure 2-1: Plasmid encoding the split-Cas9 N-terminus (split4 variant)	78
Figure 2-2: Plasmid encoding the split-Cas9 C-terminus (split4 variant)	79
Figure 2-3: Plasmid encoding sgRNAs	80
Figure 2-4: Plasmid encoding the actin-chromobody-Emerald	84
Figure 3-1: Schematic depicting the split-Cas9 system in <i>Toxoplasma</i>	91
Figure 3-2: Generation of RH-gap40sgRNA (RH-gap40), RHsplit-Cas9-gap40sgRNA (RHsCas9-gap40) and RHsplit-Cas9 (RHsCas9) parasites	92
Figure 3-3: IFA analysis and quantification of the gap40 phenotype observed in the strains RHsCas9-gap40, RH-gap40 and RHsCas9 upon Rapamycin treatment	94
Figure 3-4: Generation of strains RHsCas9-sag1sgRNA1 (RHsCas9-sag1-1), RHsCas9sag1sgRNA3 (RHsCas9-sag1-3), RHsCas9-mec17sgRNA2 (RHsCas9-mec17-2), RHsCas9-mec17sgRNA3 (RHsCas9-mec17-3) and RHsCas9-Δhx-sag1sgRNA1 (RHsCas9-Δhx-sag1-1)	95
Figure 3-5: IFA analysis and quantification of <i>Tgsag1</i> disruption with split-Cas9	97
Figure 3-6: Effect of split-Cas9 activation in parasites encoding an additional copy of the <i>sag1</i> gene	100
Figure 3-7: Effect of split-Cas9 activation in parasites encoding a lacZsgRNA ..	102
Figure 3-8: Disruption of <i>Tgsag1</i> in RH and RHΔku80 parasites	104
Figure 3-9: Effect of <i>Tgmec17</i> gene function loss in DiCre and split-Cas9 parasites	106
Figure 3-10: <i>Mec17</i> gene excision with the DiCre system and analysis of clonal RHsCas9-mec17-KO lines	108
Figure 4-1: Disruption of <i>Tgactin1</i> and <i>Tgadf</i> in RHsplit-Cas9 parasites expressing actin-chromobody-Emerald (Cb-Em or Cb)	114
Figure 4-2: Disruption of <i>Tgsag1</i> in RHsplit-Cas9 parasites expressing actin-chromobody-Emerald (RHsCas9-Cb-sag1-3)	115
Figure 4-3: Confirmation of the strains RHsCas9-ActinChromobodyEmerald-sag1sgRNA3 (RHsCas9-Cb-sag1-3), RHsCas9-ActinChromobodyEmerald-actin1sgRNA (RHsCas9-Cb-actin1) and RHsCas9-ActinChromobodyEmerald-adfsgRNA (RHsCas9-Cb-adf)	117
Figure 4-4: Parasite egress after split-Cas9 mediated gene disruption	119
Figure 4-5: Depiction of egressed and intracellular RHsCas9-CbEm-sag1-3-wt and RHsCas9-CbEm-sag1-3-KO parasites after A23187 treatment	120
Figure 4-6: Effect of A23187 treatment on intravacuolar filamentous actin structures in RHsCas9-CbEm-sag1-3-ko and RHsCas9-adf-ko parasites compared to wt parasites	122

Figure 4-7: Depiction of egressed and intracellular RHsCas9-CbEm- <i>adf-wt</i> and RHsCas9-CbEm- <i>adf-KO</i> parasites after A23187 treatment.....	124
Figure 4-8: Actin distribution in intracellular RHsCas9-CbEm- <i>actin1 wt</i> and <i>KO</i> parasites along the middle axis	126
Figure 4-9: Actin distribution in intracellular RHsCas9-CbEm- <i>adf wt</i> and <i>KO</i> parasites along the middle axis	128
Figure 4-10: Live microscopy and skeletonisation analysis investigating the interaction of the cytoplasmic actin pool and peripheral actin in the RHsCas9-CbEm- <i>adf-wt</i> line	129
Figure 4-11: Actin distribution in intracellular RHsCas9-CbEm- <i>actin1 wt</i> and <i>KO</i> parasites along the horizontal axis	130
Figure 4-12: Kymograph analysis of peripheral actin flow in intracellular <i>Toxoplasma</i> parasites	131
Figure 5-1: Investigation of <i>TgFormin2</i> (<i>FRM2</i>) localisation in <i>Toxoplasma</i>	138
Figure 5-2: Confirmation of the strains RHsCas9-ActinChromobodyEmerald- <i>DrpAsgRNA</i> (RHsCas9-Cb- <i>DrpA</i>), RHsCas9-ActinChromobodyEmerald- <i>formin2sgRNA</i> (RHsCas9-Cb- <i>formin2</i>) and RHsCas9-ActinChromobody-Emerald- <i>profilinsgRNA</i> (RHsCas9-Cb- <i>profilin</i>)	140
Figure 5-3: Disruption of <i>Tgformin2</i> in RHsplit-Cas9 parasites expressing actin-chromobody-Emerald (Cb-Em or Cb)	142
Figure 5-4: Disruption of <i>Tgformin2</i> in RHsplit-Cas9 parasites expressing actin-chromobody-Emerald (Cb-Em or Cb)	143
Figure 5-5: Generation and verification of the DiCre- <i>formin2</i> -YFPloxP strain ..	145
Figure 5-6: Effect of <i>Tgformin2</i> (<i>frm2</i>) excision with the DiCre system on apicoplast segregation and position	147
Figure 5-7: IFA attempting detection of <i>TgFormin2</i> -YFP (<i>TgFRM2</i> -YFP) without α -YFP antibody	148
Figure 5-8: IFA depicting localisation of <i>TgFormin</i> -YFP in relation to the apicoplast in DiCre- <i>frm2</i> -YFPloxP parasites	149
Figure 5-9: Transient expression of the actin-chromobody-emerald (Cb-Emerald/CbEm) in DiCre- <i>frm2</i> -YFPloxP and DiCre- <i>frm2</i> - <i>KO</i> parasites.....	150
Figure 5-10: IFA depicting the effect of <i>Tgformin2</i> depletion with the DiCre system on morphology and positioning of mitochondria and rhoptries.....	151
Figure 5-11: Disruption of <i>TgDrpA</i> in RHsplit-Cas9 parasites expressing actin-chromobody-Emerald (Cb-Em or Cb)	153
Figure 5-12: Actin distribution in intracellular RHsCas9-CbEm- <i>formin2 wt</i> and <i>KO</i> parasites along the middle axis	155
Figure 5-13: Live microscopy analysis investigating the interaction of the cytoplasmic actin pool and peripheral actin in the RHsCas9-CbEm- <i>formin2-wt</i> line	156
Figure 5-14: Skeletonisation analysis investigating actin distribution in RHsCas9-CbEm- <i>formin2-wt</i> and RHsCas9-CbEm- <i>formin2-KO</i> parasites	157
Figure 5-15: Kymograph analysis of peripheral actin flow in intracellular RHsCas9-CbEm- <i>formin2-wt</i> and <i>KO</i> parasites.....	159
Figure 6-1: Schematic depiction of the DNA damage bottle neck that a <i>Toxoplasma</i> population has to overcome after Cas9 activity	167
Figure 6-2: Schematic depicting a model for actin flow in extracellular (gliding) and intracellular <i>Toxoplasma</i> parasites	173
Figure 6-3: Disruption of <i>TgProfilin</i> in RHsplit-Cas9 parasites expressing actin-chromobody-Emerald (Cb-Em or Cb)	179
Figure 7-1: Kymograph analysis of peripheral actin flow in intracellular RHsCas9-CbEm- <i>actin1-wt</i> and <i>KO</i> parasites	181

Figure 7-2: Actin distribution and kymograph analysis in intracellular RH-GFP parasites	183
Figure 7-3: Actin distribution and kymograph analysis in intracellular RHsCas9-CbEm-adf wt and KO parasites	185
Figure 7-4: Actin distribution in intracellular RHsCas9-CbEm-formin2 wt and KO parasites along the middle axis	186
Figure 7-5: Kymograph analysis of peripheral actin flow in intracellular RHsCas9-CbEm-formin2-wt and KO parasites.....	187
Figure 7-6 Sequencing of the formin2-HA and DiCre-formin2-YFPloxP lines confirming in-frame positioning of the HA and YFP-tag at the c-terminus	188

List of Supplement Material

Movie V1, F-actin dynamics in RHsCas9-CbEm-adf-wt and RHsCas9-CbEm-KO parasites. Time-lapse movie showing Cb-Emerald signal. The movies were captured at a speed of 0.32s/frame. Scale bars are 5 μ m. Movies are depicted at 60fps. Time is shown as mm:ss.

Movie V2, F-actin dynamics in RHsCas9-CbEm-actin1-wt and RHsCas9-CbEm-actin1-KO parasites. Time-lapse movie showing Cb-Emerald signal. The movies were captured at a speed of 0.29s/frame. Scale bars are 5 μ m. Movies are depicted at 60fps. Time is shown as mm:ss.

Movie V3, Live microscopy of RH-GFP parasites. The movies were captured at a speed of 0.33s/frame. Scale bars are 5 μ m. Movies are depicted at 60fps. Time is shown as mm:ss.

Movie V4, F-actin dynamics in RHsCas9-CbEm-formin2-wt and RHsCas9-CbEm-formin2-KO parasites. Time-lapse movie showing Cb-Emerald signal. The movies were captured at a speed of 0.25s/frame. Scale bars are 5 μ m. Movies are depicted at 60fps. Time is shown as mm:ss.

Table of copyright permissions

Table 0-1: Table of copyright permissions

Publisher	Journal	Article title	Authors	Figure No. in article	Figure No.in this thesis	Copyright License
Springer Nature	Nature Reviews Microbiology	Modulation of innate immunity by <i>Toxoplasma gondii</i> virulence effectors	Christopher A. Hunter, L. David Sibley	Figure 1	Figure 1-1	4638711134319
Annual Reviews	Annual Reviews of Microbiology	Lytic Cycle of <i>Toxoplasma gondii</i> : 15 Years Later	Ira J. Blader, Bradley I. Coleman, Chun-Ti Chen, and Marc-Jan Gubbels	Figure 1	Figure 1-2 and Figure 1-3	4638721038758
Springer Nature	Nature Reviews Microbiology	Gliding motility powers invasion and egress in Apicomplexa	Karine Fréna, Jean-François Dubremetz, Maryse Lebrun, Dominique Soldati-Favre	Figure 3	Figure 1-4	4638730100889
Annual Reviews	Annual Reviews of Biophysics	CRISPR–Cas9 Structures and Mechanisms	Fuguo Jiang, Jennifer A. Doudna	Figure 1	Figure 1-6	4638781404178
John Wiley and Sons	FEBS Journal	Genetic screens and functional genomics using CRISPR/Cas9 technology	Ella Hartenian, John G. Doench	Figure 1	Figure 1-7	4638770871847
Annual Reviews	Annual Reviews of Biochemistry	Mechanism and Function of Formins in the Control of Actin Assembly	Bruce L. Goode and Michael J. Eck	Figure 2	Figure 1-9	4638780103258

Acknowledgements

I would like to thank Prof Dr Markus Meissner for providing me with the opportunity to perform my PhD studies in his laboratory. Furthermore, I am grateful for his understanding, most valuable guidance and support during my stay in Glasgow.

My second supervisor, Prof Dr Andy Waters, I would like to thank for valuable advice and discussions during my project work.

I would like to express my appreciation to Dr Richard McCulloch and Dr Charles McSharry for stimulating discussions and their guidance during my thesis work.

Working in the Meissner laboratory was a very enjoyable experience. I would like to express my gratitude to all past and present members for generating such a pleasant and productive work environment. Specifically, I would like to mention Dr Elena Jimenez Ruiz, Dr Simon Gras, Dr Javier Periz, Matthew Gow and Janessa Grech with whom I collaborated on various projects. For his technical and administrative support, I would like to thank Dr Gurman Pall. Dana Aghabi I would like to thank for being an excellent student and for making teaching a fun experience.

Furthermore, it was a great experience to collaborate with Dr Sujaan Das and to benefit from his experience.

I feel lucky to have made great friends in Glasgow. I would like to say thank you to Carmen, Natalia, Helena and Mario for the good times and their selfless support in and outside the laboratory during rough times.

Stephen, Matthias and Markus I thank for their long standing friendship, no matter how far away from home I might be.

Last but not least, an unmeasurable amount of appreciation goes to my family. I would like to thank my parents, grandmother, sister and godmother for their never ending support. My academic journey would not have been possible without them.

Author's Declaration

I, Johannes Felix Stortz hereby declare that I am the sole author of this thesis and performed all of the work presented, with the following exceptions highlighted below. No part of this thesis has been previously submitted for a degree at this or another university.

Johannes Felix Stortz

Chapter 2

- The LacZ-sgRNA plasmid was generated by Marleen Büchler under the supervision of Dr Elena Jimenez-Ruiz.
- The formin2-sgRNA plasmid and the profilin-sgRNA plasmid were generated by Dana Aghabi under my supervision.
- The strains RH Δ ku80-TgFormin2-HA and RH Δ ku80-DiCre-loxP-frm2YFP-loxP were generated by Dr Mirko Singer, who also prepared genomic DNA from the strains for sequencing by Eurofins (Appendix Figure 7-6).
- The strains RHsCas9- Δ hx-sag1-1-KO and RHsCas9-sag1KO-sag1* were generated by Matthew Gow.
- To generate the RHsCas9- Δ hx, the *hx* gene was disrupted in the RHsCas9 by Matthew Gow.
- The strain RHsCas9-lacZsgRNA was generated by Marleen Büchler under the supervision of Dr Elena Jimenez-Ruiz.
- Dr Simon Gras performed initial transfection of the actin-chromobody-emerald plasmid and FACS sorting during the generation process for the RHsCas9-CbEmerald strain.

- The strains RHsCas9-CbEm-formin2 and RHsCas9-CbEm-profilin were generated with the technical help from Dana Aghabi.
- The strain RH Δ ku80-DiCre-Pfmec17loxP was generated during my Master thesis by me prior to my PhD studies (Stortz, 2014, Master thesis, Ruprecht-Karls-University Heidelberg, Germany).

Chapter 3

- Analytical PCR confirming integration of the sag1sgRNA1 plasmid into the genome of RHsCas9- Δ hx parasites and genome sequencing for the clonal RHsCas9- Δ hx-sag1-1-KO mutant were performed by Matthew Gow (Figure 3-4 B and C).
- *TgSAG1* complementation experiments were performed by Matthew Gow (Figure 3-6).
- Transient disruption of *Tgsag1* in RH and RH Δ ku80 parasites was performed and analysed by Dr Elena Jimenez-Ruiz (Figure 3-8).

Chapter 4

- Live microscopy for RHsCas9-CbEm-actin1-wt and RHsCas9-CbEm-actin1-KO was performed by Dr Mario Del Rosario. These videos were used for analysis in Figure 4-8 A and B, Figure 4-11 and Figure 4-12 A and D. See also Appendix Figure 7-1 and Supplement Movie V2.

Chapter 5

- Analytical PCR confirming integration of plasmid DNA into the *Toxoplasma* genome was performed by Dana Aghabi under my supervision (Figure 5-2).

Publications arising from this work and collaborations

Johannes Felix Stortz, Mario Del Rosario, Mirko Singer, Jonathan M. Wilkes, Markus Meissner, and Sujaan Das (2019) “Formin-2 Drives Polymerisation of Actin Filaments Enabling Segregation of Apicoplasts and Cytokinesis in *Plasmodium Falciparum*.” *ELife* 8: e49030. <https://doi.org/10.7554/eLife.49030>.

Mario Del Rosario, Javier Periz, Georgios Pavlou, Oliver Lyth, Fernanda Latorre-Barragan, Sujaan Das, Gurman S. Pall, Johannes Felix Stortz, Leandro Lemgruber, Jamie A. Whitelaw, Jake Baum, Isabelle Tardieux and Markus Meissner (2019) “Apicomplexan F-actin is required for efficient nuclear entry during host cell invasion.” *EMBO Reports*: e48896. <https://doi.org/10.15252/embr.201948896>.

Johannes Felix Stortz*, Janessa Grech*, Matthew Gow, Markus Meissner, Elena Jimenez-Ruiz (2019) “A conditional CRISPR/Cas9 system enables phenotypic screening for novel actin binding proteins in *Toxoplasma*.” (in preparation for submission) *asterisks indicate equally contributing authors

Conference Proceedings

I presented data from my thesis at the following conferences and other local meetings:

Poster Presentations: **MPM** meeting, Woods Hole (USA) 2015

Toxo-14 meeting, Tomar (Portugal) 2017

Gordon Conference, Newport (USA) 2018

Oral Presentations: **Actin 2017** meeting, Bristol (UK), 2017

ToxoUK Day, London (UK), 2018

Definitions/abbreviations

Aa	Amino acid
ACT1 or <i>act1</i>	Actin1
ADF or <i>adf</i>	Actin depolymerisation factor
ADP	Adenosine diphosphate
AID	Auxin-inducible degron
AMA1	Apical membrane antigen 1
Amp	Ampicillin
Arg	Arginine
At	Arabidopsis thaliana
ATP	Adenosine triphosphate
a.u.	arbitrary units
α TAT1	alpha-tubulin acetyltransferase 1
BLAST	Basic Local Alignment Search Tool
BIPPO	5-Benzyl-3-isopropyl-1H-pyrazolo[4,3-d]pyrimidin-7(6H)-one
bp	Base pair
BSA	Bovine serum albumin
°C	Degree Celsius
Ca ²⁺	Calcium
cAC	Cytosolic actin centre
Cas9	CRISPR associated protein 9
CAT	Chloramphenicol acetyltransferase
cDNA	Complementary deoxyribonucleic acid
Cb	Chromobody
Cb-Em	Chromobody Emerald
CDPK	Calcium-dependent protein kinase
CIP	Calf intestinal phosphatase
C-terminal	Carboxyl terminal
CRISPR	Clustered Regularly Interspaced Short Palindromic Repeats
DD	Destabilisation domain
DHFR	Dihydrofolate reductase
DiCre	Dimerisable Cre
Dm	<i>Drosophila melanogaster</i>
DMEM	Dulbecco's Modified Eagle's Medium
DMSO	Dimethyl sulfoxide

DN	Dominant negative
DNA	Deoxyribonucleic acid
ds	Double-strand
DSB	double-strand break
dNTP	Deoxynucleotide 5'-triphosphate
<i>E. coli</i>	<i>Escherichia coli</i>
EDTA	Ethylene diamine tetraacetic acid
Em	Emerald fluorescent protein
ER	Endoplasmic reticulum
EtOH	Ethanol
FBS	Fetal bovine serum
fw	Forward
FRM or <i>frm</i>	Formin or <i>formin</i>
g	Gram or Gravity (context dependent)
GAP	Glideosome associated protein
gDNA	Genomic deoxyribonucleic acid
GFP	Green fluorescent protein
GOI	Gene of interest
GED	GTPase Effector Domain
GFP	Green Fluorescent Protein
GPI	Glycophosphatidylinositol
gRNA	Guide RNA
GTP	Guanosine triphosphate
h	Hour
H ₂ O	Water
HEPES	4-(2-Hydroxyethyl)-piperazineethanesulphonic acid
HFF	Human foreskin fibroblast
Hs	<i>Homo sapiens</i>
Hx or hxgprt	Hypoxanthine-xanthine-guanine phosphoribosyl transferase
IAA	indole-3-acetic acid
IFA	Immunofluorescence analysis
IMC	Inner membrane complex
IPP	isopentenyl pyrophosphate
K	Lysine
kbp	Kilo base pair
KD	Knockdown
kDa	Kilo Dalton

KO	Knockout
LB	Luria-Bertani
LoxP	Locus crossover in P1
Lys	Lysine
M	Molar or Methionine (amino acid)
MCS	Multiple cloning site
mg	Milligram
MIC	Micronemal protein
min	Minute
MJ	Moving Junction
ml	Millilitre
mM	Milimolar
MTOC	Microtubule organisation centre
MPA	Mycophenolic acid
mRNA	Messenger ribonucleic acid
MT	Microtubule
Myo	Myosin
NCBI	National Center for Biotechnology Information
NHEJ	Non-homologous end joining
ng	Nanogram
nm	Nanometer
N-terminal	Amino terminal
ORF	Open reading frame
<i>P. falciparum</i> or <i>Pf</i>	<i>Plasmodium falciparum</i>
PBS	Phosphate buffered saline
PCR	Polymerase chain reaction
PFA	Paraformaldehyde
Pi	Inorganic phosphate
PM	Plasma membrane
POI	Protein of interest
PV	Parasitophorous vacuole
PVM	Parasitophorous vacuole membrane
r	Resistant
RB	Residual body
rev	Reverse
RFP	Red Fluorescent Protein

RNA	Ribonucleic acid
RON	Rhoptry neck protein
rpm	revolutions per min
RT	Room temperature
s	Second
SAG1	Surface antigen 1
sCas9	Split-Cas9
SD	Standard deviation
sgRNA	Single-guide RNA
SOC	Super optimal broth with catabolite repression
ss	Single-strand
SSR	Site specific recombination
t	Time
<i>T. gondii</i> or <i>Tg</i>	<i>Toxoplasma gondii</i>
TAE	Tris-acetate-EDTA
TEMED	N,N,N',N'-tetramethylethylenediamine
term	terminus
TM	Transmembrane
Tris	Tris [hydroxymethyl] aminomethane
U	Unit
UTR	Untranslated region
UV	Ultraviolet
V	Volts
v/v	Volume/volume percentage
w/v	Weight/volume percentage
WHO	World health organisation
wt	Wild-type
Xan	Xanthosine monophosphate
X-Gal	5-bromo-4-chloro-3-indoyl- β -D-Galactopyranoside
YFP	Yellow fluorescent protein
μ g	Microgram
μ l	Microliter
μ m	Micrometer
μ M	Micromolar

1 Introduction

The single cell organism *Toxoplasma gondii* is an obligate intracellular parasite that can infect any nucleated cell in any warm-blooded animal, including humans. In this chapter, I will provide an introduction to the overall biology of this parasite. I will specifically highlight the function of the structural protein actin within the asexual lytic cycle of *Toxoplasma*. Furthermore, the recently developed molecular tool CRISPR/Cas9 will be reviewed.

1.1 Taxonomie

Toxoplasma gondii is the only species in the genus *Toxoplasma* and, therefore, will be simply referred to as *Toxoplasma* during this thesis. *Toxoplasma* is placed in the (Infra)Phylum of the Apicomplexa within the Coccidia subclass. Apicomplexans are characterised by the presence of an apical complex and a parasitic life style (LEVINE et al. 1980). It is important to note that *Plasmodium* species, the causative agent of malaria, also belong to the apicomplexan (infra)phylum (LEVINE et al. 1980). The (Infra)Phylum Apicomplexa contains about 6000 species, but a potential number of up to 10 million is estimated (Adl et al. 2007). Although all apicomplexan organisms are parasitic, there is evidence suggesting that their ancestor was living in a symbiotic relationship with corals (Moore et al. 2008; van Dooren and Striepen 2013).

The (infra)phylum Apicomplexa belongs to the superphylum of the Alveolata (Adl et al. 2012; Ruggiero et al. 2015; Adl et al. 2019). A common feature in Alveolata is a peripheral alveolar membrane system. This system contains of membrane sacs that are located directly underneath and outline the plasma membrane (Adl et al. 2019). This peripheral alveolar membrane system is referred to as IMC (Inner Membrane Complex) in Apicomplexa (Blader et al. 2015). Alveolata belong to the taxon "SAR" (Burki et al. 2007; Adl et al. 2012).

1.2 Health Impact of apicomplexan parasites

In total, *Plasmodium* was responsible for an estimated 219 million malaria cases globally, with an estimated 435,000 deaths in 2017 worldwide. Children under the age of 5 were most affected (World Health Organization: World Malaria Report 2018).

One third of the human population is infected with *Toxoplasma* (Blader et al. 2015). Most post-natal infections remain asymptomatic in healthy individuals. However, there are two situations when *Toxoplasma* infection can result in clinical disease: (1) When infected individuals become immunocompromised and (2) when an acute infection occurs in pregnant individuals since congenital infection can happen in the fetus (Blader et al. 2015). Effect of *Toxoplasma* infection on the unborn child can be dramatic, including spontaneous abortion, mental retardation (Black and Boothroyd 2000), deafness and retinal damage (Torrey and Yolken 2013). Toxoplasmic encephalitis was reported to be one of the most common AIDS-associated diseases of the central nervous system (Luft and Remington 1992). It shall also be mentioned that *Toxoplasma* infections can cause ocular disease (Torrey and Yolken 2013) and that the effect of *Toxoplasma* infection on host behaviour and mental health is under investigation (Tyebji et al. 2019).

1.3 The life cycle of *Toxoplasma*

The *Toxoplasma* life cycle (Figure 1-1) was first postulated by Frenkel and colleagues in 1970 (Frenkel, Dubey, and Miller 1970). The life cycle can be separated into three different stages: the sexual stage and the asexual stage, also known as lytic cycle. In between, there is an environmental stage when the parasite is transferred from its definitive host (sexual replication) to the intermediate host (asexual replication) (Robert-Gangneux and Dardé 2012). Noteworthy, *Toxoplasma* can be transmitted between different intermediate hosts orally, i.e. without having to complete the sexual cycle in cats. This remarkable feature of *Toxoplasma* biology was reported to be the driving force behind the clonal global expansion of *Toxoplasma* (Su et al. 2003). Throughout its life cycle *Toxoplasma* can occur in three infectious stages: rapidly dividing

tachyzoites, slow growing bradyzoites that can form tissue cysts and sporozoites which occur in oocysts that are shed by cat faeces (Torrey and Yolken 2013).

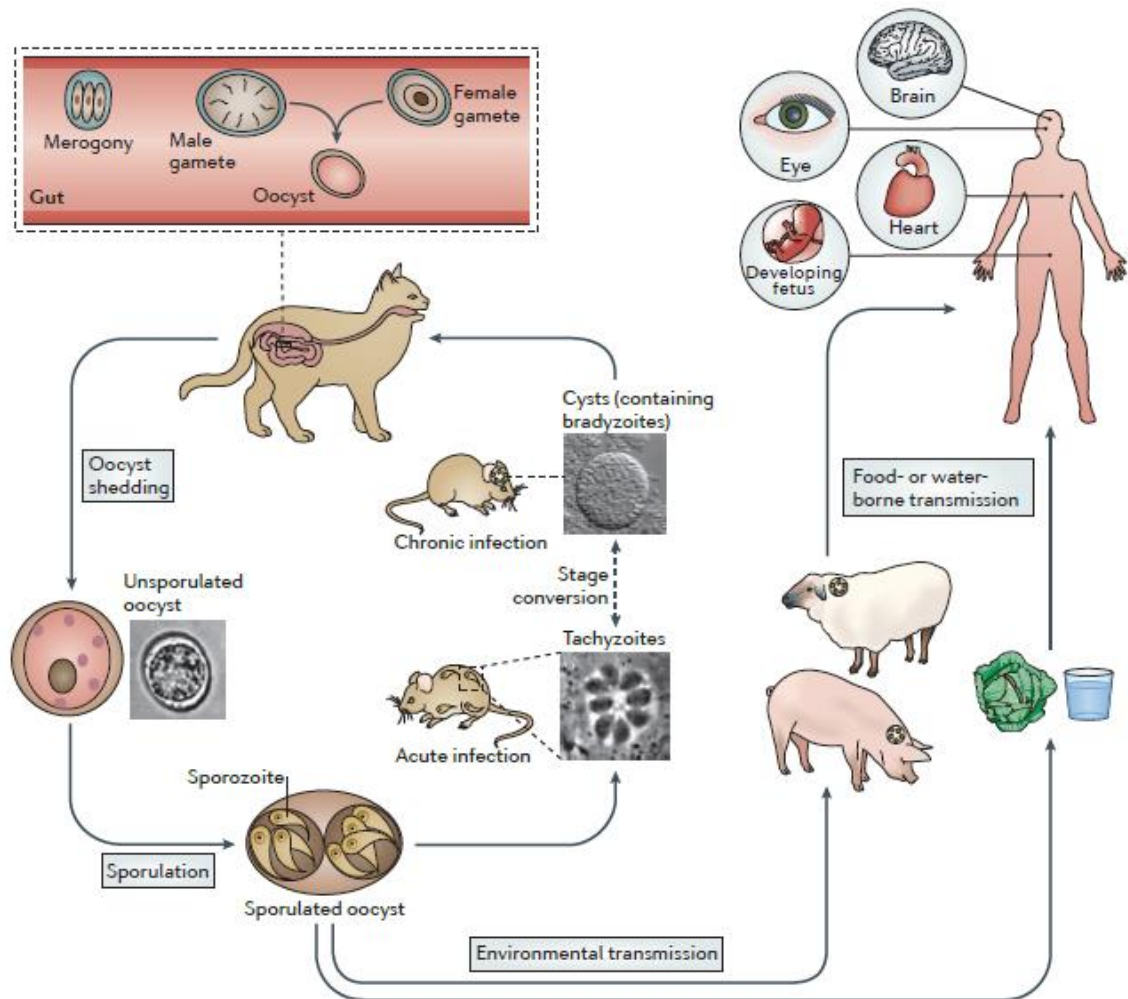


Figure 1-1: The life cycle of *Toxoplasma gondii*

The *Toxoplasma* life cycle is separated into the sexual, asexual and environmental stage. Sexual replication happens exclusively in feline species. Cats shed infective oocysts which are ingested by the intermediate host where asexual replication occurs. Asexual replication can occur in any warm-blooded animal (here depicted as mice, sheep or pig). Consumption of infected prey by the cat re-introduces *Toxoplasma* to its definite host. Humans can be infected with *Toxoplasma* when ingesting contaminated food or water. *Toxoplasma* poses a threat to immunocompromised individuals and embryos. Reprinted by permission from Springer Nature Customer Service Centre GmbH: Springer Nature, Nature Reviews Microbiology (Hunter and Sibley 2012) ©2012, License number: 4638711134319.

1.3.1 Definitive host - sexual replication

Sexual replication happens exclusively in feline species. The cat-exclusive occurrence of sexual replication was recently linked to a systemic excess of linoleic acid in felines (Di Genova et al. 2019). The excess of linoleic acid is

believed to be caused by the absence of delta-6-desaturase activity in cats (Rivers, Sinclair, and Crawford 1975; Sinclair, McLean, and Monger 1979). When the murine delta-6-desaturase was inhibited in mice that were fed a diet supplemented with linoleic acid, *Toxoplasma* was able to undergo sexual replication in mice (Di Genova et al. 2019). Cats can be infected by tachyzoites and bradyzoites (Dubey and Frenkel 1976; Dubey 2006). They can also be infected by oocysts (Dubey 2006). However, a higher number of oocysts than bradyzoites is required for establishing an infection that results in the cat shedding oocysts.

Upon oral uptake of a bradyzoite cyst by a cat, the cyst wall is destroyed by digestive enzymes. Free parasites enter epithelial cells of the small intestine (enterocytes) and replicate asexually. Eventually, merozoites are formed in schizonts, a process called schizogony. Schizogony is followed by sexual development, i.e. the formation of male and female gametocytes (gametogony). After fertilisation, an oocyst forms within an enterocyte. The oocyst is eventually released into the environment within the cat faeces (Robert-Gangneux and Dardé 2012).

1.3.2 Environmental stage

Outside the cat, sporozoites are formed within the oocyst. These sporulated oocysts can be taken up by the intermediate host through ingestion of contaminated food or water. Importantly, *Toxoplasma* undergoes meiotic reduction during sporozoite formation resulting in a haploid genome (Robert-Gangneux and Dardé 2012).

The oocyst wall consists of multiple layers (Ferguson, Hutchison, and Siim 1975; Speer, Clark, and Dubey 1998) and protects the sporozoites from the outer environment (Belli, Smith, and Ferguson 2006). It was reported that oocyst wall has similar properties to common plastic material, making it resistant to the outer environment and disinfectants (Dumetre et al. 2013). In the laboratory, oocysts can survive harsh conditions maintaining their infectiveness for hundreds of days, if not years (Dubey 1998; Yilmaz and Hopkins 1972). In the environment, oocysts were reported to remain infectious for over a year (Yilmaz

and Hopkins 1972; Frenkel, Ruiz, and Chinchilla 1975). Contamination of water supply with cat faeces can cause Toxoplasmosis outbreaks in the human population, as shown by a case study from Brazil (De Moura et al. 2006).

1.3.3 Intermediate host - asexual lytic cycle

Within the intermediate host, *Toxoplasma* replicates asexually. After oocyst uptake, the sporozoites break free and invade intestinal epithelial cells. Here, they differentiate into tachyzoites that can spread throughout the body (Robert-Gangneux and Dardé 2012). Tachyzoites can convert into bradyzoites. This stage forms cysts that can remain in the intermediate host for life (Robert-Gangneux and Dardé 2012). Upon transmission from one intermediate host to another or to the cat, bradyzoites break free from the cysts and establish a new infection (Robert-Gangneux and Dardé 2012).

1.4 The asexual lytic cycle of *Toxoplasma* tachyzoites: a closer look

The lytic cycle can be divided into several phases: gliding, host cell invasion, asexual replication and egress (**Figure 1-2**). In short, after gliding towards and invasion of a host cell, the parasite replicates within that cell and, eventually, egresses to infect another cell. Since experiments during this study were exclusively performed on asexually replicating tachyzoites, these steps will be described in more detail in the following sections. Also, the tachyzoite ultrastructure shall be introduced.

1.4.1 Tachyzoite structure

Tachyzoites show a crescent shape and are usually about 2µm in width and 6-8µm in length (Dubey, Lindsay, and Speer 1998; Joiner and Roos 2002). They possess many organelles typically found in eukaryotes, including a nucleus, a single interconnected endoplasmatic reticulum (ER) network, a single mitochondrion and a single Golgi apparatus (**Figure 1-3**) (Joiner and Roos 2002).

In addition, three distinct types of secretory organelles are present in *Toxoplasma*. These organelles are micronemes, rhoptries and dense granules (Dubey, Lindsay, and Speer 1998; Joiner and Roos 2002). Micronemes and rhoptries play important roles in gliding motility and, thus, host cell invasion and egress (please refer to sections 1.4.2., 1.4.3. and 1.4.5). The microneme secretion process is introduced in the context of parasite egress in section 1.4.5.

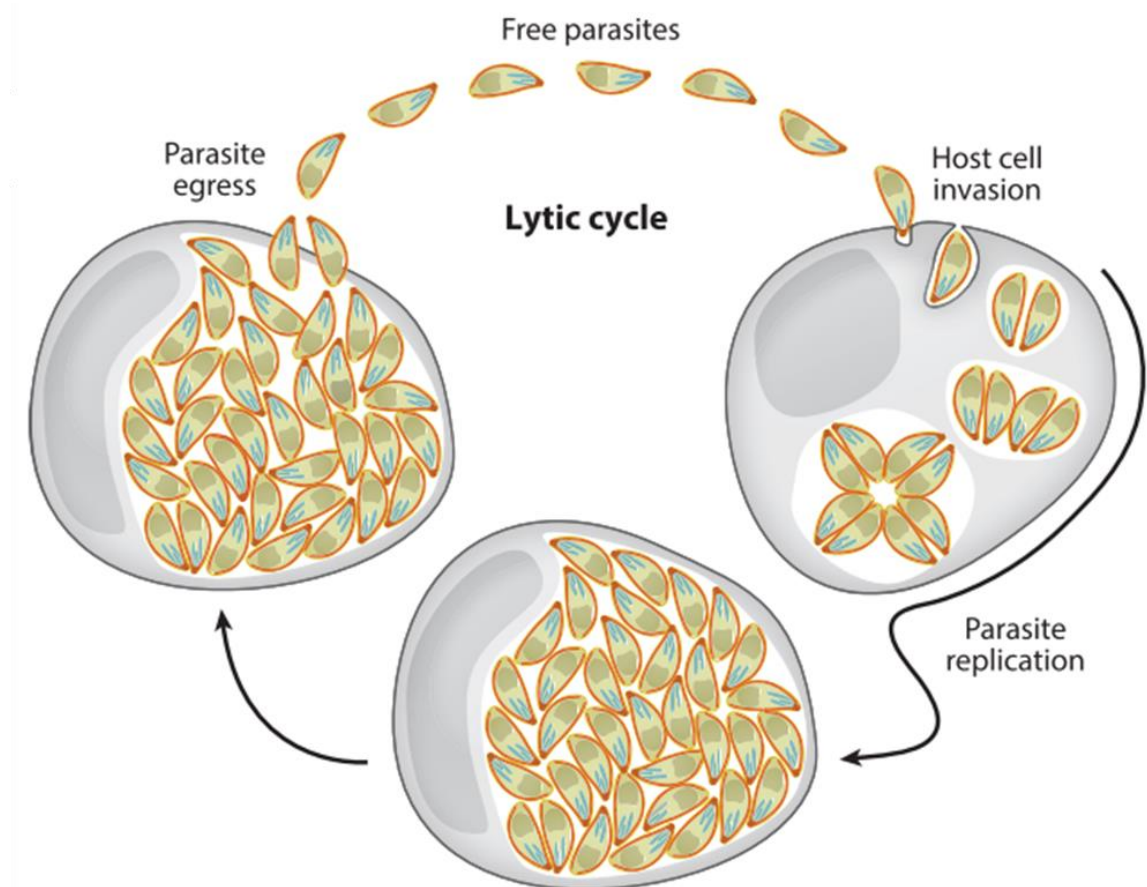


Figure 1-2: The Lytic cycle of *Toxoplasma*

Completion of the lytic cycle depends on several steps: gliding, host cell invasion, asexual replication and egress. After gliding towards and invasion of a host cell, the parasite replicates within that cell and, eventually, egresses to infect another cell. Republished with permission of Annual Reviews (Annual Reviews of Microbiology), from (Blader et al. 2015) © 2015; permission conveyed through Copyright Clearance Center, Inc. License number: 4638721038758.

Dense granules were found to be involved in the maturation of the parasitophorous vacuole (PV) (Mercier and Cesbron-Delauw 2015). For instance, the dense granule proteins GRA17 and 23 were suggested to mediate traffic of small molecules between the PV and the host cell (Gold et al. 2015). Additionally, dense granule proteins were reported to localise to the host cell

nucleus where they can impact host gene expression levels (Bougdour et al. 2013; Braun et al. 2013). Micronemes and rhoptries are localised to the apical tip of the tachyzoite and are part of the apical complex, together with the apical polar ring (APR) and the conoid (Morrissette and Sibley 2002).

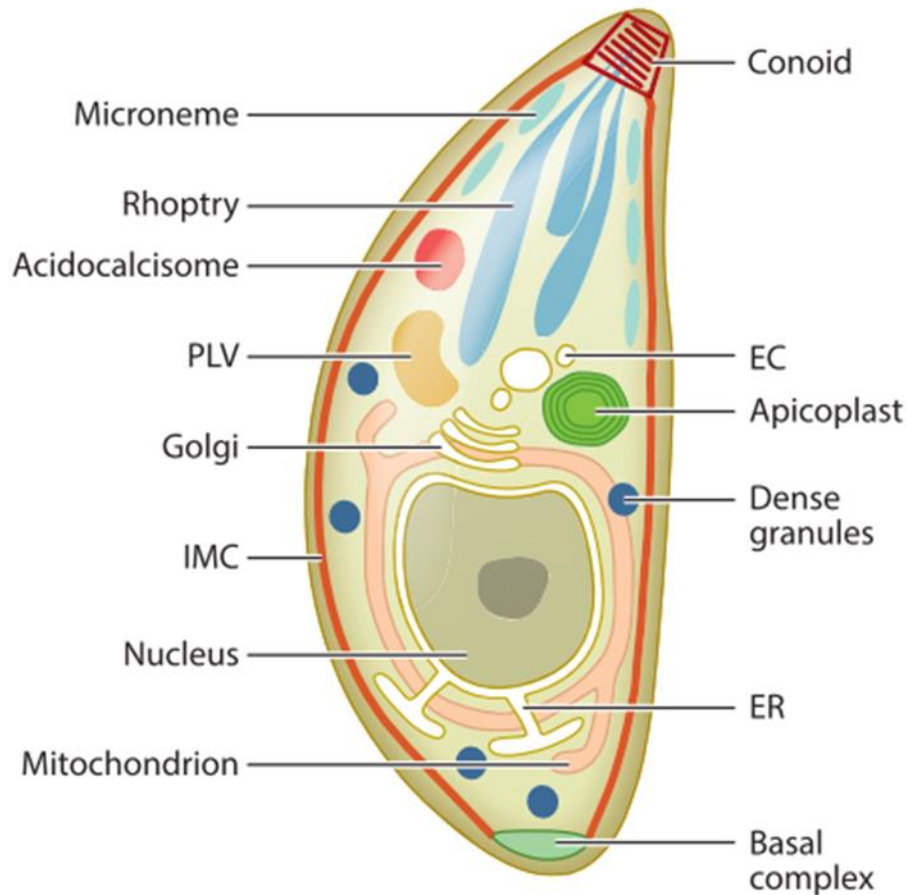


Figure 1-3: Schematic of the *Toxoplasma* tachyzoite ultrastructure

Tachyzoites possess a crescent shape and many organelles typically found in eukaryotes including a nucleus, a single interconnected endoplasmic reticulum (ER) network, a single mitochondrion and a single Golgi apparatus. The tachyzoite body is outlined by the inner membrane complex (IMC) that sits just beneath the plasma membrane and on top of the subpellicular microtubules (not depicted). The conoid is located to the apical tip of the parasite together with micronemes, rhoptries and dense granules, the three types of secretory organelles found in tachyzoites. The apicoplast is a non-photosynthetic plastid organelle and crucial for parasite survival. Abbreviations: EC - endosome compartment; PLV - plant-like vacuole. Republished with permission of Annual Reviews (Annual Reviews of Microbiology), from (Blader et al. 2015) © 2015; permission conveyed through Copyright Clearance Center, Inc. License number: 4638721038758.

Together with microtubules, the conoid is part of the tachyzoite cytoskeleton. The conoid is a cone-like structure at the apical tip of tachyzoites and consists of tubulin (Nichols and Chiappino 1987; Hu, Roos, and Murray 2002). Notably, the

tubulins forming the conoid arrange into a polymer different from typical microtubules (Hu, Roos, and Murray 2002). Conoid extrusion is part of the host cell invasion process (Nichols, Chiappino, and O'Connor 1983; Werk 1985) and was reported to depend on calcium (Mondragon and Frixione 1996). Recently, the conoid protein hub 1 (CPH1) was identified (Long, Anthony, et al. 2017). This protein localises to the conoid and is critical for conoid integrity in extracellular parasites. CPH1 also appeared to be critical for parasite motility and invasion. In addition, three calmodulin (CaM)-like proteins localise to the conoid (Long, Brown, et al. 2017). Interestingly, these proteins appear to be involved in parasite invasion, egress and motility. However, CaMs 1-3 are dispensable for conoid extrusion. CaM 1 and 2 were originally localised to the conoid by Hu and co-workers (Hu et al. 2006).

Two constituents of the APR are known: RNG1 and RNG2 (Morrisette 2015). RNG1 localises to the APR (Tran et al. 2010). Since attempts to knock-out RNG1 failed, Tran and co-workers suggested RNG1 to be critical for parasite survival. Depletion of RNG2, which also localises to the APR, inhibits host cell invasion, motility and microneme secretion (Katris et al. 2014). Interestingly, Katris and colleagues could restore microneme secretion by stimulating RNG2 depleted parasites with calcium. This finding was interpreted as implication for a function of the apical complex in the regulatory pathways for microneme secretion. The APR also functions as a microtubule organisation centre (MTOC) from which 22 subpellicular microtubules originate (Nichols and Chiappino 1987). These microtubules span about two-thirds of the tachyzoite body and form a spiralled cage. In addition to the subpellicular microtubules, two intraconoid microtubules can be found spanning the inner lumen of the conoid (Nichols and Chiappino 1987; Hu, Roos, and Murray 2002; Morrisette 2015).

The tachyzoite body is outlined by the inner membrane complex (IMC) that sits just beneath the plasma membrane and on top of the subpellicular microtubules (Harding and Meissner 2014). The IMC is composed of flattened membrane sacs (alveoli) that lie directly underneath the plasma membrane. The alveoli are supported by the subpellicular network (SPN) (Harding and Meissner 2014). The SPN was initially characterised as an interwoven network of filaments that spans the whole tachyzoite body (Mann and Beckers 2001). The network is believed to be a membrane skeleton that confers cell shape and stability. The first SPN

components to be discovered were the intermediate filament-like proteins IMC1 and 2 (Mann and Beckers 2001). Since then, a large number of additional IMC proteins (e.g. IMC3-15, IMC17-24) has been described (Gubbels, Wieffer, and Striepen 2004; Hu et al. 2006; Anderson-White et al. 2011; Chen et al. 2015). It was reported that the IMC proteins show distinct spatiotemporal distribution patterns during the tachyzoite development (Anderson-White et al. 2011). For instance, IMC15 represents a marker for early daughter cell budding (Anderson-White et al. 2011). Loss of IMC15 can cause additional daughter buds to form within the mother cell (Dubey et al. 2017).

IMC suture components (ISCs) were identified to localise to the transverse and longitudinal alveolar sutures of the IMC (Chen et al. 2015). ISCs were proposed to be involved in the establishment and/or maintenance of the tachyzoite shape, as parasites lacking ISC3 display aberrant morphology (Chen et al. 2017). Also, disruption of ISC3 caused a loss of virulence in mice (Chen et al. 2017).

1.4.1.1 The apicoplast

The apicoplast, a non-photosynthetic plastid organelle, represents a crucial organelle in *Toxoplasma* tachyzoites. The understanding of apicoplast biology is crucial for the data presented in this thesis. Therefore, this organelle shall be introduced in more detail in this section.

The apicoplast was independently described in *Toxoplasma* in 1996 and 1997 (McFadden et al. 1996; Kohler et al. 1997). Both studies localised DNA from a 35kb extrachromosomal DNA circle, originally believed to represent mitochondrial DNA (McFadden and Yeh 2017), to a distinct organelle that was identified as the apicoplast. The complete sequence of the plastid-DNA in *P. falciparum* showed that the apicoplast lacks genes required for photosynthesis (Wilson et al. 1996).

The apicoplast is believed to be derived from a red algae by secondary endosymbiosis (Janouskovec et al. 2010). It was, however, controversially debated in the past whether the apicoplast originated from a red or a green algae (Wilson 1993; Williamson et al. 1994; Kohler et al. 1997; Funes et al. 2002; Cai et al. 2003; Waller et al. 2003; Coppin et al. 2005; Waller and Keeling 2006).

The puzzle was solved by the discovery of *Chromera velia*, a photosynthetic relative of the apicomplexan parasite lineage (Moore et al. 2008). *C. velia* is a single cell organism that lives in scleractinian corals. The plastid of *C. velia* is bound by four membranes and shares an origin with the apicoplast. Examination of the plastids in *C. velia* and CCMP3155, another photosynthetic alveolate closely related to apicomplexans, revealed that the apicoplast in apicomplexans is derived from a red algae (Janouskovec et al. 2010).

Apicoplast division is coordinated with nucleus replication (Striepen et al. 2000). Dividing and non-dividing apicoplasts are associated with the centrosome throughout the parasite life cycle (Striepen et al. 2000). It was reported that disruption of microtubule formation impacts apicoplast replication (Striepen et al. 2000). Proper actin dynamics are also critical for apicoplast replication and segregation (Andenmatten et al. 2013; Jacot, Daher, and Soldati-Favre 2013; Haase et al. 2015; Whitelaw et al. 2017). Disruption of actin dynamics results in vacuoles containing parasites devoid of the apicoplast. *TgMyoF* and *TgDrpA* represent additional key players in apicoplast division. *TgMyoF* was reported to be involved in centrosome positioning and apicoplast inheritance (Jacot, Daher, and Soldati-Favre 2013). The dynamin-related protein *TgDrpA* is critical for apicoplast fission (van Dooren et al. 2009). The enzyme ensures the cutting of the dividing apicoplast so that both daughter cells receive one single apicoplast.

The apicoplast is essential for parasite survival (Roos and Fichera 1997; He et al. 2001). It is important to note, however, that apicoplast loss does not immediately abolish *Toxoplasma* growth. Parasites usually die within the 2nd lytic cycle after apicoplast loss, a phenomenon referred to as the “delayed death phenotype” (Roos and Fichera 1997; He et al. 2001). Intriguingly, as long as one parasite within the vacuole possesses an apicoplast, the vacuole as a whole shows almost normal growth even in the 2nd lytic cycle (He et al. 2001). This shows that one single apicoplast can keep a whole vacuole of parasites alive.

The apicoplast hosts fatty acid synthesis via the FASII pathway (Waller et al. 1998; Ramakrishnan et al. 2012) and synthesis of isopentenyl pyrophosphate (IPP) which is a precursor of isoprenoids (Jomaa et al. 1999; Nair et al. 2011). It is further believed that the apicoplast is involved in the synthesis of iron sulphur clusters (Kumar et al. 2011; Gisselberg et al. 2013; Geoffrey Ian McFadden and

Yeh 2017) and haem synthesis (Sato et al. 2004; Dhanasekaran et al. 2004; Nagaraj et al. 2008, 2009; Goldberg and Sigala 2017). In *Plasmodium*, asexual blood stage parasites that are lacking the apicoplast can survive indefinitely when supplemented with exogenous IPP (Yeh and DeRisi 2011). This makes IPP synthesis the only essential apicoplast function in malaria blood stages. Lack of isoprenoid precursors was suggested to interfere with protein prenylation and cellular vesicle trafficking, resulting in the fragmentation of the digestive vacuole in parasites experiencing delayed death (Kennedy et al. 2019).

1.4.2 Gliding motility

Experiments with tachyzoites in 2D identified three distinct types of movement: circular gliding, upright twirling and helical rotation (Hakansson et al. 1999). More recently, tachyzoite gliding was analysed in a more biologically relevant 3D environment (Leung et al. 2014). These experiments revealed that tachyzoites move in irregular corkscrew-like trajectories. It was suggested that the different gliding styles that were observed in 2D reflect the different types of movement that are necessary to perform corkscrew-like trajectories in 3D (Leung et al. 2014; Frénal, Dubremetz, et al. 2017).

The key concept of apicomplexan motility is the gliding on a surface which requires cell-cell contact between gliding parasite and substrate (**Figure 1-4**). This presents a remarkable feature as parasites do not utilise ciliary or flagellar propulsion as is often the case in unicellular organisms. The exact mechanisms by which this type of forward movement is achieved are currently under investigation. One of the proposed models is the so-called actomyosin motor complex. This complex consists, among other factors, of the structural protein actin and MyosinA (MyoA). Another key player are the micronemes, a set of secretory organelles (Frénal, Dubremetz, et al. 2017).

In brief, the proposed mode of action of the actomyosin motor complex is depicted in the following (Frénal, Dubremetz, et al. 2017): The MyoA tail domain is linked to the IMC via MLC1 while the MyoA head interacts with actin filaments between the IMC and the parasite plasma membrane. This complex is kept in place by the gliding-associated proteins (GAPs), GAP40, GAP45 and GAP50. When

gliding is initiated, micronemes are exocytosed at the apical tip of the tachyzoite and adhesion molecules are integrated into the parasite plasma membrane. These adhesins span the plasma membrane and interact with receptor molecules on the substrate surface outside the parasite. The actin filaments are connected to adhesins via a glideosome-associated connector (GAC). Overall, this molecular set up anchors the actin-myosin motor to the IMC and, at the same time, the outside surface of the substrate. This allows MyoA-mediated force generation by translocation of actin filaments alongside the tachyzoite periphery towards the basal end of the parasite.

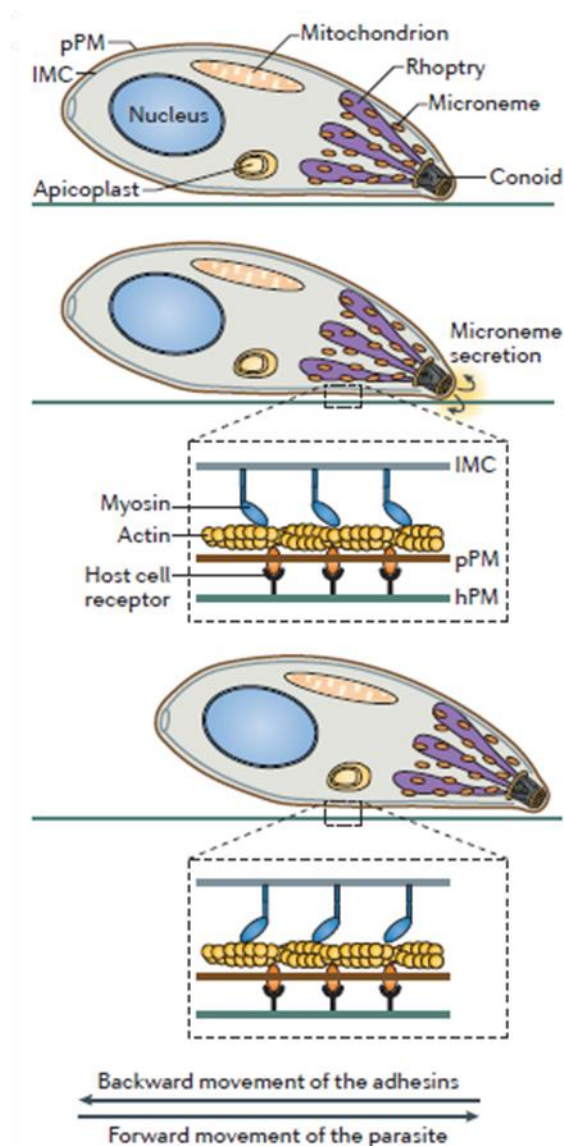


Figure 1-4: Gliding motility in *Toxoplasma tachyzoites*

Tachyzoite movement on a host cell plasma membrane (hPM) requires contact between the gliding parasite and the substrate. Forward movement is achieved by the actomyosin motor complex. This complex consists, among other factors, of the structural protein actin and MyosinA (MyoA). Another key player are the micronemes, a set of secretory organelles. MyoA is linked to the IMC and interacts with actin filaments between the IMC

and the parasite plasma membrane (pPM). When gliding is initiated, micronemes are exocytosed at the apical tip of the tachyzoite and adhesion molecules are integrated into the pPM. These adhesins span the pPM and interact with receptor molecules on the hPM. Forward movement is achieved by MyoA-mediated translocation of actin filaments alongside the tachyzoite periphery towards the basal end of the parasite. Abbreviations: IMC - inner membrane complex; pPM - parasite plasma membrane; hPM - host plasma membrane. Reprinted by permission from Springer Nature Customer Service Centre GmbH: Springer Nature, Nature Reviews Microbiology (Frénal, Dubremetz, et al. 2017) ©2017, License number: 4638730100889.

Numerous studies were conducted to support the current view of the actomyosin system and its components. Myosin A was reported to possess kinetic properties similar to myosins in muscle cells, thus explaining its capacity in generating force together with actin (Herm-Götz et al. 2002). The same study identified myosin light chain (MLC1) to bind MyoA (Herm-Götz et al. 2002). In addition, Myosin A was found to be essential for parasite gliding and invasion (Meissner, Schlüter, and Soldati 2002).

The gliding associated proteins GAP45 and 50 were identified and localised to the IMC (Gaskins et al. 2004). Subsequently, GAP40 was identified and GAP45 was further characterised to be essential for motility, egress and invasion (Frénal et al. 2010). Recently, GAC was proposed to connect the actomyosin complex with micronemal adhesins (Jacot et al. 2016). GAC appears to be critical for gliding, egress and invasion. Interestingly, experimental data suggest actin stabilising properties for GAC (Jacot et al. 2016). Noteworthy, experiments were performed on *Plasmodium falciparum* actin, not *Toxoplasma* actin.

Several adhesion molecules are known to function in *Toxoplasma* (Paing and Tolia 2014; Frénal, Dubremetz, et al. 2017). For instance, loss of the microneme protein MIC2 negatively impacted tachyzoite attachment to the host cell surface and reduced helical gliding movements in 2D assays (Huynh and Carruthers 2006).

In summary, these studies highlight the importance of this complex for the lytic cycle and overall parasite morphology. Nevertheless, it is still debated whether the actomyosin system is exclusively responsible for parasite gliding and invasion. Some of the proposed actomyosin motor complex components were suggested to be dispensable as clonal tachyzoite lines lacking the *myoA* or *mic2* gene were able to survive (Andenmatten et al. 2013). Although lack of MIC2

impacted overall motility, clonal *mic2* knock-out parasites were still able to perform gliding at the same maximum speed as wild-type parasites (Gras et al. 2017). Taken together, these observations could suggest an alternative gliding and invasion mechanism. Conditional depletions of other components of the actomyosin system support the existence of such an alternative system (Egarter et al. 2014; Whitelaw et al. 2017). Whitelaw and co-workers suggested a role for the actomyosin complex in surface attachment, rather than force generation during parasite gliding (Whitelaw et al. 2017). A recent study suggested retrograde membrane flow as a driving force for tachyzoite gliding motility (Gras et al. 2019). Gras and colleagues reported that extracellular parasites are capable of taking up exogenous material such as labelled lipids. After uptake, these lipids appear to be secreted again upon activation of gliding motility during attachment and invasion (Gras et al. 2019). Based on these findings, the authors proposed the existence of an endocytosis-secretion cycle in *Toxoplasma*. Furthermore, fluorescent microscopy and transmission electron microscopy (TEM) provide evidence that extracellular parasites are capable of endocytosing surface proteins (e.g. SAG1) (Gras et al. 2019). This observation indicates that membrane recycling occurs in *Toxoplasma*. Based on these findings, a retrograde membrane flow (fountain flow model) was suggested to be involved in movement generation in *Toxoplasma* (**Figure 1-5**). Bead translocation experiments indicated that the retrograde membrane flow occurs independently from the actomyosin motor complex (Whitelaw et al. 2017; Gras et al. 2019). It was further hypothesized that the membrane flow and the actomyosin motor complex might work together to enable parasite movement (Gras et al. 2019).

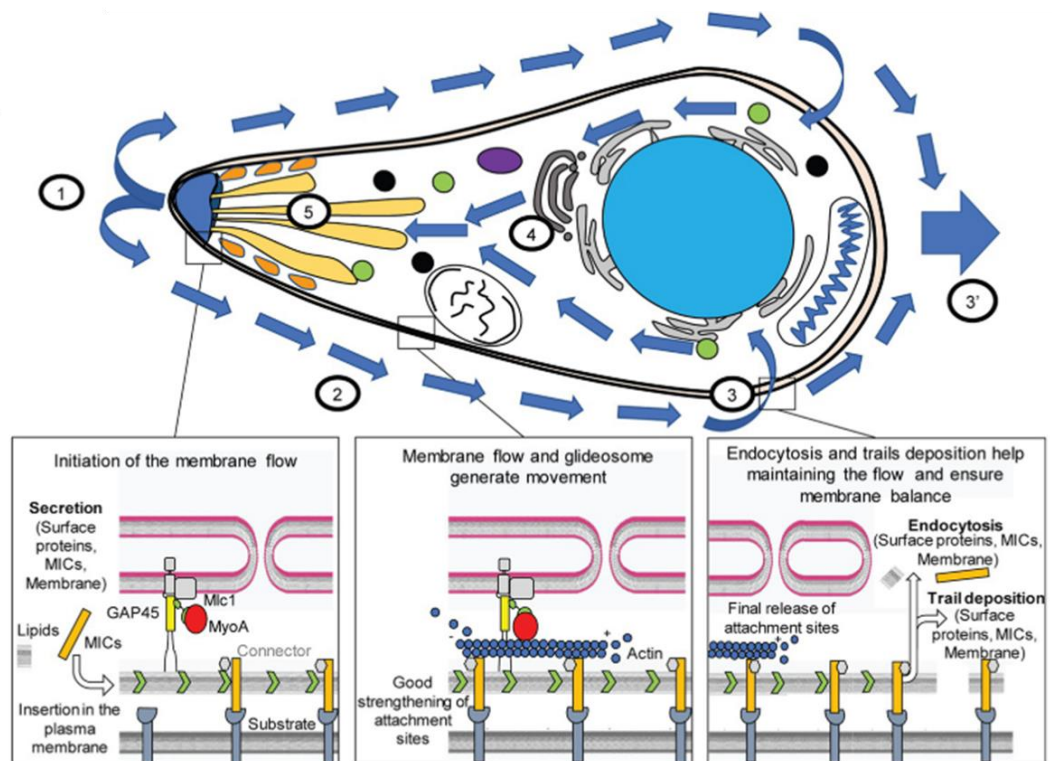


Figure 1-5: Cartoon depicting the involvement of the retrograde membrane flow (fountain-flow model) in *Toxoplasma* motility

The endocytic-secretory cycle (1-5) generates retrograde membrane flow and maintains membrane volume. Several steps occur during the endocytic-secretory cycle: (1) Secretion of secretory organelles, (2) retrograde membrane flow, (3) membrane recycling or (3') trail deposition and (4,5) trafficking of recycled lipids and secretory organelles back to the secretory organelles. Reprinted from PLOS Biology (Gras et al. 2019) under the Creative Commons Attribution 4.0 International License.

1.4.3 Invasion

Successful host cell invasion relies on (1) attachment to the host cell, (2) secretion of microneme content, (3) reorientation so that apical tip of tachyzoite faces the host cell, (4) rhoptry secretion and finally (5) motility-driven propulsion of the parasite into the host cell (Fréchal, Dubremetz, et al. 2017).

It is important to note that the invasion process relies on parasite motility. To exploit the actomyosin system for host cell invasion, the parasite has to be firmly anchored to the host cell membrane. Tachyzoites achieve this by establishing a structure referred to as the moving junction (MJ). In brief, the MJ is formed by exocytosis of the micronemal protein AMA1 to the parasites

surface. In addition, rhoptry proteins including RON2 are secreted and inserted into the host cell surface, acting as a receptor for AMA1. AMA1 is linked to the actomyosin motor, thus allowing force transduction to propel the parasite into the host cell (Besteiro, Dubremetz, and Lebrun 2011; Frénal, Dubremetz, et al. 2017).

In *Toxoplasma*, AMA1 was reported to localise to the micronemes and to be secreted by extracellular tachyzoites, with calcium strongly increasing secretion (Donahue et al. 2000). AMA1 was first linked to invasion by Hehl and co-workers based on the reduction of parasite invasion after treatment with antiserum against AMA1 (Hehl et al. 2000). In addition, this study confirmed that AMA1 localises to the micronemes in intracellular parasites and that AMA1 is secreted by extracellular parasites. Conditional depletion of AMA1 strongly impaired tachyzoite invasion while overall motility appeared unaffected in a 2D gliding assay (Mital et al. 2005). This presented further evidence for AMA1 to be specifically involved in host cell invasion. AMA1 was also suggested to be involved in the rhoptry secretion process (Mital et al. 2005).

The rhoptry proteins RON2, 4, 5 and 8 are present at the MJ (Besteiro et al. 2009). While RON4, 5 and 8 were suggested to be exposed to the host cell cytoplasm (Besteiro et al. 2009), RON2 was proposed to be a transmembrane protein with parts of the protein being present on both sides of the host cell membrane (Lamarque et al. 2011). An interaction between RON2 and AMA1 was suggested by metabolic labelling and immunoprecipitation (Besteiro et al. 2009). This interaction was later supported *in vivo* on the surface of extracellular parasites amongst other binding assays (Lamarque et al. 2011).

Although the MJ junction model is based on numerous publications, the exact mechanism underlying *Toxoplasma* invasion is still controversially debated. For instance, AMA1 was suggested to play a critical role in attachment of the tachyzoite to the host cell surface, but to be dispensable for MJ formation (Giovannini et al. 2011; Bargieri et al. 2013). Strikingly, a clonal AMA1 null mutant was able to survive in culture displaying reduced host cell invasion (Bargieri et al. 2013). Although reduced in numbers, observed invasion events for this strain showed similar kinetics to wild-type parasites. Based on this, AMA1 was proposed to be involved in host cell attachment, but not directly in the

invasion process. Another study offered redundancy in AMA and RON proteins as possible explanation for the residual invasion in AMA1 null mutants (Lamarque et al. 2014). Specifically, AMA2 and AMA4 (together with RON2_{L1}) were suggested to functionally compensate in the absence of AMA1.

All in all, it would appear that many details of the tachyzoite invasion process remain to be elucidated. This becomes apparent with the description of a novel RON protein, RON4_{L1} that appears to be a member of the AMA1/RON2/RON4/RON5/RON8 complex (Guérin et al. 2017). RON4_{L1} faces the host cytoplasm of the MJ. RON4_{L1} is not critical for parasite growth in culture. However, a slightly decreased virulence in mice was observed upon RON4_{L1} depletion.

When invading the host cell, tachyzoites engulf themselves in a parasitophorous vacuole (PV). Once the parasite has fully entered the host, the PV is pinched off via a fission pore (Suss-Toby, Zimmerberg, and Ward 1996). This closes the PV and creates an extra compartment for the parasite to replicate. The PV is established by invagination of the host cell membrane so that most, if not all, of the PV membrane (PVM) is derived from the host (Suss-Toby, Zimmerberg, and Ward 1996). Importantly, host transmembrane proteins are excluded from the PVM at the MJ during invasion, rendering the PV nonfusogenic (Mordue et al. 1999; Clough and Frickel 2017). Thus, the PV avoids the host cell lysosomal system.

The PV creates a closed compartment for the parasite by presenting a physical barrier to the host cell cytoplasm. Nevertheless, the PVM allows for small molecule exchange between the PV and the host cell cytoplasm (Schwab, Beckers, and Joiner 1994; Gold et al. 2015), granting the parasites access to essential nutrients from the host. Noteworthy, the PVM is the structure that is recognized by the host immune system. This makes the PV a place of high host-parasite interaction. While the host employs mechanisms to kill *Toxoplasma*, the parasite combats these efforts to guarantee its own survival (Clough and Frickel 2017).

1.4.4 Asexual replication

Asexual replication of *Toxoplasma* tachyzoites within the PV happens via endodyogeny (Goldman, Carver, and Sulzer 1958; Sheffield and Melton 1968). In this mode of replication, two daughter cells bud within the mother cell, which is destroyed at the end of this process. The budding daughter cells IMCs are formed on the apical side from the maternal nucleus. The daughter cells take up organelles through their open basal end (Goldman, Carver, and Sulzer 1958; Sheffield and Melton 1968; Hu et al. 2002).

An extensive study by Nishi and colleagues provided a detailed timetable for daughter cell formation and organelle distribution (Nishi et al. 2008). When the daughter cells continue to grow, they first receive the divided Golgi and apicoplast. The nucleus, ER and the mitochondrion follow. Micronemes and rhoptries are synthesised *de novo* within the forming daughter cells. In total, this process takes about 6 hours to complete. Hence, every 6 hours, the parasite burden within a host cell doubles. As the daughter cells continue to enlarge, they eventually fill out the entire mother cell. At this point the maternal IMC disappears and the two daughter cells are engulfed by the maternal plasma membrane (Sheffield and Melton 1968). Photobleach and Photoactivation studies revealed that the daughter IMC is initially synthesised *de novo* and later supplemented with recycled maternal IMC (Ouologuem and Roos 2014). Noteworthy, Periz and co-workers recently reported that micronemes, in addition to being synthesised *de novo*, can also be recycled from the mother to the daughter cells (Periz et al. 2019).

The centrosome was identified as platform for daughter cell budding in replicating tachyzoites (Chen and Gubbels 2013). Together with the replication of the Golgi apparatus and the apicoplast, centrosome division is among the first observable steps of endodyogeny in *Toxoplasma* (Hu et al. 2002; Hartmann et al. 2006; Nishi et al. 2008). Two centrosomes become visible near the nucleus before the start of the daughter IMC budding. Centrosome division starts with the re-localisation of the centrosome from the apical site of the nucleus to the basal site of the nucleus. After division, the two centrosomes migrate back to their apical position (Hartmann et al. 2006). More in depth analysis revealed that the centrosome is made up of two cores, the inner and the outer core (Suvorova

et al. 2015). Interestingly, the two cores seem to fulfil independent functions during endodyogeny. The outer core is critical for daughter cell budding, while the inner core is involved in nuclear division. It was reported that cells that lack the outer core components do not show any daughter buds, but are still capable of dividing the nucleus (Suvorova et al. 2015).

Within the PV, tachyzoites grow in a rosette-like organisation with individual parasites being attached to a common residual body with their basal end (Dubey, Lindsay, and Speer 1998; Muniz-Hernández et al. 2011). The residual body was suggested to be involved in establishing the rosette formation (Muniz-Hernández et al. 2011). Work published by Periz and co-workers suggested that vesicular trafficking occurs through the residual body between individual parasites (Periz et al. 2017). This finding was subsequently supported by experimental data from Frénal and co-workers indicating that the residual body connects the cytoplasm of all parasites within a vacuole, allowing for molecule transport between individual parasites (Frénal, Jacot, et al. 2017). The residual body also harbours acidocalcisomes which contain calcium (Attias, Miranda, and De Souza 2019). This observation gave rise to hypothesis that the residual body might be involved in the egress process in which Calcium-signalling is involved as a requirement for microneme secretion (Blader et al. 2015) (see section 1.4.5). Together, these findings indicate that the residual body fulfils specific functions during the asexual life cycle.

1.4.5 Egress

There are several reasons for tachyzoites to initiate egress from their host cell (Blader et al. 2015). For instance, the host cell immune response or damage to the host cell can trigger parasite egress. In the absence of abiotic factors impacting egress, a potential quorum sensing mechanism might initiate egress when a certain tachyzoite density is reached in the host cell (Blader et al. 2015).

As egress from the host cell relies on parasite mobility (gliding), microneme secretion is a critical requirement for this process (Blader et al. 2015). A complex network of multiple factors is believed to be involved in the process of microneme secretion (Bullen, Bisio, and Soldati-Favre 2019). Roughly, the model

suggests that, prior to microneme secretion, the signalling molecule inositol 1,4,5-triphosphate (IP₃) mediates calcium release from the ER. Elevated calcium levels activate calcium-dependent protein kinases (CDPKs), which are critical for microneme secretion. At the same time, the phospholipid Phosphatidic Acid (PA) is integrated into the parasite plasma membrane. PA is recognised by the acylated pleckstrin homology (PH) domain-containing protein (APH). APH is anchored to the microneme and acts as PA sensor, allowing for microneme exocytosis.

The critical role of calcium in *Toxoplasma* egress was first described in 1982 (Endo, Sethi, and Piekarski 1982). CDPK1 is essential for calcium dependent microneme secretion (Lourido et al. 2010). The kinase was shown to play a significant role in gliding motility, invasion and egress. Interestingly, CDPK3 is dispensable for invasion, but required for egress and gliding motility (Lourido, Tang, and Sibley 2012). Noteworthy, microneme secretion appeared only dependent on CDPK3 when calcium was used to initiate secretion. In contrast to this, microneme exocytosis relies on CDPK1 regardless of the applied initiator substance (calcium or ethanol) (Lourido, Tang, and Sibley 2012). These data indicate that *Toxoplasma* utilises distinct signalling pathways for triggering microneme secretion. Another study confirmed the critical role for CDPK3 in calcium-mediated egress, but not invasion (McCoy et al. 2012). Interestingly, this study did not observe any impact of CDPK3 depletion on overall parasite motility. McCoy and colleagues further reported that CDPK3 depletion had no effect on microneme secretion in extracellular parasites (McCoy et al. 2012). This strengthens the view that CDPK3 is exclusively involved in egress of intracellular parasites. A forward screen also identified CDPK3 as important for rapid egress of intracellular parasites (Garrison et al. 2012). Gaji and colleagues reported phosphorylation of *TgMyoA* as function of *TgCDPK3* during parasite egress (Gaji et al. 2015). *TgCDPK3*-dependent phosphorylation of *TgMyoA* appeared important for egress and motility as shown by 2D motility assays exploiting *TgCDPK3* mutants and *TgMyoA* phosphorylation mutants.

APH was recently identified by Bullen and co-workers (Bullen et al. 2016). APH was localised to the micronemes and its depletion impaired parasite egress. Experiments performed by Bullen and colleagues suggested APH binding to PA. It was further reported that APH is highly selective for PA (Darvill et al. 2018).

Darvill and colleagues identified two major PA binding sites within the APH domain. This causes APH to bind to more than one PA molecule.

The involvement of IP₃ in calcium release in *Toxoplasma* was suggested to be based on the negative impact of an IP₃ receptor antagonist on microneme secretion, invasion and attachment (Lovett et al. 2002). Based on these findings the phosphoinositide-specific phospholipase (PLC) was suggested to be involved in IP₃ synthesis. Indirect evidence for PLC involvement had previously been provided by a study showing that a PLC-inhibitor blocks parasite egress (Moudy, Manning, and Beckers 2001). PI-PLC was first characterised in *Toxoplasma* in 2006 (Fang, Marchesini, and Moreno 2006) and later described as critical to the lytic cycle (Bullen et al. 2016).

Calcium release does not only initiate motility for egress, but also the release of the perforin-like protein 1 (PLP1) (Kafsack et al. 2009). PLP1 was reported to be released from micronemes and to mediate pore formation in the PVM. Depletion of PLP1 heavily impaired the parasite ability to escape the PV. The lecithin:cholesterol acyltransferase (LCAT) is also involved in enabling parasite egress (Pszenny et al. 2016). Upon secretion from intracellular parasites, this dense granule enzyme localises to the lumen of the PV. Pszenny and co-workers proposed that the membrane-remodelling properties of LCAT could benefit the egress process by supporting parasite escape from the host cell. LCAT depleted parasites also depicted a slower growth rate and reduced virulence in mice. A follow-up study confirmed the involvement of LCAT in parasite egress, but failed to reproduce its importance for growth in culture and virulence in mice (Schultz and Carruthers 2018).

Overall, calcium-dependent motility plays a critical role in the completion of the lytic life cycle as it is crucial for invasion and egress. Distinct signalling pathways appear to exist in *Toxoplasma* for enabling calcium release in different scenarios.

The final stage of the lytic cycle is the differentiation of tachyzoites into bradyzoites residing in tissue cysts (White, Radke, and Radke 2014). Bradyzoites are very similar to tachyzoites in structure and tissue cysts can persist in a host for life (Dubey, Lindsay, and Speer 1998). It was proposed that bradyzoites are

non-replicative (Radke et al. 2003). However, more recent data suggested active endodyogeny to occur in bradyzoites (Watts et al. 2015).

1.5 Molecular Tools to dissect *Toxoplasma* biology

The haploid nature of the tachyzoite genome allows for genetically modification of genes with relative ease. Since the permanent loss of some genes is detrimental to the parasite, conditional systems are required to explore the function of these essential genes. In *Toxoplasma*, gene function can be conditionally controlled on the genomic level, the transcriptional level and the protein level (Meissner et al. 2007; Jiménez-Ruiz et al. 2014).

Gene transcription can be regulated with the tetracycline inducible transactivator system which was first exploited to describe the function of *MyoA* in *Toxoplasma* (Meissner, Schlüter, and Soldati 2002). In this system the transactivator TATi is constitutively expressed in tachyzoite parasites. The parasites were modified to encode for an additional copy of *myoA* (*myoA-i*) under the control of a so-called Tet-promoter. After the introduction of the extra *myoA-i* copy, the endogenous *myoA* gene was deleted. The Tet-promoter remains active only in the presence of TATi. Gene translation can be suppressed by adding anhydrotetracycline (ATc) which sequesters TATi, thus preventing its binding to the Tet-promoter. Due to the inactivity of the Tet-promoter, the *myoA-i* gene is not translated resulting in a gene knock-down. Further adaptation of the system by Sheiner and colleagues allows for direct replacement of the endogenous promoter of the gene of interest (GOI) with the Tet-promoter (Sheiner et al. 2011). This was achieved by generating a parental TATi- Δ ku80 line that allows for reliable promoter replacement by double homologous recombination. By exploiting the transactivator TRAD4, the transactivator system was also successfully used for studying essential *Plasmodium* genes (Pino et al. 2012).

Protein stability can be regulated by fusing the protein of interest to a destabilisation (ddFKBP) domain. The ddFKBP domain was shown to cause rapid protein degradation in mammalian cells (Banaszynski et al. 2006). The authors were able to prevent ddFKBP-mediated protein degradation by culturing the

cells with Shld-1, the ligand for ddFKBP, in a reversible fashion. This technology was adapted for *Toxoplasma* (Herm-Götz et al. 2007) and *Plasmodium* (Armstrong and Goldberg 2007). Another system that enables conditional protein degradation in *Toxoplasma* is the auxin-inducible degron (AID) system (Brown, Long, and Sibley 2017; Brown, Long, and Sibley 2018). The system was first described in yeast, chicken and mammalian cells (Nishimura et al. 2009). It has also found application in *Plasmodium falciparum* (Kreidenweiss, Hopkins, and Mordmüller 2013) and *Plasmodium berghei* (Philip and Waters 2015). In brief, the protein of interest (POI) is tagged with the AID sequence. Addition of auxin promotes binding of the E3 ubiquitin ligase TIR to AID, resulting in POI degradation. Since the auxin-dependent degradation machinery, including TIR, is derived from plants (Teale, Paponov, and Palme 2006; Leyser 2018), the E3 ubiquitin ligase TIR has to be expressed in the respective organism for the system to function (Kreidenweiss, Hopkins, and Mordmüller 2013; Philip and Waters 2015; K. M. Brown, Long, and Sibley 2017; K. Brown, Long, and Sibley 2018).

Conditional gene depletion (knock-out) via the DiCre system was made available in *Toxoplasma* in 2013 (Andenmatten et al. 2013). In this system, the Cre-recombinase is split into two subunits which are fused to the rapamycin binding domains FKBP and FRB. Both subunits are expressed in the parasite. The GOI is flanked with two loxP sites. Upon rapamycin treatment, these two DiCre domains are brought together and the recombinase resumes activity, excising the DNA sequence between the loxP sites. The use of an YFP reporter gene downstream the loxP site indicates successful excision of the target gene. The DiCre system was originally described in mammalian cells (Jullien et al. 2003) and in mice (Jullien et al. 2007).

1.5.1 The type II CRISPR/Cas9 system

The CRISPR/Cas9 system (CRSIPR: clustered regularly interspaced short palindromic repeats) was recently introduced as a novel tool for genomic editing in various organisms. In this system, an endonuclease is guided by a guide RNA (gRNA) to the genomic DNA sequence complementary to the gRNA. The endonuclease then cleaves the double-stranded DNA (dsDNA) leading to gene

disruption by small insertions or deletions of nucleotides (Doudna and Charpentier 2014; Hartenian and Doench 2015; Jiang and Doudna 2017). The CRISPR-Cas9 system naturally occurs in prokaryotes where it acts as an adaptive immune system that protects the organism from foreign DNA, e.g. bacteriophages (**Figure 1-6**). DNA sequences encoding gRNAs are present in the prokaryotic genome as clustered regularly interspaced short palindromic repeats (CRISPRs) (Doudna and Charpentier 2014; Hartenian and Doench 2015; Jiang and Doudna 2017).

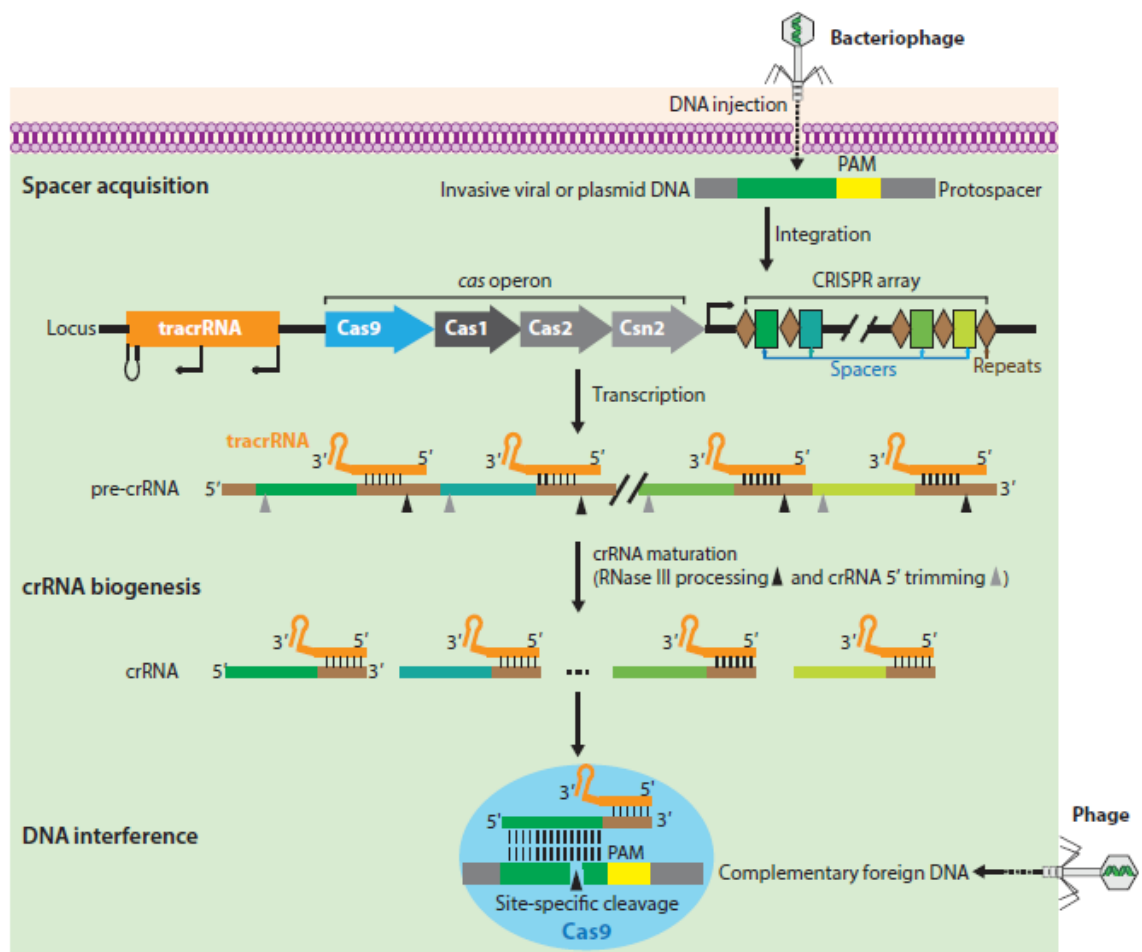


Figure 1-6: The type II CRISPR/Cas9 system in prokaryotes

The CRISPR-Cas9 system acts as an adaptive immune system that protects prokaryotes from foreign DNA, e.g. bacteriophages. The *cas* operon codes for the Cas9 endonuclease as well as additional Cas proteins. The CRISPR array contains the spacer sequences that are acquired from foreign DNA. Activity of the type II CRISPR/Cas9 system relies on the transcription of the CRISPR repeats. The spacers mature into CRISPR RNAs (crRNAs) and hybridise with the trans-activating crRNA (tracrRNA). This RNA hybrid molecule associated with the Cas9 endonuclease. The crRNA then guides the complex to its complementary DNA sequence which will be cut by Cas9. Importantly, a protospacer adjacent motif (PAM) is critical for DNA cleavage to occur. Republished with permission of Annual Reviews (Annual Reviews of Biophysics), from (Jiang and Doudna 2017) © 2017; permission conveyed through Copyright Clearance Center, Inc. License number: 4638781404178.

CRISPRs were first described in *E. coli* in 1987 as repeats of unknown function (Ishino et al. 1987). Subsequently, the term CRISPR was proposed (Jansen et al. 2002). Jansen and co-workers also reported the presence of CRISPR-associated (Cas) genes adjacent to the CRISPR loci. CRISPR systems are characterized based on, amongst other factors, their respective protein-coding Cas genes (Makarova et al. 2011; Makarova, Wolf, and Koonin 2018). They are categorized into two major classes consisting of six different types of CRISPR systems (types I - VI) (Makarova, Wolf, and Koonin 2018).

Activity of the type II CRISPR/Cas9 system relies on the transcription of palindromic repeats which, subsequently, get cut into individual CRISPR RNAs (crRNAs) (**Figure 1-6**). The hybridization of a crRNA with a so-called trans-activating crRNA (tracrRNA) is followed by the association of this RNA hybrid molecule to the Cas9 endonuclease. The crRNA then guides the complex to its complementary DNA sequence which will be cut by Cas9 (Doudna and Charpentier 2014; Hartenian and Doench 2015; Jiang and Doudna 2017).

Although the CRISPR system type II encodes for additional proteins, the Cas9 endonuclease was reported to be the only enzyme necessary for DNA cleavage (Sapranauskas et al. 2011). Two independent studies showed that Cas9 is an RNA-guided endonuclease (Gasiunas et al. 2012; Jinek et al. 2012). The RNA confers site-specific DNA cleavage as only DNA sequences complementary to the guide RNA are cleaved (Gasiunas et al. 2012; Jinek et al. 2012). Moreover, Jinek and co-workers succeeded in fusing the crRNA and tracrRNA to one chimeric RNA molecule (Jinek et al. 2012). This chimeric DNA together with Cas9 proved to be programmable for cleaving specific DNA sequences such as *gfp* (Jinek et al. 2012). The Cas9 enzyme possesses two nuclease domains, HCH and RuvC-like (Sapranauskas et al. 2011; Gasiunas et al. 2012; Jinek et al. 2012). Each of the two nuclease domains cleaves one of the two opposite DNA strands (**Figure 1-7**) (Gasiunas et al. 2012; Jinek et al. 2012).

Of relevance, the *Streptococcus pyogenes* type II Cas9 system requires a protospacer adjacent motif (PAM) for DNA cleavage to occur (Jinek et al. 2012). This PAM sequence is proximal to the target DNA sequence and its sequence is

NGG (Jinek et al. 2012). It was reported that Cas9 cleaves DNA three nucleotides upstream of the PAM sequence (Gasiunas et al. 2012; Jinek et al. 2012).

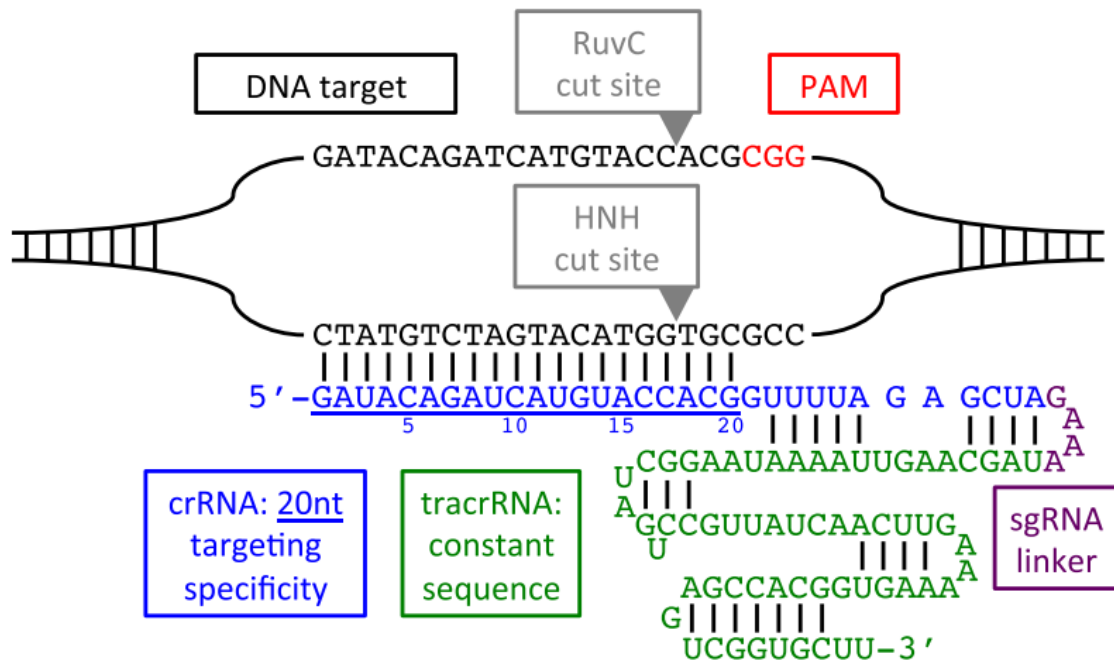


Figure 1-7: Schematic of the sgRNA-mediated gene specificity of the type II CRISPR/Cas9 system

Fusing of the crRNA and tracrRNA to one single guide RNA (sgRNA) via a linker sequence enables Cas9-mediated gene targeting. Each of the two Cas9 endonuclease domains, HCH and RuvC, cleaves one of the two opposite DNA strands. The protospacer adjacent motif (PAM) sequence is proximal to the target DNA sequence and, for the type II CRISPR/Cas9 system, its sequence is NGG. Cas9-mediated DNA cleavage occurs three nucleotides upstream of the PAM sequence. Reprinted by permission from John Wiley & Sons, Inc.: John Wiley and Sons, FEBS Journal (Hartenian and Doench 2015) ©2015. License number: 4638770871847.

Taken together, the type II CRISPR/Cas9 system presents a convenient application for gene modifications in other organisms. Only one recombinant enzyme together with one chimeric gRNA should be sufficient for gene disruption. Indeed, the type II CRISPR/Cas9 system was successfully applied for genome editing purposes in various organisms, including human cells (Jinek et al. 2013; Mali et al. 2013), woody plants (Fan et al. 2015), beetles (Gilles, Schinko, and Averof 2015) and rabbits (Yan et al. 2014). Furthermore, the CRISPR/Cas9 technology enables genome wide screens in mammalian cells (Shalem et al. 2014; Wang et al. 2014; Jiang et al. 2019; Korkmaz et al. 2019). In *Toxoplasma*, the CRISPR/Cas9 was shown to be effective for single target gene disruption and site-specific insertions (Shen et al. 2014; Sidik et al. 2014). In

2016, a genome-wide CRISPR/Cas9 screen identified novel fitness-conferring genes in *Toxoplasma* (Sidik et al. 2016; Sidik, Huet, and Lourido 2018).

Various efforts have been made to exploit the CRISPR/Cas9 as conditional system (Zhou and Deiters 2016). For instance, different approaches exploiting the split-Cas9 concept have been reported in mammalian cells (Nihongaki et al. 2015; Truong et al. 2015; Wright et al. 2015; Zetsche, Volz, and Zhang 2015; Schmelas and Grimm 2018). For this concept, the Cas9 enzyme is split into its N- and C-terminus which allows for different ways of promoting sub-unit reunion. In two independent studies, the sub-units were linked to fusion proteins which can be induced to promote reunion of the N- and C-terminus, resulting in Cas9 activity. Nihongaki and co-workers exploited photo-inducible dimerization domains that promote Cas9 activity in response to blue light (Nihongaki et al. 2015). Zetsche and colleagues used the rapamycin-binding domains FRB and FKBP12 to enable conditional Cas9 activity (Zetsche, Volz, and Zhang 2015). In *Toxoplasma*, a conditional nuclear Cas9 fused to ddFKBP was described and applied to identify factors involved in the nuclear export of RNA (Serpeloni et al. 2016).

1.6 Actin in eukaryotes

1.6.1 Structure of actin monomers and filaments

The structural protein actin is highly abundant and conserved in eukaryotic cells (Baum et al. 2006; Pollard and Cooper 2009; Pollard 2016). Actin fulfils various critical functions within eukaryotic cells including cytokinesis, cargo trafficking and cellular motility (Pollard and Cooper 2009). In a eukaryotic cell, actin occurs in two different states, the globular (G-actin) and filamentous (F-actin) form (Baum et al. 2006; Pollard and Cooper 2009; Dominguez and Holmes 2011).

The atomic structure of monomeric G-actin was first described in 1990, revealing that the G-actin protein consists of 4 subdomains (Kabsch et al. 1990). G-actin binds ATP or ADP in the cleft between the subdomains 2 and 4 (Kabsch et al. 1990; Otterbein, Graceffa, and Dominguez 2001). It was reported that G-actin-ATP and G-actin-ADP show conformational differences in subdomain 2 (Otterbein, Graceffa, and Dominguez 2001; Graceffa and Dominguez 2003).

G-actin monomers can polymerise to form F-actin. Electron microscopy in 1963 proposed that F-actin consists of two actin strands that intertwine to form a right-handed helical filament (Hanson and Lowy 1963). More recently, the F-actin structure was described by cryo-electron microscopy (Fujii et al. 2010). Based on these data, it was suggested that the F-actin structure actually represents a single left-handed helix (Dominguez and Holmes 2011). Dominguez and Holmes argued that, since the twist per actin molecule is -166° (close to -180°), the F-actin filament structure only appears like two strands that slowly turn in a right-handed fashion. Hence, the F-actin structure can either be described as a two-start right-handed helix or a single-start left-handed helix.

One critical factor for the transition between G-actin and F-actin (actin treadmilling) is the hydrolysis of ATP (**Figure 1-8**) (Korn, Carlier, and Pantaloni 1987; Baum et al. 2006). The actin treadmilling cycle starts with the addition of G-actin-ATP to “barbed” (plus) end of the F-actin filament. During this polymerisation step, ATP is hydrolysed to ADP and inorganic phosphate (P_i). Hydrolysis of ATP results in stable F-actin filaments with bound $ADP+P_i$ (F-actin- $ADP-P_i$). Slow release of P_i results in F-actin-ADP and destabilises the filament, resulting in the release of G-actin-ADP from the F-actin filament. In a growing F-actin strand, F-actin-ADP accumulates at the “pointed” (minus) end where the depolymerisation of G-actin-ADP occurs. Subsequently, ADP can be replaced with ATP, generating a new G-actin-ATP molecule. It was suggested that the addition of a new G-actin-ATP molecule to the F-actin barbed end causes a conformational change in the adjacent actin molecule (Murakami et al. 2010). Murakami and co-workers proposed this structural change to initiate ATP hydrolysis.

Of relevance, the amount of monomeric G-actin has to be above a certain threshold for polymerisation to occur. This threshold is referred to as the critical concentration. All G-actin monomers above this concentration are available for polymerisation (Pollard and Borisy 2003). Importantly, the critical concentration for polymerisation to happen at the barbed end is lower than the concentration needed to allow for polymerisation at the pointed end (Pollard and Borisy 2003; Pollard 2016). It should also be mentioned that the critical concentration needed for G-actin-ATP to polymerise was reported to be lower than the concentration required for G-actin-ADP (Cooke 1975; Pollard 1984). This means that actin

polymerisation is more likely to happen at the barbed end of an F-actin strand by attaching G-actin-ATP monomers.

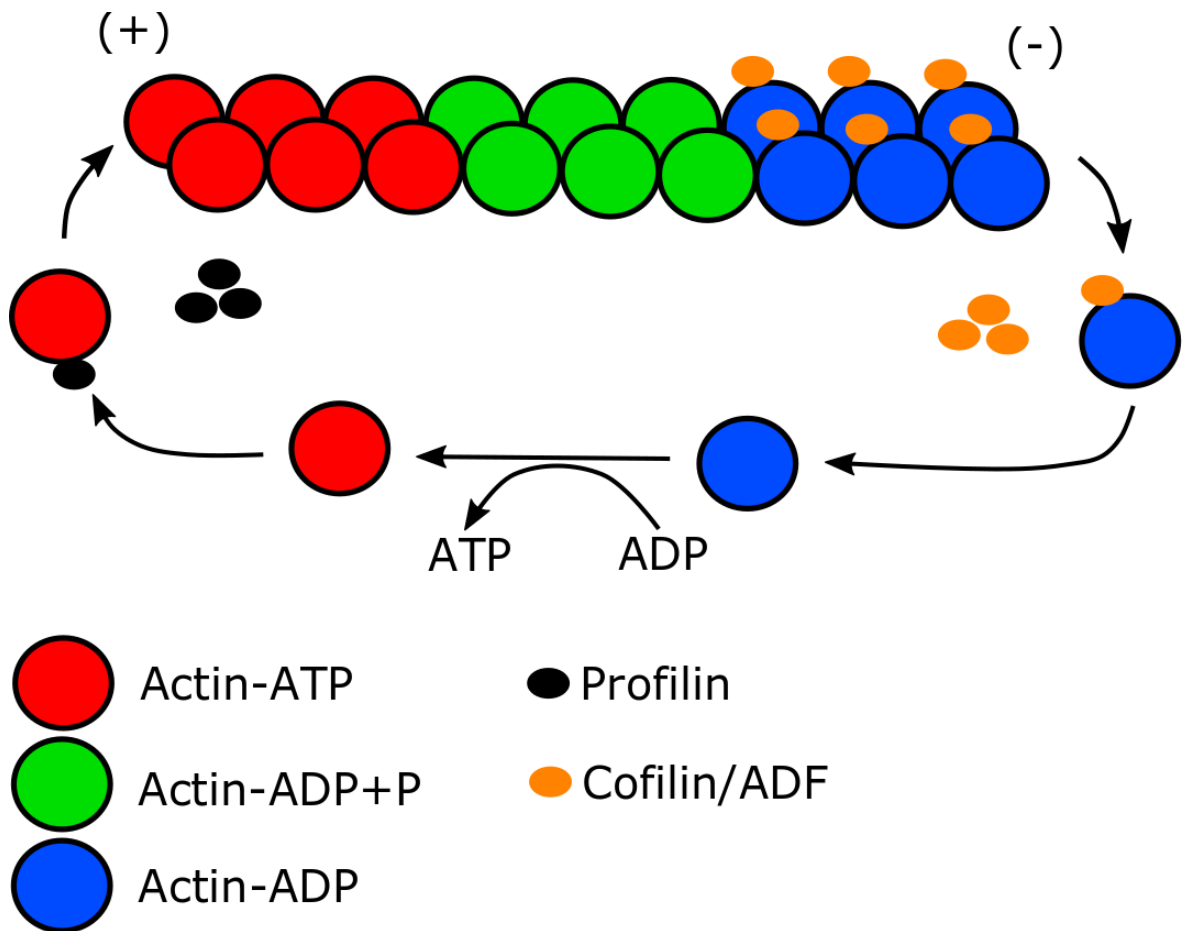


Figure 1-8: Actin treadmilling in eukaryotes

F-actin filaments are dynamic structures that can undergo growth and shrinkage by addition or disassociation of actin monomers, respectively. The actin treadmilling cycle starts with the addition of G-actin-ATP to “barbed” (+) end of the F-actin filament. During this polymerisation step, ATP is hydrolysed to ADP and inorganic phosphate (P_i). Hydrolysis of ATP results in stable F-actin filaments with bound ADP+ P_i (Actin-ADP- P_i). Slow release of P_i results in Actin-ADP and destabilises the filament, resulting in the release of Actin-ADP from the F-actin filament. In a growing F-actin strand, Actin-ADP accumulates at the “pointed” (-) end where the depolymerisation occurs. Subsequently, ADP can be replaced with ATP, generating a new Actin-ATP molecule. ADF/cofilin destabilizes F-actin filaments, thus increasing the amount of available G-actin monomers. ADF/cofilin binds to F-actin filaments and causes F-actin depolymerisation. While depolymerisation happens at the (-) end during the treadmilling process, F-actin filament elongation occurs at the (+) end. Profilin binds to Actin-ATP promoting actin polymerisation. Profilin also binds Actin-ADP increasing the exchange rate of actin-bound ADP for ATP (not depicted). Abbreviations: ATP - adenosine triphosphate; ADP - adenosine diphosphate; P - monophosphate. This figure was inspired by (Baum et al. 2006).

The first step of *de novo* F-actin filament formation is called actin nucleation. Actin nucleation refers to the formation of a new F-actin filament by the assembly of G-actin monomers (Pollard, Blanchoin, and Mullins 2000). Inevitably,

this process requires the formation of actin dimers and trimers, a process that is kinetically unfavourable (Sept and McCammon 2001; Deeks and Hussey 2005; Pollard 2016). From this point onwards however, G-actin monomer assembly to the actin trimer was proposed to occur with the same rate as G-actin polymerisation on existing F-actin filaments (Sept and McCammon 2001). It is therefore believed that the assembly of this trimer nucleus presents the critical step that has to be overcome for *de novo* F-actin formation (Sept and McCammon 2001; Deeks and Hussey 2005).

To efficiently control many of the kinetically unfavourable steps of actin dynamics, eukaryotic cells exploit a vast number of actin binding proteins (ABPs) (Pollard 2016). For instance, these ABPs are involved in facilitating the transition between G-actin and F-actin (actin treadmilling) and *de novo* filament synthesis. Some of the eukaryotic key players involved in this process shall be briefly described in the following section.

1.6.2 Function of Actin binding proteins (ABPs)

1.6.2.1 Actin treadmilling

Several ABPs are involved in the actin treadmilling process, including the factors adf/cofilin and profilin (**Figure 1-8**). Proteins belonging to the ADF/cofilin family destabilize F-actin filaments, thus increasing the amount of available G-actin monomers (Moon and Drubin 1995). Initially, *in vitro* studies reported that cofilin binds to F-actin filaments (Nishida, Maekawa, and Sakai 1984) and causes F-actin depolymerisation (Yonezawa, Nishida, and Sakai 1985). The role of cofilin in F-actin turnover and depolymerisation was confirmed *in vivo* in yeast (Lappalainen and Drubin 1997). Cofilin mutants depicted increased numbers of actin patches within the cell indicating a role for cofilin in actin depolymerisation and turnover. In a comparative study, ADF was later shown to depolymerise F-actin filaments more potently than cofilin (Yeoh et al. 2002). Both proteins bind to F-actin with similar affinity and sever F-actin filaments with comparable potency. Cofilin and ADF have higher affinity to G-Actin-ADP than to G-Actin-ATP. Furthermore, ADF has a higher affinity to F-actin-ADP than

F-actin-ATP or F-actin-ADP-P_i and increases the depolymerisation rate from the pointed end (Carlier et al. 1997).

Based on these results, a treadmilling model was proposed by Yeoh and co-workers in which ADF/cofilin bind to F-actin-ADP causing filament fragmentation at the pointed end (Yeoh et al. 2002). Disassembly of F-actin at the pointed end is followed by nucleotide exchange (G-actin-ADP to G-actin-ATP) and new filament formation. Recently, it was suggested that ADF/cofilin-mediated filament depolymerisation might also occur at the barbed end (Wioland et al. 2017). Maintaining actin treadmilling by F-actin severing and depolymerisation has physiological importance as cofilin is critical for proper embryonic development in mice (Gurniak, Perlas, and Witke 2005). Furthermore lack of ADF function causes corneal defects in mice (Ikeda et al. 2003; Bellenchi et al. 2007). Co-depletion of cofilin and ADF in mammalian cells leads to stress fiber accumulation affecting nuclear integrity (Kanellos et al. 2015).

While depolymerisation happens at the pointed end during the treadmilling process, F-actin filament elongation occurs at the barbed end. One of the proteins involved in mediating filament assembly is the polymerisation factor profilin which binds monomeric G-actin (Baum et al. 2006; Pollard 2016). A role for profilin in actin treadmilling was first suggested in 1977 (Carlsson et al. 1977), while its ability to promote actin polymerisation was proposed in 1993 (Pantaloni and Carlier 1993). It was further shown that profilin binds to G-actin-ATP and G-actin-ADP with similar affinity while drastically increasing the exchange rate of actin-bound ADP for ATP (Selden et al. 1999). Based on these findings, Selden and co-workers suggested that rapid profilin-mediated regeneration of the G-actin-ATP pool depicts a key step in actin treadmilling. This is because the maintenance of the G-actin-pool at a level above the critical concentration is necessary for continued actin assembly.

For F-actin elongation at the barbed end, profilin acts together with a protein called formin (see below). Together, profilin and formin can achieve a dramatic increase of F-actin elongation rates compared to the rates shown by actin alone or actin with only formin (Romero et al. 2004; Kovar et al. 2006). Another factor impacting F-actin filament dynamics are so-called capping proteins. These

proteins are able to bind to free barbed ends and prevent addition or removal of actin monomers (Edwards et al. 2014; Pollard 2016).

1.6.2.2 Actin nucleation

Since actin nucleation is kinetically unfavourable, eukaryotic cells exploit so-called nucleation factors to overcome the initial steps of *de novo* filament formation. Three different types of actin nucleators have been described: the Arp2/3 complex, the formin protein family and spire (**Figure 1-9**) (Goode and Eck 2007).

First described in 1994, the Arp2/3 complex consists of seven sub-units including the actin related proteins Arp2 and Arp3 (Machesky et al. 1994). The complex was shown to associate with the sides of F-actin filaments (Mullins, Stafford, and Pollard 1997) and to promote actin polymerisation (Welch, Iwamatsu, and Mitchison 1997). In brief, further research revealed that Arp2/3 causes the branching of novel daughter actin filaments from already existing mother filaments at an angle of 70° (Mullins, Heuser, and Pollard 1998). It was further proposed that the two actin related proteins of the complex (Arp2 and 3) act as the first subunits of the newly forming daughter filament (Volkman et al. 2001; Rouiller et al. 2008). As a consequence, the arp2/3 complex is associated with the pointed end of F-actin filaments.

Due to the localisation of some of its components to the lamellipodia in stationary and motile cells, the Arp2/3 complex was suggested to be involved in lamellipodia protrusion (Welch et al. 1997). The function of Arp2/3-mediated actin network assembly in cell migration was confirmed in fibroblasts lacking a functional Arp2/3 complex (Suraneni et al. 2012). These cells were incapable of forming lamellipodia and showed a defect in performing directional migration.

Another type of actin nucleator, Spire, was identified in the fly *Drosophila* in 2005 (Quinlan et al. 2005). Quinlan and colleagues showed that spire is able to promote actin assembly *in vitro*. Spire possesses four WASP homology 2 (WH2) domains and all four domains are required for maximum nucleation potential (Quinlan et al. 2005). It was proposed that spire attracts four G-actin monomers (one to each WH2 domain) to create a nucleation complex (Quinlan et al. 2005).

Interestingly, it was suggested that spire and formins can interact with each other in a regulatory fashion during actin nucleation (Quinlan et al. 2007). A model was proposed in which spire recruits formin to the barbed end of F-actin causing fast formin-mediated filament growth (Montaville et al. 2014).

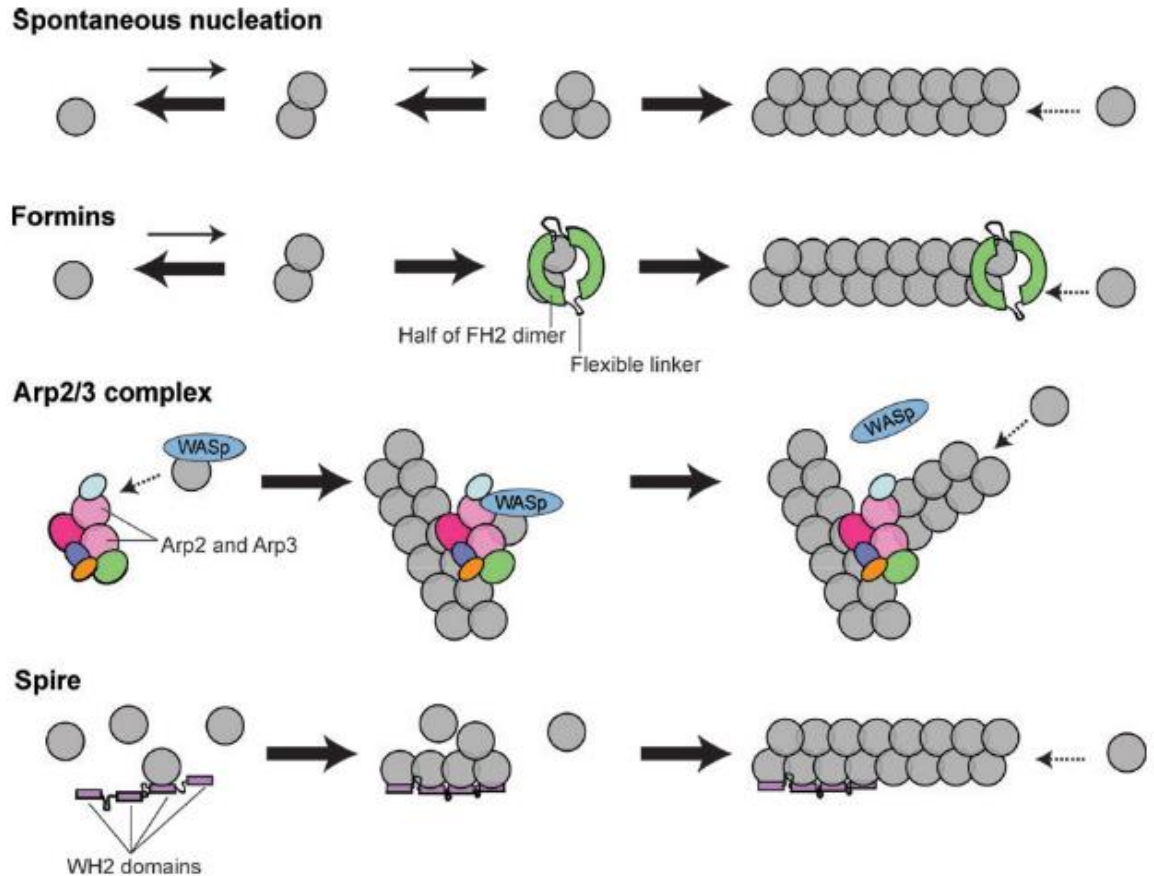


Figure 1-9: The three types of actin nucleation factors in eukaryotes

Since spontaneous actin nucleation is highly unfavourable, eukaryotic cells exploit nucleation factors to overcome the initial steps of *de novo* filament formation. The three different types of actin nucleators are the Arp2/3 complex, formins and spire. Formins form a dimer and stabilise actin dimers to initiate F-actin assembly. The formin dimer stays associated with the barbed end of the growing actin filament while promoting addition of G-actin. This mode of action is referred to as “processive capping”. A flexible linker between the two formin proteins enables repositioning of the dimer which is necessary when additional actin monomers are added to the barbed end. The Arp2/3 complex (together with WASp) mediates *de novo* filament polymerisation on already existing filaments at an angle of 70° . Spire possesses four WH2 domains and all four domains are required for maximum nucleation potential. Spire attracts four G-actin monomers (one to each WH2 domain) to create a nucleation complex. Dotted line arrows indicate the barbed end of the respective actin filament. Republished with permission of Annual Reviews (Annual Reviews of Biochemistry), from (Goode and Eck 2007) © 2007; permission conveyed through Copyright Clearance Center, Inc. License number: 4638780103258.

The actin nucleation mechanism of formins is of high importance for this thesis. Therefore, formin biology shall here be described in more detail. The first gene was introduced as a formin in 1990 (Woychik et al. 1990). Since then, many members of the formin family have been described in various organisms (Evangelista, Zigmond, and Boone 2003; Goode and Eck 2007). Members of the formin family were reported to nucleate actin and to mediate “processive capping” of F-actin filaments (Goode and Eck 2007; Courtemanche 2018). Formins share two domains, the formin homology domain 1 and 2 (FH1 and FH2) (Castrillon and Wasserman 1994; Wasserman 1998). The FH1 domain was reported to interact with profilin (Evangelista et al. 1997; Imamura et al. 1997), while the FH2 domain appeared critical for formin-mediated actin assembly (Sagot et al. 2002; Pruyne et al. 2002).

It was shown that formin is required for the assembly of F-actin cables in yeast (Feierbach and Chang 2001; Evangelista et al. 2002; Sagot, Klee, and Pellman 2002). This formin-mediated F-actin assembly requires profilin *in vivo* (Evangelista et al. 2002). *In vitro* experiments with a minimal form of the yeast formin Bni1 suggested that actin assembly can happen without profilin, but is enhanced in the presence of profilin (Sagot et al. 2002). Pring and colleagues proposed that Bni1 promotes actin nucleation by stabilising an actin dimer to allow for further actin assembly (Pring et al. 2003).

Based on *in vitro* data, Sagot and co-workers proposed that yeast formin Bni1 promotes formation of unbranched actin filaments, while Arp2/3 promotes the formation of branched actin filaments (Sagot et al. 2002). Interestingly, a minimal version of yeast Bni1 (Bni1pFH1FH2) localised to the barbed end of unbranched filaments *in vitro* as determined by electron microscopy (Pruyne et al. 2002). Association of the Bni1FH2 domain with the barbed end was further supported by its ability to promote actin filament assembly in the presence of capping proteins (Zigmond et al. 2003; Moseley et al. 2004). Barbed end protection from capping proteins was also reported for the FH1FH2 core of the mouse formin FRL α , indicating that barbed-end localisation is a universal formin trait (Harris, Li, and Higgs 2004).

The barbed end localisation of formins, together with their proposed (FH2-dependent) dimerization (Harris, Li, and Higgs 2004; Moseley et al. 2004; Xu et

al. 2004), gave rise to the “processive capping” model for formin-dependent actin nucleation and filament elongation. In this model, the formin dimer associates with the barbed end while promoting addition of G-actin to the growing F-actin strand. During filament elongation, formin repositions to maintain persistent association with the growing barbed end (Goode and Eck 2007; Courtemanche 2018). It is important to note that the exact structural mechanism of formin-mediated processive filament elongation at the growing barbed end is still under investigation (Paul and Pollard 2009; Thompson et al. 2013; Courtemanche 2018).

The model is supported by structural analyses of the formin dimer. The formin dimer was described as a stable, but flexible structure (Xu et al. 2004). Xu and colleagues proposed that a flexible link between the two formin proteins allows for repositioning of the dimer upon actin addition to the barbed end. Another study provided the crystal structure of the complex between the yeast BnipFH2 domain with actin (Otomo et al. 2005). The study suggests that the formin dimer can switch between two states, either promoting actin monomer addition to or promoting actin disassociation from the F-actin filament. Structural analysis by Otomo and co-workers also supports the model of formin enabling actin nucleation by stabilising an actin dimer that acts as nucleus for further actin assembly. More recently, continuous association of the mouse formin mDia1 to the growing actin filament was made visible by single-molecule fluorescence microscopy in real time (Breitsprecher et al. 2012). The same technology was later used to confirm the existence of a processive formin (AtFH14) in the plant *Arabidopsis* (Zhang et al. 2016).

Several cellular functions have been proposed for formins in various organisms (Evangelista, Zigmond, and Boone 2003). For example, it was shown that formins are required for the formation of the cytokinetic actin ring and the completion of cytokinesis in yeast (Tolliday, VerPlank, and Li 2002). In addition, plants lacking the formin AtFH5 were compromised in cytokinesis in the seed endosperm (Ingouff et al. 2005). In mice, the formin family member Fhod3 is critical for heart development in embryos (Kan-o et al. 2012) and postnatal juveniles (Ushijima et al. 2018).

1.7 Actin in *Toxoplasma*

Toxoplasma encodes actin on a single copy gene, *Tgactin1* (*Tgact1*) (Dobrowolski, Niesman, and Sibley 1997). The *TgACT1* protein shares 93% sequence similarity with *Plasmodium falciparum* actin, but only about 80% with other eukaryotic actins (Dobrowolski, Niesman, and Sibley 1997; Baum et al. 2006). Initial studies assessing the physical state of actin in *Toxoplasma* used cell fractionation by centrifugation for separating F-actin from G-actin (Dobrowolski, Niesman, and Sibley 1997). This experimental set up failed to detect actin in the pellet fraction where F-actin is expected to accumulate. Dobrowolski and colleagues therefore suggested that actin is mainly present in its monomeric G-actin state in *Toxoplasma*.

In a comparative approach with recombinant actin *in vitro*, *Toxoplasma* actin formed shorter (ca. 0.1 μ m) and more unstable filaments than rabbit actin (ca. 2 μ m) (Sahoo et al. 2006). It was proposed that amino acid residues on the *Toxoplasma* actin monomer surface differ from conventional actin and that these differences contribute to filament instability (Sahoo et al. 2006; Skillman et al. 2011). *In vitro*, the critical concentration required for *Toxoplasma* actin to polymerise was proposed to be lower than for conventional actins, resulting in the understanding that *TgACT1* filaments possess a rapid assembly and turnover rate (Sahoo et al. 2006). Since stabilisation of *TgACT1* affected parasite gliding, the general instability of *TgACT1* filaments was suggested to be an adaptation that enables parasite motility (Skillman et al. 2011).

The concept of rapid apicomplexan F-actin turnover was supported by findings in the related apicomplexan parasite *Plasmodium falciparum* (Schmitz et al. 2005). *Plasmodium* actin1 (*PfACT1*) also formed shorter filaments (ca 0.1 μ m) when compared to rabbit actin (ca 3.5 μ m) *in vitro*. Another study reported inefficient filament assembly by recombinant *PfACT1* *in vitro* (Schüler, Mueller, and Matuschewski 2005). More recently, pyrene fluorescence assays suggested kinetics for *PfACT1* similar to canonical actin (Kumpula et al. 2017). Of relevance, the depolymerisation rate for *PfACT1* appeared faster than for canonical actins. Structural differences to canonical actins were proposed to cause the instability and, consequently, the short nature of *Plasmodium* F-actin (Vahokoski et al. 2014). Electron cryo-microscopy revealed differences in the

contact sites between *Pf*ACT1 molecules as reason for the filament instability (Pospich et al. 2017). Based on crystallography studies for *Pf*ACT1, it was reported that the conformation of the Arg178/Asp180-containing A-loop plays a key role in *Plasmodium* filament destabilisation (Kumpula et al. 2019). Within the *Pf*ACT1 molecule, for instance, the A-loop interacts with the *Plasmodium*-specific residue Lys(K)270, enabling a conformational stage that promotes actin filament fragmentation (Kumpula et al. 2019). When *Pf*ACT1 was mutated to a K270M variant, reflecting canonical actin and blocking interaction with the A-loop, longer actin filaments were formed *in vitro* (Kumpula et al. 2019). Noteworthy, *Toxoplasma* actin1-K270M mutants were found to increase polymerisation in comparison to wild-type *Tg*ACT1 (Skillman et al. 2011).

Actin sedimentation assays later questioned the existence of a critical concentration for actin polymerisation in *Toxoplasma* (Skillman et al. 2013). This was because the concentration of monomeric actin in the supernatant fraction continuously increased when more actin was used for polymerisation assay prior to centrifugation. In the case of actin polymerisation that depends on critical concentration, the concentration of monomeric actin in the supernatant should reach a plateau (representing the critical concentration) since all monomeric actin molecules above this threshold are assembled into actin filaments (Pollard and Borisy 2003). This was the case for yeast actin as shown by Skillman et al. (Skillman et al. 2013). Based on the results from the sedimentation assays, Skillman and co-worker proposed that an isodesmic model would be best suited to explain the observed *Tg*ACT1 kinetics (Skillman et al. 2013). According to this model, actin assembly and disassembly occur at the same rate. Thus, the kinetically unfavourable actin nucleation prior to filament elongation would not present a rate limiting step. It was argued by Skillman and colleagues that F-actin formation could therefore happen independently from nucleation-promoting factors. In addition, the model was applied to explain the previously reported presence of short and unstable actin filaments in *Toxoplasma* (Sahoo et al. 2006).

Actin sedimentation assays based on ultracentrifugation were later proposed to be unreliable for the determination of the critical concentration of apicomplexan actin (Kumpula et al. 2017). This is because the short length of apicomplexan actin filaments prevents their sedimentation. A method exploiting

pyrene-labelled actin was applied to measure the critical concentration for *Pf*ACT1 (ca. 0.1 μ M) *in vitro* (Kumpula et al. 2017). Kumpula and colleagues argued that *Pf*ACT1 shows similar kinetics to canonical actins with F-actin formation depending on nucleation. Crystallography studies recently suggested that unique structural features in the *Pf*ACT1 molecule promote filament destabilisation and, eventually, fragmentation (Kumpula et al. 2019).

It should be mentioned that a previous study by Olshina et al. suggested that *Pf*ACT1 might not be correctly folded by heterologous expression systems *in vitro* (Olshina et al. 2016). However, since the authors used *in vitro* cell free expression systems that differ from systems applied in other literature for *Pf*ACT1 expression (Schmitz et al. 2005; Schüler, Mueller, and Matuschewski 2005; Ignatev et al. 2012; Vahokoski et al. 2014; Kumpula et al. 2017, 2019), this general conclusion might have to be considered with caution.

As part of the actomyosin motor complex (Fréna, Dubremetz, et al. 2017), *Tg*ACT1 is highly important for all processes that require parasite motility. For instance, *Tg*ACT1 was reported to be essential for parasite egress from the host cell (Egarter et al. 2014; Whitelaw et al. 2017). *Tg*ACT1 was further reported to be important, but not essential, for parasite gliding (Egarter et al. 2014; Whitelaw et al. 2017). Although most parasites lost their ability to glide after *Tg*ACT1 depletion, a small number of tachyzoites remained able to glide at speeds similar to control parasites (Whitelaw et al. 2017). In addition, depletion of *Tg*ACT1 causes apicoplast loss in parasites (Andenmatten et al. 2013; Whitelaw et al. 2017). Also, dense granule trafficking appears to rely on actin and myosins (Heaslip, Nelson, and Warshaw 2016; Whitelaw et al. 2017).

Involvement of *Tg*ACT1 in host cell invasion (and motility) was first suggested in 1996 (Dobrowolski and Sibley 1996). Although Cre-Lox-mediated conditional depletion of *Tg*ACT1 rendered most parasites incapable of host cell invasion, some parasites (ca. 10-25%) were still able to invade (Egarter et al. 2014; Whitelaw et al. 2017). It was further reported that conditional *Tg*ACT1-depleted parasites were unable to establish strong attachment to surfaces (Whitelaw et al. 2017). Based on these findings, Whitelaw and co-workers suggested a role for the actomyosin complex in surface attachment, rather than force generation during the invasion process.

The suggestion that actual host cell penetration can occur in the absence of *TgACT1* sparked controversy. Another study suggested that host cell invasion by *TgACT1*-depleted parasites is facilitated by residual actin after Cre-Lox gene excision (Drewry and Sibley 2015). In the context of this debate, potential cross-reactivity of the exploited antibodies against *TgACT1* were discussed (Drewry and Sibley 2015; Whitelaw et al. 2017).

Overall, *TgACT1* is essential for parasite survival since no clonal *Tgact1* knock-out line could be generated so far (Andenmatten et al. 2013; Egarter et al. 2014). Interestingly, the intracellular replication rate in culture appears to be largely unaffected by *TgACT1* depletion (Egarter et al. 2014; Periz et al. 2017). Noteworthy, however, depletion of *TgACT1* causes asynchronous replication in *Toxoplasma* (Periz et al. 2017). In addition, parasites lack the typical rosette formation within the PV (Periz et al. 2017). Actin was also reported to be involved in residual body formation (Periz et al. 2017).

The recent visualisation of *Toxoplasma* actin via actin-chromobodies allowed for a more detailed investigation of actin function in intracellular parasites (Periz et al. 2017). Periz and colleagues reported that individual parasites are connected by a filamentous actin network. This network appeared to contribute to vesicular trafficking between individual parasites within the PV and IMC recycling (Periz et al. 2017). Disassembly and reassembly of these intravacuolar filaments occur during parasite replication (Periz et al. 2017). A follow-up study by Periz et al. proposed that F-actin facilitates recycling of maternal micronemes during daughter cell budding (Periz et al. 2019). Further exploitation of the chromobody technology suggested a novel function for actin in the host cell invasion process (Del Rosario et al. 2019). According to Del Rosario and colleagues, the parasite nucleus presents a major obstacle for efficient host cell entry. To allow for efficient nuclear entry, actin is thought to stabilise the junction and to push the parasite nucleus into the host cell (Del Rosario et al. 2019).

1.7.1 Actin binding proteins (ABPs) in *Toxoplasma*

Apicomplexan parasites, including *Toxoplasma* and *Plasmodium* species, possess a limited set of ABPs (Baum et al. 2006) (Table 1-1). For example, *Toxoplasma* encodes a single gene each for ADF and profilin, while three genes encode formins. As perspective, humans possess 5 *profilin* genes, 14 *adf/cofilin* genes and 16 *formin* genes (Baum et al. 2006). Strikingly, the nucleation factors spire (Baum et al. 2006) and Arp2/3 (Gordon and Sibley 2005) are missing in *Toxoplasma*, making formins the only known actin nucleator.

Table 1-1: Depiction of selected actin binding proteins (ABPs) found in apicomplexan and eukaryotic genomes

Please note that this table is not a complete list of ABPs present in the depicted genomes. Data presented in this table was reproduced from (Baum et al. 2006). Abbreviations: *Pf* – *Plasmodium falciparum*, *Tg* - *Toxoplasma gondii*, *At* - *Arabidopsis thaliana*, *Dm* - *Drosophila melanogaster*, *Hs* - *Homo sapiens*.

Functional class	Protein domain	Number of proteins detected in the genome				
		<i>Pf</i>	<i>Tg</i>	<i>At</i>	<i>Dm</i>	<i>Hs</i>
Monomer treadmilling	Profilin	1	1	5	4	5
	CAP	1	1	1	1	2
	Cofilin	2	1	14	7	14
Nucleation	Formins (FH2)	2	3	20	14	16
	Spire	0	0	0	4	2
	ARPC1/p41	1	0	3	3	2
	ARPC2/p34	0	0	2	1	2
	ARPC3/21	0	0	1	3	2
	ARPC4/p20	0	0	1	1	1
Crosslinking / bundling	ARPC5/p16	0	0	1	1	2
	WAVE/WASp	0	0	0	13	11
	Coronin	1	1	2	8	8

*Tg*ADF was first described in 1997 as a single copy gene (Allen et al. 1997). Recombinant *Tg*ADF is capable of binding to G-actin and of depolymerising F-actin (Allen et al. 1997). *In vivo*, a cytosolic localisation was reported for *Tg*ADF by antibody staining and endogenous tagging (Allen et al. 1997; Mehta and Sibley 2011; Haase et al. 2015). Depletion of *Tg*ADF compromises host cell invasion, egress and overall gliding motility, making *Tg*ADF essential for the lytic replication cycle (Mehta and Sibley 2011).

In vitro sedimentation assays with rabbit actin suggested that *TgADF* does not stably associate with F-actin (Mehta and Sibley 2010). In the same study, *TgADF* also displayed a weaker severing activity than the canonical yeast cofilin and appeared to prevent F-actin assembly mainly by sequestering monomeric G-actin. According to structural analysis, *TgADF* has enhanced affinity for G-actin (Yadav et al. 2011). *In vivo*, lack of *TgADF* causes the accumulation of actin structures within the parasite (Mehta and Sibley 2011; Periz et al. 2017).

Initially, conditional depletion of *TgFormin1* with the TATi-system was applied to report that *TgFormin1* is not important for intracellular replication and not critical for egress (Daher et al. 2010). Instead, Daher and co-workers suggested *TgFormin1* to be involved in tachyzoite motility and host cell invasion. A follow-up publication confirmed *TgFormin1* importance for gliding and invasion, but also indicated a critical role in parasite egress (Tosetti et al. 2019). Plaque assays suggested that *TgFormin1* is essential for the completion of the asexual lytic cycle in culture (Tosetti et al. 2019).

By obtaining a clonal *TgFormin2*-KO line, Tosetti and colleagues showed that *TgFormin2* is not essential for the completion of the lytic cycle (Tosetti et al. 2019). However, the *Formin2*-KO strain was outgrown by wild-type parasites in growth competition assays. It should be mentioned that the *Formin2*-KO line was obtained by applying CRISPR/Cas9 to delete a large part of the open reading frame (ORF). *TgFormin2* is involved in intracellular replication as its deletion causes an increase in aberrant daughter cell orientation (Tosetti et al. 2019). *TgFormin1* and 2 were initially localised to the tachyzoite pellicle (Daher et al. 2010). Subsequent reports localised *TgFormin1* to the apical tip of the parasite and *TgFormin2* to the vicinity of the apicoplast (Jacot et al. 2016; Tosetti et al. 2019).

TgFormin3-KO tachyzoites do not depict any replication defects, making *TgFormin3* dispensable for the lytic cycle (Daher et al. 2012). Initially, *TgFormin3* was localised to the apical and the basal pole as well as around the mitochondrion (Daher et al. 2012). Later, *TgFormin3* localisation was re-defined to the basal pole and the residual body based on endogenous tagging (Tosetti et al. 2019). Asynchronous replication was observed in parasites lacking *TgFormin3* (Tosetti et al. 2019). In addition, recovery of fluorescence in bleaching

experiments was slower for *TgFormin3*-KO parasites when compared to wild-type parasites. Tosetti and colleagues therefore suggested a role for *TgFormin3* in cell-cell communication.

Evidence suggests the all three *Toxoplasma* Formins can nucleate actin *in vitro*. The FH2 domains of *TgFormin1* and 2 were reported to initiate nucleation of rabbit actin (Daher et al. 2010) and *Toxoplasma* actin (Skillman et al. 2012) *in vitro*. The *TgFormin3* FH2 domain also nucleates rabbit actin (Daher et al. 2012). Skillman and colleagues interpreted fluorescence microscopy data as indication for the promotion of short filament bundles by *TgFormin1* and 2 (Skillman et al. 2012). Electron microscopy suggested that, *in vitro*, *TgFormin1* causes *TgACT1* to form an interconnected network, while *TgFormin2* mediates the formation of straight actin filament bundles (Skillman et al. 2012).

Intriguingly, *TgFormin*-mediated actin polymerisation was inhibited by *TgProfilin* *in vitro* (Skillman et al. 2012). These observations stand in direct contrast to observations made *in vitro* with yeast Profilin, which was reported to enhance Formin-mediated F-actin assembly (Sagot et al. 2002). Co-immunoprecipitation with *TgFormins* failed to precipitate *TgProfilin* (Daher et al. 2010). This lack of interaction was further supported by isothermal titration calorimetry and crystal structure analysis (Kucera et al. 2010). Taken together, these observations made Skillman et al. suggest that the main function of *TgProfilin* might be to sequester *TgACT1*, rather than enhancing *TgFormin2*-mediated F-actin assembly (Skillman et al. 2012).

TgProfilin is critical for the completion of the lytic life cycle as depletion of *TgProfilin* rendered parasite defective in gliding motility, invasion and host cell egress (Plattner et al. 2008). Intracellular replication was not affected by *TgProfilin* loss.

The ABPs *TgFormin2* (Jacot, Daher, and Soldati-Favre 2013; Tosetti et al. 2019), *TgADF* (Jacot, Daher, and Soldati-Favre 2013; Haase et al. 2015) and *TgProfilin* (Jacot, Daher, and Soldati-Favre 2013) are involved in apicoplast segregation in *Toxoplasma* tachyzoites.

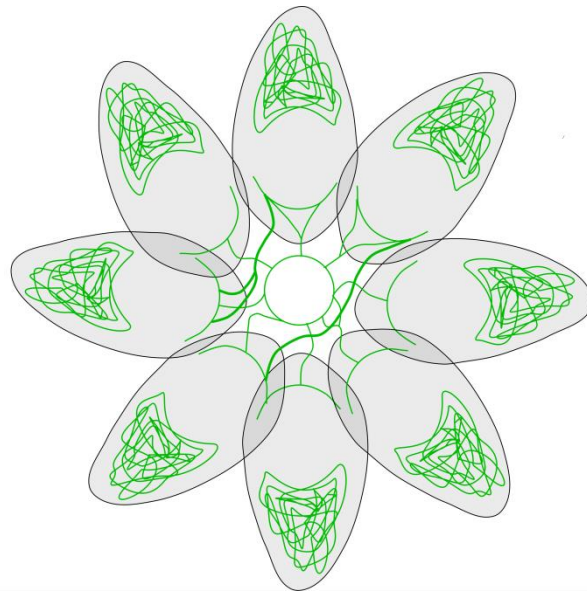


Figure 1-10: Schematic of the actin network in *Toxoplasma*

In intracellular tachyzoites, actin (green) forms a network that connects parasites within the parasitophorous vacuole. Individual parasites display actin accumulation in their apical region. The schematic is based on results published by Periz and co-workers (Periz et al. 2017).

1.8 Aims of this study

Although actin and its ABPs in *Toxoplasma* have been the focus of intense investigation, the overall conclusions were limited by the lack of a reliable method for actin visualisation. Because of this, the action of different ABPs on actin dynamics was mainly examined *in vitro*, making conclusion about their exact functions *in vivo* challenging.

The visualisation of actin structures in *Toxoplasma* was recently achieved by exploiting actin-chromobodies (Periz et al. 2017). These findings presented a major advancement in apicomplexan actin biology since actin visualisation had been a major obstacle. Classical antibody staining proved to be unreliable (Drewry & Sibley, 2015; Whitelaw et al., 2017) and other fluorogenic actin probes could not be expressed in *Toxoplasma* (Tardieux 2017; Periz et al. 2017). Expression of anti-actin-chromobodies in *Toxoplasma* revealed an extensive actin network that connects intracellular parasites within the parasitophorous vacuole (PV) (Figure 1-10) (Periz et al. 2017). In addition, Periz and colleagues identified a highly dynamic actin accumulation centre anterior to the nucleus in individual parasites.

Overcoming the challenge of actin visualisation opens the door to in-depth analysis of actin dynamics *in vivo*. In addition, the actin-chromobody could potentially be used for screening approaches aiming at the identification of novel ABPs. Since actin is critical for completion of the lytic cycle in *Toxoplasma* (Andenmatten et al. 2013; Egarter et al. 2014), a conditional gene disruption system might be advantageous for investigating potentially novel and essential actin dynamic factors.

Recently, a conditional type II CRSIPR/Cas9 system (split-Cas9) was described in mammalian cells (Zetsche, Volz, and Zhang 2015). In this system, the Cas9 enzyme is split into two sub-units (N- and C-terminus) which are fused to a FKBP or FRB domain. Upon rapamycin treatment, the two sub-units are re-united and become active. In theory, this system should have phenotypic screening potential. A gRNA library could be transfected into parasites while the conditional nature of the split-Cas9 system would allow for controlled phenotype induction. In addition, this system should enable rapid targeting of known ABPs.

The novel ability to visualize F-actin in fixed or live *Toxoplasma* cells presents an exciting opportunity to further investigate actin dynamics *in vivo* in unprecedented detail. Combination of the split-Cas9 system and the actin-chromobody technology could potentially give, for the first time, insights into the exact functions of ABPs within the *Toxoplasma* actin network *in vivo*. Therefore, the overall aims of this study were defined as follows:

- 1) The split-Cas9 system shall be established in *Toxoplasma* to allow for reliable analysis of gene function.
- 2) Overall actin dynamics in *Toxoplasma* shall be investigated by combining the split-Cas9 and actin-chromobody technologies.
- 3) The specific role of ABPs in maintaining actin dynamics during the lytic cycle in *Toxoplasma* shall be addressed.
- 4) A medium-throughput screen aiming at identifying novel ABPs in *Toxoplasma* shall be initiated.

2 Materials and Methods

2.1 Equipment

Table 2-1: Equipment

Applied Precision	DeltaVision® Core microscope
BD Biosciences	Syringes, Needles (23-25 gauge), FACS tubes with cell strainer cap
BioRad	Agarose gel electrophoreses equipment, UV transilluminator, SDS-PAGE system, Blotting apparatus (Transblot SD and Mini transblot electrophoretic transfer cell), gel documentation system, gene Pulser Xcell, Micropulser, S3e™ Cell sorter
BTX	Electroporation cuvettes and system (ElectroSquare Pore 830)
Eppendorf	Thermocycler (Mastercycler Eppgradient), Thermomixer compact
Fished Scientific	Ultrasound water bath FB15047
Grant	Water bath
Heraeus Instruments	Incubator
KD scientific	Syringe pump
Kuehner	Shaking incubator (ISF-1-W)
Lonza	4D-Nucleofactor™X electroporation unit, Single 100 µl Nucleovette™
Milipore	MilliQ water deionising facility, 3 µm Millipore filters
Photometrics	CoolSNAP HQ2CCD camera
Sanyo	CO ₂ -incubator for tissue culture
Satorius	Analytical balances
Sciquip	Sigma 6K 15 centrifuge (1150 rotor and 12500 rotor)
StarLab	ErgoOne Single & Multi-Channel pipettes, StarPet Pro pipette controller
Stuart	Heat block, Roller mixer, Orbital Shaker
ThermoFisher scientific	CO ₂ -incubator for tissue culture, Nanodrop spectrophotometer, Centrifuge (sorrall legend XFR), Table top centrifuge Heraeus Pico 21, Tabletop cooling centrifuge Heraeus Fresco 21
Zeiss	Axioskop 2 (mot plus) fluorescence microscope with Axiocam MRm CCD camera, Primo Vert (light microscope), Axiovert 40 CFL fluorescence microscope with Axiocam ICc1, Axiovert A1 fluorescence microscope with Axiocam IMc1, ELYRA PS.1 Super-resolution microscope, sCMOS pco SIM camera, Plan Apochromat 63x lens

2.2 Computer Software

Table 2-2: Computer software

Adobe Systems Inc.	Adobe Acrobat Reader DC
Inkscape Project	Inkscape™: Open Source Scalable Vector Graphics Editor
AcaClone software	pDraw32
Applied Precision	SoftWoRx explorer and SoftWoRx suite
BioRad	ProSort™
Carl Zeiss Microscopy	Zen Black and Zen Blue
Microsoft Corporation	Windows 7, Microsoft Office 2010
National Institute for Biotechnology Information (NCBI)	Basic Local Alignment search tool (BLAST), Primer-BLAST
National Institute of Allergy and Infectious Diseases (NIAID)	ToxoDB (Kissinger et al. 2003; Gajria et al. 2008)
National Institutes of Health (NIH)	ImageJ, Fiji (Schneider, Rasband, and Eliceiri 2012; Schindelin et al. 2012)
New England Biolabs (NEB)	NEB tools™: Double Digest Finder, Enzyme Finder, NEBCutter®, NEBBioCalculator®, Tm Calculator
Thermo Scientific	Thermo Scientific web tools: Tm Calculator
Mendeley Ltd.	Mendeley Desktop
University of Utah	ApE Plasmid Editor v2.0.53c Copyright© by M. Wayne Davies
University of Georgia	Eukaryotic Pathogen gRNA Design Tool (EuPaGDT) (Peng and Tarleton 2015)

2.3 Consumables, biological and chemical reagents

Table 2-3: Biological and Chemical reagents

Company	Reagents
Formedium	Tryptone, yeast extract
Life technologies	Phosphate buffered saline 1X (PBS), Trypsin/EDTA (0.05%), DNaseI, Platinum Taq DNA Polymerase High Fidelity, NuPage SDS loading buffer and reducing agent, Sodium bicarbonate, Ultrapure agarose
Melford	Agar, ditriothreitol, IPTG, X-Gal
NEB	1kb DNA ladder, all Restriction enzymes and associated buffers, T4 DNA ligase, Taq polymerase,

	Q5® high-fidelity DNA polymerase, Calf intestinal phosphatase (CIP)
Phenix Research Products	GelRed nucleic acid stain
Promega	pGEM®-T Easy vectors system
Roche	MgSO ₄ × 7H ₂ O, potassium hydroxide, paraformaldehyde
Sigma	Ammonium persulfate, Bromophenol blue sodium salt, Casein hydrosylate, Dulbecco's Modified Eagle Medium (DMEM), Ficoll, Ethylene glycol tetraacetic acid, Isopropanol, Sodium dodecyl sulfate (SDS), dimethyl sulfoxide (DMSO), N,N,N',N'-tetramethylethylenediamine, Triton X-100, Rapamycin, Giemsa stain, L-glutathione reduced, Adenosine 5'-triphosphate disodium salt hydrate, Glutamine, 30% acryl-bisacrylamide mix, Sodium deoxycholate, K ₂ HPO ₄ , Magnesium chloride, Bleomycin (BLEO), Ampicillin sodium salt, Gentamicin, Xanthine
Southern Biotech	DAPI-Fluoromount G
Thermo Scientific	Bovine serum albumin (BSA), Ethylene diamine tetraacetic acid, Glycerol, Glycine, Methanol, Tris, Sodium chloride, 40nM FluoSpheres® Carboxylate-Modified Microspheres, Platinum Taq DNA Polymerase High Fidelity, 1kb plus DNA ladder
VWR	CaCl ₂ × 2 H ₂ O, Glacial acetic acid, Ethanol, HEPES, Potassium chloride, Na ₂ HPO ₄ , KH ₂ PO ₄
Zeiss	Immersion oil

2.4 Kits

Table 2-4: Kits

Company	Kits
Qiagen	Spin Mini-prep, Plasmid Midi-prep, PCR Purification MinElute, QIAquick gel extraction Kit, DNeasy blood and tissue Kit
Roche	High Pure PCR product purification Kit
New England Biolabs	Q5® Site-Directed Mutagenesis Kit

2.5 Buffers, solutions and media

Table 2-5: Buffers for DNA analysis

Buffer	Components
50X TAE buffer	2M Tris, 0.5M Na ₂ EDTA, 5.71% glacial acetic acid (v/v)
5X loading dye	15% Ficoll (v/v), 20 mM EDTA, 0.25% Bromophenol Blue in H ₂ O
1kb plus DNA ladder	150 µl 1kb ladder (1 µg/µl), 300 µl 5X DNA loading buffer, 1050 µl H ₂ O

Table 2-6: Buffers and media for bacterial culture

Buffer	Components
LB medium	10 g/l tryptone, 5 g/l yeast extract, 5 g/l NaCl
LB agar	1.5% (w/v) agar in LB medium
SOB medium	2% tryptone (w/v), 0.5% yeast extract (w/v), 0.05% NaCl (w/v), 2.5 mM KCl, 10mM MgCl ₂
SOC medium	20 mM glucose in SOB medium
NYZ broth	5 g/l NaCl, 2 g/l MgSO ₄ *7H ₂ O, 5 g/l yeast extract, 10 g/l casein hydrolysate, pH adjusted to 7.5 with NaOH
Ampicillin (1000X)	100 mg/ml in H ₂ O
IPTG (100 µl/petri dish)	100 mM IPTG in H ₂ O
X-Gal (10 µl/Petri dish)	50 mg/ml in N,N-dimethylformamide

Table 2-7: Buffers and media for Toxoplasma and mammalian cell culture

Buffer	Components
DMEM _{COMPLETE}	500 ml DMEM, 10 % FCS (v/v), 2 mM glutamine, 20 µg/ml gentamicin
DMEM Fluorobrite _{COMPLETE}	500 ml DMEM, 10 % FCS (v/v), 2 mM glutamine, 20 µg/ml gentamicin
2 x Freezing solution	25 % FCS (v/v), 10 % DMSO (v/v) in DMEM _{COMPLETE}
Electroporation buffer (Cytomix)	10 mM K ₂ HPO ₄ /KH ₂ PO ₄ , 25 mM HEPES, 2 mM EGTA pH 7.6, 120 mM KCl, 0.15 mM CaCl ₂ , 5 mM MgCl ₂ with 5 mM KOH adjusted to pH 7.6, 3 mM ATP, 3 mM GSH
MPA (500X)	12.5 mg/ml in methanol
XAN (500X)	20 mg/ml, 1M KOH
Pyrimethamine (1000X)	1 mM in EtOH
Rapamycin (1000X)	50 µM in DMSO
FACS buffer	1 % FCS, 1 mM EDTA in PBS
PFA fixing solution	4 % PFA (w/v) in PBS
Permeabilisation solutions	0.2 % triton X-100 (v/v) in PBS
Blocking solution	% BSA (w/v) in permeabilisation solution

2.6 Antibodies

Table 2-8: Antibodies

Abbreviations: 1st - primary antibody, 2nd - secondary antibody.

Antibody	Species of origin	Dilution IFA	Source
anti-gap40 (1 st)	rabbit	1:250	Dr Dominique Soldati-Favre
anti-IMC1 (1 st)	mouse	1:1000	Dr Gary Ward
anti-SAG1 (1 st)	mouse	1:500	Dr Sebastian Lourido
anti-MIC8 (1 st)	rabbit	1:500	Dr Markus Meissner
anti-K40acteylation (1 st)	mouse	1:500	Sigma, cat# T6793
anti-gap45 (1 st)	rabbit	1:2000	Dr Dominique Soldati-Favre
anti-HSP60 (apicoplast) (1 st)	rabbit	1:2000	Dr Lilach Sheiner
anti-HA (1 st)	rat	1:500	Roche, cat# 1187431001
anti-GFP/YFP (1 st)	rabbit	1:500	Abcam, cat #ab6556
anti-Atrx1 (apicoplast) (1 st)	mouse	1:500	Dr Lilach Sheiner
anti-G2Trx (apicoplast) (1 st)	rabbit	1:500	Dr Lilach Sheiner
anti-TOM40 (1 st)	rabbit	1:1000	Dr Lilach Sheiner
anti-Rop 2,4 T34A7 (1 st)	mouse	1:500	Dr Jean-François Dubremetz
AlexaFluor594 anti-rabbit (2 nd)	goat	1:3000	Life Technologies
AlexaFluor488 anti-rabbit (2 nd)	goat	1:3000	Life Technologies
AlexaFluor594 anti-mouse (2 nd)	goat	1:3000	Life Technologies
AlexaFluor488 anti-mouse (2 nd)	goat	1:3000	Life Technologies
AlexaFluor594 anti-rat (2 nd)	goat	1:3000	Life Technologies
AlexaFluor488 anti-rat (2 nd)	goat	1:3000	Life Technologies

2.7 Oligonucleotides

Table 2-9: Oligonucleotides

1- PCR amplification, 2 - Integration PCR, 3-sequencing

Oligonucleotide	Sequence (5` - 3`)	Purpose
sCas9-C-term-split4-fw	GAATTCGaCAAAATGGCCCCAAAGAAGAAGCG	1
sCas9-C-term-split4-rev	cTTAATTAACTTACTTTTTCTTTTTGCCTGGCCGG	1
sCas9-N-term-split4-fw	GAATTCGaCAAAATGCTAGATTTAGCTAGC	1
sCas9-N-term-split4-rev	CTTAATTAACTTACTGCTTGCTGATTCTTC	1
Q5-universal-rev	AACTTGACATCCCCATTTAC	1
sag1-sgRNA3-fw	GAATGTCGCAAGGTGCTCCTAGTTTTAGAGCTAGAAATAGC	1
mec17-sgRNA2-fw	GTGTTCTGCGACTTTTCGTCTGTTTTAGAGCTAGAAATAGC	1
mec17-sgRNA3-fw	GCTCAAGGGCCTCACCCGACGTTTTAGAGCTAGAAATAGC	1
actin1-sgRNA-fw	GTCCATTCCGACCATGATACCGTTTTAGAGCTAGAAATAGC	1
adf-sgRNA-fw	GAGATCCGCAAGACGGTGAAGGTTTTAGAGCTAGAAATAGC	1
formin2-sgRNA-fw	GTGGTTACTCGGAGTCAGCGAGTTTTAGAGCTAGAAATAGC	1
profilin-sgRNA-fw	GCCAATCCAAACACCGTTAGGTTTTAGAGCTAGAAATAGC	1
drpA-sgRNA-fw	GTCGGCTTCTGCAGAAAACAGGTTTTAGAGCTAGAAATAGC	1
actin1-gRNA-cutside-fw	GCGGATGAAGAAGTGCAAGC	1
actin1-gRNA-cutside-rev	GGAGGTGGTGAAGCCGTATC	1
adf-gRNA-cutside-fw	GCTACGTCCGAGGTGTGAAA	1
adf-gRNA-cutside-rev	TTCGACTGAACACCCGAACA	1
formin2-gRNA-cutside-fw	CCTTCGTTCCGAGTCTGTCTTC	1
formin2-gRNA-cutside-rev	AGAGCTGCTTGTGTGCTAAA	1
mec17-gRNA-cutside-fw	cctataATGCATGAAGTTCGGTTTGAATTTCTGCAC	1
mec17-gRNA-cutside-rev	GTCTTGAGTGTGAGCCACCA	1
DiCre-formin2-3`-fw	GGTGAAAGTTGTTCCCTCG	2
DiCre-formin2-3`-rev	ATCCCTTCCCTGCAGGAG	2
DiCre-formin2-5`-loxP-fw	CACTTTTCATAGTATAGGATAACTTCG	2
DiCre-formin2-5`-rev	CCATTTTGCCTGTTCAAGTG	2
DiCre-formin2-excision-fw	TTCTCATTITTAGCTTCACCACG	2
pGEM-sequencing -fw	TGTAATACGACTCACTATAGGGC	3

pGEM-sequencing - rev	ATTTAGGTGACACTATAGAATACTC	3
C-term-Cas9_seq-fw1	TGGAGCTGCTGAAGCTGGAG	3
C-term-Cas9_seq-fw2	GACAGCCTGACCTTTAAAGAGG	3
C-term-Cas9_seq-fw3	GATGAAGAACTACTGGCGGC	3
C-term-Cas9_seq-fw4	CTCTGATCGAGACAAACGGC	2, 3
N-term-Cas9_seq-fw1	AGAAGTACCCACCATCTACC	3
N-term-Cas9_seq-fw2	ATAGTACGCCGACCTGTTTCTG	2, 3
TUB8-sequencing-fw1	GTTCTTGCGGAAACTACTCG	3
TUB8-sequencing-fw2	CGCCCTTTCCTTCTCTTTGCG	3
sequencing-rev	CCACAGCGGAACAACTCAGTTTC	2, 3
Int-gRNA-fw	CAGTCACGACGTTGTAAAC	2
Int-RNA-rev	CAAGTTGATAACGGACTAGCC	2
gRNA-sequencing-rev	GACAGCAGACAACTTTCC	3
pU6-gRNA-sequencing-fw	CTTGCGCAGCATACACTCGAAGC	3

2.8 Plasmids

Table 2-10: Plasmids

*Please note that the lacZ-sgRNA plasmid was generated by Marleen Büchler under the supervision of Dr Elena Jimenez-Ruiz. The formin2- and the profilin-sgRNA plasmids were created by Dana Aghabi under my supervision.

Plasmid		reference
sgRNA-plasmids	pU6_sgRNA_dhfr_Amp	This study*
sCas9-N-term-split4	pTUB8_NES_N-terminus-Cas9-split4_FRB_HX_Amp	This study
sCas9-C-term-split4	pTUB8_NLS_FKBP_C-terminus-Cas9-split4_NLS_Amp	This study
Actin-chromobody-emerald	pDHFR_Actin-Chromobody_Emerald_Amp	(Periz et al. 2017)

2.9 Cell strains

2.9.1 Bacteria strains and mammalian cell lines

Table 2-11: Bacteria strains

Strain	Competence	Source
DH5 α	Chemically competent	New England BioLabs
One Shot Top10	Chemically competent	Thermo Fisher Scientific
XL-10 Gold	Chemically competent	Stratagene

Table 2-12: Mammalian cells

Cells	Organism	Source
Human foreskin fibroblasts (HFF), primary cell line	Homo sapiens	ATCC® SCRC-1041™

2.9.2 *Toxoplasma* strains

Table 2-13: *Toxoplasma* strains

Strain	Genotype	Reference
RH	RH Δ hx	(Donald et al. 1996)
RH Δ ku80	RH Δ ku80 Δ hx	(Fox et al. 2009; Huynh and Carruthers 2009)
RH Δ ku80-DiCre	RH_DiCre_T2A_ Δ ku80 Δ hx_CAT	(Hunt et al. 2019)
RH-gap40	RH_gap40sgRNA_dhfr_ Δ hx	this study
RHsCas9-gap40	RH_Cas9-N-Termius-split4_split-Cas9-C-Terminus-split4_gap40sgRNA_dhfr_hx	this study
RHsCas9	RH_Cas9-N-Termius-split4_split-Cas9-C-Terminus-split4_hx	this study
RHsCas9- Δ hx	RH_Cas9-N-Termius-split4_split-Cas9-C-Terminus-split4_ Δ hx	Matthew Gow, unpublished
RHsCas9-sag1-1	RH_Cas9-N-Termius-split4_split-Cas9-C-Terminus-split4_sag1sgRNA1_dhfr_hx	this study
RHsCas9-sag1-1-KO	RH_Cas9-N-Termius-split4_split-Cas9-C-Terminus-split4_sag1sgRNA1_dhfr_hx_sag1disrupted	this study
RHsCas9- Δ hx-sag1-1-KO	RH_Cas9-N-Termius-split4_split-Cas9-C-Terminus-split4_sag1sgRNA1_dhfr_ Δ hx_sag1disrupted	Matthew Gow, unpublished
RHsCas9-sag1-	RH_Cas9-N-Termius-split4_split-Cas9-C-	this study

3	Terminus-split4_sag1sgRNA3_dhfr_Δhx	
RHsCas9-sag1KO-sag1*	RH_Cas9-N-Terminus-split4_split-Cas9-C-Terminus-split4_sag1sgRNA1_dhfr_hx_sag1disrupted_sag1* (sag1* represents a mutated sag1 gene variant)	Matthew Gow, unpublished
RHsCas9-lacZ	RH_Cas9-N-Terminus-split4_split-Cas9-C-Terminus-split4_lacZsgRNA_dhfr_hx	Marleen Büchler and Dr Elena Jimenez-Ruiz, unpublished
RHsCas9-mec17-2	RH_Cas9-N-Terminus-split4_split-Cas9-C-Terminus-split4_mec17sgRNA2_dhfr_Δhx	this study
RHsCas9-mec17-3	RH_Cas9-N-Terminus-split4_split-Cas9-C-Terminus-split4_mec17sgRNA3_dhfr_Δhx	this study
RHΔku80-DiCre-Pfmec17loxP	RHΔku80_DiCre_loxP-Pfmec17-loxP_dhfr_hx	Stortz 2014, Master Thesis, Ruprecht-Karls-University of Heidelberg
RHsCas9-CbEmerald	RH_Cas9-N-Terminus-split4_split-Cas9-C-Terminus-split4_actin-chromobody-Emerald_dhfr_Δhx	this study, in collaboration with Dr Simon Gras
RHsCas9-CbEm-actin1	RH_Cas9-N-Terminus-split4_split-Cas9-C-Terminus-split4_actin-chromobody-Emerald_actin1sgRNA_dhfr_Δhx	this study
RHsCas9-CbEm-adf	RH_Cas9-N-Terminus-split4_split-Cas9-C-Terminus-split4_actin-chromobody-Emerald_adfsgRNA_dhfr_Δhx	this study
RHsCas9-CbEm-sag1-3	RH_Cas9-N-Terminus-split4_split-Cas9-C-Terminus-split4_actin-chromobody-Emerald_sag1sgRNA3_dhfr_Δhx	this study
RHΔku80-TgFormin2-HA	RHΔku80_formin2_HA_Δhx	Dr Mirko Singer, (Stortz et al. 2019)
RHΔku80-DiCre-loxP-frm2YFP-loxP	RHΔku80_DiCre_loxP_formin2_YFP_loxP_Δhx	Dr Mirko Singer, (Stortz et al. 2019)
RHsCas9-CbEm-formin2	RH_Cas9-N-Terminus-split4_split-Cas9-C-Terminus-split4_actin-chromobody-Emerald_formin2sgRNA_dhfr_Δhx	this study, in collaboration with Dana Aghabi
RHsCas9-CbEm-profilin	RH_Cas9-N-Terminus-split4_split-Cas9-C-Terminus-split4_actin-chromobody-Emerald_profilinsgRNA_dhfr_Δhx	this study, in collaboration with Dana Aghabi
RHsCas9-CbEm-DrpA	RH_Cas9-N-Terminus-split4_split-Cas9-C-Terminus-split4_actin-chromobody-	this study

	Emerald_drpAsgRNA_dhfr_Δhx	
RH-GFP	RHΔhx_GFP	Dr Musa Hassan

2.10 Microbiology Methods

2.10.1 Liquid cultures and cryopreservation stocks of *E. coli*

After a growth period of 14-17h on an agar plate, a single bacterial colony was picked and added to LB-medium containing ampicillin (100µg/ml). Liquid cultures were incubated at 37°C while shaking. Cryopreservation was achieved by mixing freshly grown *E. coli* liquid cultures with freezing media (LB-Medium containing 40% glycerol and 2% peptone) in a ratio 1:2. Cryostocks were stored at -80°C.

2.10.2 Transformation of chemically competent *E. coli*

For transformation purposes, chemically competent *E. coli* cells were defrosted on ice. After this, DNA was added to 25µl of bacterial suspension, followed by an incubation time of 45min on ice. The heat-shock was performed at 42°C for 30s. Subsequently, bacteria were again incubated in ice for 2min. The bacterial suspension was then spread on ampicillin-containing (100µg/ml) LB-agar plates (1.5 % (w/v) agar in LB medium) and incubated at 37°C for 14-17h.

When the pGEM®-T Easy vectors system (Promega) was used for transformation, the LB-agar plates were treated with IPTG and X-Gal prior to bacteria spreading. This allowed for blue/white colony screening.

2.11 Molecular Biology Methods

2.11.1 Polymerase Chain Reaction (PCR)

PCR was performed to amplify DNA fragments from various template DNAs. The PCR mix (25µl) contained the following reagents: template DNA, 2.5µl 10 x PCR reaction buffer, 0.5µl dNTPs (stock: 10mM, final: 0.2mM), 1µl forward primer (stock: 10pmol/µl, final: 0.4pmol/µl), 1µl reverse primer (stock:10pmol/µl,

final: 0.4pmol/ μ l) (for primers refer to **Table 2-9**), 0.1 μ l Platinum Taq DNA polymerase High-Fidelity (Invitrogen), 1 μ l of the Q5[®] high-fidelity DNA polymerase or 0.125 Taq DNA polymerase (New England Biolabs) and water (Fisher Scientific, DNA grade). Platinum Taq DNA polymerase High Fidelity (Invitrogen) required addition of 1 μ l MgSO₄ (stock: 50mM, final: 2mM). If necessary, betaine solution (Sigma-Aldrich) was added (stock: 5M, final: 0.2M). The Q5 high CG enhancer was added to the reaction mix when the Q5[®] high-fidelity DNA polymerase was used. All Polymerases were used with their respective buffers as supplied by the manufacturer. High-fidelity Polymerases were exploited to avoid mutations during DNA fragment amplification. The Taq DNA Polymerase was used for analytical purposes.

PCR cycles were set to an initial denaturation at 95°C for 3-10min, followed by 30 repeats of denaturation (95°C, 30 sec), annealing (30 sec) and elongation. A final elongation step was performed for 5-10min. The annealing temperature depended on the melting temperature of the primers used. Elongation duration was calculated according to the size of the amplified DNA fragment. The temperature for the elongation steps was chosen based on the specific Tag polymerase requirements as described by the manufacturer.

2.11.2 Agarose Gel Electrophoresis (AGE)

To separate DNA fragments, agarose gel electrophoresis (AGE) was performed. Depending on the size range of DNA fragments gels containing 0.8-1.2% agarose in 1x TAE buffer were exploited. The DNA was visualized by UV light. For this purpose, gels were supplemented with 1/100 GelRed Nucleic Acid Stain (Phenix research products). A 6x loading dye was used for DNA loading onto the gel. DNA ladders were used to calculate the size of the DNA fragments.

2.11.3 DNA restriction

Restriction enzymes (New England BioLabs) and their respective buffers were used according to the manufacturer's instructions. Duration of the restriction reaction was calculated depending on the DNA amount and the number of units

per ml (U/ml) of the enzyme stock. Usually, analytic restriction digests were performed in a total volume of 30µl for 1-4h, while preparative restriction digests were usually incubated overnight. When plasmid backbones were prepared for future sub-cloning by restriction digest, the reaction was treated with CIP (10U, New England BioLabs) at 37°C for 1h.

When larger amounts of DNA were digested, e.g. for *Toxoplasma* transfections, reactions were incubated for 14-17h in total volume of 100-120µl. To maximise restriction efficiency, the reactions were topped up with their respective enzymes after the initial 14-17h and incubated again for 1h.

2.11.4 DNA purification

DNA fragments were purified from PCR using either the *MinElute PCR Purification Kit* (Qiagen) or *High Pure PCR Product Purification Kit* (Roche). To extract DNA from an agarose gel, the *MinElute Gel Extraction Kit* (Quiagen) was exploited. The procedures were performed according to the manufacturer's instructions. DNA was eluted in water (Fisher Scientific, DNA grade).

2.11.5 DNA ligation

For sub-cloning purposes, the T4-DNA-Ligase (New England BioLabs) was applied to ligate restricted DNA fragments. The ligation mix had a total volume of 10µl. The mix contained 1µl of T4-DNA-Ligase and 1µl of 10x T4-DNA ligase buffer (New England BioLabs). When DNA fragments were ligated into the pGEM®-T Easy vector (Promega), the ligation mix was set up according to the manufacturer's instructions. Ligation reactions were incubated at 4°C for at least 12h.

2.11.6 Isolation of plasmid DNA from *E.coli*

Isolation of plasmid DNA from bacterial liquid cultures was performed according to the *QIAprep Spin Miniprep Kit* (Qiagen) or the *QIAGEN Plasmid Plus Midi Kit*

(Qiagen). To achieve maximum elution efficiency, DNA was incubated with water (Fisher Scientific, DNA grade) at room temperature for 10min, followed by a centrifugation step of 3min at 13,000rpm.

Alternatively, the *QIAprep Spin Miniprep Kit* (Qiagen) was followed until the centrifugation step (10min, 13,000 rpm). Then, the supernatant was taken off and mixed with 100% Isopropanol (ice-cold) in a ratio 1:1. The samples were stored at -80°C for at least 1h. To pellet the plasmid DNA, the mixture was centrifuged at 14,000rpm at 4°C. The DNA pellet was washed twice with 70% Ethanol. After this, the pellet was air dried and finally resuspended in 100µl water (Fisher Scientific, DNA grade).

2.11.7 Alcohol precipitation of plasmid DNA for *Toxoplasma* transfections

Toxoplasma transfection required DNA to be purified and concentrated via ethanol precipitation. To achieve this, DNA was mixed with 2.5 volume of ice-cold 100% ethanol and 1/10 NaAc (3M, pH5). This mix was incubated at -20°C for at least 14h. The DNA was subsequently pelleted for 60min at 4°C and maximum speed. After two washing steps with ice-cold 70% ethanol (centrifugation: 10min, 4°C, maximum speed), the supernatant was removed under sterile conditions. The DNA pellet was air dried for approximately 15-45min. Depending on the transfection system, the DNA was resuspended in cytomix (BioRad® system) or P3 buffer (Amaya® system). DNA was stored until transfection at 4°C for up to 2 days or at -20°C until use.

2.11.8 Isolation of genomic DNA (gDNA) from *Toxoplasma*

To isolate genomic DNA from tachyzoites, the *DNeasy Blood & Tissue Kit* (Qiagen) was applied according to the manufacturer's instructions. Prior to Kit application, freshly lysed tachyzoites (0.4-1ml) were pelleted by centrifuging at 6,000rpm for 10min. Genomic DNA was eluted in 100µl of water (Fisher Scientific, DNA grade) after an incubation time of 5-10min.

2.11.9 Sub-cloning of the split-Cas9 plasmids

The N and C-terminus of the Cas9 enzyme (split4 variant) (Figures 2-1 and 2-2) were amplified from the original plasmids provided by Zetsche and colleagues (Zetsche, Volz, and Zhang 2015) via PCR. The PCR amplicons were ligated into the pGEM®-T Easy vector and sequenced. Subsequently, the Cas9 N and C-terminus were cloned into a *Toxoplasma* expression vector via the restriction enzymes *EcoRI* and *PacI*. For the C-term-Cas9 vector, the *hx* selection marker was removed by restriction with *SacII*. Correct positioning of the Cas9 N and C-terminus in the expression vector was confirmed by sequencing.

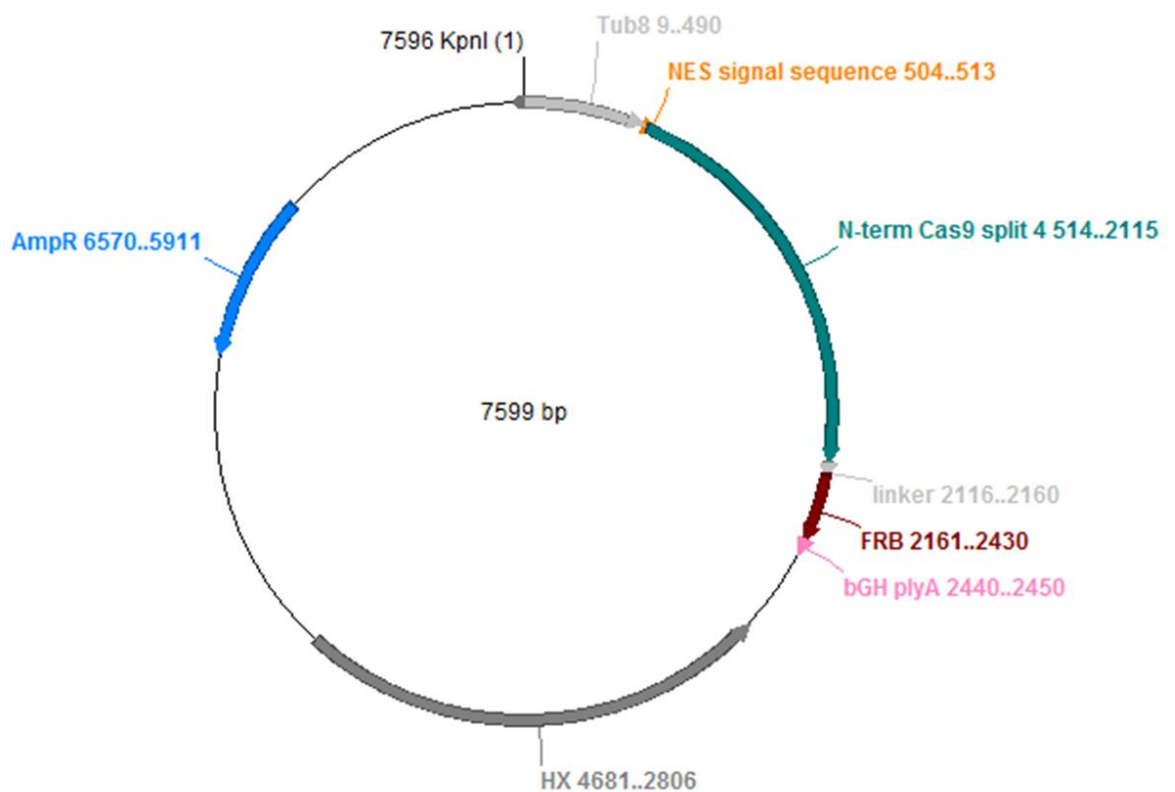


Figure 2-1: Plasmid encoding the split-Cas9 N-terminus (split4 variant)

The Cas9-N-terminus was expressed under the TUB8 promoter. The restriction site *KpnI* was used to linearize the plasmid for transfection. The plasmid codes for the *hx* selection marker

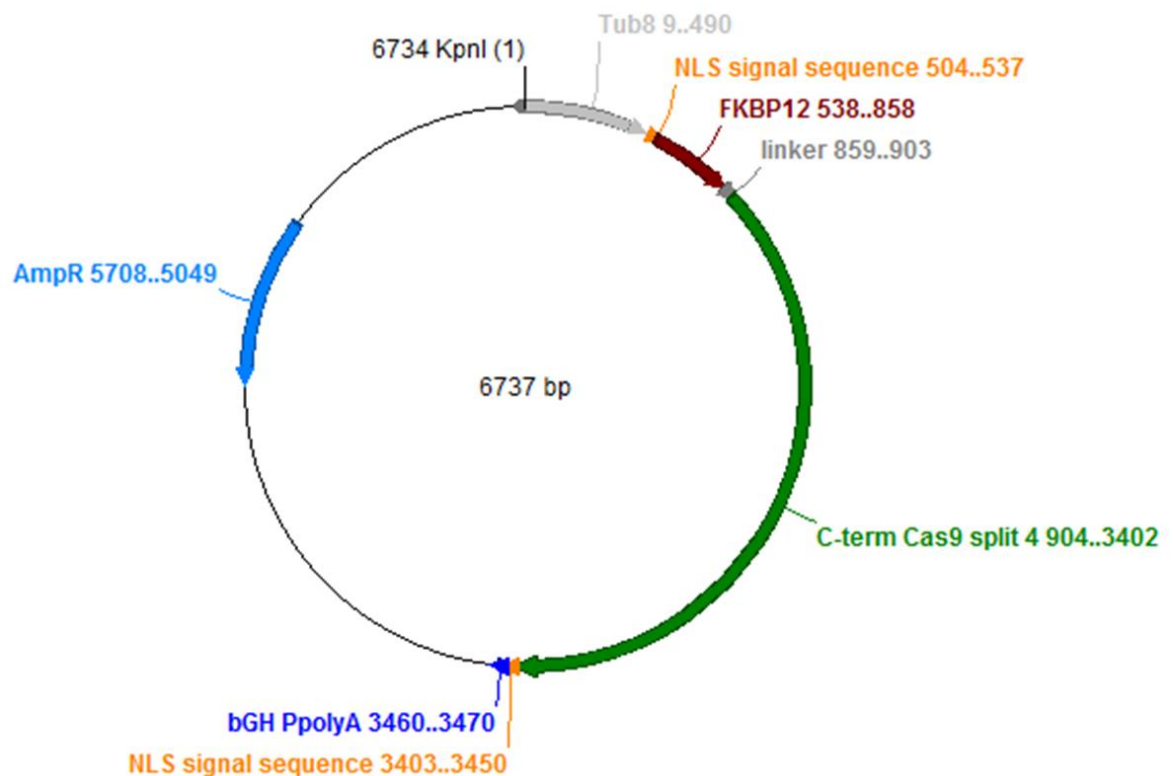


Figure 2-2: Plasmid encoding the split-Cas9 C-terminus (split4 variant)

The Cas9-C-terminus was expressed under the TUB8 promoter. The restriction site *KpnI* was used to linearize the plasmid for transfection. Please note that this plasmid does not code for a selection marker.

2.11.10 Sub-cloning of gRNA plasmids

The Q5® Site-Directed Mutagenesis Kit (New England Biolabs) was used to insert gene-specific sgRNAs into the universal sgRNA plasmid (Figure 2-3) according to the manufacturer's instructions. Importantly, a universal reverse primer was used together with a forward primer to which the whole sgRNA sequenced was attached (Table 2-9). All sgRNA-plasmids were sequenced to confirm proper sgRNA insertion and sequence.

2.11.11 DNA sequencing

Plasmid DNA was sequenced by Eurofins (GATC services, LightRun Tubes). DNA was prepared for sequencing in accordance with the company's protocol.

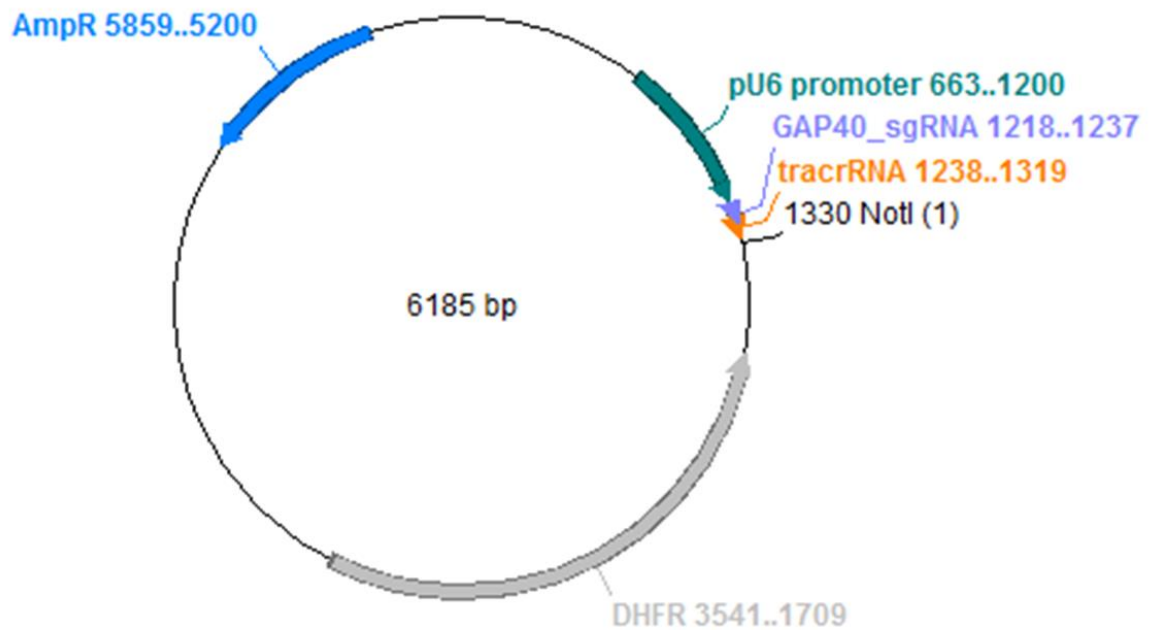


Figure 2-3: Plasmid encoding sgRNAs

The sgRNA (gene-specific gRNA and tracrRNA) were expressed under a pU6 promoter. The selection marker is dhfr. The restriction site NotI was used to linearize the plasmid for transfection. This figure shows the gap40sgRNA plasmid as an example. All other gRNA plasmids possess the same sequence with the gene-specific gRNA being the only difference.

2.12 Biochemistry Methods

2.12.1 Indirect Immunofluorescence Analysis (IFA)

For IFA analysis, tachyzoites were grown in HFFs cells on glass coverslips until fixation with 4%PFA for 20min at RT. Samples were then washed with 1xPBS and, subsequently, permeabilised with 0.2% Triton X-100/1xPBS for 20min at RT. A 3%BSA (in 0.2% Triton X-100/1xPBS) solution was used for blocking purposes. Samples were incubated with the blocking solution for at least 20min at RT. Subsequently, primary antibodies (diluted in 3%BSA/0.2%TritonX-100/1xPBS) were applied to the sample for 60min at RT. After washing the samples with 1xPBS, the secondary antibodies were applied for 45-60min at RT. Another washing step with 1xPBS was performed prior to coverslip mounting with Dapi fluoromount G (Southern Biotech). To protect fluorescent proteins from bleaching, all steps were carried out in the dark. Please refer to **Table 2-8** for a full list of primary and secondary antibodies.

2.13 Cell Culture

2.13.1 Culturing host cells (HFFs) and *Toxoplasma*

Human foreskin fibroblasts (HFFs) were cultured in DMEMcomplete at 37°C and 5%CO₂. HFFs are a primary cell line and were used until passage 25. *Toxoplasma* tachyzoites were grown on a HFF monolayer at 37°C and 5%CO₂ in DMEMcomplete. After complete lysis of the host cell monolayer, parasites were inoculated onto a fresh monolayer. Please refer to **Table 2-13** for the complete list of *Toxoplasma* lines used in this study.

2.13.2 Cryopreservation of *Toxoplasma*

Cryopreservation was performed to enable long term storage of *Toxoplasma* lines. For this purpose, host cells containing large vacuoles of intracellular parasites were taken up in DMEM only and added to 2x freezing mix (pure DMEM, 25% FCS, 10% DMSO) in a ratio of 1:1. These stabilates were frozen at -80°C and, subsequently, stored in liquid nitrogen.

Cryopreserved parasites were thawed at 37°C and immediately inoculated onto a fresh HFF cells. The medium was changed every 48h until healthy parasites were detectable.

2.13.3 Stable and transient transfections of *Toxoplasma*

Stable transfections

In this study, freshly lysed *Toxoplasma* tachyzoites were transfected with the Bio-Rad[®] or the Amaxa[®] system. For the Bio-Rad[®] electroporator, parasites were resuspended in 640µl cytomix together with 30µl ATP (100mM), 30µl GSH (100mM) and 100µl of linearized plasmid DNA (30-60µg). This mix was transferred into an electroporation cuvette. After electroporation (1700V, 2 pulses for 0.2s), parasites were inoculated on HFF cells. About 1ml of freshly

lysed parasites from a 6cm dish (total volume 4ml) were used for the Bio-Rad[®] electroporator.

The Amaxa[®] system required the resuspension of parasites in 10 μ l (transfection in strips) or 50 μ l (transfection in cuvettes) P3 buffer. For strips, parasites were mixed with 10 μ l of linearized DNA in P3 buffer. For cuvettes, 50 μ l of linearized DNA in P3 buffer was added to the parasites. Between 20-35 μ g of DNA was used for Amaxa[®] transfections. 100 μ l (strips) or 200 μ l (cuvettes) of freshly lysed parasites from a 6cm dish (total volume 4ml) were used for Amaxa[®] transfections.

Selection for stable plasmid integration into the *Toxoplasma* genome was achieved by culturing transfected population with selection markers. In this study, parasites were selected with 25mg/ml MPA in combination with 40mg/ml XAN when parasites were selected for the *hx* gene (Donald et al. 1996). When selected for the *dhfr* resistance marker, parasites were treated with 1 μ M pyrimethamine (Donald and Roos 1993).

Transient transfections

For transient transfections, circular plasmid DNA was used. Apart from this, the same protocols as described for stable transfections were applied. Transiently transfected parasites were used for IFA analysis (refer to section 2.12.1) 24-72h after transfection.

2.13.4 Generation of the parental split-Cas9 (sCas9) strain

The Cas9 N and C-terminus plasmids (**Figures 2-1 and 2-2**) were co-transfected into RH Δ hx parasites. Parasites were selected with 25mg/ml MPA in combination with 40mg/ml XAN for the *hx* gene (Donald et al. 1996). Prior to transfection, the plasmids had been linearized with the restriction enzyme *KpnI* (New England BioLabs). This restriction enzyme was added to the transfection mix prior to electroporation to allow for Restriction Enzyme Mediated Insertion (REMI) (Black et al. 1995). Clonal lines were obtained from this transfection by serial dilution.

Analytic PCR confirmed the presence of the Cas9 N and C-terminus in the parasite genome. Split-Cas9 activity was confirmed by transient transfection of RHsCas9 parasites with the *gap40*-sgRNA and subsequent induction with rapamycin.

2.13.5 Generation of sCas9-sgRNA strains

RHsCas9 or RHsCas9-CbEmerald parasites were transfected with linearized sgRNA-plasmids. sgRNA plasmids were linearized via the *NotI* restriction enzyme. *NotI* was also added to the transfection mix to enable Restriction Enzyme Mediated Insertion (REMI) (Black et al. 1995). Transfected parasites were cultured with 1 μ M pyrimethamine which selects for the *dhfr* resistance marker (Donald and Roos 1993). Presence of the sgRNA-plasmid in the parasite genome was verified via integration PCR.

2.13.6 Generation of RHsCas9-CbEmerald strain

The RHsCas9-CbEmerald strain was generated in collaboration with Dr Simon Gras. Initial transfection of the actin-chromobody-emerald plasmid (**Figure 2-4**) and enrichment of positive parasites via FACS sorting was performed by Dr Simon Gras. Subsequently, I isolated clonal RHsCas9-CbEmerald lines and tested them for split-Cas9 activity. For this purpose, I transfected parasites with the *gap40*-sgRNA in transient, induced with rapamycin and analysed split-Cas9 activity by quantifying vacuoles depicting a *gap40* phenotype.

2.13.7 Serial dilution of transfected *Toxoplasma* parasites

Serial dilution was performed to isolate clonal parasite lines from the transfection pool after drug selection. For this purpose, parasites were serially diluted on 96 well plates and cultivated for 5-7 days in the presence of the respective selection marker under normal culturing conditions. Eventually, each well of the 96 well plates was examined for plaque formation. A single plaque

indicated a clonal parasite line. Clonal populations were subsequently cultured under normal conditions for further examination and experiments.

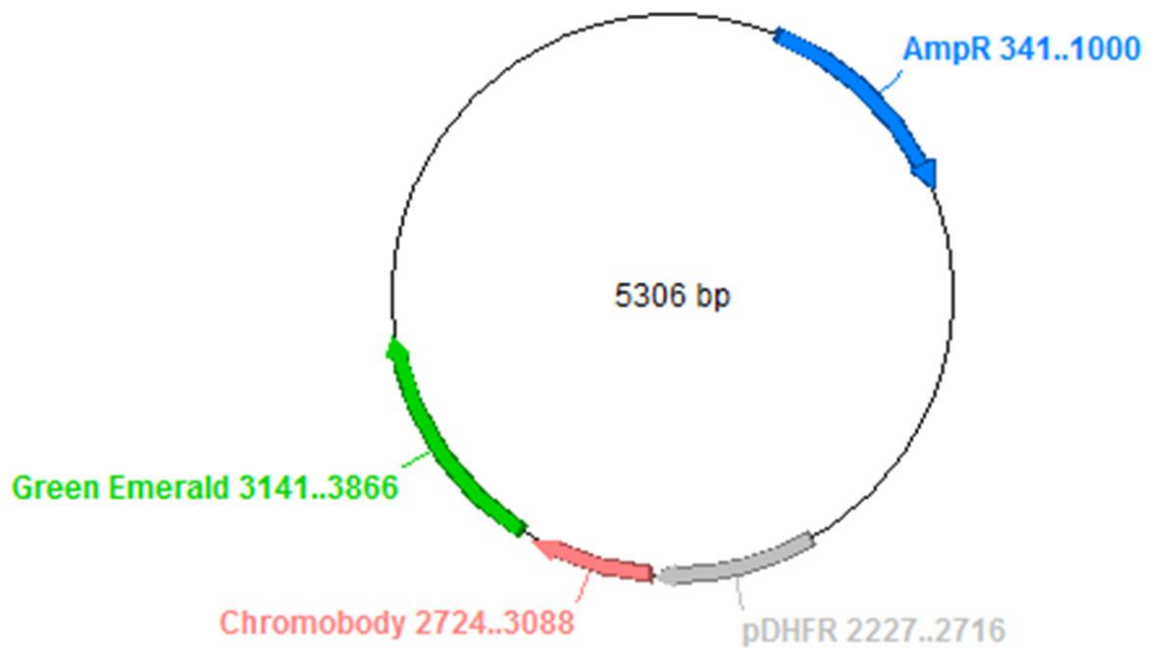


Figure 2-4: Plasmid encoding the actin-chromobody-Emerald

The actin-chromobody-emerald was expressed under the DHFR promoter. Please note that this plasmid does not code for a selection marker.

2.13.8 Induction of the split-Cas9 or DiCre system in *Toxoplasma*

Conditional split-Cas9 or DiCre mutants were obtained by adding 50nM rapamycin to the parental lines. Parasites were incubated for 1h (split-Cas9) or 4h (DiCre) at 37°C and 5% CO₂ and then cultured as described above (refer to section 2.13.1). Alternatively, parasites were treated with 50nM rapamycin until fixation. To enrich RHsCas9-CbEm-actin1-KO mutants for time-lapse microscopy, these parasites were cultured in DMEMcomplete supplemented with 2.5% dextran sulphate at 24h after induction. This was done to inhibit re-invasion of wild-type parasites.

Successful gene targeting by the respective gRNAs was confirmed by sequencing the predicted DNA cleavage site after rapamycin induction. For this purpose, RHsCas9 parasites were induced for 1h with 50nM rapamycin. After 48h, gDNA

was isolated from induced parasites and the predicted DNA cleavage sites were amplified by PCR. After sub-cloning into the pGEM®-T Easy vector (Promega), the cleavage sites were sequenced. The disruption of *Tgmec17* and *Tgsag1* genes was confirmed in clonal knock-out populations. The obtained sequences were compared to the predicted wild type sequence (*Tgadf*, *Tgactin1*, *Tgmec17* and *Tgsag1*) or to the non-induced strain (*Tgformin2*).

2.13.9 Egress Assay

Induced (50nM Rapamycin, 1h) and non-induced RHsCas9-CbEm parasites were grown for 48h. Egress was then induced by incubating parasites with 2 μ M A23187 for 5-8min under normal culturing conditions (refer to section 2.13.1). Subsequently, parasites were fixed with 4%PFA and IFA was performed as described above (refer to section 2.12.1).

2.14 Microscopy

2.14.1 Light microscopy

Fluorescent microscopy was performed on a DV Core microscope (AppliedPrecision, GE) attached to a CoolSNAP HQ2 CCD camera. Images were de-convolved with SoftWoRx Suite 2.0 (Applied Precision, GE). Images were processed with ImageJ (Schneider, Rasband, and Eliceiri 2012; Schindelin et al. 2012).

Super-resolution microscopy was conducted on an ELYRA PS.1 microscope (Zeiss). A Plan Apochromat 63 \times , 1.4 NA oil immersion lens was used together with a CoolSNAP HQ camera (Photometrics). Structure Illumination was achieved exploited ZEN Black software (Zeiss). Images were processed with ImageJ and Fiji (Schneider, Rasband, and Eliceiri 2012; Schindelin et al. 2012).

2.14.2 Time-lapse video microscopy for *Toxoplasma*

Conditional split-Cas9 strains were grown on fresh HFF cells for 72h as described above. Subsequently, parasites were mechanically lysed and inoculated on glass bottom dishes (MaTek) for another 24h. RH-GFP parasites were inoculated on glass bottom dishes (MaTek) for 24h. Prior to live microscopy, the DMEMcomplete culturing media was replaced with FluoroBrite DMEM media supplemented with 10% FBS, 2 mM L-glutamine and 25 mg/mL gentamycin. The dish was then transferred to the DV Core microscope (AppliedPrecision, GE) and maintained under standard culturing conditions (37°C, 5% CO₂). Images were taken at a speed of 10 frames per second using a 100x oil objective lens. Please note that the actual movie frame rate differs. Deconvolution was performed using SoftWoRx Suite 2.0 (Applied Precision, GE). Videos were processed with ImageJ and Fiji (Schneider, Rasband, and Eliceiri 2012; Schindelin et al. 2012).

2.15 Bioinformatics

2.15.1 Design of gRNAs for *Toxoplasma*

In this study, sgRNAs design was based on the available literature at the time. It was reported that a so-called seed sequence within the CRISPR/Cas9 target sequence is important for DNA cleavage. This seed sequence is located at the 3' region of the protospacer, adjacent to the crucial PAM motif (Gorski, Vogel, and Doudna 2017).

Jinek and co-workers provided data indicating that mutations within the seed sequence close to the PAM can interfere with CRISPR/Cas9 mediated cutting (Jinek et al. 2012). Further studies revealed that single-nucleotide mismatches up to 11bp upstream of the PAM sequence prevent CRISPR/Cas9-activity in mammalian cells (Cong et al. 2013). Yet another study supported the concept of a seed sequence by showing that mutations within the 12 nucleotides upstream of the PAM stopped DNA cutting by CRISPR/Cas9 (Jiang et al. 2013). The same study, however, also pointed out that only certain nucleotide exchanges prevent cleavage, depending on their position in the seed sequence. Mutations are more likely to terminate Cas9-mediated DNA cutting when they take place closer to

the PAM (Jiang et al. 2013). Outside the seed sequence, a number of 8 consecutive mismatches at the position 13-20 upstream of the PAM sequence was required to render the Cas9 nuclease ineffective (Jinek et al. 2012).

It was proposed that, after PAM recognition and binding, the Cas9-gRNA complex scans the protospacer seed sequence for its gRNA complementarity (Sternberg et al. 2014; Jiang et al. 2015). Sternberg and colleagues suggested that mismatches within the seed sequence would cause Cas9 to abort further target sequence interrogation (Sternberg et al. 2014). Importantly, the PAM was shown to be critical for target DNA cleavage by the *Streptococcus pyogenes* type II Cas9 system (Jinek et al. 2012). Jinek and co-workers suggested that this is because the PAM is required for CRISPR/Cas9 binding to the target DNA. The PAM sequence is NGG (Jinek et al. 2012).

Based on these findings, it was proposed that the lack of a PAM sequence adjacent to a potential genomic off-target sequence should prevent Cas9-mediated DNA cleavage (Jiang et al. 2013; Sternberg et al. 2014). In the presence of a PAM sequence, Jiang and co-workers suggested that multiple mutations in the seed sequence could protect from nuclease activity (Jiang et al. 2013). In *Toxoplasma*, two mismatches within the seed sequence dramatically decreased the gRNA efficiency (Shen et al. 2014).

As described previously for the CRISPR/Cas9 system in *Toxoplasma*, sgRNAs were designed to have a length of 20 nucleotides (Shen et al. 2014; Sidik et al. 2014, 2016; Sidik, Huet, and Lourido 2018). In addition, a leading “G” was added to the 5’ end when the complementary sgRNA sequence did not naturally start with a “G” (Sidik et al. 2016; Sidik, Huet, and Lourido 2018).

The observed findings described above were taken into account to avoid off-target gene disruption by the sgRNA-Cas9 complex. A newly designed sgRNA was only considered suitable for specific gene targeting if potential off-target sequences (1) lacked a complete PAM and/or (2) had at least one mismatch within the seed sequence defined as the 11bp adjacent to the PAM and/or (3) showed at least 8 mismatches outside the seed sequence.

To ensure the application of these guidelines, a two-step process was applied for the purpose of sgRNA design. First, sgRNAs were designed exploiting the

Eukaryotic Pathogen gRNA Design Tool (EuPaGDT) (Peng and Tarleton 2015). Settings were chosen to reflect the guidelines described above. Only sgRNAs predicted to have no off targets were accepted. Secondly, the accepted sgRNAs were blasted against the *Toxoplasma* genome and the Cb-Emerald sequence (if present in the genome) using NCBI BLAST (<https://blast.ncbi.nlm.nih.gov/Blast.cgi>) to manually check for potential off-targets.

2.15.2 Kymograph analysis

Colour-coded kymographs were generated by applying the ImageJ plugin “KymographClear” as described previously (Mangeol, Prevo, and Peterman 2016). In short, a track was defined on a maximum intensity image that was calculated from an image sequence (movie). A kymograph was then generated, depicting particle movement alongside the chosen track. Fourier filtering of the kymograph enables the distinction between forward-moving (red), backward-moving (green) and static (blue) particles.

Kymograph data was exported to the stand-alone software “KymographDirect” to generate time-averaged local intensity profiles (Mangeol, Prevo, and Peterman 2016). Intensity profiles depict Cb-Emerald or GFP intensity along the measured axis over the entire duration of the movie. Background corrections were performed for all imported kymographs.

2.15.3 Skeletonization analysis

Image sequences (movie) were skeletonized with the ImageJ plugin “Skeleton” (Schindelin et al. 2012). Prior to skeletonization, thresholding was performed on the movie stacks to create binary images. These binary images were then used for skeletonization. Skeletonized images in this study represent collapsed t-stacks.

3 Establishment of a novel conditional CRISPR/Cas9 system for reliable gene disruption in *Toxoplasma*

The overall aim of this thesis is to gain insights into actin factors and dynamics in the apicomplexan parasite *Toxoplasma gondii* by exploiting the recently introduced Chromobody technology for actin visualization (Periz et al. 2017). This endeavour will require the generation of several strains and, eventually, shall initiate a medium throughput screen to identify potentially novel actin binding proteins. Therefore, initial experiments of this study will focus on establishing a reliable and rapid CRISPR/Cas9-based methodology that allows investigation of genes on a screening scale.

Prior to this study, CRISPR/Cas9 systems had been established successfully for genome modification in *Toxoplasma*. Single target gene disruption and site-specific insertions were achieved (Shen et al. 2014; Sidik et al. 2014). CRISPR/Cas9 also enabled genome-wide screening leading to the discovery of novel fitness-conferring apicomplexan genes (Sidik et al. 2016; Sidik, Huet, and Lourido 2018). In addition, a conditional nuclear Cas9 fused to ddFKBP was introduced and applied to identify factors involved in the nuclear export of RNA (Serpeloni et al. 2016).

Despite significantly advancing the understanding of *Toxoplasma* biology, CRISPR/Cas9 systems are also associated with certain challenges. For instance, data suggest that constitutive or prolonged Cas9 expression negatively impacts parasite fitness (Sidik et al. 2016; Serpeloni et al. 2016; Markus et al. 2019). Transient Cas9 expression was suggested to cause aberrant mitochondria morphology (Lacombe et al. 2019). Furthermore, disruption of non-essential genes was reported to sometimes result in parasites displaying aberrant morphology (Serpeloni et al. 2016). Finally, the conditional Cas9-ddFKBP system appears to suffer from background activity leading to undesired disruption of the target gene in the parental strain (Dr Elena Jimenez-Ruiz, unpublished data).

Since actin is highly crucial for the lytic cycle of *Toxoplasma* (Andenmatten et al. 2013; Egarter et al. 2014), a conditional gene disruption system is advantageous for investigating potentially essential actin dynamic factors. Therefore, I aimed at further exploring the potential of conditional CRISPR/Cas9

systems in *Toxoplasma* research. To circumvent reported issues with previous systems, I chose to establish the conditional split-Cas9 system that had recently been described in mammalian cells (Zetsche, Volz, and Zhang 2015) (**Figure 3-1**). In this rapamycin-inducible system, the Cas9 enzyme is split into two sub-units (N- and C-terminus) which are fused to a FKBP or FRB domain. Split-Cas9 activity was reported to be tightly regulated due to spatial separation of the Cas9 N- and C-terminus which are linked to a nuclear localisation sequence (NLS) or nuclear export signal (NES). In addition, the re-assembled split-Cas9 enzyme possesses decreased nuclease activity compared to the wild-type Cas9 enzyme. This aspect might be beneficial for parasite tolerance towards prolonged Cas9 presence within the cell.

In this chapter, I will present results that illustrate split-Cas9 functionality and shed further light on the advantages and disadvantages of CRISPR/Cas9-based gene analysis in *Toxoplasma*.

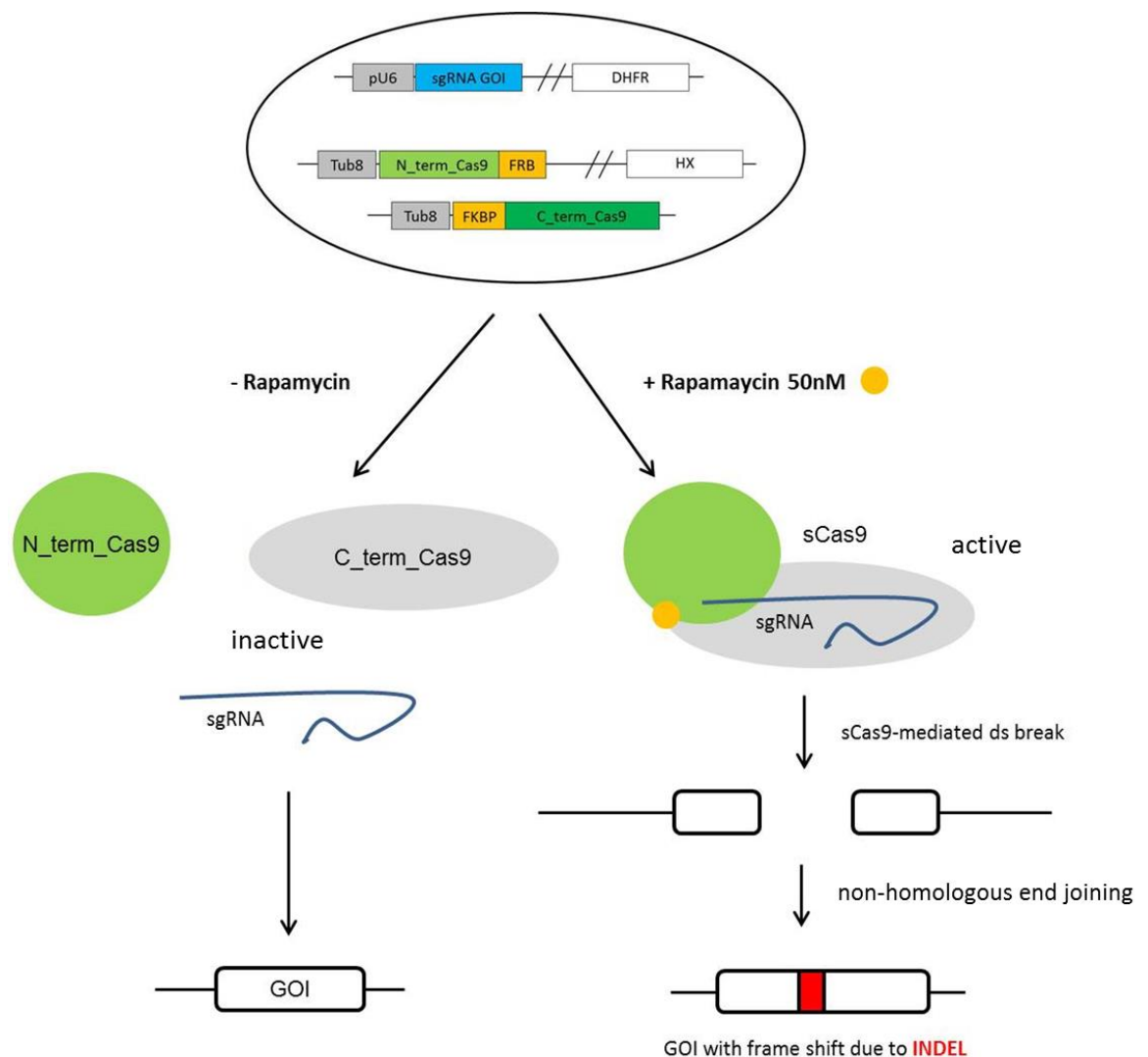


Figure 3-1: Schematic depicting the split-Cas9 system in *Toxoplasma*

Please see page 90 for the schematic. Parasites are expressing the two split-Cas9 sub-units together with a single-guide RNA (sgRNA). The system remains inactive in the absence of rapamycin. Activation of split-Cas9 by reassembly of the sub-units results in gene disruption due to insertion or deletion of nucleotides (INDELS).

3.1 Proof of Principle I: Targeting *Tggap40* with split-Cas9

To verify functionality of split-Cas9 in *Toxoplasma*, I chose to target the essential *Tggap40* gene (Harding et al. 2016). This decision was based on the severe and very distinguishable phenotype that is caused by loss of *Tggap40* gene function (Harding et al. 2016). In addition, *Tggap40* had previously been exploited as a successful proof of principle target for CRISPR/Cas9 systems (Serpeloni et al. 2016).

For this purpose, I decided to adapt the split 4 variant of the split-Cas9 system (Zetsche, Volz, and Zhang 2015). A parasite line coding for the two split-Cas9 sub-units (RHsCas9), a parasite expressing a *gap40*sgRNA (RH-gap40) and a line that encoded the two split-Cas9 units together with the *gap40*sgRNA (RHsCas9-gap40) were created (**Figure 3-1 and 3-2**). The *gap40*sgRNA plasmid and the split-Cas9 sub-units were randomly integrated into the parasite genome. Integration was confirmed by analytical PCR amplifying specific plasmid DNA sequences present in successfully transfected parasites, but not the parental strains (**Figure 3-2**).

Upon rapamycin treatment, a *gap40* phenotype as described in the literature (Harding et al. 2016) was observed in up to 95% of RHsCas9-gap40 parasites, but not in RH-gap40 or RHsCas9 parasites (**Figure 3-3**). Induced RHsCas9-gap40 parasites showed a lack of TgGAP40 protein in IFA, indicating that the *Tggap40* gene was successfully disrupted by the split-Cas9 system (**Figure 3-3 A**). No difference in *Tggap40* gene disruption efficiency was detected when RHsCas9-gap40 parasites were treated with rapamycin for 1h or 48h (**Figure 3-3 B**). About 10% of non-induced RHsCas9-gap40 parasites displayed a partial *gap40* phenotype, potentially hinting towards a certain degree of split-Cas9 background activity (**Figure 3-3 A and B**).

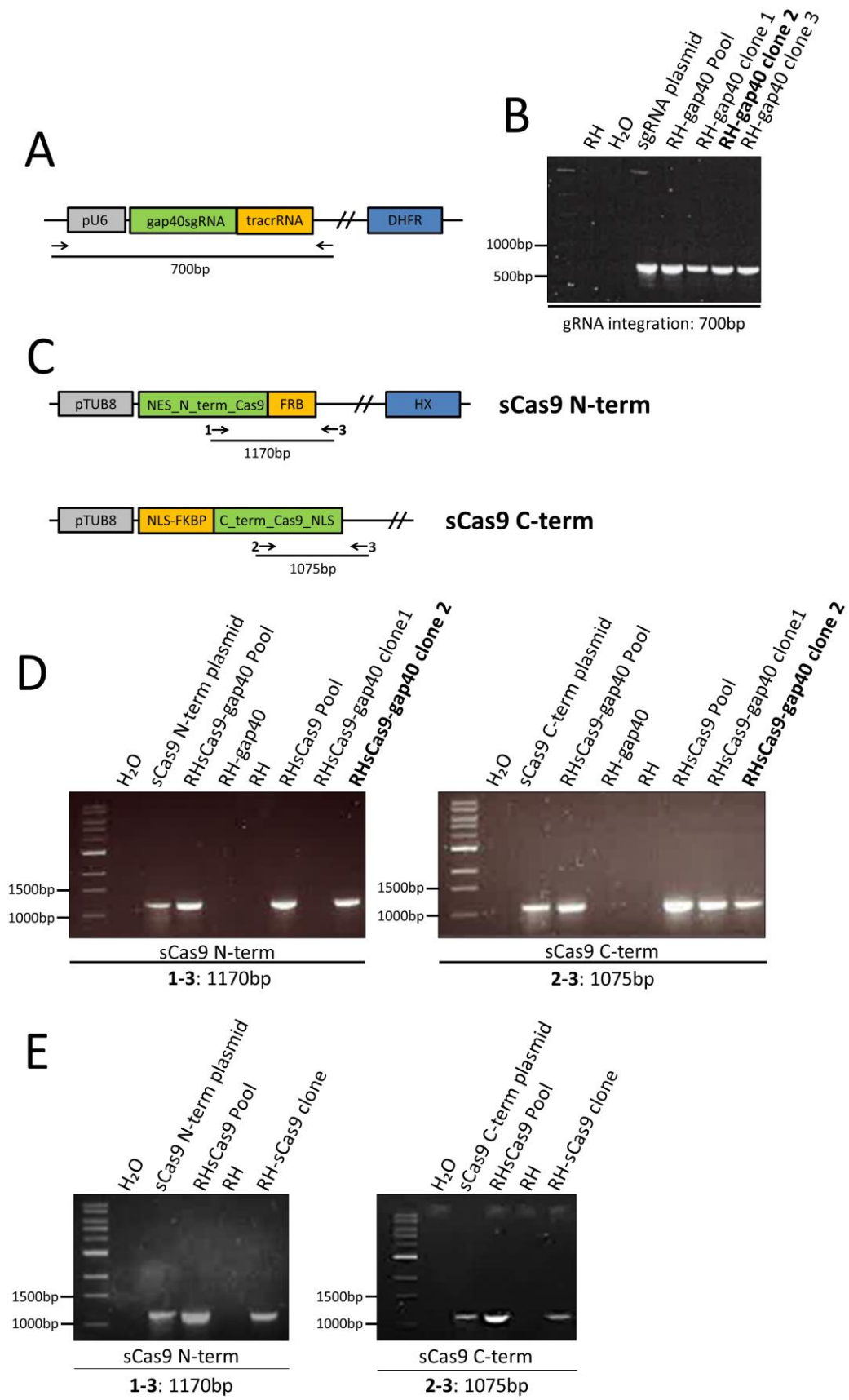


Figure 3-2: Generation of RH-gap40sgRNA (RH-gap40), RHsplit-Cas9-gap40sgRNA (RHsCas9-gap40) and RHsplit-Cas9 (RHsCas9) parasites

Figure 3-2 continued: **(A)** Plasmid coding for the *gap40* single-guide gRNA (sgRNA). This plasmid was universally used for sgRNA expression in this thesis. Arrows indicate PCR amplicon for verification of plasmid integration (see (B)). **(B)** Analytical PCR confirming integration of sgRNA-plasmid into the parasite genome. **(C)** Plasmids coding for the N- and C-terminus of the Cas9 enzyme (split 4 variant). Arrows indicate PCR amplicon for verifying plasmid integration (see (D)). **(D)** Analytical PCR confirming integration of split-Cas9 plasmids into the genome of RH-*gap40* parasites. **(E)** Analytical PCR confirming of integration of split-Cas9 plasmids into the RH parasites. If more than one clonal line was obtained, the one used for further experiments in this study is highlighted.

Interestingly, Cas9-mediated *Tggap40* disruption impacts nuclear replication as nuclei appear to be heavily deformed and, potentially, not properly divided (**Figure 3-3 A**). Depletion of *Tggap40* was reported to have no effect on nuclear replication (Harding et al. 2016). Although data presented by Harding and colleagues would suggest some impact of *Tggap40* loss on the morphology of single nuclei, nuclear division in general seems unaffected. Due to the detrimental effect of *Tggap40* loss on the overall parasite fitness and morphology, it is difficult to finally conclude whether these observations represent a secondary effect of *Tggap40* loss or a potential artefact caused by split-Cas9 expression or activity.

Since reports have been made about negative effects of Cas9 on *Toxoplasma* (Sidik et al. 2016; Serpeloni et al. 2016; Lacombe et al. 2019), I decided to further analyse the effect of (split-)Cas9 expression and activity on parasite fitness. I chose to target the genes *Tgsag1* (refer to sections 3.2 - 3.4) and *Tgmec17* (refer to section 3.5) with the spit-Cas9 system. The major tachyzoite surface protein TgSAG1 is considered to be dispensable for parasite survival (Kim and Boothroyd 1995; Lekutis et al. 2001). *TgMec17* acts as an α -tubulin acetyltransferase in *Toxoplasma* and was suggested to be important for nuclear division (Varberg et al. 2016). I hypothesized that these two genes could be exploited to further investigate the impact of Cas9-based systems on nuclear morphology and replication.

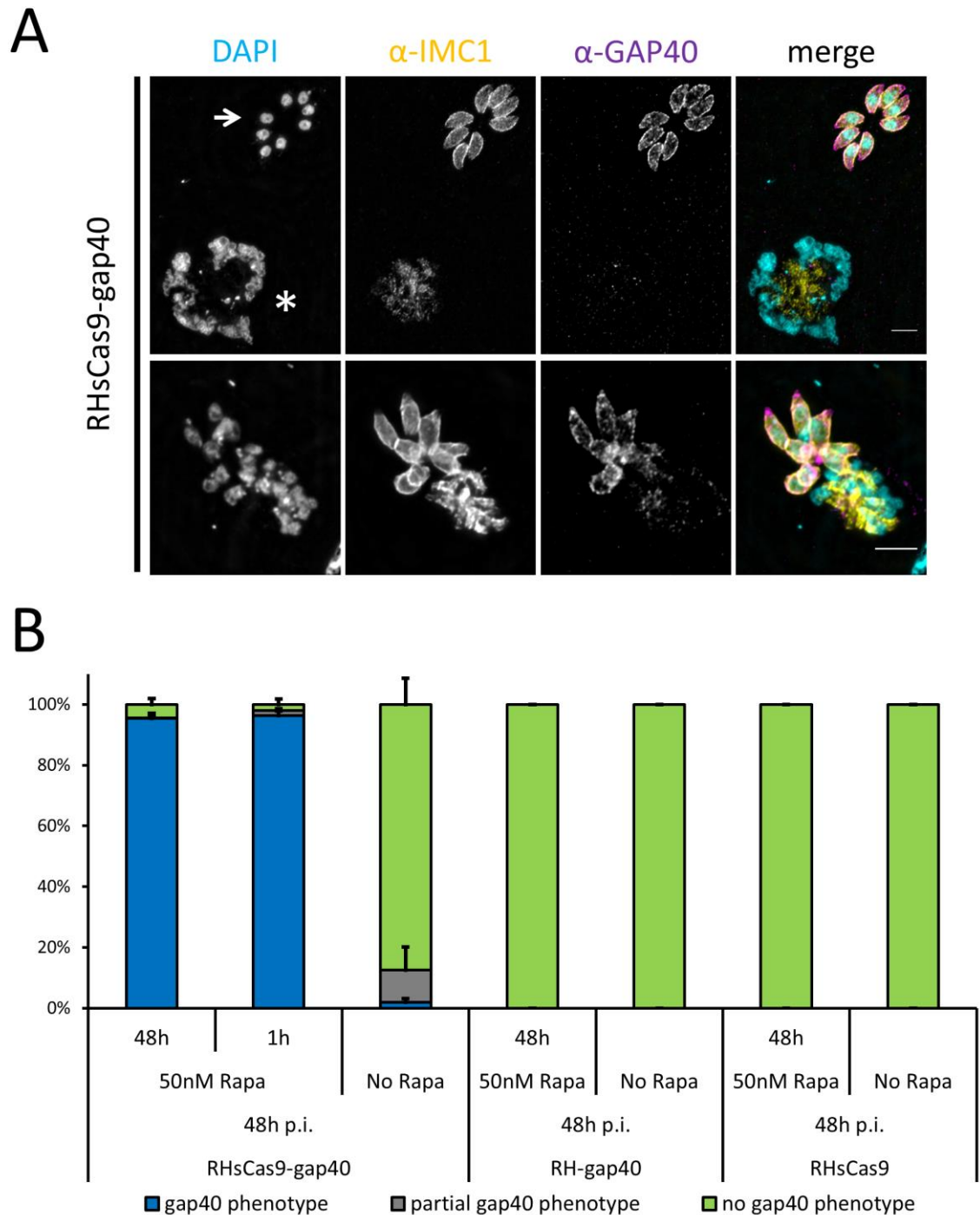


Figure 3-3: IFA analysis and quantification of the gap40 phenotype observed in the strains RHsCas9-gap40, RH-gap40 and RHsCas9 upon Rapamycin treatment

(A) IFA depicting the three phenotypes observed in this experiment: the gap40 phenotype with collapsed IMC and loss of GAP40 expression (top panel, asterisk); a partial gap40 phenotype where only parts of the vacuole show a collapsed IMC and loss of GAP40 signal (bottom panel); and wild type parasites with normal IMC and GAP40 localisation (top panel, arrow). Images show RHsCas9-gap40 parasites that were treated with 50nM rapamycin for 48h. Parasites were grown for a total of 48h and fixed with 4%PFA. IFA analysis was performed using α -GAP40 and α -IMC antibodies. Nuclei were stained with DAPI. Scale bars are 5 μ m. **(B)** Quantification of gap40 phenotypes in different strains 48h post inoculation (p.i.). Only parasites expressing both, the gap40sgRNA and the split-

Cas9 system, presented a gap40 phenotype after rapamycin treatment. Parasites were treated with rapamycin for 1h or the whole growth period of 48h as indicated. Data represents three independent experiments. For each condition 100 vacuoles were counted (total n=300).

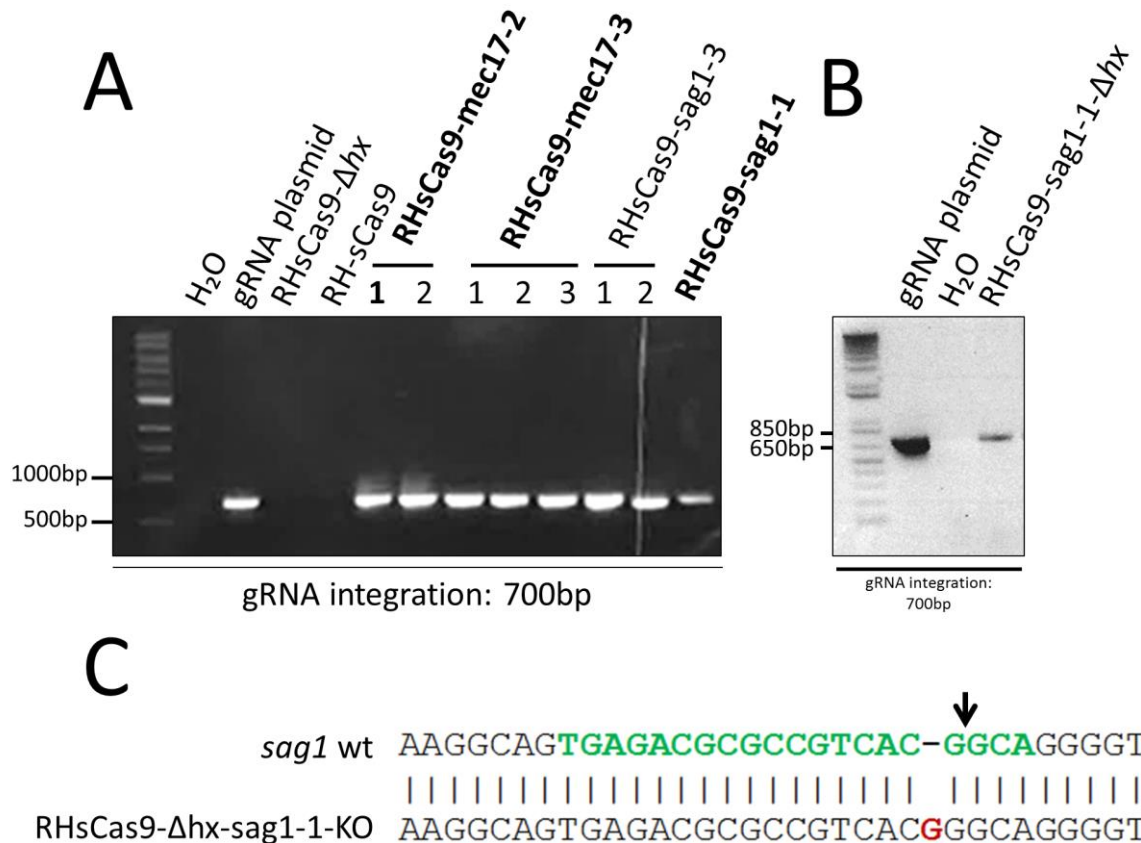


Figure 3-4: Generation of strains RHsCas9-sag1sgRNA1 (RHsCas9-sag1-1), RHsCas9sag1sgRNA3 (RHsCas9-sag1-3), RHsCas9-mec17sgRNA2 (RHsCas9-mec17-2), RHsCas9-mec17sgRNA3 (RHsCas9-mec17-3) and RHsCas9-Δhx-sag1sgRNA1 (RHsCas9-Δhx-sag1-1)

(A) Analytical PCR confirming integration of indicated sgRNA-plasmids into the parasite genome. (B) Analytical PCR confirming integration of the sag1sgRNA1 plasmid into the genome of RHsCas9-Δhx parasites. For (A) and (B), integrated plasmids were amplified from the genome as described in Figure 3-2 A. (C) Genome sequencing performed for the clonal RHsCas9-Δhx-sag1-1-KO mutant. Green letters indicates sgRNA sequence. Red letters represent nucleotide insertion in the mutant strain, causing a frame shift and, thus, the functional knock-out of the *Tgsag1* gene. The black arrow indicates the predicted cut side. Please note that data presented in parts (B) and (C) of this figure were generated by Mr Matthew Gow.

3.2 Proof of Principle II: Targeting *Tgsag1* with split-Cas9

Since loss of *Tgsag1* gene function is not linked to any detrimental effects in *Toxoplasma* (Kim and Boothroyd 1995; Lekutis et al. 2001), I argued that disruption of *Tgsag1* with split-Cas9 should have no measureable effects on the morphology and behaviour of the parasite. To investigate this, split-Cas9 parasites were stably transfected with the *sag1sgRNA1* to generate RHsCas9-*sag1sgRNA1* (RHsCas9-*sag1*-1) parasites (**Figure 3-4 A**). When treated with rapamycin for 1h or 48h, RHsCas9-*sag1*-1 parasites lost their SAG1 signal in IFA, strongly suggesting *Tgsag1* gene disruption (**Figure 3-5 A**). Strikingly, 54% (± 6.1) and 52.3% (± 2.1) of parasites showed aberrant nuclei and morphology in addition to TgSAG1 loss after 1h and 48h rapamycin induction time, respectively (**Figure 3-5 A and B**). This phenotype was only present in rapamycin-treated parasites expressing split-Cas9 together with the *sag1sgRNA1*. No impact on parasites morphology was observed in non-induced RHsCas9-*sag1*-1 parasites or RHsCas9 parasites (cultured with or without rapamycin present).

To further understand the occurrence of aberrant parasites, I induced RHsCas9-*sag1*-1 parasites for 1h with rapamycin and mechanically lysed the parasites after 48h of growth. These parasites were then inoculated again (without rapamycin) and fixed for IFA after 48h, thus representing the 2nd lytic cycle (2nd generation) of parasites after rapamycin induction. The number of parasites with aberrant nucleus and cellular morphology was comparable to the background seen in non-induced RHsCas-*sag1*-1 parasites (**Figure 3-5 B**). About 79% (± 4.8) of 2nd generation parasites were TgSAG1 negative in IFA and displayed a normal nucleus and cell morphology.

A TgSAG1 negative clonal line (RHsCas9-*sag1*-1-KO) was created by inducing RHsCas9-*sag1*-1 parasites and, subsequently, cloning them out by serial dilution. These parasites displayed normal nuclear and cellular morphology while TgSAG1 could not be detected by IFA. In addition, another sgRNA targeting the *Tgsag1* gene (*sag1sgRNA3*) was stably transfected into RHsCas9 parasites (**Figure 3-4 A**). This was done to exclude sgRNA off-targets as a reason for the detrimental effect on parasites appearance. The obtained clonal lines of RHsCas9-*sag1*-3 parasites displayed highly similar behaviour upon rapamycin treatment (**Table 3-1**).

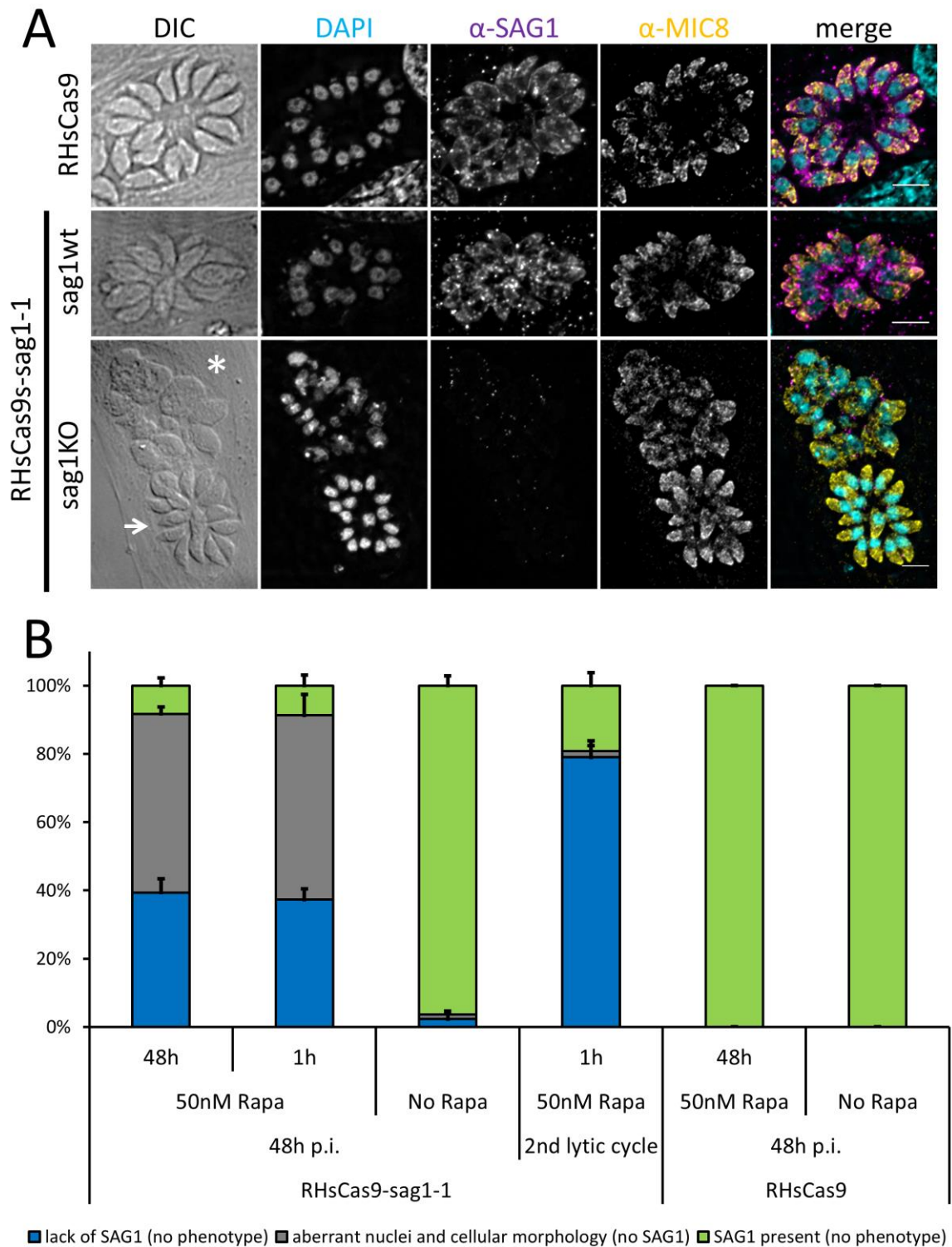


Figure 3-5: IFA analysis and quantification of *Tgsag1* disruption with split-Cas9

(A) IFA depicting the three phenotypes observed in this experiment: healthy vacuoles with SAG1 expression on the parasite surface (top and middle panel); healthy vacuoles lacking SAG1 expression (bottom panel, arrow); and parasites lacking SAG1 while displaying aberrant nuclei and cellular morphology (bottom panel, asterisk). Images show the strains RHsCas9 and RHsCas9-sag1-1. RHsCas9-sag1-1 parasites were treated with 50nM Rapamycin for 48h. Parasites were grown for a total of 48h and fixed with 4%PFA. IFA analysis was performed using α -SAG1 and α -MIC8 antibodies. Nuclei were stained with

DAPI. Scale bars are 5 μ m. **(B)** Quantification of the phenotypes 48h post inoculation (p.i.) as described in (A). Aberrant nuclei and cellular morphology was observed only when *sag1* was disrupted (KO) by split-Cas9 activation. Abundance of non-healthy parasites was reduced to background levels when induced RHsCas9-*sag1*-1 parasites were mechanically lysed, transferred onto fresh host cells and grown again for 48h in this second lytic cycle (total incubation of 96h). Parasites were treated with rapamycin for 1h or the whole growth period of 48h as indicated. Data represent three independent experiments. For each condition 100 vacuoles were counted (total n=300).

Table 3-1: Phenotypic characterisation of the lines RHsCas9-*sag1*-3 clone1 and 2

Numbers were obtained by analysing IFA results. IFAs were conducted as described in **Figure 3-5**. The asterisk (*) indicates vacuoles that lack *TgSAG1* signal and display aberrant nuclei and cellular morphology.

	Rapamycin	SAG1	lack of SAG1	lack of SAG1*	# vacuoles
RHsCas9- <i>sag1</i> -3 clone 1	50nM (1h)	7	31	62	100
	50nM (48h)	4	35	61	100
	none	99	1	0	100
RHsCas9- <i>sag1</i> -3 clone 2	50nM (1h)	7	36	57	100
	50nM (48h)	4	45	51	100
	none	100	0	0	100

Data obtained so far suggest that the observed abnormalities occur within the 1st lytic cycle after split-Cas9 activation. To the author's knowledge no conditional *Tgsag1* knock-out mutant has been described to this point. Therefore, three hypotheses might explain the phenomenon in question. For one, the affected nuclear and cellular morphology might represent a *sag1*-specific phenotype that only half of the parasites lacking *TgSAG1* are able to overcome. Another explanation could be that the double stranded break caused by split-Cas9 is causing the described effects. Finally, the sgRNA/split-Cas9 complex might cause the aberrant appearance independently of DNA cutting.

3.3 Investigating the effect of split-Cas9 activation on *Toxoplasma* I: *TgSAG1* complementation studies

To finally clarify what causes the aberrant appearance of the nucleus and overall cellular morphology in the 1st lytic cycle after split-Cas9 induction, a *TgSAG1*

negative strain (RHsCas9-sag1-1-KO) was complemented with an additional *Tgsag1** gene that was modified to prevent the sag1sgRNA1 from cutting (**Figure 3-6 A**). In addition, the mutated *Tgsag1** gene was also introduced into *TgSAG1* positive parasites (RHsCas9-sag1-1-wt) (**Figure 3-6 A**). Since both lines were generated in the RHsCas9-sag1-1 background, they expressed the split-Cas9 components and sag1sgRNA1.

The strain RHsCas9-sag1-1-sag1KO-sag1* should have no valid target for the sag1sgRNA as the endogenous gene had already been mutated due to previous split-Cas9 activation and the modified *sag1* version was altered to prevent sgRNA recognition. RHsCas9-sag1-1-sag1wt-sag1* parasites still coded for the original version of the endogenous gene and, thus, presented one valid sag1sgRNA target.

To generate both strains, the *hx* gene in RHsCas9 parasites was disrupted to generate RHsCas9- Δ hx parasites. These parasites were transfected with sag1sgRNA1 (**Figure 3-4 B**). Subsequently, the stable RHsCas9- Δ hx-sag1-1 line was induced and cloned out to obtain a *TgSAG1* negative clonal line (RHsCas9- Δ hx-sag1-1-sag1KO). Disruption of the endogenous *Tgsag1* gene was confirmed by sequencing (**Figure 3-4 C**). Re-generation of an *hx* deficient *TgSAG1* negative line was necessary to allow insertion of the modified *Tgsag1* gene resulting in the strain RHsCas9- Δ hx-sag1-1-sag1KO-sag1*. As described above, this strain should not have any valid sag1sgRNA target. In both gene copies (*Tgsag1* and *Tgsag1**), the target site is mutated either due to previous Cas9-mediated cutting (endogenous *Tgsag1*) or due to design (*Tgsag1**). The mutated *Tgsag1** gene was also introduced into the non-induced RHsCas9- Δ hx-sag1-1 strain, thus generating RHsCas9- Δ hx-sag1-1-sag1wt-sag1* parasites. This strain encodes two *Tgsag1* versions (*sag1wt* and *sag1**) from which only the endogenous *Tgsag1* should be cut by the sag1sgRNA1.

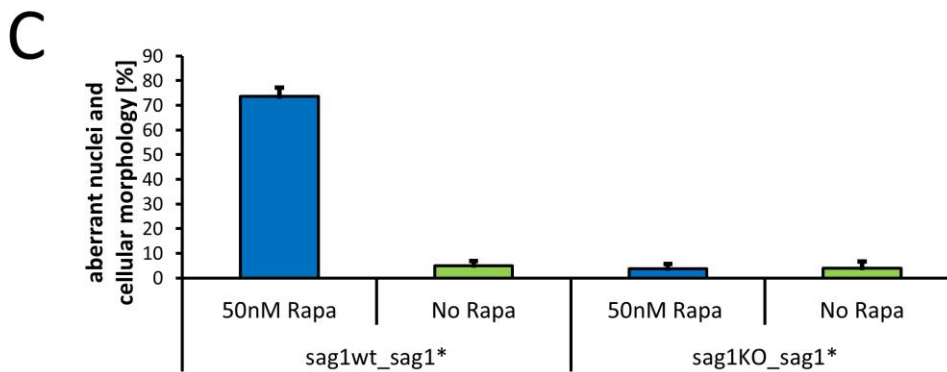
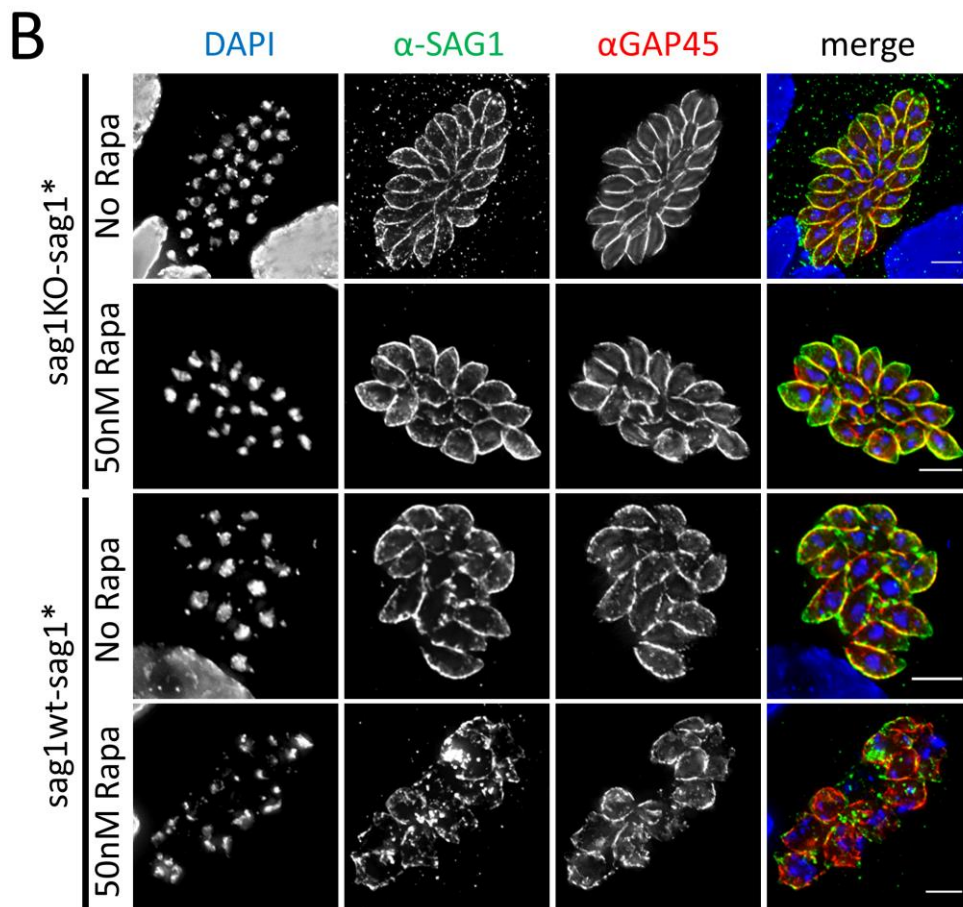
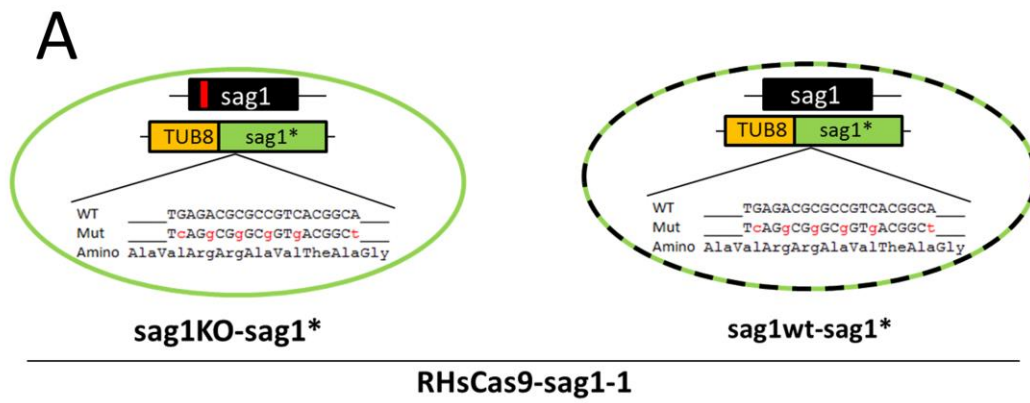


Figure 3-6: Effect of split-Cas9 activation in parasites encoding an additional copy of the *sag1* gene

(A) Schematic depiction of the strains *sag1KO-sag1** and *sag1wt-sag1**. Both strains were generated in the RHsCas9-*sag1-1* background and, thus, express split-Cas9 and the *sag1sgRNA1*. The endogenous *Tgsag1* gene in the *sag1KO-sag1** line had been disrupted by prior split-Cas9 activation (refer to Figure 3-4 C). The endogenous *Tgsag1* gene of *sag1wt-sag1** is still intact. Both lines express an additional *sag1* copy that has been modified as indicated to be resistant to *sag1sgRNA1* recognition. **(B)** IFA depicting the impact of split-Cas9 activation on *sag1KO-sag1** and *sag1wt-sag1** parasites. Parasites were induced with 50nM rapamycin for 1h or in the absence of rapamycin. Parasites were grown for a total of 48h and fixed with 4%PFA. IFA analysis was performed using α -SAG1 and α -GAP45 antibodies. Nuclei were stained with DAPI. Scale bars are 5 μ m. **(C)** Quantification of vacuoles displaying aberrant nuclei and cellular morphology after split-Cas9 activation at 48h post inoculation. High abundance of vacuoles displaying aberrant nuclei and cellular morphology were observed upon rapamycin treatment only in the *sag1wt-sag1** strain. Levels of aberrant parasites did not increase in *sag1KO-sag1wt* parasites compared to the non-induced population. Data represent three independent experiments. For each condition at least 100 vacuoles were counted (total $n \geq 300$). Please note that data shown in this figure were generated by Mr Matthew Gow.

When RHsCas9- Δ hx-*sag1-1-sag1KO-sag1** parasites were induced with rapamycin, parasites did not display any abnormalities and did not lose *TgSAG1* on the surface (**Figure 3-6 B and C**). This confirms that the mutated copy of *Tgsag1* (*sag1**) cannot be cut by Cas9 and that *TgSAG1* remains on the parasites surface. It also suggests that the sheer assembly of the sgRNA/split-Cas9 complex without having a valid target has no impact on parasites fitness. Split-Cas9 activation in parasites coding for the non-disrupted endogenous *Tgsag1* gene and the mutated *Tgsag1** gene (RHsCas9- Δ hx-*sag1-1-sag1wt-sag1**) caused the parasites to display the nuclear phenotype while still showing SAG1 on their surface (**Figure 3-6 B and C**).

In sum, this data indicate that aberrant nuclei and morphology in parasites do not represent a *sag1*-specific phenotype. This is because parasites still express *TgSAG1* on their surface. Split-Cas9 is able to cut the endogenous copy of *Tgsag1*, but not the mutated version. If the aberrant phenotype was due to *TgSAG1* loss on the surface, no phenotype should have been observed in RHsCas9- Δ hx-*sag1-1-sag1wt-sag1** parasites. Instead these results strongly indicate that the nuclear phenotype is most likely linked to Cas9-mediated DNA cutting since it only occurs in parasites after a double stranded break has been introduced into their genome by Cas9.

I confirmed this observation with RHsCas9-lacZsgRNA (RHsCas9-lacZ) parasites (**Figure 3-7 A**). The lacZsgRNA targets an exogenous sequence and, therefore, has no predicted target in the *Toxoplasma* genome. Upon split-Cas9 activation, no aberrant parasites were observed (**Figure 3-7 B**). The same results had been obtained previously for the ddFKBP-Cas9 system (Serpeloni et al. 2016). This suggests that the aberrant phenotype is caused by Cas9-mediated double-strand breaks (DSBs) in genomic DNA.

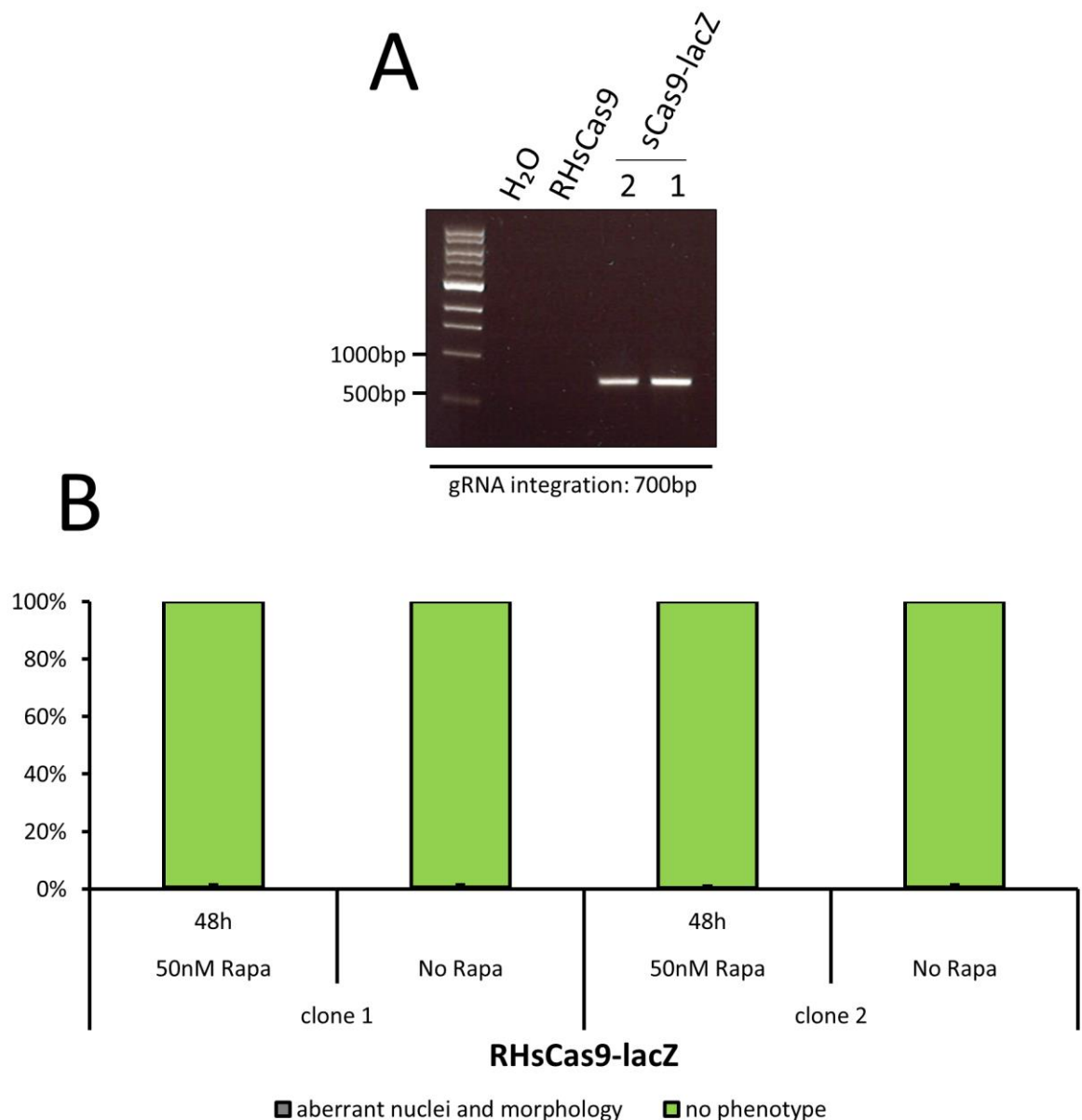


Figure 3-7: Effect of split-Cas9 activation in parasites encoding a lacZsgRNA
(A) Analytical PCR confirming integration of lacZsgRNA into the parasite genome. Integrated plasmids were amplified from the genome as described in Figure 3-2 A. **(B)** Quantification of vacuoles displaying aberrant nuclei and cellular morphology upon treatment with 50nM rapamycin for 48h. Parasites were fixed at 48h post inoculation.

Split-Cas9 activation did not cause aberrant nuclei or morphology in RHsCas9-lacZsgRNA (RHsCas9-lacZ) parasites. Data represents three independent experiments. For each condition at least 100 vacuoles were counted (total n=300). Please note that the RHsCas9-lacZsgRNA strains were generated by Marleen Büchler under the supervision from Dr Elena Jimenez-Ruiz. Experiments shown in this figure represents my own work.

3.4 Investigating the effect of split-Cas9 activation on *Toxoplasma* II: Disruption of *Tgsag1* in RH vs RH Δ ku80 parasites

Since introduction of DNA DSBs appear to be required for the aberrant nuclei and morphology to emerge, I argued that the observed phenotype might be the consequence of unrepaired DNA damage. To test this hypothesis, RH Δ ku80 parasites were transiently transfected with a plasmid coding for Cas9-YFP and the sag1sgRNA2. The RH Δ ku80 strain lacks the *ku80* gene which has been reported to be important in non-homologous end joining (NHEJ), a process that allows eukaryotes to repair DSBs their genomes (Critchlow and Jackson 1998). I hypothesized that RH Δ ku80 parasites should not be able to repair the Cas9-mediated double strand break and display the aberrant phenotype as response to Cas9 activity. Indeed, 99.15% (\pm 1.5) of transfected RH Δ ku80 parasites displayed the aberrant nuclei and morphology (**Figure 3-8**).

In comparison, 53.8% (\pm 14%) of RH parasites appeared aberrant when transiently transfected with the Cas9-YFP-sag1sgRNA2 plasmid. 40.5% (\pm 11.1) of RH parasites were TgSAG1 negative and did not show any morphological defect (**Figure 3-8**). Thus, the RH strain showed very similar behaviour to the RHsCas9-sag1-1 strain upon split-Cas9 activation. This strongly indicates that the described aberrant effects are not split-Cas9 specific, but a general CRISPR/Cas9 phenomenon.

The fact that the lack of the *ku80* gene makes *Toxoplasma* more susceptible to displaying the aberrant phenotype indicates that proper DNA repair is vital for recovery from the effects of Cas9 activity. Hence, aberrant nuclei and morphology are most likely the result of parasites failing to repair the Cas9-mediated DNA damage.

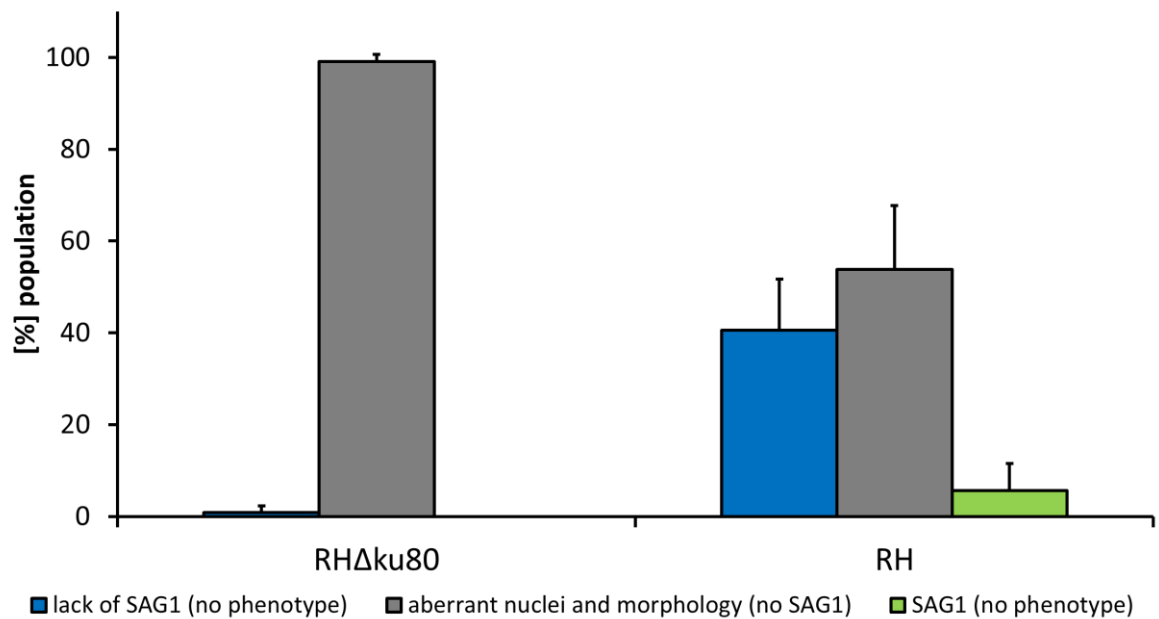


Figure 3-8: Disruption of *Tgsag1* in RH and RHΔku80 parasites

RH and RHΔku80 parasites were transiently transfected with a Cas9-YFP-sag1sgRNA2 plasmid. Parasites were fixed 48h after transfection with 4%PFA and IFA analysis was performed to allow for subsequent quantification. Only parasites that had been transfected successfully were counted. Transfected parasites were identified by YFP signal (Cas9-YFP) in the nucleus or loss of SAG1. Data represents three independent experiments. Transfection efficiencies were 21.5% (± 4.8) for RHΔku80 and 13.2% (± 3.6) for RH parasites. Total n=129 (RHΔku80), total n=79 (RH). Please note that data shown in this figure were generated by Dr Elena Jimenez-Ruiz.

3.5 A case study: Disruption of *TgMec17*-mediated tubulin acetylation via the split-Cas9 and DiCre systems

In 2010, two research groups independently reported α -tubulin acetyltransferase 1 (Mec17, also named α TAT1) to specifically mediate α -tubulin acetylation at lysine (K) 40 in a variety of eukaryotic organisms (Akella et al. 2010; Shida et al. 2010). Recently, this enzyme was also described to be responsible for acetylation of lysine 40 of α -tubulin in *Toxoplasma* (Varberg et al., 2016). Varberg and co-workers further reported that acetylation of α -tubulin at the lysine 40 residue is essential for asexual replication in culture. Cas9-mediated disruption of *Tgmec17* led to the lack of acetylation and to deformed and fragmented nuclei within the first generation of parasites after transient Cas9-mediated DNA cutting.

The phenotype described by Varberg and colleagues highly resembled the aberrant nuclei caused by Cas9-activity as described above. To clarify whether the nuclear replication phenotype was specific to *Tgmec17* loss of function or caused by Cas9 activity, I decided to target the *Tgmec17* gene with two independent conditional systems, namely the split-Cas9 system and the DiCre system (Andenmatten et al. 2013). For this purpose, the RHsCas9-mec17sgRNA2 (RHsCas9-mec17-2) line was generated (**Figure 3-4 A**). In addition, an RH Δ ku80-DiCre-Pfmec17loxP strain, that I had created prior to my thesis studies (Stortz 2014, Master thesis, Ruprecht-Karls-University of Heidelberg), was used for experiments. In this strain the endogenous *Tgmec17* gene was replaced by the *P. falciparum* (*Pf*) *mec17* orthologue flanked with loxP sites as described previously by Andenmatten et al. (Andenmatten et al. 2013). This was done because amplification of the full *Tgmec17* cDNA was not possible.

After split-Cas9 activation with 50nM rapamycin for 48h, 40.3% (\pm 12.7) of vacuoles showed a lack of acetylated α -tubulin at the lysine 40 residue without displaying any abnormalities (**Figure 3-9**). In some parasites (16% [\pm 5.2]), the absence of α -tubulin acetylation was accompanied with aberrant nuclei and cell morphology. Highly similar results were obtained when parasites were induced for only 1h or when *Tgmec17* was targeted with a different sgRNA (RHsCas9-mec17-3) (**Table 3-2; Figure 3-4 A**).

In addition, I induced RHsCas9-mec17-2 parasites and cloned them out by serial dilution to obtain five independent clonal lines. All lines lacked α -tubulin acetylation. In only two lines 1% of vacuoles showed morphological defects, while no abnormalities could be observed in the other lines (**Figure 3-10 C**). Exemplarily, the sgRNA region was sequenced for one of the clonal lines revealing a frame shift in the *Tgmec17* gene (**Figure 3-10 B**).

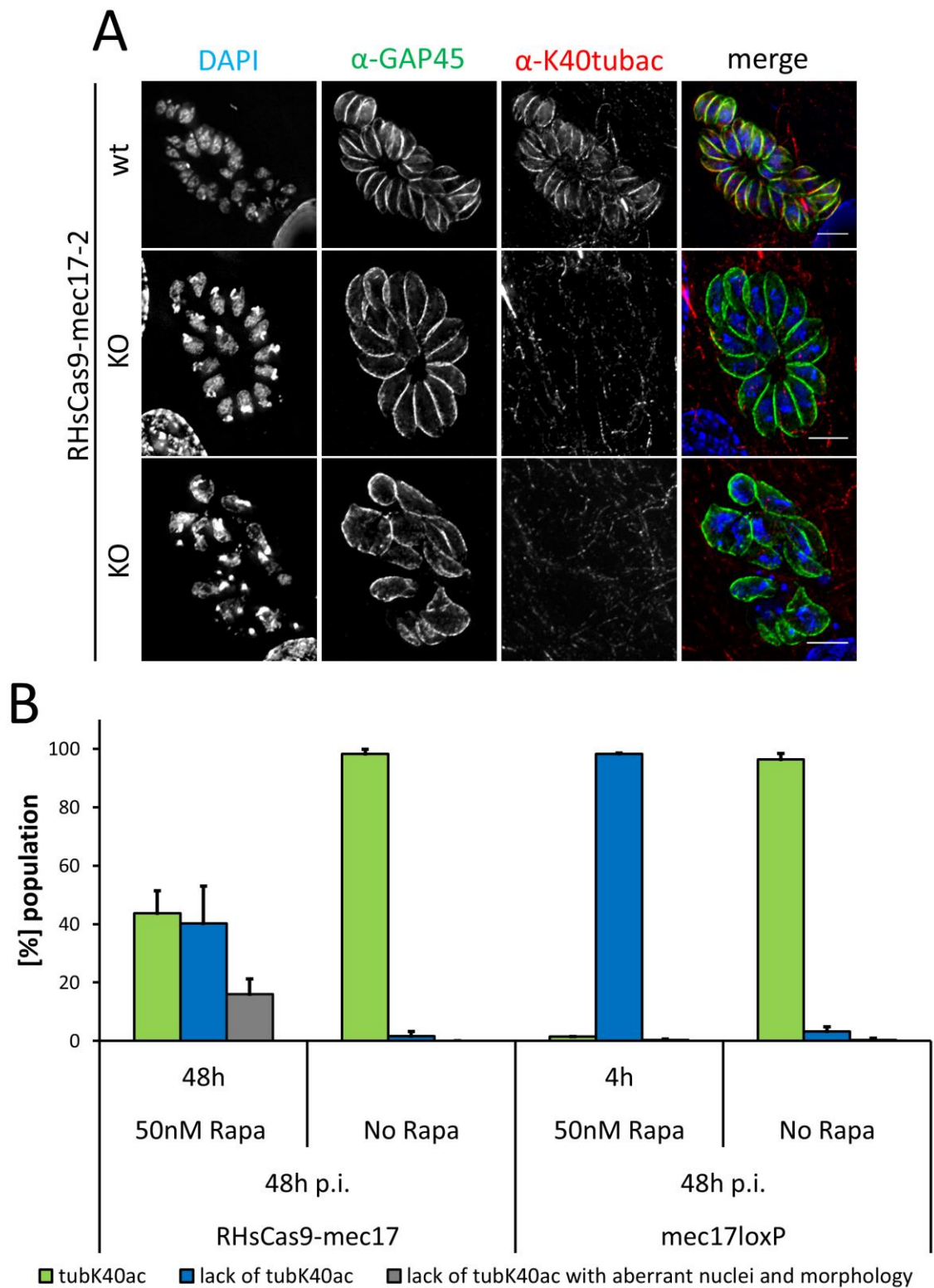


Figure 3-9: Effect of *Tgmec17* gene function loss in DiCre and split-Cas9 parasites

(A) IFA depicts α -tubulin acetylation at lysine (K) 40 (K40tubac) in RHsCas9-mec17-2 (wt) and RHsCas9-mec17-2-KO (KO) parasites. Acetylation of α -tubulin K40 was lost upon *mec17* gene disruption. In some vacuoles, loss of acetylation was associated with aberrant nuclei and morphology (bottom panel). Other vacuoles appeared healthy (middle

panel). Parasites were incubated in the presence or absence of 50nM rapamycin for 48h. Parasites were then fixed with 4%PFA and stained with α -K40tubac and α -GAP45 by IFA. Nuclei were stained with DAPI. Scale bars are 5 μ m. **(B)** Quantification of parasites presenting aberrant nuclei and morphology after *mec17* gene disruption in the RHsCas9-*mec17*-2 (RHsCas9-*mec17*) line and *mec17* gene excision in RH Δ ku80-DiCre-*Pfmec17loxP* (*mec17loxP*) parasites. While parasites lost α -tubulin acetylation after loss of *mec17* gene function in both conditional systems, only split-Cas9 parasites showed aberrant nuclei and morphology. Parasites were grown with or without 50nM rapamycin as indicated. Cells were fixed 48h post inoculation (p.i.). Data represent three independent experiments. For each condition 100 vacuoles were counted (total n=300).

Table 3-2: Phenotypic characterisation of the lines RHsCas9-*mec17*-2 and RHsCas9-*mec17*-3

Numbers were obtained by analysing IFA results. IFAs were conducted as described in Figure 3-9. The asterisk (*) indicates vacuoles that lack α -tubulin acetylation at lysine 40 (K40ac) and display aberrant nuclei and cellular morphology.

	Rapamycin	K40ac	lack of K40ac	lack of K40ac*	# vacuoles
RHsCas9- <i>mec17</i> -2	50nM (1h)	38	45	17	100
RHsCas9- <i>mec17</i> -3	50nM (1h)	43	27	30	100
	50nM (48h)	42	29	29	100
	none	98	2	0	100

With the DiCre system, excision of *Pfmec17* led to the loss of K40 acetylated α -tubulin in 98.2% (\pm 0.29) of parasite vacuoles after 48h (**Figure 3-9 B** and **Figure 3-10 A**). Aberrant nuclei together with loss of acetylation were observed in 0.33% (\pm 0.29). In the non-induced population, 3.33% of vacuoles (\pm 1.6) lacked α -tubulin acetylation. Loss of acetylation and aberrant nuclei were observed in 0.33% (\pm 0.58%). This shows that the level of aberrant nuclei was not elevated when α -tubulin acetylation was increasingly lacking in the parasite population (induced vs non-induced population). I therefore propose that aberrant nuclei do not represent a result of *Pfmec17* excision and the subsequent loss of acetylation.

All in all, *Tgmec17* and *Pfmec17* appear to be responsible for microtubule acetylation at the lysine 40 residue of α -tubulin, as previously reported (Varberg et al. 2016). A nuclear replication phenotype, however, was only observed in some parasites when α -tubulin acetylation was disrupted with the split-Cas9 system. The discrepancy between the split-Cas9 and DiCre system regarding

nuclear integrity is most likely rooted in their different mode of actions. CRSIPR/Cas9 induces a DSB in the genome and leaves the organisms DNA repair machinery to repair the damage (Doudna and Charpentier 2014). The Cre system recombines the organisms genomic DNA in the process of excising the target sequence, thus preserving genome integrity (Nagy 2000). Based on data presented in this chapter, I am proposing that the described replication defect is not caused by loss of microtubule acetylation, but rather represents the effect of Cas9-mediated DNA damage in the 1st lytic cycle of *Toxoplasma* parasites.

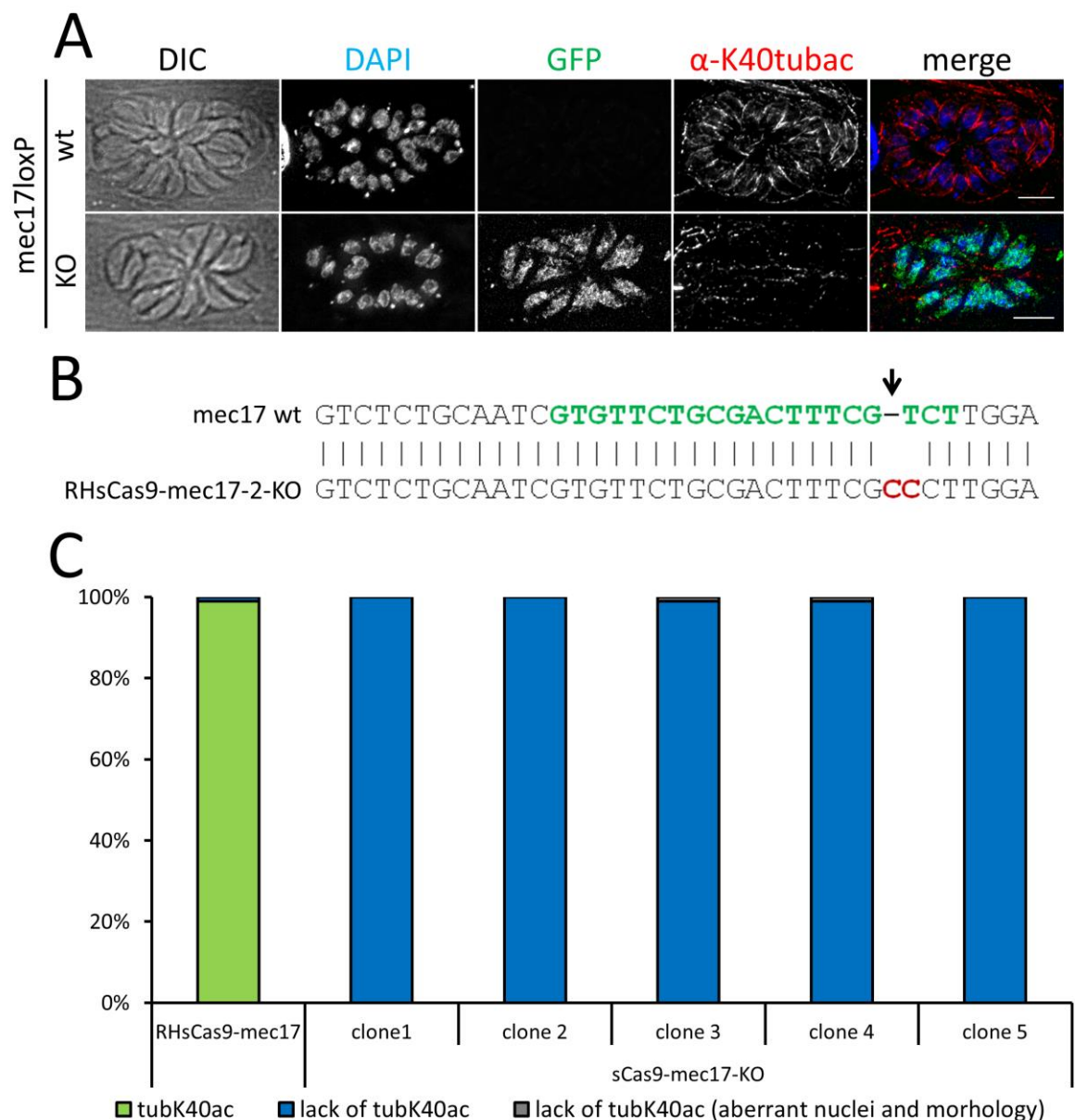


Figure 3-10: *Mec17* gene excision with the DiCre system and analysis of clonal RHsCas9-*mec17*-KO lines

(A) IFA depicting α -tubulin acetylation at lysine 40 (K40tubac) in RH-DiCre-Pfmec17loxP (wt) and RH-DiCre-*mec17*-KO (KO) parasites. To achieve *mec17* gene excision, parasites were incubated with 50nM rapamycin for 4h. Successful gene excision resulted in GFP expression

(lower panel). Loss of *mec17* gene function resulted in parasites lacking α -tubulin acetylation. Parasites were grown for 48h and fixed with 4%PFA. Parasites were stained with α -K40tubac by IFA. Nuclei were stained with DAPI. Scale bars are 5 μ m. **(B)** Genome sequencing performed for the RHsCas9-*mec17*-2-KO line (clone 1). Green letters indicates sgRNA sequence. Red letters represent nucleotide insertion in the mutant strain, causing a frame shift and, thus, the functional knock-out of the *mec17* gene. The black arrow indicates the predicted cut site. **(C)** Quantification of parasite vacuoles presenting aberrant nuclei and morphology in clonal RHsCas9-*mec17*-2-KO populations. Parasites were grown for 48h and fixed with 4%PFA. IFA analysis was performed to allow for quantification. For each clone, one experiment was conducted (n=100).

3.6 Summary and conclusions

In this chapter, the split-Cas9 system (Zetsche, Volz, and Zhang 2015) was introduced to the apicomplexan parasite *Toxoplasma*. The genes *Tggap40* (Harding et al. 2016), *Tgsag1* (Kim and Boothroyd 1995; Lekutis et al. 2001) and *Tgmec17* (Varberg et al. 2016) were targeted and previously described phenotypes were successfully reproduced. Interestingly, my data most strongly suggest that Cas9-mediated DSBs in the genome cause *Toxoplasma* to display a DNA damage phenotype. This phenotype features aberrant and fragmented nuclei as well as abnormal cell shape. Most likely, this phenotype occurs in parasites that fail to repair the DSB introduced by Cas9 activity. It became apparent that DNA damage only occurs when split-Cas9 was activated in the presence of a sgRNA targeting the parasite genome (Table 3-3).

Table 3-3: Prerequisites for DNA damage to occur in *Toxoplasma* upon split-Cas9 activation

Toxoplasma displays DNA damage at 48h post inoculation only when split-Cas9 is activated by Rapamycin in the presence of a sgRNA with an actual target sequence and the parasite genome.

split-Cas9	sgRNA (valid target)	sgRNA (no target)	rapamycin	DNA damage
+	-	-	-	-
-	+	-	-	-
-	-	-	+	-
+	+	-	-	-
+	-	-	+	-
-	+	-	+	-
+	-	+	+	-
+	+	-	+	+

A detrimental effect of Cas9 activity on *Toxoplasma* fitness had been suggested previously. Transient transfection of a Cas9-sag1sgRNA plasmid impacted parasite fitness as measured by plaque assay immediately after transfection (Sidik et al. 2014). The effect was observed in RH parasites and, to a greater extent, in RH Δ ku80 parasites. Sidik and co-workers hypothesised that DNA damage caused by Cas9 could be responsible for this decrease in fitness, especially in the RH Δ ku80 strain. Data presented in this chapter stands in strong agreement with this hypothesis. Unsurprisingly, the repair of DSB in the parasite genome appears to present the bottleneck for parasite recovery after CRISPR-Cas9 activity.

It was also shown that stabilisation of conditional ddFKBP-Cas9 for longer than 4h led to aberrant parasite morphology (Serpeloni et al. 2016). Constitutive expression of Cas9 in *Toxoplasma* could not be achieved, unless the enzyme was expressed together with a decoy sgRNA (Sidik et al. 2016). A fitness advantage was later reported for parasites expressing Cas9 together with a sgRNA versus parasites expressing only Cas9 (Markus et al. 2019). Cas9 toxicity was proposed to be caused by endogenous RNA mediating Cas9 activity (Sidik et al. 2016) and/or by secondary non-targeted Cas9 nuclease activity in the absence of any sgRNA (Markus et al. 2019). Markus and co-workers hypothesized that the co-expression of a sgRNA might sequester Cas9 enzymes, thus preventing undesired nuclease activity (Markus et al. 2019).

As hypothesized at the beginning of this chapter, this problem was not observed with the split-Cas9 system. Activation of the system over a period of 48h without sgRNA did not have any noticeable effects on parasite morphology. The activated split-Cas9 system is less efficient than the wild-type Cas9 enzyme at inducing nucleotide insertions or deletions at the specific target site (Zetsche, Volz, and Zhang 2015). This reduced efficiency of the split-Cas9 system might explain the apparent lack of toxicity when activated without genome targeting sgRNA. I concluded from this, that expression of a decoy sgRNA, as proposed previously for constitutive Cas9 expression (Sidik et al. 2016; Markus et al. 2019), is not necessary for the split-Cas9 system.

In the ddfKBP-Cas9 system, stable transfection of a sag1sgRNA caused accumulation of sag1-KO mutants in the parasite population without ddfKBP-Cas9 activation (Dr Elena Jimenez-Ruiz, unpublished data). This level of background activity is not present in the split-Cas9 system, suggesting tighter regulation by Cas9 sub-unit separation.

All in all, the split-Cas9 system is capable of reliably disrupting genes in *Toxoplasma*. The DNA damage caused by Cas9 activity is only apparent in the 1st lytic cycle. I therefore argue that phenotypic analysis of split-Cas9 mutants is possible in the 2nd lytic cycle. In addition, the obvious nature of the DNA damage allows for exclusion of this phenotype during analysis. It is of most importance to note, however, that the split-Cas9 system is not suitable for investigating nucleus replication or cell replication. Also, any experimental set up with the split-Cas9 system should include a control that allows for the estimation of how DNA damage affects the process that is being researched.

Published research strongly indicates that *Tgactin1*, although critical for completion of the lytic life cycle, is not essential for intracellular growth and replication (Andenmatten et al. 2013; Egarter et al. 2014; Periz et al. 2017; Whitelaw et al. 2017). Lack of *Tgactin1* affects vacuole organisation (Periz et al. 2017). However, effects on overall nuclear integrity or parasite morphology, as described here for the DNA damage, have not been reported. The same is true for the actin depolymerisation factor (*TgADF*) (Mehta and Sibley 2011; Haase et al. 2015; Periz et al. 2017). Therefore, the split-Cas9 system should be applicable for investigating actin-related phenotypes or for screening approaches aiming at identifying novel actin binding proteins. I argue that the clear nature of the DNA damage phenotype should allow for its exclusion from phenotypic analysis. Noteworthy, Lacombe and co-workers recently suggested a negative impact of transient Cas9 expression on mitochondria morphology (Lacombe et al. 2019). This finding indicates that Cas9 expression might affect additional cellular processes, a phenomenon that requires further investigation in the future. In sum, subsequent confirmation of the gene-specific phenotype with other conditional systems such as the DiCre system (Andenmatten et al. 2013) is recommended when applying (split-)Cas9-based strategies.

4 Combining the split-Cas9 and actin-chromobody technology to investigate actin distribution and dynamics in *Toxoplasma*

In the previous chapter, the split-Cas9 technology was established as molecular tool for targeted gene disruption in *Toxoplasma*. To investigate and visualize the impact of actin binding proteins on actin dynamics, combination of this conditional CRSIPR/Cas9 system with the actin-chromobody technology presented the next step of this study.

Chromobodies are nanobodies which are derived from single-heavy chain antibodies found in Camels (Hamers-Casterman et al. 1993). These nanobodies can be fused to fluorescent proteins (Melak, Plessner, and Grosse 2017) and have been used to visualize actin filaments in a variety of organisms ranging from animal cells (Panza et al. 2015; Plessner et al. 2015) to plants (Rocchetti, Hawes, and Kriechbaumer 2014).

Expression of anti-actin-chromobodies in *Toxoplasma* revealed an extensive actin network consisting of (probably short) F-actin bundles in intracellular parasites (Periz et al. 2017). This network connects parasites within the parasitophorous vacuole (PV) via intravacuolar filaments. Parasites also possess a highly dynamic actin accumulation centre anterior to the nucleus (also referred to as cytosolic actin centre [cAC]). Periz and co-workers demonstrated that these structures depend on actin and the actin treadmilling machinery. Loss of *TgActin* caused intravacuolar, filamentous structures to disappear while depletion of *TgADF* abolished actin dynamics in the cytoplasm. Furthermore, absence of *TgADF* resulted in strong actin accumulation at the basal and (to a lesser extent) at the apical pole.

In the past, actin visualisation in *Toxoplasma* presented a challenge. Detection of actin with classical antibody staining was controversially discussed with regards to antibody specificity and background staining (Drewry & Sibley, 2015; Whitelaw et al., 2017). Other fluorogenic actin probes such as Lifeact (Riedl et al. 2008) could not be expressed in the parasite and, thus, were not useful in order to detect filamentous actin (F-actin) in *Toxoplasma* (Tardieux 2017; Periz et al. 2017).

The novel ability to visualize F-actin in fixed or live *Toxoplasma* cells presented an exciting opportunity to re-evaluate actin dynamics and to precisely dissect the function of known actin factors within this complex cytoskeletal network. In this chapter, I will demonstrate that different aspects of actin biology can be explored by combining split-Cas9 and the actin-chromobody technology in *Toxoplasma*.

4.1 Disruption of *Tgactin1* and *Tgadf* with the split-Cas9 system

To combine the split-Cas9 system with the chromobody technology, the actin-chromobody fused to the fluorescent protein EmeraldFP (Cb-Emerald) (Periz et al. 2017) was randomly integrated into the genome of RHsCas9- Δ hx parasites. RHsCas9-CbEmerald parasites were enriched in the transfected population by flow cytometry. Subsequent serial dilution resulted in a clonal RHsCas9- Δ hx-CbEmerald (referred to as RHsCas9-CbEmerald) line. This line displayed the actin network features previously described (Periz et al. 2017): long intravacuolar F-actin network and actin accumulation anterior to the nucleus (**Figure 4.1 A and C, wt panels**).

Next, I confirmed that the split-Cas9 system can be applied to investigate actin dynamics in *Toxoplasma*. For this purpose, an actin1sgRNA and adfsgRNA were transfected into the RHsCas9-CbEmerald to create the two lines RHsCas9-CbEmerald-actin1sgRNA and RHsCas9-CbEmerald-adfsgRNA (**Figure 4-3 A**). Upon disruption of *Tgactin1*, parasites lost their actin structures as previously described (Periz et al. 2017) (**Figure 4-1 A and Figure 4-3 B**). In the absence of intravacuolar filaments and the cytosolic actin accumulation centre, parasites showed ubiquitous Cb-Emerald distribution in the cytoplasm. This most likely represents diffusion of unbound Cb-Emerald throughout parasite lacking actin structures. Disruption of *Tgactin1* also resulted in apicoplast loss as previously described (Andenmatten et al. 2013; Egarter et al. 2014; Whitelaw et al. 2017). Of relevance, in non-induced parasites, apicoplasts localised to the actin accumulation centre in the cytosol (**Figure 4-1 A, wt panels**).

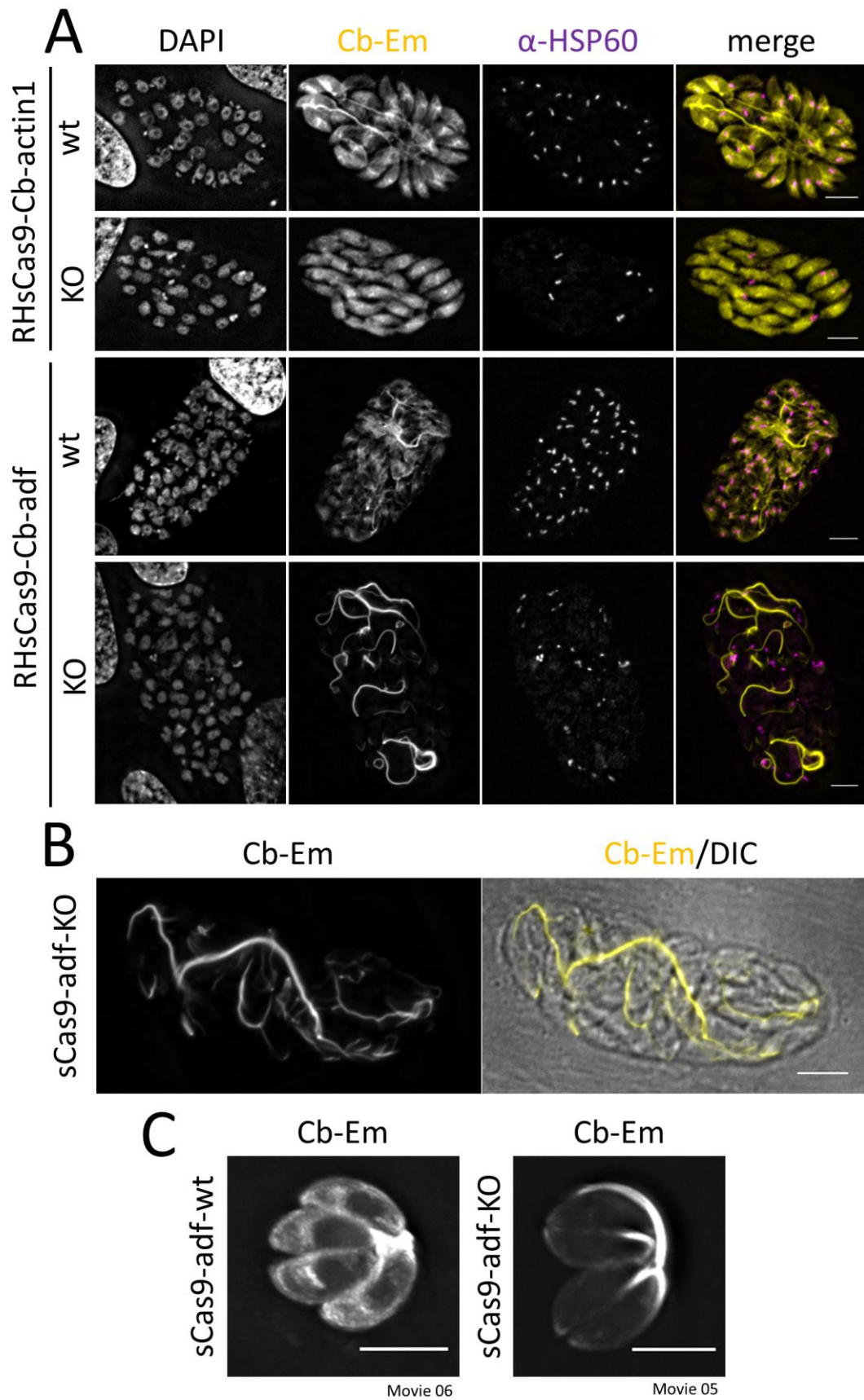


Figure 4-1: Disruption of *Tgactin1* and *Tgadf* in RHsplit-Cas9 parasites expressing actin-chromobody-Emerald (Cb-Em or Cb)

Figure 4-1 continued: (A) and (B) IFA depicting the effect of *Tgactin1* (RHsCas9-Cb-actin1) or *Tgadf* (RHsCas9-Cb-adf) disruption on the actin network (Cb-Emerald) and apicoplast segregation (HSP60). To achieve gene disruption (KO), parasites were incubated with 50nM rapamycin for 1h. Parasites were fixed after 48h. Apicoplasts were stained with α -HSP60 by IFA. Nuclei were stained with DAPI. Scale bars are 5 μ m. **(C)** Images depicting collapsed t-stacks obtained from live microscopy for RHsCas9-Cb-*adf* parasites. Parasites were grown in the presence or absence of 50nM rapamycin for 1h, followed by growth for another 72h. Parasites were then mechanically lysed and inoculated for 24h prior to live microscopy. Scale bars are 5 μ m. See also **Supplement Movie V1**.

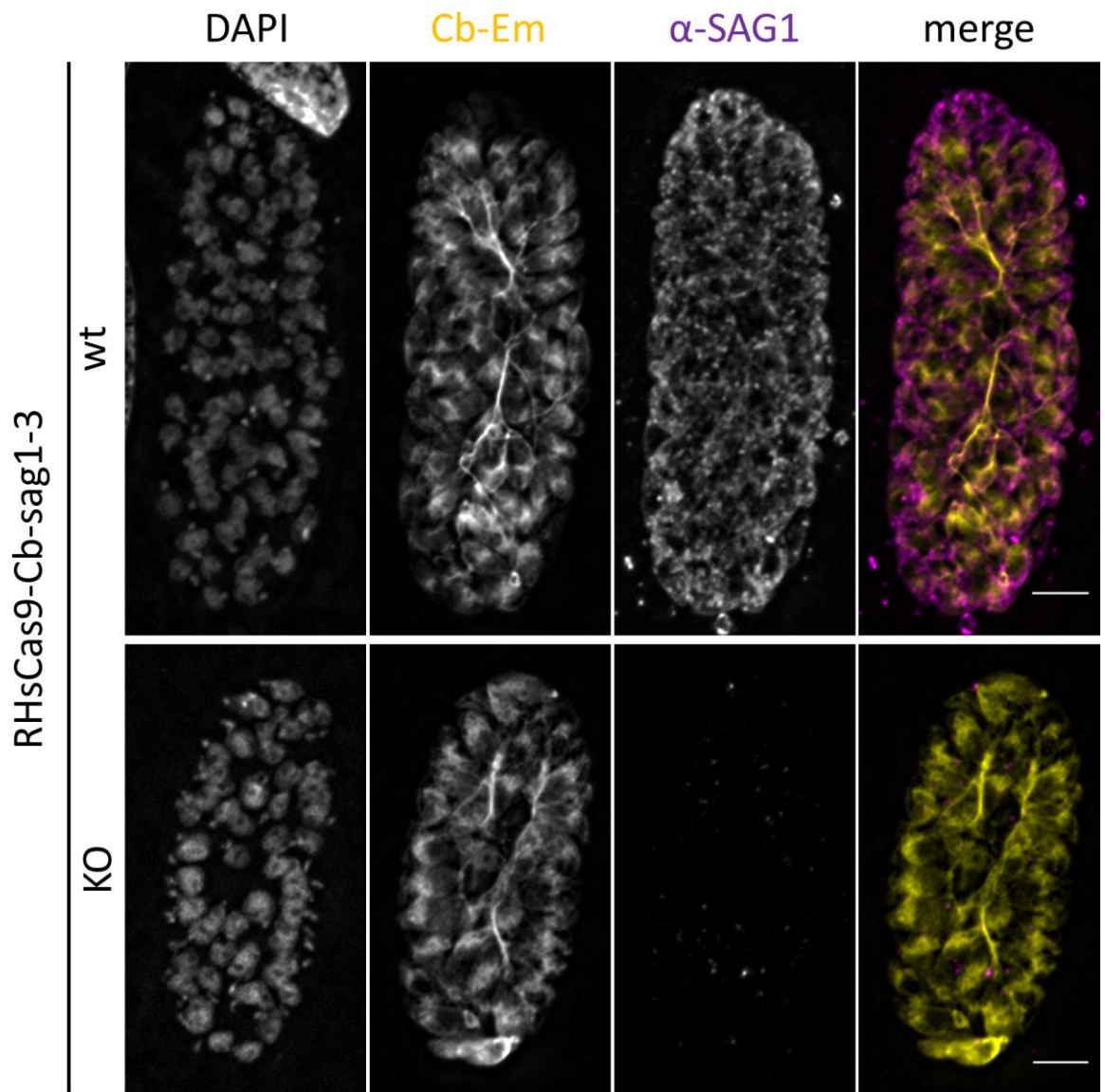


Figure 4-2: Disruption of *Tgsag1* in RHsplit-Cas9 parasites expressing actin-chromobody-Emerald (RHsCas9-Cb-sag1-3)

IFA depicts the effect of *Tgsag1* disruption on the actin network (Cb-Emerald). To achieve gene disruption (KO), parasites were incubated with 50nM rapamycin for 1h. Parasites were fixed after 48h and stained with α -SAG1 by IFA. Nuclei were stained with DAPI. Scale bars are 5 μ m.

In smaller vacuoles (**Figure 4-1 C**) (**Supplement Movie V1**), disruption of *Tgadf* reproduced the published phenotype of actin accumulation at the basal and (to a lesser extent) at the apical pole together with loss of actin structures in the cytosol (Periz et al. 2017). Interestingly, the split-Cas9 system identified the accumulation of thick intravacuolar filaments as a characteristic feature of *Tgadf* disruption in larger vacuoles (**Figure 4-1 A and B**). Actin was almost exclusively observed in these filamentous structures which can span the entirety of the vacuole (**Figure 4-1 B**). As reported previously, parasites displayed an apicoplast replication defect upon loss of *TgADF* (Jacot, Daher, and Soldati-Favre 2013; Haase et al. 2015). Disruption of the *Tgadf* and *Tgactin1* genes upon split-Cas9 activation was confirmed by sequencing (**Figure 4-3 C**).

Finally, I wanted to exclude that Cas9-mediated gene disruption has a universal impact on the actin network by targeting the dispensable gene *Tgsag1* (Kim and Boothroyd 1995; Lekutis et al. 2001). For this purpose, the RHsCas9-CbEmerald-sag1-3 strain was generated (**Figure 4-3 A**). Activation of split-Cas9 resulted in *TgSAG1* loss on the parasite surface (**Figure 4-2**) strongly indicating *Tgsag1* gene disruption. Loss of *TgSAG1* did not affect overall actin distribution as parasites still displayed intravacuolar actin filaments and cytosolic actin accumulation.

In summary, the disruption of the genes *Tgactin1*, *Tgadf* and *Tgsag1* showed that the split-Cas9 system can be applied to depict different actin network phenotypes. Previously reported phenotypes with the DiCre (Andenmatten et al. 2013) and TATi-1 (Meissner, Schlüter, and Soldati 2002) systems were successfully confirmed.

represent nucleotide insertion in the mutant strain, causing a frame shift and, thus, the functional disruption of the indicated gene. Black arrows indicate the predicted cut side.

4.2 Investigating the impact of *Tgadf* disruption on actin filament dynamics

Upon loss of *Tgadf* gene function, actin appears to accumulate mostly in thick intravacuolar filamentous structures. I hypothesised that this phenomenon could be explained by the previously suggested involvement of *TgADF* in actin filament turnover (Mehta and Sibley 2010, 2011). Loss of *TgADF* might prevent the depolymerisation of actin filaments and, thus, the re-introduction of actin monomers into the available actin pool in *Toxoplasma*. As consequence, the enrichment of filamentous actin structures depletes free monomeric actin from the overall actin pool that is required for maintaining sites of highly dynamic actin, i.e. the cytosol.

To test this idea, I was eager to address the impact of *TgADF* loss on the overall dynamics of filamentous actin structures in the parasites. One process that was associated with highly dynamic disassembly of F-actin structures was parasites egress (Periz et al. 2017). Upon the induction of egress with a calcium-ionophore, but prior to parasite movement, the large intravacuolar actin filaments were disassembled in a rapid fashion. I argued that, if *TgADF* is indeed responsible for actin turnover, actin filament disassembly should be diminished in *sCas9-adf-KO* parasites.

4.2.1 Analysis of egress behaviour in conditional *sCas9* mutants

Before analysing the role of *TgADF* in F-actin disassembly upon egress, it was critical to determine whether the split-Cas9 system is suitable for analysis of this process. For this purpose, it had to be excluded that Cas9-mediated DNA damage, which can lead to aberrant nuclei and overall cell morphology (see chapter 3), diminishes the parasites ability to egress. The egress of *sCas9-sag1-3-KO*, *sCas9-actin1-KO* and *sCas9-adf-KO* parasites were measured and normalized to the respective non-induced wild-type lines (**Figure 4-4 A and B**). In addition,

abundance of DNA damage and the rate of gene disruption after split-Cas9 activation were measured for all strains (Figure 4-4 C).

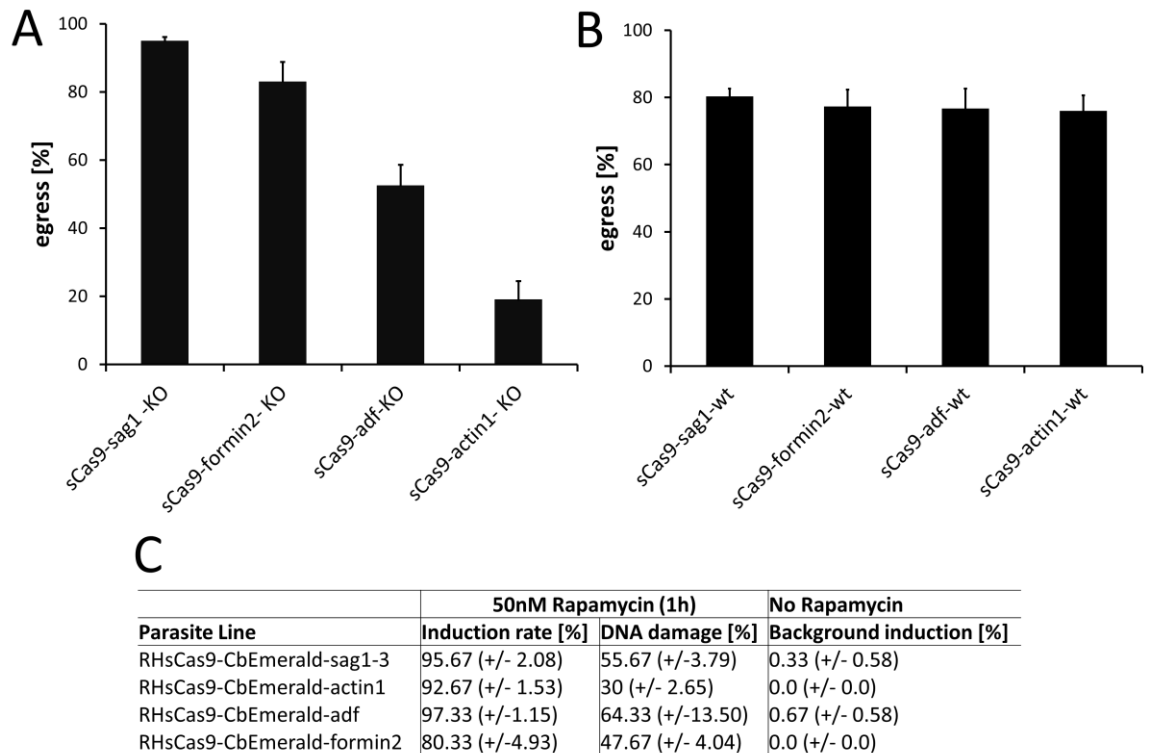


Figure 4-4: Parasite egress after split-Cas9 mediated gene disruption

(A) and (B) Induced (50nM rapamycin, 1h or 48h) and non-induced RHsCas9-CbEm parasites were grown for 48h. Egress was then induced by incubating parasites with 2 μ M A23187 for 5-8min. Egress percentage of the sCas9-KO parasites in (A) was normalized to the egress percentage of the respective sCas9-wt parasites depicted in (B). Egress percentage was obtained from three independent egress assays. Experiments were stopped for wt and KO populations at the same time, when the wt populations showed egress of about 80%. Time for egress in the individual wt vs KO experiments was as follows: sag1 – 8min, 8min, 8min; formin2 – 5min, 7min, 7min; adf – 8min, 8min, 5min; actin1 – 8min, 5min, 7min. For each condition 100 vacuoles were counted (total n=300). (C) The table gives information about the overall induction rate and DNA damage in the respective parasite populations at 48h after rapamycin induction (50nM, 1h). Numbers were obtained from three independent experiments for each strain and condition. For each condition 100 vacuoles were counted (total n=300). For the formin2, adf and actin1 sCas9 strains, one biological repeat was performed with a rapamycin incubation time of 48h. For analysis of the RHsCas9-CbEm-formin2 strain, please refer to chapter 5.

Disruption of the non-essential *Tgsag1* gene (Kim and Boothroyd 1995; Lekutis et al. 2001) caused DNA damage in 55.67% (\pm 3.79) of parasites. In comparison with the wt parental line, however, egress was reduced by only 5% (\pm 1.1) in sCas9-sag1-3KO parasites. IFA analysis confirmed that parasites were able to egress

despite displaying a DNA damage phenotype (**Figure 4-5**). In agreement with studies that reported *Tgactin1* as critical for parasite egress (Egarter et al. 2014; Whitelaw et al. 2017), the sCas9-actin1-KO population showed an egress reduction of 80.8% (± 5.4) at 48h post split-Cas9 activation. Disruption of *Tgadf* caused a reduction of egress by 47.5% (± 6.1). This result can be seen as support for the previously reported egress phenotype for *TgADF* depletion (Mehta and Sibley 2011). Mehta and Sibley showed that *TgADF*cKO parasites were slower to egress due to impaired motility. In their experiments, not all *TgADF*cKO parasites managed to egress at the 5-8min mark post egress induction, the cut-off time I chose in my egress experiments. Together these data suggest that the split-Cas9 system is capable of reliably describing a wide range of egress phenotypes in parasites mutants.

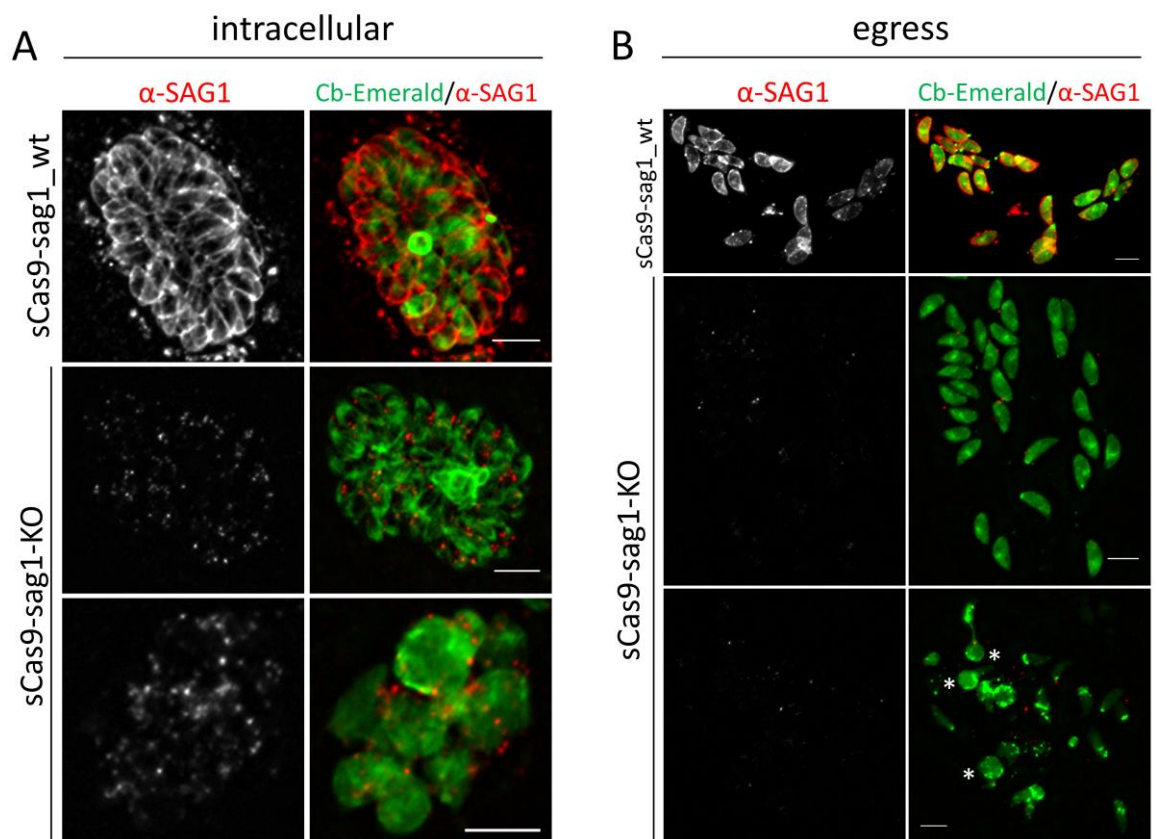


Figure 4-5: Depiction of egressed and intracellular RHsCas9-CbEm-sag1-3-wt and RHsCas9-CbEm-sag1-3-KO parasites after A23187 treatment

For this experiment, induced (50nM rapamycin, 1h) and non-induced RHsCas9-CbEm-sag1 parasites were grown for 48h. Egress was then induced by incubating parasites with 2 μ M A23187 for 8min. After fixation with 4%PFA, parasites were stained for *TgSAG1* by IFA. **(A)** Depiction of *sag1*-wt and *sag1*-KO parasites that remained intracellular after A23187 treatment. For *sag1*-KO parasites, the top panel shows a healthy vacuole while the bottom panel represents DNA damage (aberrant morphology). **(B)** Depiction of egressed *sag1*-wt and *sag1*-KO parasites. For *sag1*-KO parasites, healthy parasites are

depicted in the top panel. The bottom panel shows egressed *sag1*-KO parasites representing DNA damage (asterisks). Scale bars are 5µm.

4.2.2 Impact of *Tgadf* disruption on filament disassembly upon egress

Next, the impact of *Tgadf* disruption on disassembly of the large intravacuolar filaments upon parasite egress was investigated. To this end, the abundance of large filamentous actin structures before and after egress in wild-type and mutant parasites were compared to each other. Fixed assays revealed that in a growing wild-type population, 73.3% (RHsCas9-CbEm-*sag1*-3) and 83.3% (RHsCas9-CbEm-*adf*) show intravacuolar filaments (**Figure 4-6 and Figure 4-7**).

After treatment with calcium-ionophore (2µM A23187), these filamentous actin structures usually could not be detected anymore in the proximity of freshly egressed parasites or within still intracellular vacuoles (**Figure 4-6- and 4-7**). This was true for the majority of sCas9-*sag1*-wt, sCas9-*sag1*-KO and sCas9-*adf*-wt parasites (**Figure 4-6**). In sCas9-*sag1*-wt parasites only 4.6% (egressed) and 22% (intracellular) of parasites displayed intravacuolar filaments after calcium-ionophore treatment. In the sCas9-*sag1*-ko population these numbers were 1.8% (egressed) and 8% (intracellular). For sCas9-*adf*-wt, 21% (egressed) and 40% (intracellular) of parasites showed large intravacuolar filaments or their remainders. In total, sCas9-*sag1*-wt and sCas9-*sag1*-KO parasites show a strong reduction of intravacuolar filaments from 73.3% down to 4.6% (wt) and 1.8% (KO) upon egress. In sCas9-*adf*-wt parasites they dropped from 83.3% to 21.3%. In striking contrast, the large majority of sCas9-*adf*-KO parasites still displayed large actin filaments throughout the vacuole and in close proximity to freshly egressed parasites (**Figure 4-6 and 4-7**). 79.3% of egressed parasites still showed large intravacuolar filaments. For intracellular parasites it was 94.4%.

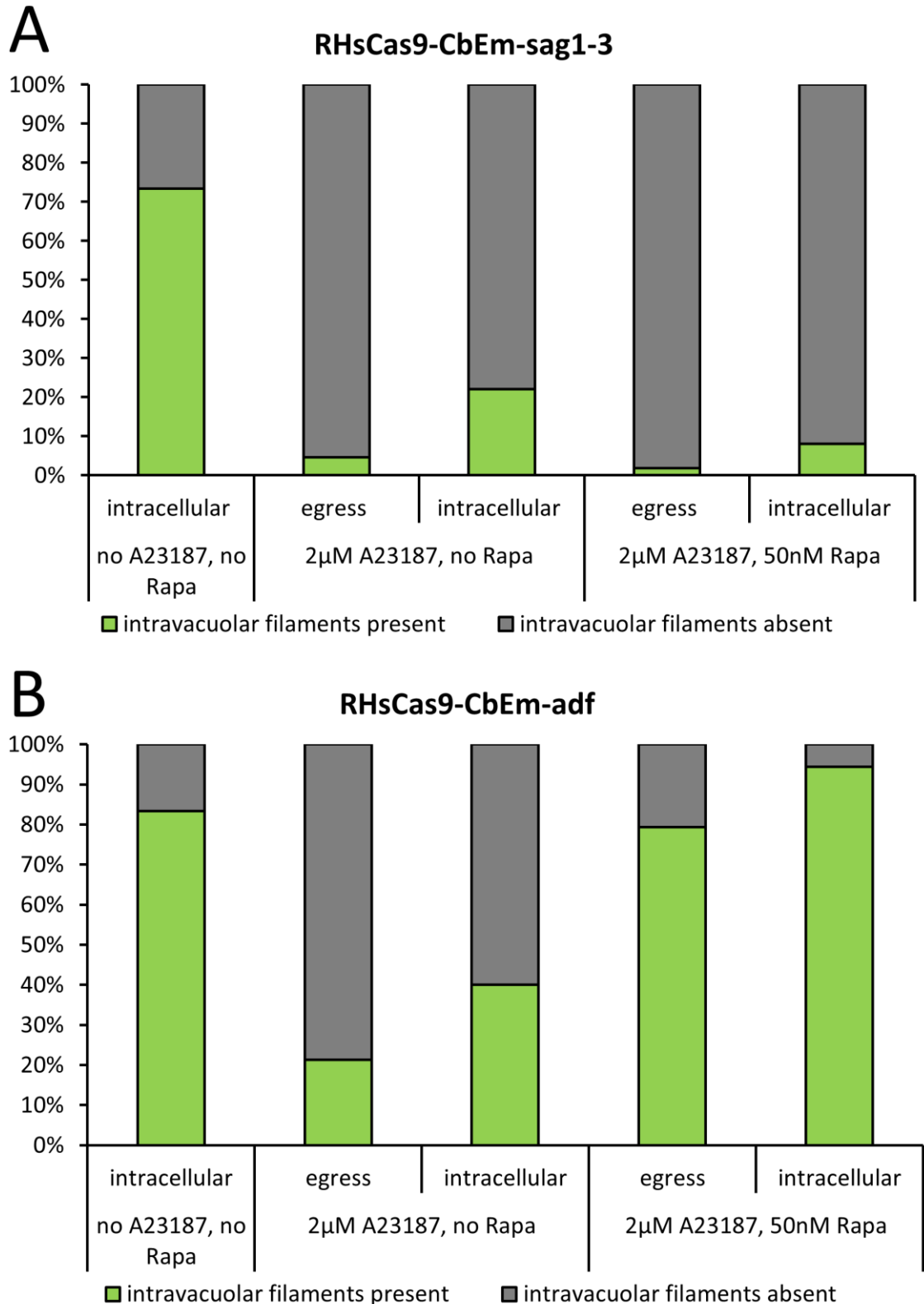


Figure 4-6: Effect of A23187 treatment on intravacuolar filamentous actin structures in RHsCas9-CbEm-sag1-3-ko and RHsCas9-adf-ko parasites compared to wt parasites

This figure depicts the abundance of large intravacuolar filamentous actin structures in *sag1*-wt/KO (A) and *adf*-wt/KO (B) parasites after A23187 treatment for 5-8min or no treatment. See **Figure 4-4** for overall egress rates and **Figure 4-7** for representative

images. Analysis is based on three independent experiments. For RHsCas9-CbEm-sag1-3: no A23187/no Rapa: n=300; 2 μ M A23187/no Rapa: n=241 (egress), n=59 (intracellular); 2 μ M A23187/50nM Rapa: n=225 (egress), n=75 (intracellular). For RHsCas9-CbEm-adf: no A23187/no Rapa: n=300; 2 μ M A23187/no Rapa: n=230 (egress), n=70 (intracellular); 2 μ M A23187/50nM Rapa: n=121 (egress), n=179 (intracellular).

In summary, RHsCas9-sag1-wt/KO and RHsCas9-adf-wt parasites showed loss of actin filaments upon egress induction, while RHsCas9-adf-KO parasites show no reduction in these structures compared to the non-treated intracellular wild-type population. It would therefore appear that regulation of *TgADF* is critical for F-actin disassembly during parasite egress. Furthermore, disassembly of actin network seems to be associated with parasite egress, but not essential for this process to happen. In the past, actin sedimentation assays revealed that actin is more stable in parasites depleted of *TgADF* (Mehta and Sibley 2011). The here described phenotype in the RHsCas9-CbEm-adf-KO line visualized this previous finding within the parasite.

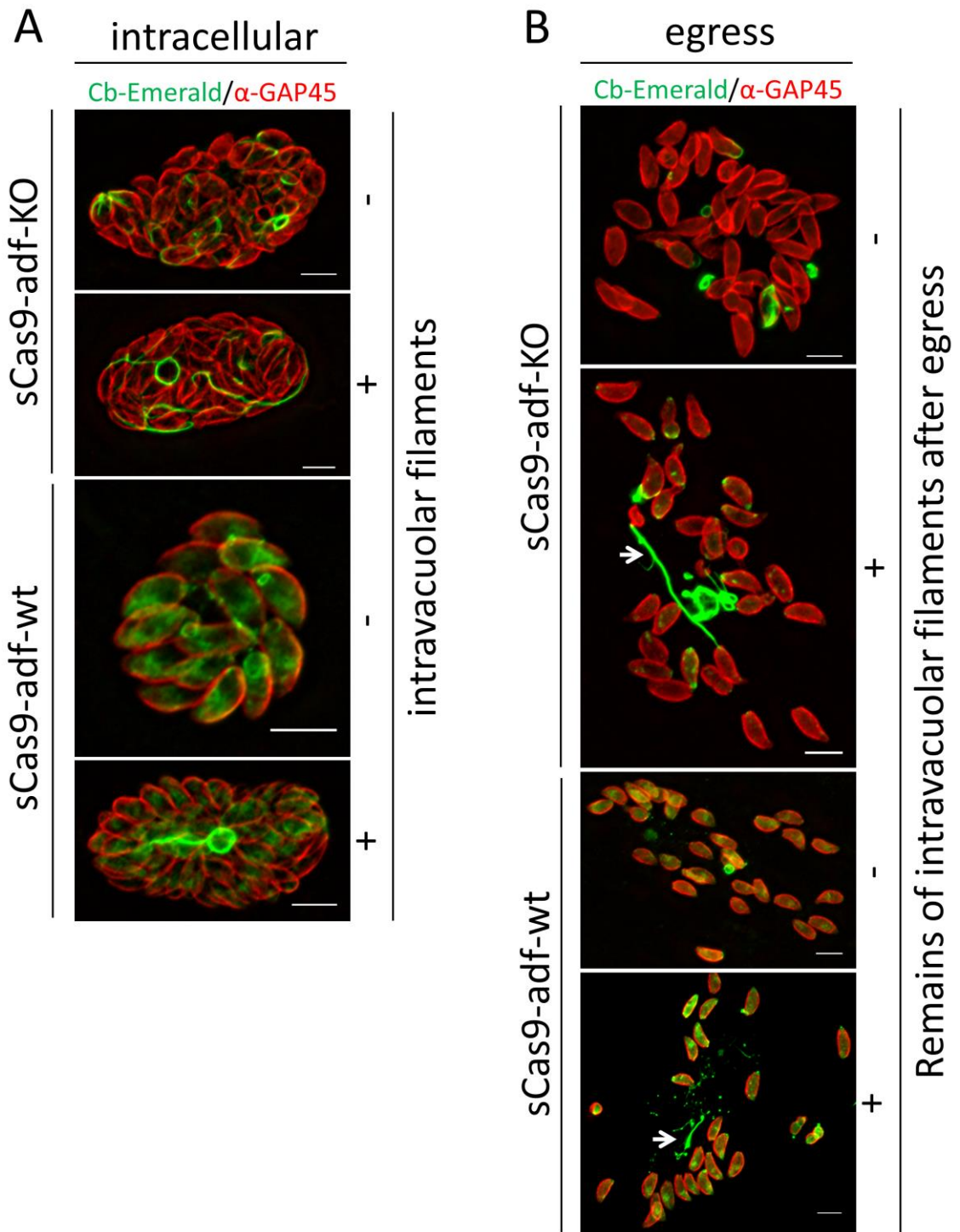


Figure 4-7: Depiction of egressed and intracellular RHsCas9-CbEm-adf-wt and RHsCas9-CbEm-adf-KO parasites after A23187 treatment

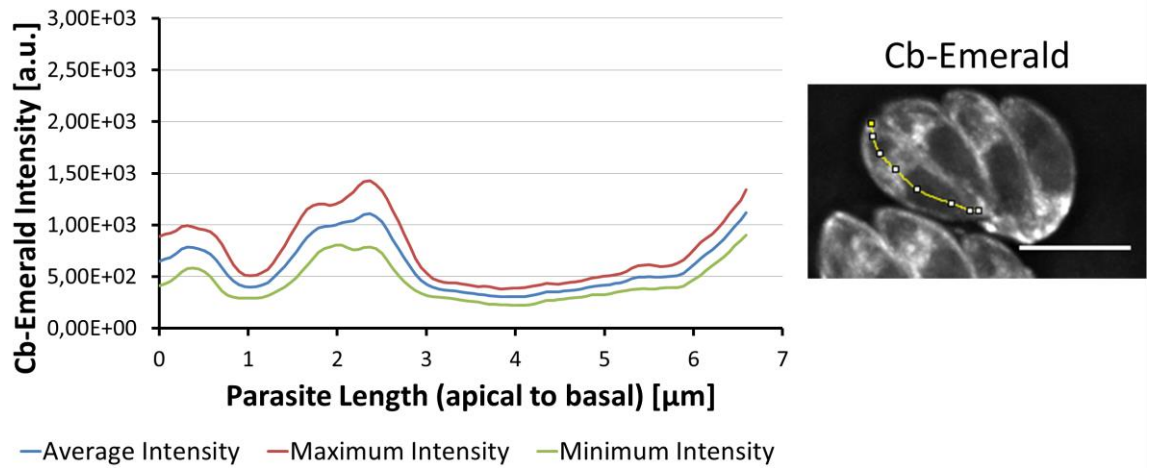
For this experiment, induced (50nM rapamycin, 1h) and non-induced RHsCas9-CbEm-adf parasites were grown for 48h. Egress was then induced by incubating parasites with 2 μ M A23187 for 5-8min. After fixation with 4%PFA, parasites were stained for GAP45 by IFA. Images depict intracellular (**A**) and egressed (**B**) vacuoles with (+) or without (-) intravacuolar filamentous actin structures. See **Figure 4-4** and **4-6** for corresponding numerical analysis. White arrows indicate the remains of intravacuolar filaments after parasite egress. Scale bars are 5 μ m.

4.3 Re-defining intracellular actin distribution and dynamics

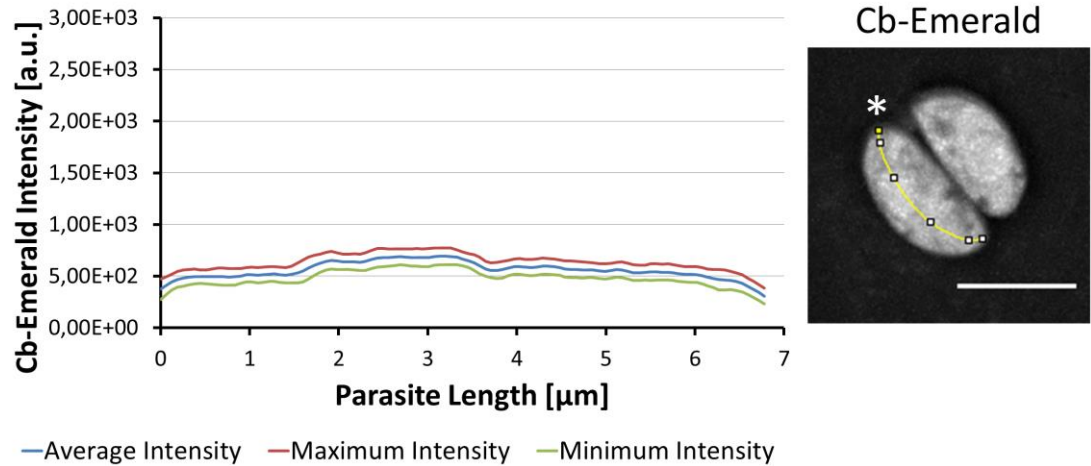
After performing analysis on intravacuolar actin structures that manifest outside the parasite body, I aimed at re-visiting actin distribution and dynamics within the parasite. A highly dynamic cytosolic actin accumulation centre had been described by Periz and colleagues (Periz et al. 2017). However, no further analysis of actin distribution or dynamics was performed. To further explore actin dynamics I applied kymograph analysis as described by Mangeol and co-workers (Mangeol, Prevo, and Peterman 2016). For this purpose, live microscopy was performed on Cb-Emerald expressing parasites. I then conducted Kymograph analysis on the obtained movies to measure particle flow, representing actin flow alongside a chosen track. Fourier filtering allowed for the distinction between different flow directions. Furthermore, I used kymograph data for the generation of time-averaged local intensity profiles. These profiles depict Cb-Emerald intensity, i.e. actin distribution, in live parasites over the entire duration of the movie.

In wild-type parasites, time-averaged local intensity profiling showed the highest Cb-Emerald intensities at the two poles and anterior to the nucleus (**Figure 4-8 A** and **Figure 4-9 A**) (**Supplement Movie V1** and **V2**) (**Appendix Figure 7-3**). Disruption of *Tgactin1* resulted in the absence of any directed actin distribution (**Figure 4-8 B**) (**Supplement Movie V2**). Loss of *Tgadf* function led to strong actin accumulation at the basal end (**Figure 4-9 B**) (**Supplement Movie V1**) (**Appendix Figure 7-3**). Thus, intensity profiling confirmed numerically the phenotypes described for these genes by IFA (**Figure 4-1**). Of relevance, distribution of GFP throughout the parasites differed distinctively from the Cb-Emerald pattern (**Figure 4-8 C**) (**Supplement Movie V3**) (**Appendix Figure 7-2**). Time-lapsed video microscopy revealed that the cytosolic actin centre is highly dynamic and frequently interacts with the parasite periphery (**Figure 4-10 B**) (**Supplement Movie V1**). Wild-type parasites showed actin accumulation in the periphery as confirmed by intensity profile measurement and skeletonisation analysis (**Figure 4-10A** and **Figure 4-11**) (**Supplement Movie V1** and **V2**).

A RHsCas9-Cb-actin1-wt (movie 03A)



B RHsCas9-Cb-actin1-KO (movie 02A)



C RH-GFP (movie 23A)

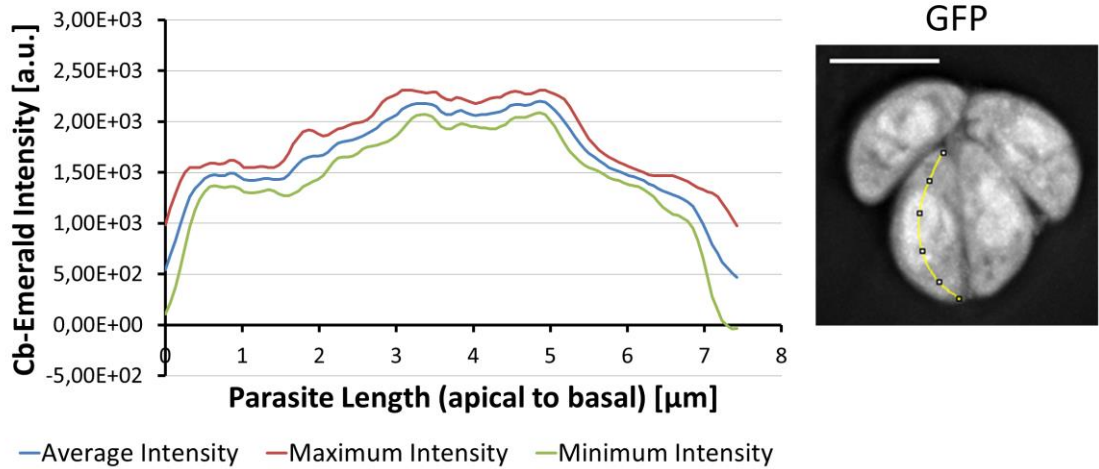


Figure 4-8: Actin distribution in intracellular RHsCas9-CbEm-actin1 wt and KO parasites along the middle axis

Figure 4-8 continued: (A) and (B) Time-averaged intensity profiling along the parasites middle axis in RHsCas9-CbEm-actin1-wt and RHsCas9-CbEm-actin1-KO parasites. Parasites were incubated with or without 50nM rapamycin for 1h. After a growth period of 72h, cultures were mechanically lysed and incubated on a fresh host cell monolayer for another 24h prior to live microscopy. **(C)** Time-averaged intensity profiling along the parasites middle axis for the RH-GFP line. Parasites were grown for 24h prior to live microscopy. At least 5 (actin1) or 10 (GFP) independent movies were produced and analysed for each condition. Movies are depicted as images representing collapsed t-stacks. Intensity profiles depict Cb-Emerald or GFP intensity along the measured axis (yellow line) over the entire duration of the movie. As polarity is difficult to define for RHsCas9-actin1-KO parasites, the start point of the measurement is indicated with an asterisk. The figure shows representative images. Scale bars are 5µm. See also **Supplement Movies V2** and **V3**, as well as **Appendix Figure 7-2**. Please note that live microscopy for the RHsCas9-CbEm-actin strain was performed by Dr Mario Del Rosario.

Recently, a model of actin flux to the basal pole alongside the parasite periphery was proposed for extracellular *Toxoplasma* parasites (Tosetti et al. 2019). As the periphery presents a place of high actin abundance in intracellular parasites, I was eager to investigate actin flow at this location. Kymograph analysis on wild-type parasites showed trajectories representing Cb-Emerald particle flow to the apical and the basal pole (**Figure 4-12 A and B**) (**Supplement Movie V1 and V2**) (**Appendix Figure 7-1 and 7-3**). This finding demonstrates bi-directional actin flow alongside the lateral axis of intracellular parasites. Strikingly, upon *Tgactin1* disruption, kymographs did not display any obvious particle tracks (**Figure 4-12 A**) (**Supplement Movie V2**) (**Appendix Figure 7-1**). This interpretation is supported by the strong resemblance of sCas9-actin1-KO kymographs to measurements performed on the movie background (**Figure 4-12 D**) (**Supplement Movie V2**) (**Appendix Figure 7-1**). Disruption of *Tgadf* caused kymographs to depict strong accumulation of static actin at the basal end (**Figure 4-12 B**) (**Supplement Movie V1**) (**Appendix Figure 7-3**). Measurements performed on RH-GFP parasites resulted in more diffuse and, thus, highly distinguishable kymographs when compared to wild-type Cb-Emerald kymographs (**Figure 4-12 C**) (**Supplement Movie V3**) (**Appendix Figure 7-2**). This strongly indicates that the kymograph analysis presented here is capable of specifically depicting actin dynamics.

Data suggest that intracellular *Toxoplasma* parasites possess four sites of major actin abundance. These sites are the two poles, the cytosolic region anterior to the nucleus and the periphery. Bi-directional actin flow appears to occur at the

periphery. Based on these findings, I am proposing that cytosolic actin flow connects these different sites of actin accumulation.

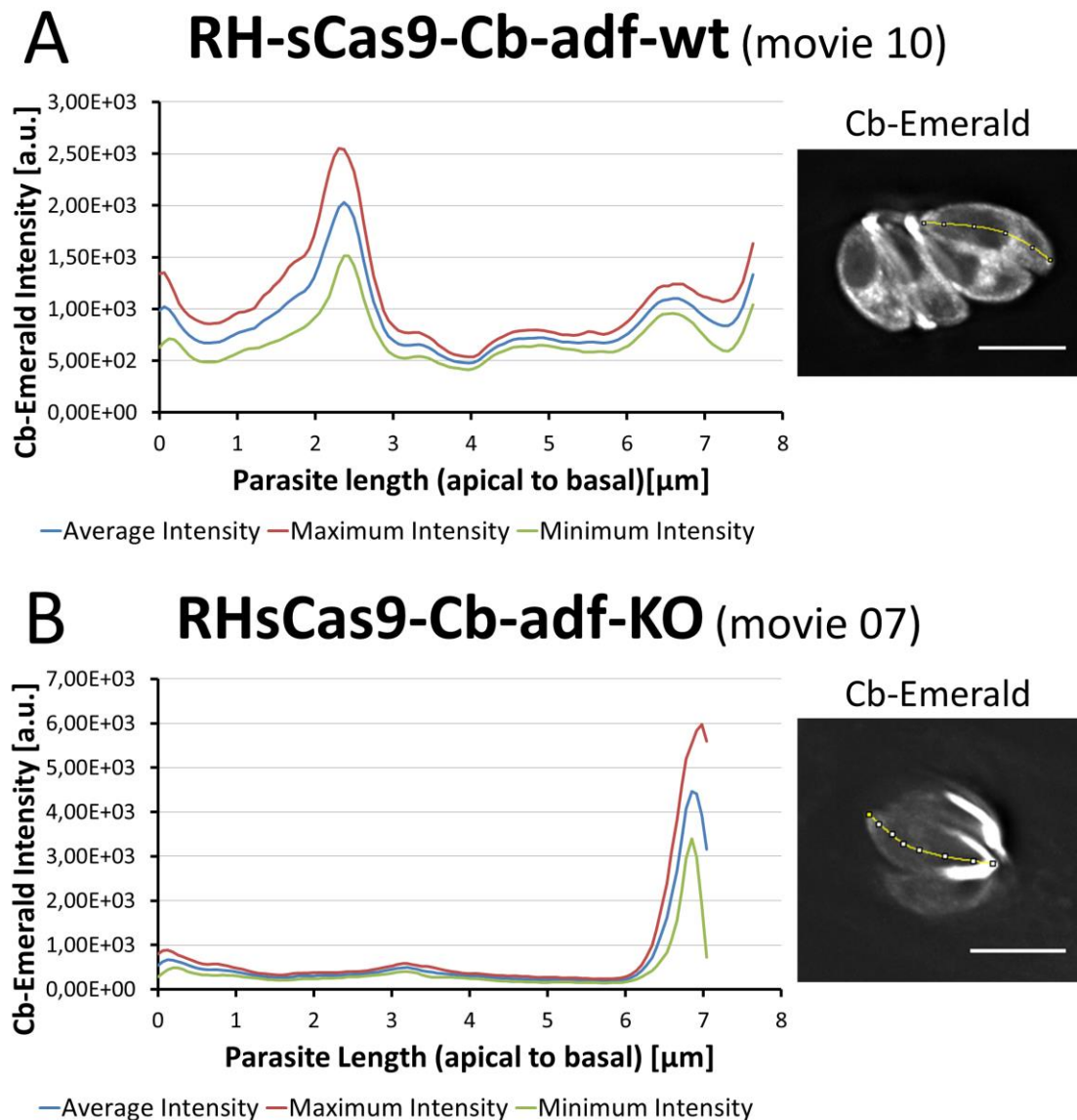


Figure 4-9: Actin distribution in intracellular RHsCas9-CbEm-*adf* wt and KO parasites along the middle axis

(A) and (B) Time-averaged intensity profiling along the parasites middle axis in RHsCas9-CbEm-*adf*-wt and RHsCas9-CbEm-*adf*-KO parasites. Parasites were incubated with or without 50nM rapamycin for 1h. After a growth period of 72h, cultures were mechanically lysed and incubated on a fresh host cell monolayer for another 24h prior to live microscopy. At least 10 independent movies were produced and analysed for each condition. Movies are depicted as images representing collapsed t-stacks. Intensity profiles depict Cb-Emerald intensity along the measured axis (yellow line) over the entire duration of the movie. The figure shows representative images. See also **Supplement Movie V1** and **Appendix Figure 7-3**. Scale bars are 5μm.

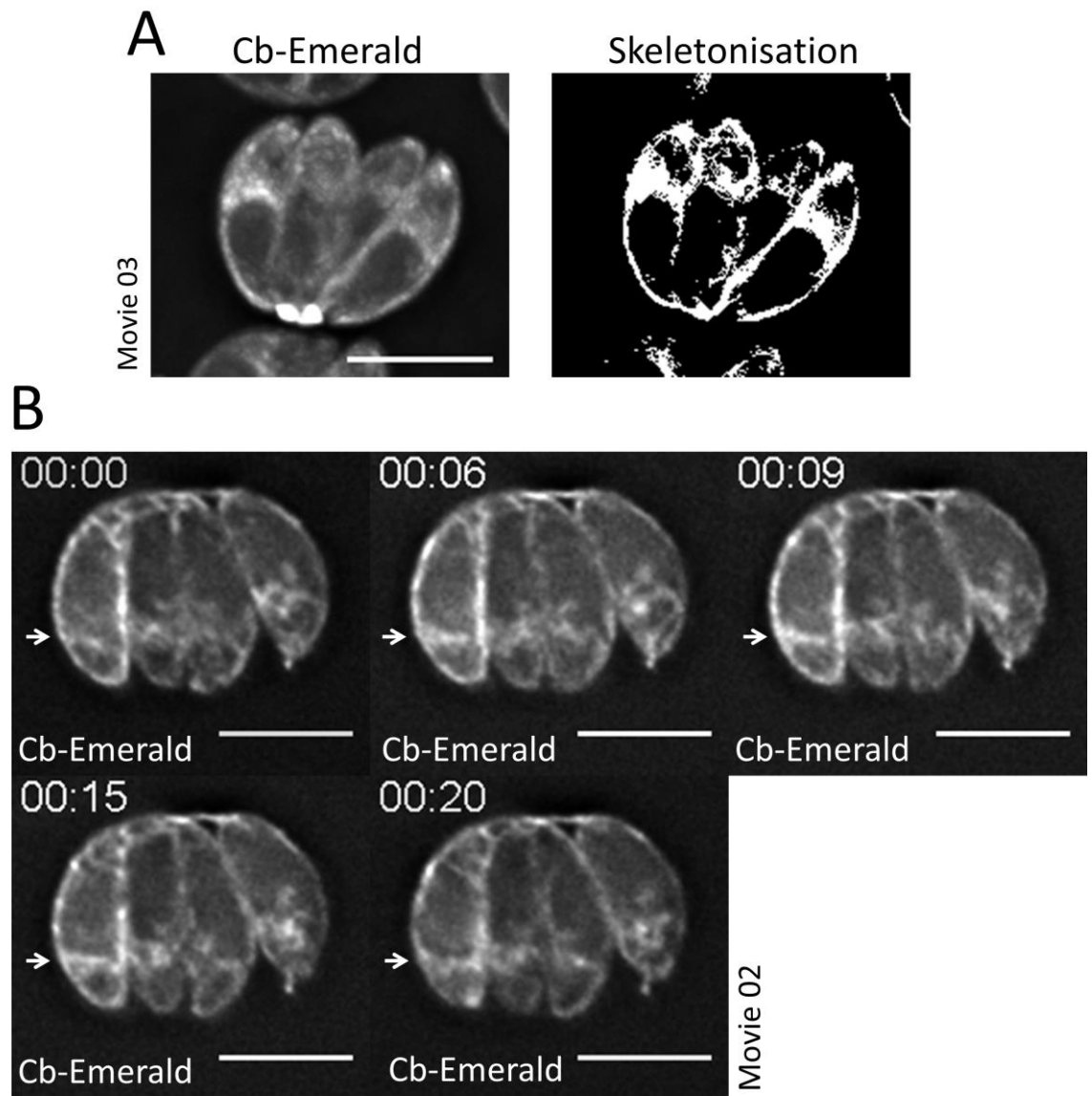
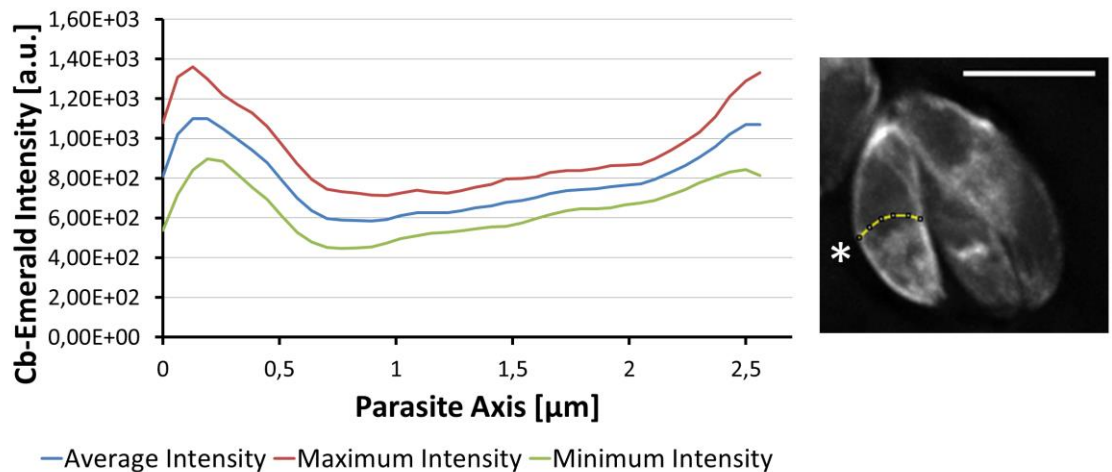


Figure 4-10: Live microscopy and skeletonisation analysis investigating the interaction of the cytoplasmic actin pool and peripheral actin in the RHsCas9-CbEm-*adf-wt* line

Parasites were grown for 72h. Cultures were then mechanically lysed and incubated on a fresh host cell monolayer for another 24h prior to live microscopy. **(A)** Skeletonisation analysis (right panel) for the depicted Cb-Emerald movie (left panel). The movie is depicted as collapsed t-stacks. **(B)** Live microscopy depicting the contact of the cytoplasmic actin pool with peripheral actin (white arrows). At least 10 independent movies were produced and analysed. The figure shows representative images. Time is depicted as mm:ss. Scale bars are 5µm. See also **Supplement Movie V1**.

A RHsCas9-Cb-actin1-wt (movie 03C)



B RHsCas9-Cb-actin1-KO (movie 02A)

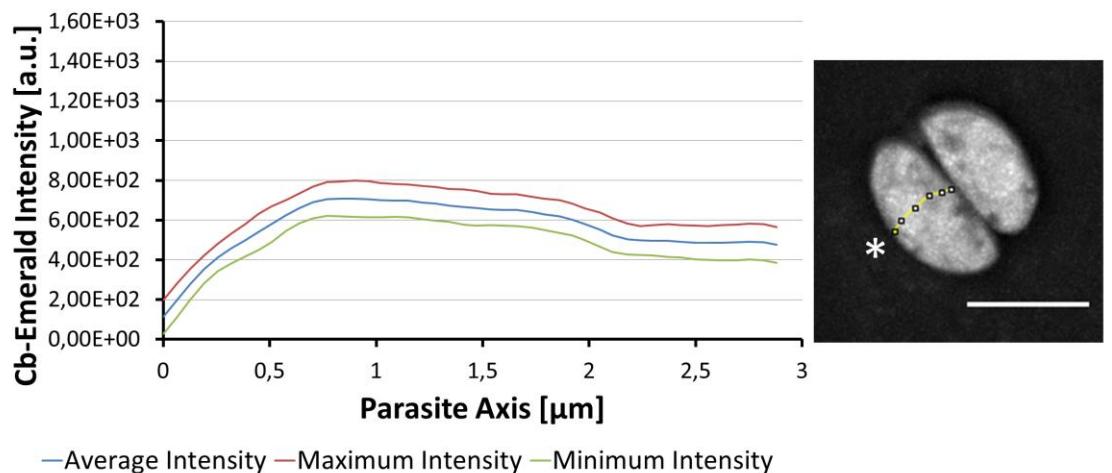
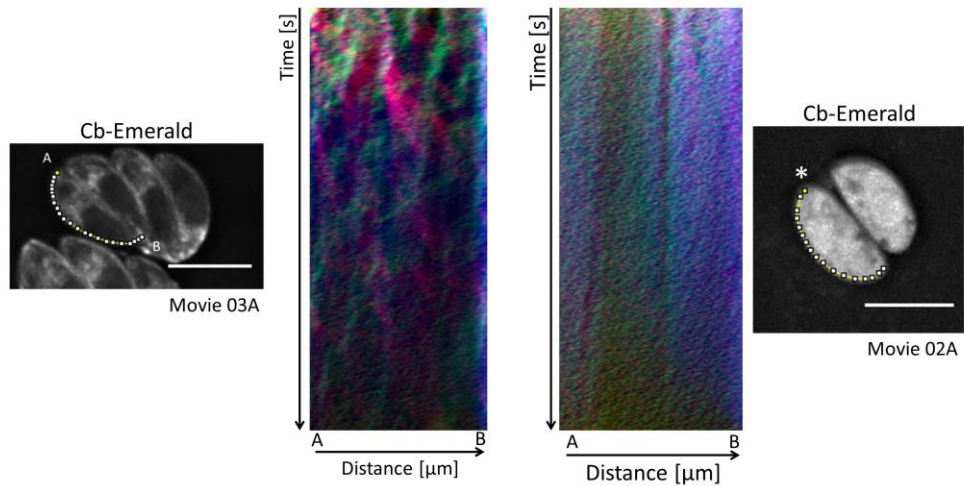


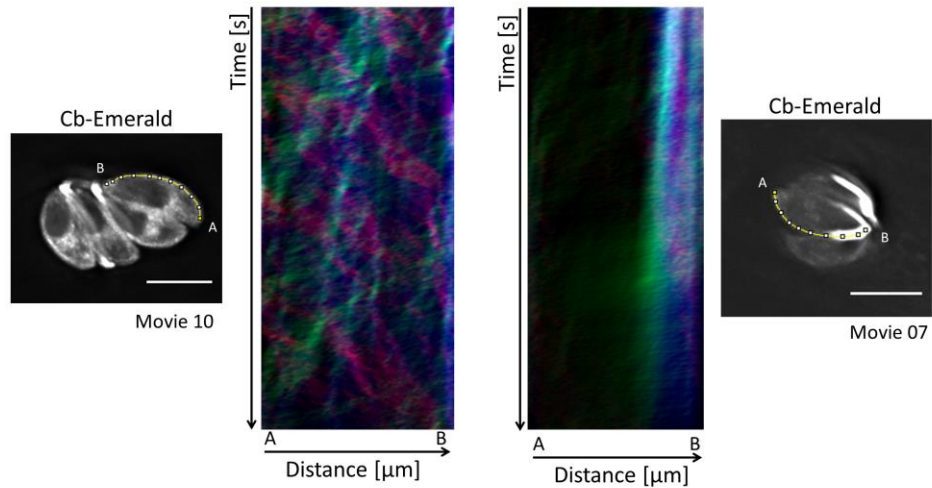
Figure 4-11: Actin distribution in intracellular RHsCas9-CbEm-actin1 wt and KO parasites along the horizontal axis

(A) and (B) Time-averaged intensity profiling along the parasites horizontal axis in RHsCas9-CbEm-actin1-wt and RHsCas9-CbEm-actin1-KO parasites. Parasites were incubated with or without 50nM rapamycin for 1h. After a growth period of 72h, cultures were mechanically lysed and incubated on a fresh host cell monolayer for another 24h prior to live microscopy. Movies are depicted as images representing collapsed t-stacks. Intensity profiles depict Cb-Emerald intensity along the measured axis (yellow line) over the entire duration of the movie. The start point of each measurement is indicated with an asterisk. Scale bars are 5 μ m. See also **Supplement Movie V2**. Please note that live microscopy for the RHsCas9-CbEm-actin strain was performed by Dr Mario Del Rosario.

A RHsCas9-Cb-actin1-wt RHsCas9-Cb-actin1-KO



B RHsCas9-Cb-actin1-wt RHsCas9-Cb-actin1-KO



C RH-GFP **D** background

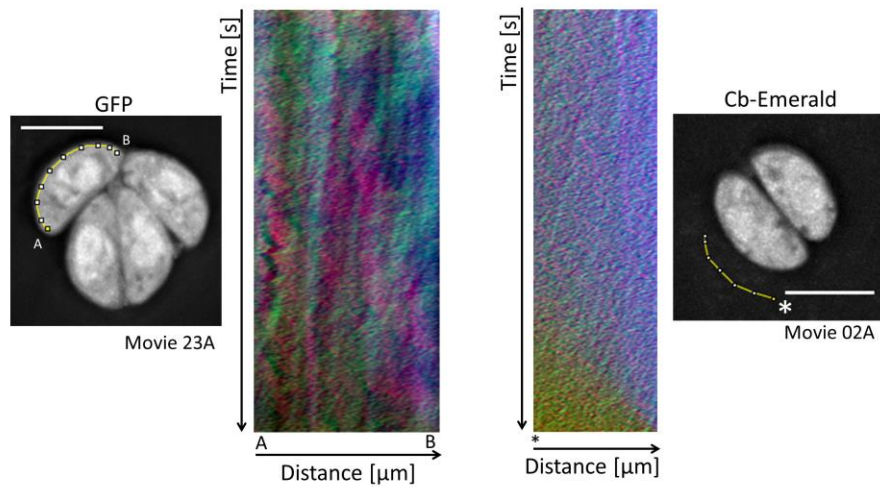


Figure 4-12: Kymograph analysis of peripheral actin flow in intracellular *Toxoplasma* parasites

Figure 4-12 continued: Kymograph analysis is shown for **(A)** RHsCas9-CbEm-actin1-wt/KO, **(B)** RHsCas9-CbEm-*adf*-wt/KO and **(C)** RH-GFP parasites. **(D)** Kymograph analysis was performed on the movie background for RHsCas9-CbEm-actin1-KO. Particle movement alongside the periphery is depicted via three colour-coded kymographs. Red tracks represent particles moving to the basal end, green tracks show particle flow to the apical end and blue depicts static particles. The yellow line represents the area of kymograph measurement. Particle movement was measured from the apical (A) to the basal pole (B). As polarity is difficult to define for sCas9-actin1-KO parasites, the start point of the flow measurement is indicated with an asterisk. The same is true for the background measurement. Parasites were incubated with or without 50nM rapamycin for 1h. After a growth period of 72h, cultures were mechanically lysed and incubated on a fresh host cell monolayer for another 24h prior to live microscopy. RH-GFP parasites were grown for 24h prior to live microscopy. Images represent videos as collapsed t-stacks. At least 5 (actin) or 10 (others) independent movies were produced and analysed for each depicted condition. The figure shows representative kymographs. Scale bars are 5µm. See also **Supplement Movies V1, V2 and V3**. Additional analysis can be found in **Appendix Figures 7-1, 7-2 and 7-3**. Please note that live microscopy for the RHsCas9-CbEm-actin strain was performed by Dr Mario Del Rosario.

4.4 Summary and conclusions

In this chapter, the split-Cas9 system was combined with the actin chromobody technology (Periz et al. 2017) to investigate the actin network in *Toxoplasma*. By doing so, I was able to re-produce previously reported effects on the intracellular actin network for the genes *Tgactin1* and *Tgadf* (Periz et al. 2017). The impact of these genes on parasite egress was also investigated with the split-Cas9 system. My findings support previous publications for *Tgactin1* (Egarter et al. 2014; Whitelaw et al. 2017) and *Tgadf* (Mehta and Sibley 2011). Taken together, these data suggest that phenotypical analysis is possible for actin factors despite the occurrence of DNA damage upon Cas9 activity.

Interestingly, the abundance of DNA damage within a population depended on the targeted gene. For example, the number of vacuoles displaying DNA damage after *Tgadf* disruption was twice as high as the number of vacuoles after *Tgactin1* targeting. It would therefore appear that some genomic loci are more challenging to repair than others. When applying split-Cas9 for phenotypic characterisation, it remains crucial to include proper controls such as the RHsCas9-*sag1* strain. Furthermore, one has to determine the applicability of the split-Cas9 system for each assay individually.

Due to successful confirmation of known actin phenotypes, I argued that the split-Cas9 system should be suitable for a phenotypical screening approach, aiming at identifying potentially novel actin binding proteins. While a CRISPR/Cas9-based screening approach previously addressed overall parasite fitness (Sidik et al. 2016), a screen allowing for immediate insights into actin dynamics or other well discriminated phenotypes would present a powerful tool for future phenotypic screens. Therefore a medium through-put screen was initiated during my PhD studies (refer to chapter 5, section 5.5).

Disruption of *Tgadf* abolished intravacuolar filament disassembly upon parasite egress. In other organisms, ADF activity depends on its phosphorylation status (Mizuno 2013). ADF activity is inhibited by LIM kinase-dependent phosphorylation (Arber et al. 1998; Yang et al. 1998). The SSH phosphatase can mediate ADF dephosphorylation, thus leading to its re-activation (Niwa et al. 2002). It was also reported that SSH phosphatases can decrease LIM kinase activity by dephosphorylating the kinase itself (Soosairajah et al. 2005). Applying these findings to *Toxoplasma* biology, one could speculate that a calcium-dependent pathway might exist that mediates dephosphorylation of *TgADF* prior to egress. Activation of *TgADF* located to the large filamentous structures might explain their disassembly within seconds, as shown by Periz and co-workers (Periz et al. 2017). More experiments would have to be conducted to support this hypothesis.

Importantly, filament disassembly does not appear to be critical for successful parasite egress. I am therefore proposing that the disassembly process might serve the purpose of recycling actin by reintroducing monomeric actin to the cytosolic actin pool. Since actin was shown to be critical for parasite egress (Egarter et al. 2014; Whitelaw et al. 2017), increasing the overall actin concentration within the parasite might increase the chance for successful egress and subsequent host cell invasion.

Overall actin distribution was re-defined for intracellular parasites by performing live microscopy and kymograph analysis. I identified four actin accumulation sites: the apical and basal end, the cytosolic region anterior to the nucleus and the periphery. In addition, bi-directional actin flow appears to connect these actin polymerisation centres with each other. Based on live microscopy presented in this chapter, I was hypothesising that the cytosolic actin

polymerisation centre is fuelling the lateral actin flow. To gather supporting evidence for this theory, I wanted to focus on identifying the actin factors responsible for this highly dynamic actin site.

5 Investigating the role of *TgFormin2* within the intracellular actin network

In chapter 4, I redefined actin distribution in intracellular *Toxoplasma* parasites. The split-Cas9 system successfully reproduced previously reported actin phenotypes for the genes *Tgactin1* and *Tgadf*. In addition, four major actin accumulation sites were described: the two poles, the cytosolic region anterior to the nucleus and the periphery. The cytosolic actin centre (cAC) showed a highly dynamic nature and frequently interacted with the parasite periphery. Based on these observations, I hypothesised that the cAC is critical for the lateral actin flow in intracellular *Toxoplasma* parasites.

To explore this hypothesis, it was critical to identify the actin binding protein responsible for maintaining the cAC. I argued that rapid actin nucleation and polymerisation must be mediating the highly dynamic nature of this distinct actin site. The *Toxoplasma* genome codes for a limited set of actin binding proteins (Baum et al. 2006). For example, *Toxoplasma* lacks key components of the Arp2/3 actin nucleation complex (Gordon and Sibley 2005), which is a major contributor to actin polymerisation in other eukaryotes (Gould and Machesky 1999; Pollard and Beltzner 2002; Pollard 2007, 2016). Therefore, I reasoned that the remaining actin nucleation factors present in *Toxoplasma*, namely *TgFormin1-3* (Baum et al. 2006; Gupta, Thiyagarajan, and Sahasrabuddhe 2015), could be involved in maintaining the cAC.

The FH2 domains of *TgFormin1* and 2 were reported to initiate nucleation of rabbit actin (Daher et al. 2010) and *Toxoplasma* actin (Skillman et al. 2012) *in vitro*. Initially, *TgFormin1* and 2 were localised to the parasite periphery (Daher et al. 2010). A more recent study mentions that endogenously-tagged *TgFormin1* accumulates at the apical tip of the parasite, while endogenously-tagged *TgFormin2* locates to the vicinity of the apicoplast (Jacot et al. 2016). No experimental evidence was provided to support this claim for *TgFormin2*. The *TgFormin3* FH2 domain also nucleates rabbit actin and the enzyme was localised to the apical and the basal pole as well as around the mitochondrion (Daher et al. 2012). Overall, the localisation to the vicinity of the apicoplast made *TgFormin2* the prime candidate for mediating the cytosolic actin centre. I

followed this line of reasoning as the apicoplast frequently co-localised with the cytosolic actin centre anterior to the nucleus (Figure 4-1 A, wt panels).

It shall be mentioned that investigating the function of actin nucleation factors *in vivo* addresses a relevant conundrum of *Toxoplasma* actin biology. Although nucleation activity was shown for *TgFormins* *in vitro* (Daher et al. 2010, 2012; Skillman et al. 2012), an isodesmic polymerisation model was proposed as underlying mechanisms for actin filament formation in *Toxoplasma* (Skillman et al. 2013). According to this model, actin filaments assemble in a nucleation-independent fashion rendering nucleation factors unnecessary. It was further suggested that polymerisation and depolymerisation rate of actin filaments happen at equal rates. The model was applied to explain the previously reported presence of short and unstable actin filaments in *Toxoplasma* (Sahoo et al. 2006). It was recently proposed that *Plasmodium* actin kinetics behave similar to canonical actin *in vitro* (Kumpula et al. 2017). The observation that the depolymerisation rate for *PfACT1* appeared faster than for canonical actins (Kumpula et al. 2017) was later explained by unique structural features in the *PfACT1* molecule, promoting filament destabilisation and, consequently, depolymerisation (Kumpula et al. 2019).

In this chapter, the tools established in chapter 4 will be used to investigate the function of the actin nucleation factor *TgFormin2* within the complex actin network of *Toxoplasma*. I will demonstrate that the actin-chromobody technology presents a powerful tool for addressing actin dynamics in their natural environment, the parasite itself.

5.1 Localisation and function of *TgFormin2* within the actin network of intracellular *Toxoplasma*

Literature available during the process of data generation for this thesis made conflicting reports regarding *TgFormin2* localisation. According to one study, *TgFormin2* accumulated mainly to the periphery for *Toxoplasma* (Daher et al. 2010), while another reported the enzyme in close proximity to the apicoplast (Jacot et al. 2016). To clarify *TgFormin2* localisation, *TgFormin2* was endogenously-tagged with a c-terminal HA-tag (Figure 5-1 A). Correct

integration of the HA-tag into the parasite genome was confirmed by analytic PCR (**Figure 5-1 B**) and sequencing (**Appendix Figure 7-6 A**). In intracellular parasites, *TgFormin2*-HA accumulated in close proximity to the apicoplast (**Figure 5-1 C and D**). Transient expression of the actin-chromobody in *TgFormin2*-HA parasites revealed that *TgFormin2* co-localises with cytosolic sites of actin accumulation (**Figure 5-1-E**).

To explore *TgFormin2* function, I generated the RHsCas9-CbEmerald-formin2 strain which expressed a *formin2*-sgRNA together with the split-Cas9 system and the actin-chromobody. Analytic PCR confirmed integration of the sgRNA-plasmid into the parasite genome (**Figure 5-2 A**). Upon disruption of *Tgformin2*, 68% (± 6.6) of parasites lost the cytosolic actin centre (cAC) at 48h post split-Cas9 activation (1st lytic cycle) (**Figure 5-3A and Figure 5-4 B**). The untreated control population showed a baseline for cAC loss of 1.3% (± 1.2). The disruption of *Tgformin2* did not affect intravacuolar filament formation (**Figure 5-3**).

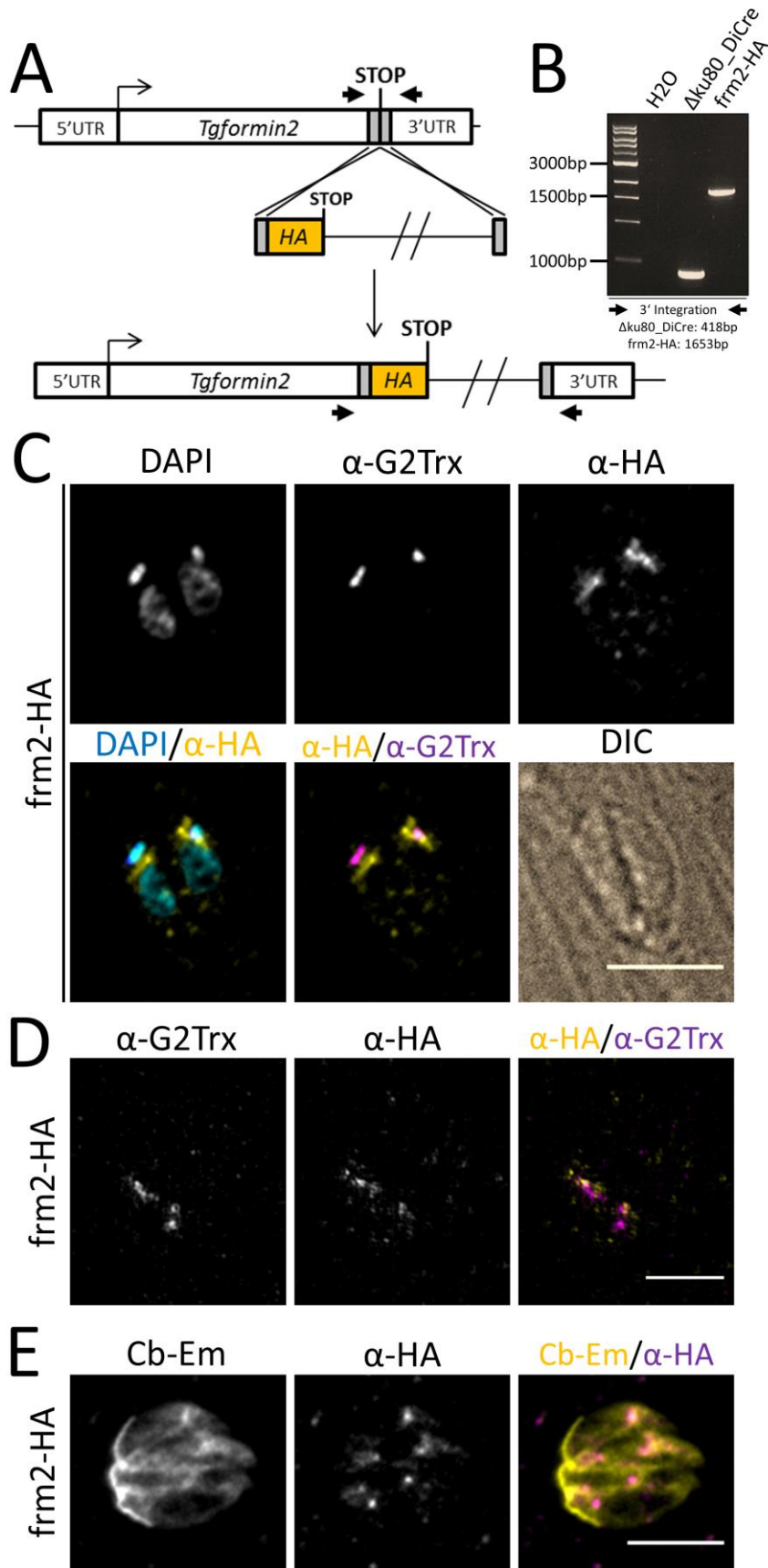


Figure 5-1: Investigation of *TgFormin2* (FRM2) localisation in *Toxoplasma*
(A) Cartoon depicting the insertion of an HA-tag at the 3' end of the *Tgformin2* (*frm2*) gene. Arrows indicate primers used for analytic PCRs shown in **(B)**. **(B)** Analytical PCR

confirming integration of the HA-tag into the parasite genome at the c-terminus of *Tgformin2* (*frm2*). The recognition sites of the colour-coded primers (arrows) are shown in (A). **(C)** IFA depicting *TgFRM2*-HA localisation in *Toxoplasma*. Parasites were grown for 24h and fixed with 4%PFA prior to IFA. Samples were stained with α -G2Trx (apicoplast) and α -HA (*TgFRM2*-HA). **(D)** Super-resolution microscopy confirming *TgFRM2*-HA localisation. Parasites were treated as described in (C). **(E)** Position of *TgFRM2*-HA within the actin network in intracellular *Toxoplasma* parasites. Samples were transiently transfected with the Cb-Emerald plasmid, inoculated for 48h and fixed with 4%PFA. Parasites were stained with α -HA (*TgFRM2*-HA) by IFA. The figure shows representative images. Nuclei were stained with DAPI. All scale bars are 5 μ m. Please note that the *TgFRM2*-HA strain was generated by Dr Mirko Singer. Experiments shown in this figure represent my own work.

Tgformin2 disrupted parasites lacking the cAC anterior to the nucleus displayed an apicoplast segregation phenotype (**Figure 5-3**). Two types of phenotypes were observed. Some vacuoles contained parasites simply being devoid of apicoplasts (**Figure 5-3 A, middle panel**). In other vacuoles, the lack of apicoplasts within the parasites was associated with the accumulation of apicoplast material to distinct locations within the vacuole (**Figure 5-3 A and B**). Most likely, apicoplasts accumulated outside the parasite bodies, i.e. the residual body or bodies, as *Tgformin2* disrupted parasites often egressed without containing an apicoplast (**Figure 5-4 A**). The apicoplasts were left behind outside the parasites upon egress. Of relevance, overall egress was not significantly affected by *Tgformin2* disruption (**Figure 4-4 A and B**).

Quantification of the apicoplast phenotype in parasites lacking the cAC was performed to provide a more detailed overview. After 48h post Cas9 activation (1st lytic cycle), 59.7% (± 5) of vacuoles depicted parasites devoid of the apicoplast without accumulation of apicoplast material to a specific location (**Figure 5-4 C**). Accumulation of apicoplasts in the residual body was observed in 31.7% (± 5.7) of vacuoles. In the 2nd lytic cycle (96h), apicoplast mislocalisation to the residual body was detected in 75% (± 4.4) of vacuoles, while 24% (± 5.3) of vacuoles contained parasites lacking the apicoplast without noticeable relocation to the residual body. In the non-treated control population, 11% (± 1) (1st lytic cycle) and 12.3% (± 1.6) (2nd lytic cycle) of vacuoles contained parasites lacking the apicoplast. Accumulation of apicoplasts within residual bodies of vacuoles was never observed in the control populations. Noteworthy, only vacuoles without any signs of DNA damage were included in the phenotypic

analysis (Figure 4-4 C). Disruption of the *Tgformin2* gene was confirmed by sequencing at 48h post induction (Figure 5-2 B).

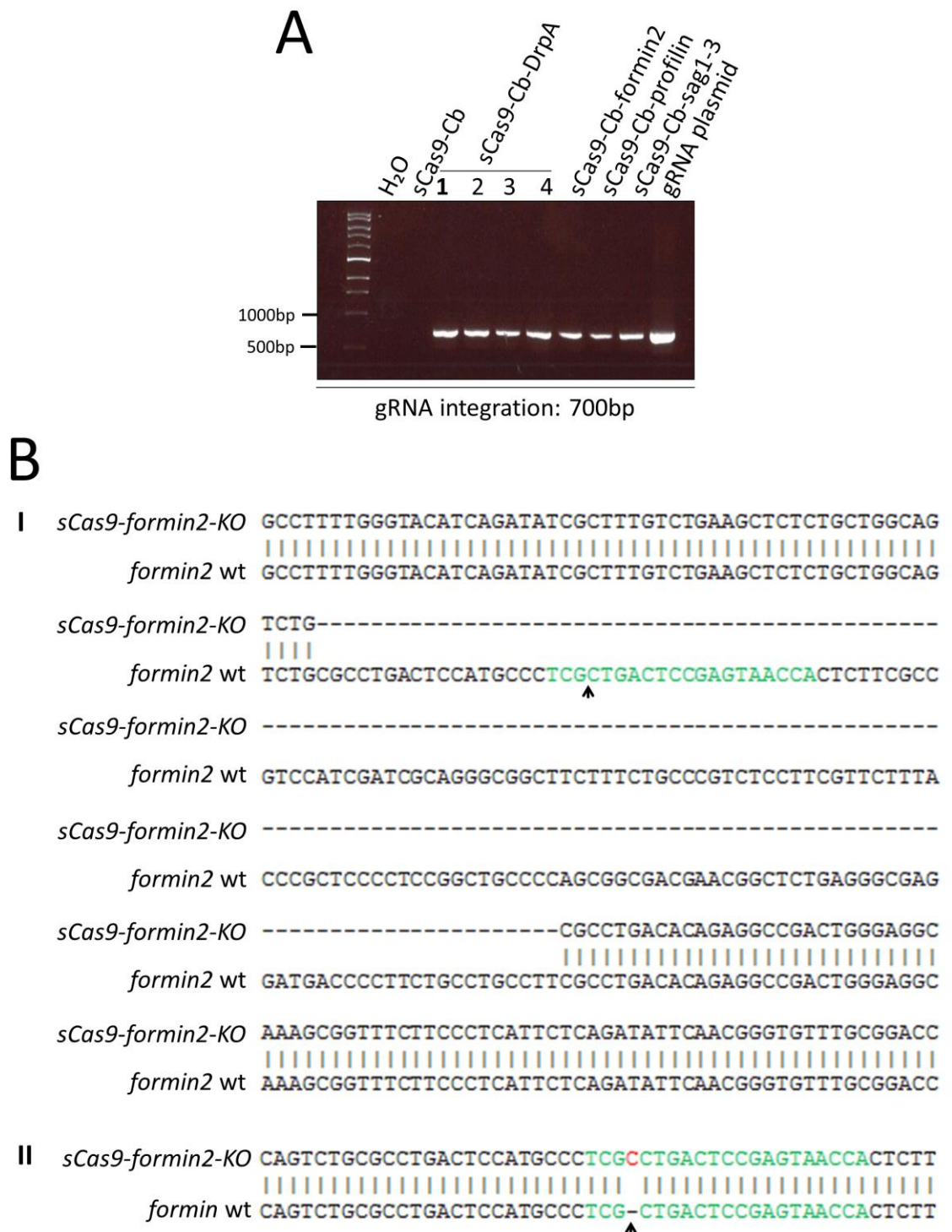


Figure 5-2: Confirmation of the strains RHsCas9-ActinChromobodyEmerald-DrpAsgRNA (RHsCas9-Cb-DrpA), RHsCas9-ActinChromobodyEmerald-formin2sgRNA (RHsCas9-Cb-formin2) and RHsCas9-ActinChromobodyEmerald-profilinsgRNA (RHsCas9-Cb-profilin)

(A) Analytical PCR confirming integration of indicated sgRNA-plasmids into the parasite genome. Integrated plasmids were amplified from the genome as described in Figure 3-2

A. **(B)** Sequencing performed on the sgRNA cut side of RHsCas9-Cb-formin2-KO. For this purpose, cultures were induced with 50nM rapamycin for 1h. Parasites were grown for 48h prior to gDNA collection. The sgRNA cut site was amplified by PCR. Amplicons (I, II) were cloned into the pGEM vector and sequenced. Green letters indicates sgRNA sequence. Red letters represent nucleotide insertion in the mutant strain, causing a frame shift and, thus, the functional knock-out of the indicated gene. Black arrows indicate the predicted cut side. Please note that the analytical PCR (A) was performed by Dana Aghabi under my supervision.

In summary, data presented here strongly indicate that the nucleation factor *TgFormin2* is critical for maintaining the cytosolic actin centre (cAC) in intracellular parasites. *TgFormin2* localisation to the vicinity of the apicoplast and to actin accumulation centres supports this finding. The previously reported *TgFormin2* localisation by Jacot and co-workers (Jacot et al. 2016) was confirmed. *TgFormin2* driven actin nucleation appears to be essential for apicoplast inheritance. The process of apicoplast inheritance had been linked to *TgFormin2* previously by overexpressing the *TgFormin2* FH2 domain in *Toxoplasma* (Jacot, Daher, and Soldati-Favre 2013). Most interestingly, conditional disruption of *Tgformin2* with the split-Cas9 system caused the apicoplast mislocalisation to the residual body. The importance of actin dynamcis on apicoplast inheritance is well documented in *Toxoplasma* (Andenmatten et al. 2013; Jacot, Daher, and Soldati-Favre 2013; Haase et al. 2015; Whitelaw et al. 2017). However, massive accumulation of apicoplast material outside the parasite upon *Tgformin2* disruption presents a unique feature among actin-related apicoplast phenotypes.

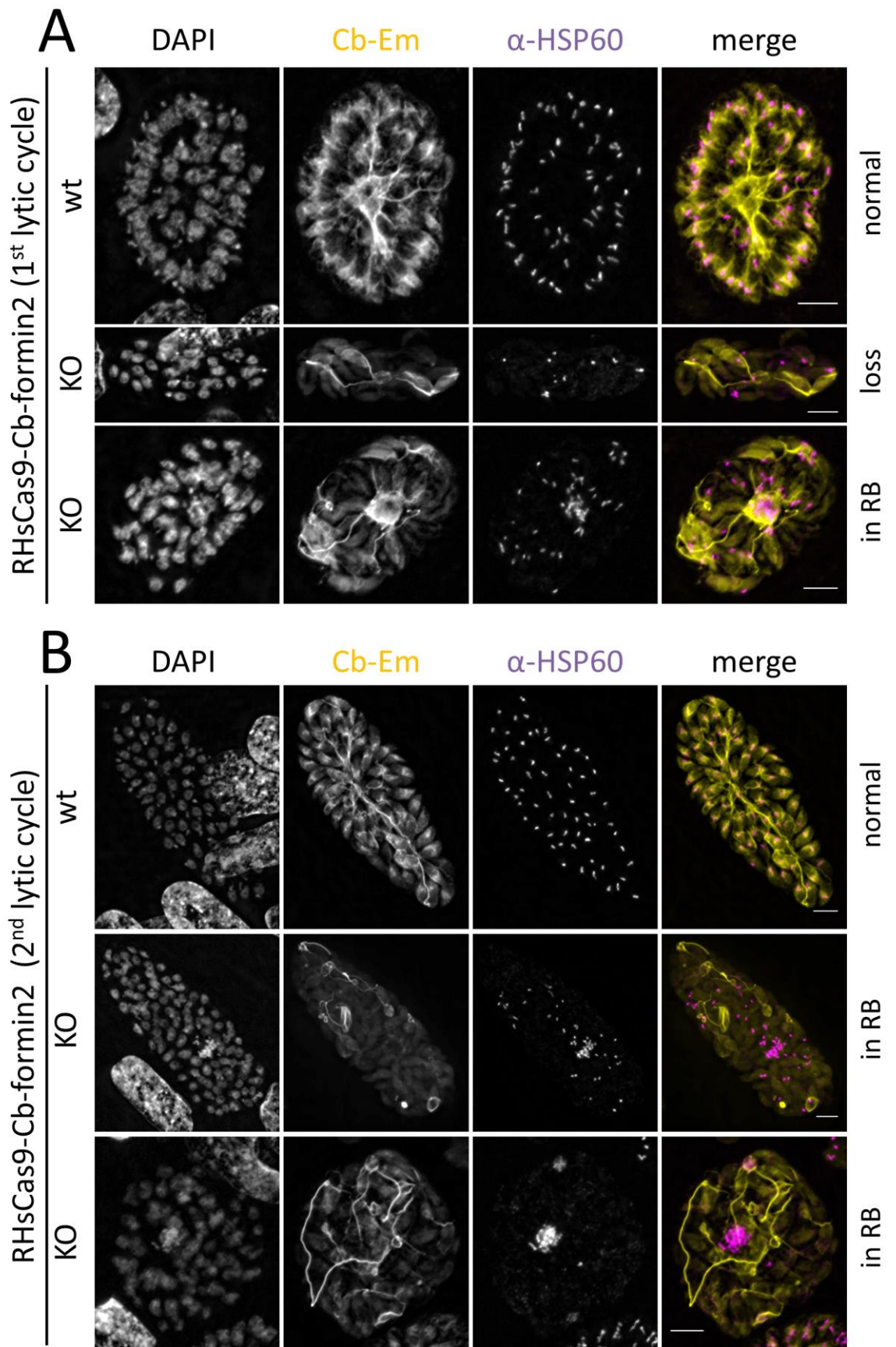


Figure 5-3: Disruption of *Tgformin2* in RHsplit-Cas9 parasites expressing actin-chromobody-Emerald (Cb-Em or Cb)

Figure 5-3 continued: IFA depicts the effect of *Tgformin2* (RHsCas9-Cb-formin2) disruption on the actin network (Cb-Emerald) and apicoplast segregation (HSP60). *Tgformin2*-wt parasites showed normal apicoplast numbers and localisation (normal), while *Tgformin2*-KO parasites depicted apicoplast loss (loss) or the accumulation of apicoplast material in the residual body (RB) (in RB). Quantification of these phenotypes can be found in Figure 5-4. **(A)** To achieve gene disruption (KO), parasites were incubated with 50nM rapamycin for 1h. Parasites were fixed after 48h with 4%PFA (1st lytic cycle). **(B)** Parasites were treated with 50nM rapamycin for 1h (KO). Parasites were grown for 48h, mechanically lysed and inoculated again for another 48h prior to fixing with 4%PFA (2nd lytic cycle). Apicoplasts were stained with α -HSP60 by IFA. Nuclei were stained with DAPI. Scale bars are 5 μ m.

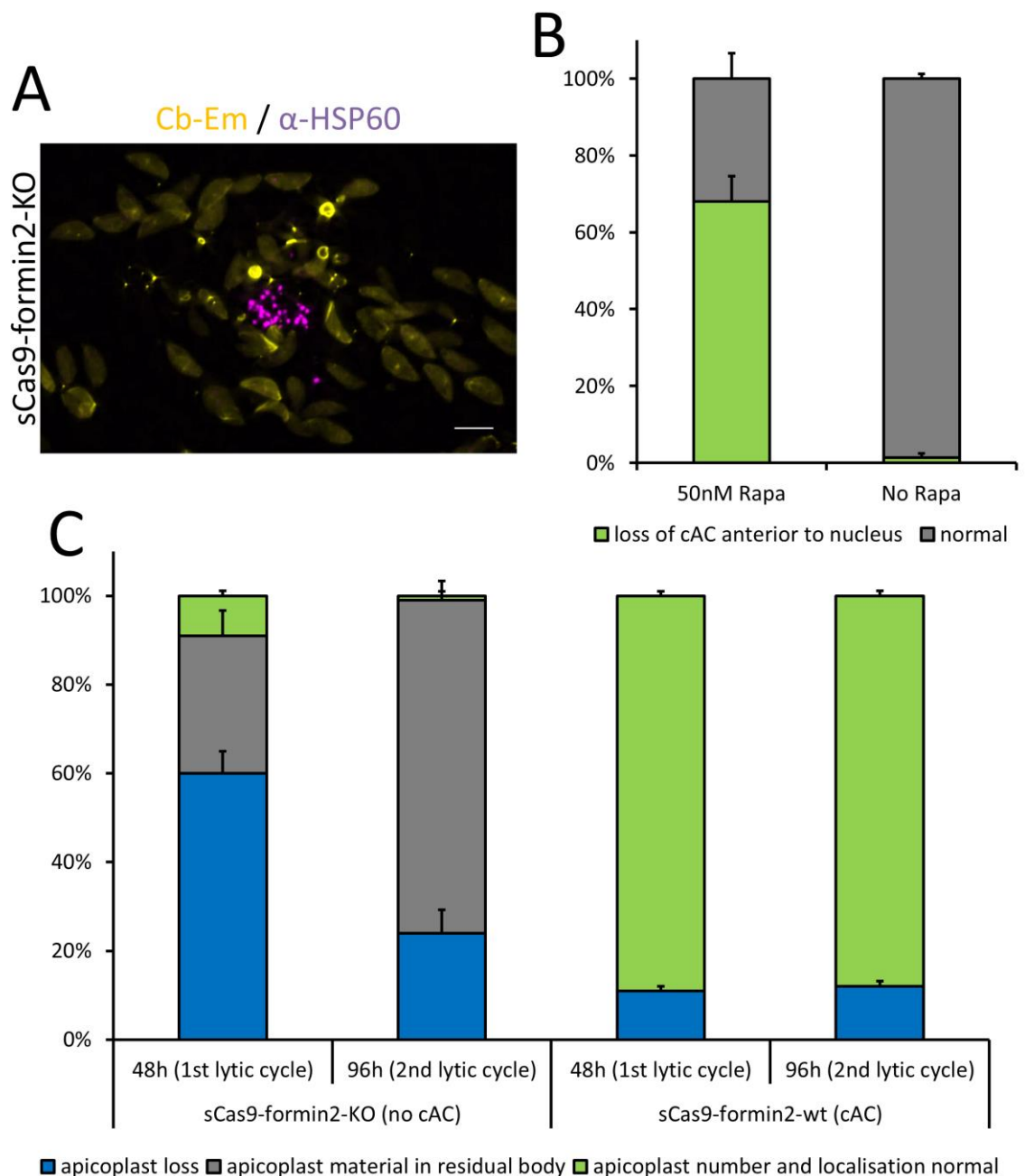


Figure 5-4: Disruption of *Tgformin2* in RHsplit-Cas9 parasites expressing actin-chromobody-Emerald (Cb-Em or Cb)

(A) IFA depicting natural egress of RHsCas9-CbEm-formin2-KO parasites. To achieve gene disruption (KO), parasites were incubated with 50nM rapamycin for 1h. Parasites were fixed after 48h with 4%PFA and stained with α -HSP60 (apicoplast) by IFA. Scale bar is 5 μ m. **(B)** Quantification of IFA depicted in Figure 5-3 A. The graph quantifies the loss of the cytosolic actin centre (cAC) anterior to the nucleus in rapamycin-treated (50nM) and untreated populations of the RHsCas9-CbEm-formin2 strain. For this experiment, parasites were stained by IFA after 48h of growth (see Figure 5-3 A). **(C)** Quantification of the different apicoplast phenotypes depicted in the IFAs in Figure 5-3 A and B. RHsCas9-CbEm-formin2-wt parasites showing the natural cytosolic actin centre (cAC) anterior to the nucleus were compared to RHsCas9-CbEm-formin2-KO parasites lacking the cAC. For both conditions, parasites of the 1st and the 2nd lytic cycle were investigated. Parasites were treated as described in Figure 5-3 A and B. Quantifications presented in (B) and (C) were obtained from three independent experiments for each condition. For each condition 100 vacuoles were counted (total n=300).

5.2 Confirmation of *TgFormin2* function with the DiCre system

The effect of *Tgformin2* disruption with split-Cas9 presented a complete novelty with regards to actin dynamics in intracellular parasites. To ensure that the DNA damage observed in some parasites after split-Cas9 activation (see chapter 3) did not cause the observed phenotype, I decided to validate the function of *TgFormin2* using the DiCre system (Andenmatten et al. 2013) as an independent conditional approach. Due to its mode of action, the DiCre system allows gene excision without causing a double-stranded DNA break. As demonstrated for *TgMec17* (see chapter 3, **Figure 3-9** and **Figure 3-10**), no underlying effects are to be expected upon gene excision.

For this purpose, the *Tgformin2* gene was flanked with two *loxP* sites and, at the same time, c-terminally-tagged with *yfp* to generate the DiCre-formin2-YFPloxP strain (**Figure 5-5 A**). Genome modifications and gene excision upon DiCre activation via rapamycin were confirmed via analytic PCRs (**Figure 5-5 B**). Sequencing analysis revealed in-frame integration of the *yfp*-tag into the genome (**Appendix Figure 7-6 B**).

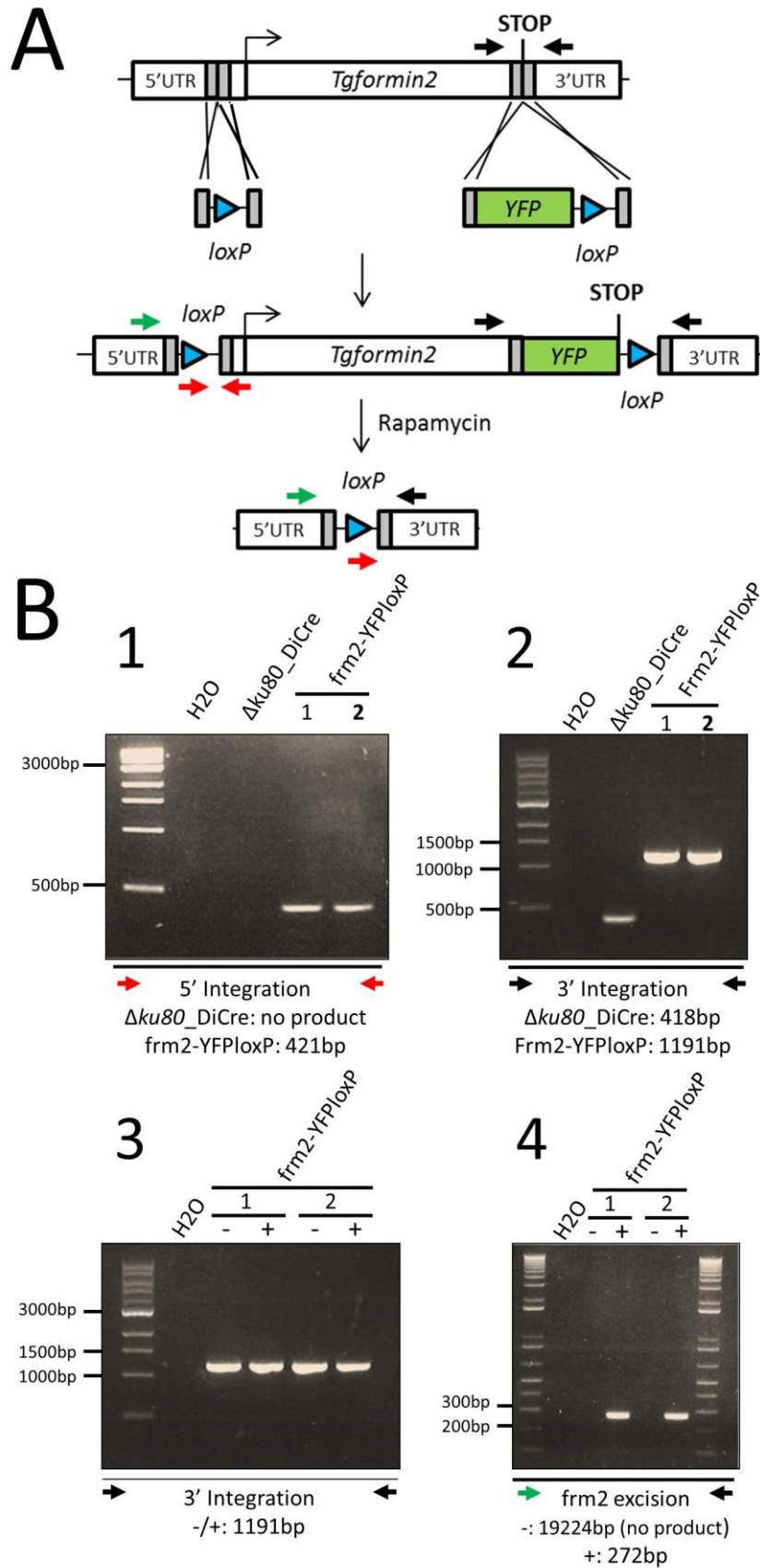


Figure 5-5: Generation and verification of the DiCre-formin2-YFPloxP strain
 (A) Cartoon depicting the strategy of flanking the *Tgformin2* gene with two loxP sites and, at the same time, inserting a YFP-tag at the 3' end of the gene. Upon rapamycin

treatment, the endogenous *Tgformin2* locus is excised. Arrows indicate primers used for analytic PCRs shown in (B). **(B)** Analytical PCR confirming integration of the loxP sites and the YFP-tag into the parasite genome. PCRs 1 and 2 confirm 5' and 3' integration, respectively. To confirm the excision of the *Tgformin2* (*frm2*) gene upon rapamycin treatment, parasites were inoculated with (+) or without (-) 50nM rapamycin. Samples of gDNA were collected after 48h. Excision of *Tgfrm2* was confirmed by PCR 4. The amplification of the 3' integration product in PCR 3 indicates incomplete gene excision in the rapamycin-induced *frm2*-YFPloxP population. The recognition sites of the colour-coded primers (arrows) are shown in (A). Please note that the DiCre-formin2-YFPloxP strain was generated by Dr Mirko Singer. Experiments shown in this figure represents my own work.

Localisation of *TgFormin2* to the vicinity of the apicoplast was confirmed by detecting *TgFormin2*-YFP with an anti-YFP antibody (**Figure 5-6 A, top panel**). Interestingly, the YFP signal was not detectable without antibody use (**Figure 5-7**), probably suggesting low expression levels for *TgFormin2*. Closer examination revealed that 30% of *TgFormin2*-YFP signal partially overlaps with the apicoplast (**Figure 5-8**). In other cases, *TgFormin2* was found adjacent to the apicoplast with (58%) or without (12%) being in contact with the apicoplast periphery. Taken together, this quantification suggests that *TgFormin2* preferentially accumulates in close proximity to the apicoplast in intracellular parasites.

Rapamycin treatment resulted in loss of *TgFormin2*-YFP in 35.7% ($\pm 3.8\%$) of parasites as determined by IFA (**Figure 5-6 A**). The same two types of apicoplast phenotypes as for the split-Cas9 system (**Figure 5-3 and Figure 5-4**) were observed upon excision of *Tgformin2*-YFP with the DiCre system (**Figure 5-6**). In 23.3% (± 3.8) of vacuoles, some parasites were devoid of the apicoplast without accumulation of apicoplast material to a specific location within the vacuole (**Figure 5-6 A and B**). Lack of apicoplasts within the parasites was associated with the accumulation of apicoplast material to the residual body in 41.3% (± 3.1) of vacuoles. In the untreated control population, 1% (± 0) of parasites showed an apicoplast segregation phenotype. No apicoplast material was detectable in the residual body in the control population. In addition, *TgFormin2*-YFP excision resulted in loss of the cAC anterior to the nucleus when parasites were transiently transfected with the actin-chromobody-emerald (**Figure 5-9**).

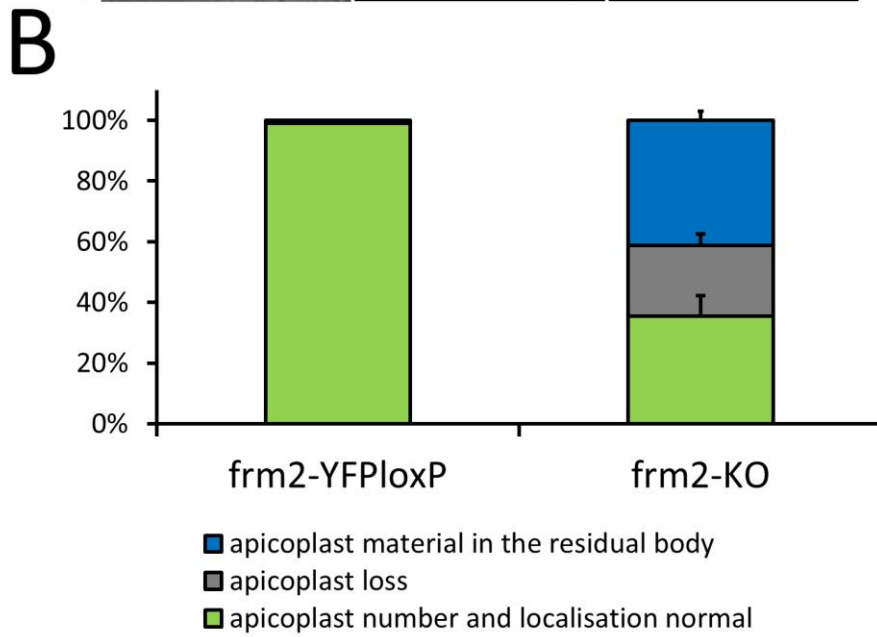
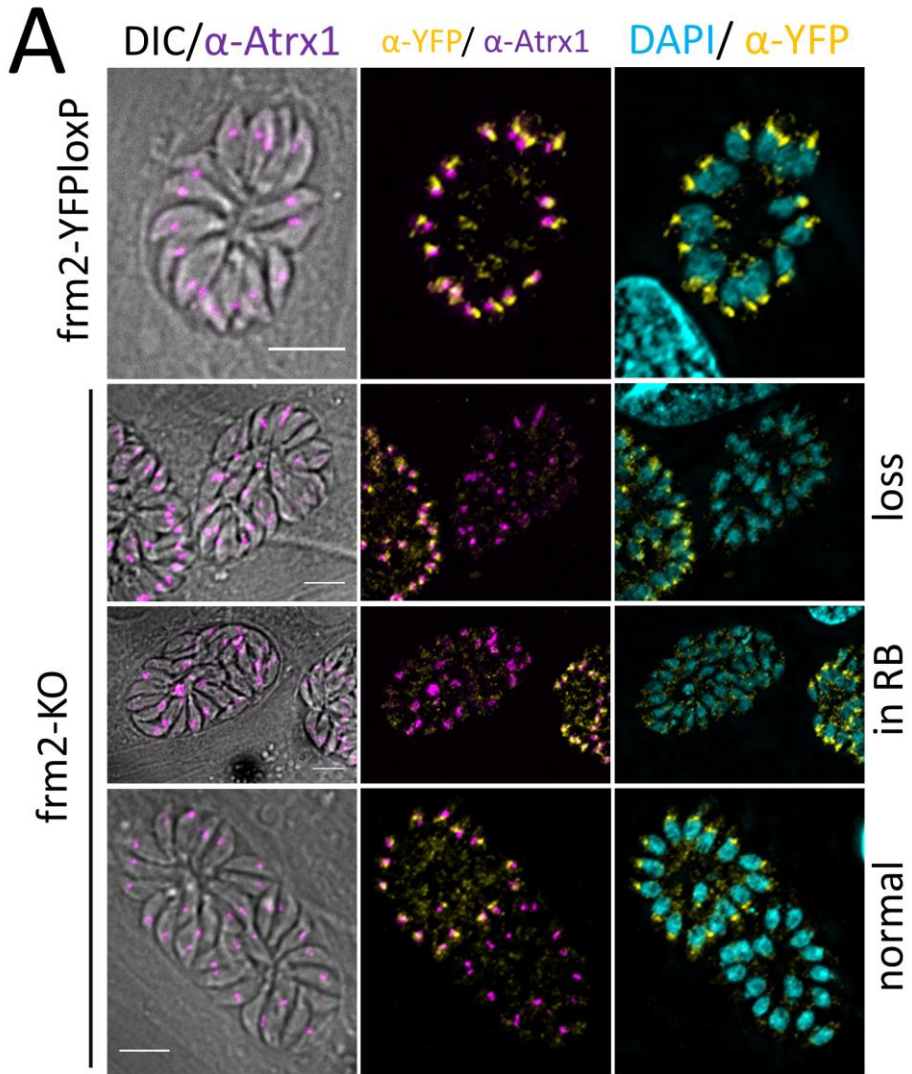


Figure 5-6: Effect of *Tgformin2* (*frm2*) excision with the DiCre system on apicoplast segregation and position

Figure 5-6 continued: (A) IFA depicting apicoplast fate in DiCre-frm2-YFPloxP and DiCre-frm2-KO parasites. DiCre-frm2-YFPloxP parasites showed normal apicoplast numbers and localisation (normal). The DiCre-frm2-KO population depicted normal apicoplast numbers (normal), apicoplast loss (loss) or the accumulation of apicoplast material in the residual body (RB) (in RB). DiCre-frm2-YFPloxP and DiCre-frm2-KO parasites were grown for 48h without or with 50nM rapamycin, respectively. After fixation with 4%PFA, apicoplasts were stained with α -Atrx-1 and Formin2-YFP was detected with α -YFP by IFA. Nuclei were stained with DAPI. Scale bars are 5 μ m. **(B)** Quantification of apicoplast phenotypes observed in IFA as presented in (A). Numbers were obtained from three independent experiments for each condition. For each condition 100 vacuoles were counted (total n=300).

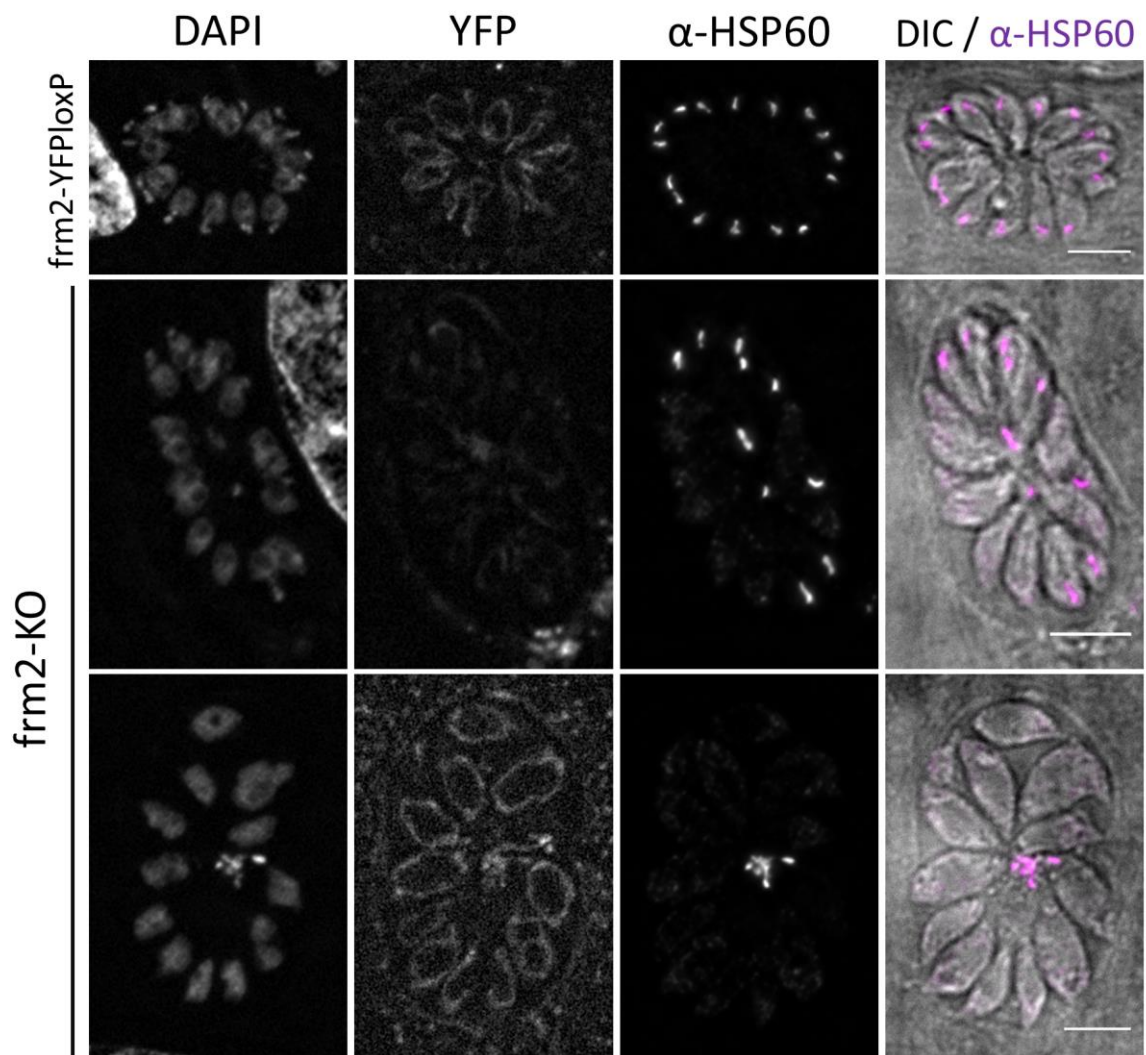


Figure 5-7: IFA attempting detection of *Tg*Formin2-YFP (*Tg*FRM2-YFP) without α -YFP antibody

DiCre-frm2-YFPloxP and DiCre-frm2-KO parasites were grown for 72h without or with 50nM rapamycin, respectively. After fixation with 4%PFA, apicoplasts were stained with α -HSP60 by IFA. Nuclei were stained with DAPI. The YFP channel shows background fluorescence. In the DiCre-frm2-YFPloxP population, YFP-tagged *Tg*FRM2 was not detectable in the absence of an YFP-antibody. The figure shows representative images. Scale bars are 5 μ m.

I was also interested in examining whether actin dynamics mediated by *TgFormin2* were involved in the replication and localisation of other organelles. While parasites displayed the characteristic apicoplast phenotypes after *TgFormin2*-YFP excision, parasites did not show any defect in mitochondria replication and morphology (**Figure 5-10 A**). Some rhoptry material accumulated in the residual body upon *Tgformin2* loss (**Figure 5-10 B**). However, further studies will have to be conducted to elucidate the role of actin dynamics in rhoptry biogenesis and overall morphology.

In summary, the DiCre system confirmed *TgFormin2* function in intracellular *Toxoplasma* parasites. Localisation studies with YFP-tagged *TgFormin2* stressed the close proximity between the nucleation factor and the apicoplast in intracellular parasites. I decided to further investigate this phenomenon in the next section.

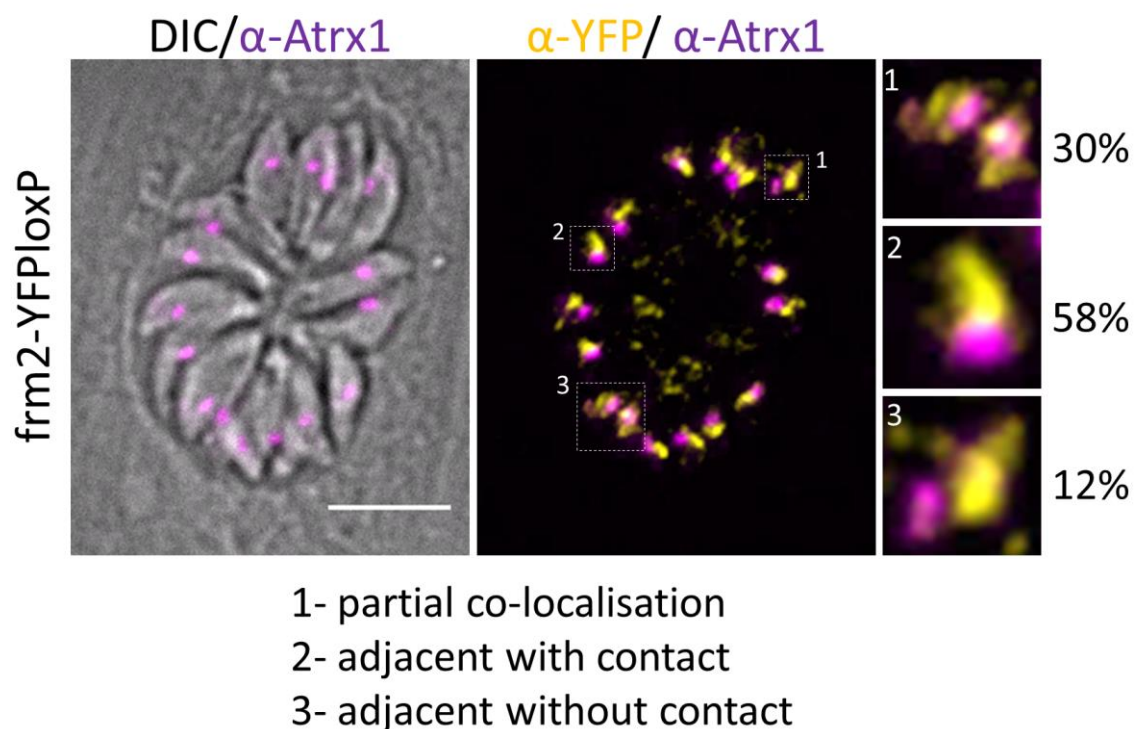


Figure 5-8: IFA depicting localisation of *TgFormin*-YFP in relation to the apicoplast in DiCre-frm2-YFPloxP parasites

Parasites were grown for 48h and fixed with 4%PFA. Apicoplasts were stained with α -Atrx-1 and *TgFormin2*-YFP was detected with α -YFP. Three different types of positioning were identified for *TgFormin2*-YFP. In 30% of parasites, *TgFormin2* and the apicoplast partially co-localise (1). In 58% of parasites, there is overlap in the periphery of *TgFormin2* accumulation site and the apicoplast (2). Other parasites (12%) show *TgFormin2* in close proximity to the apicoplast without signal overlap (3). Quantification is based on n=142

parasites from 22 independent vacuoles. This figure shows representative images. Scale bar is 5 μ m.

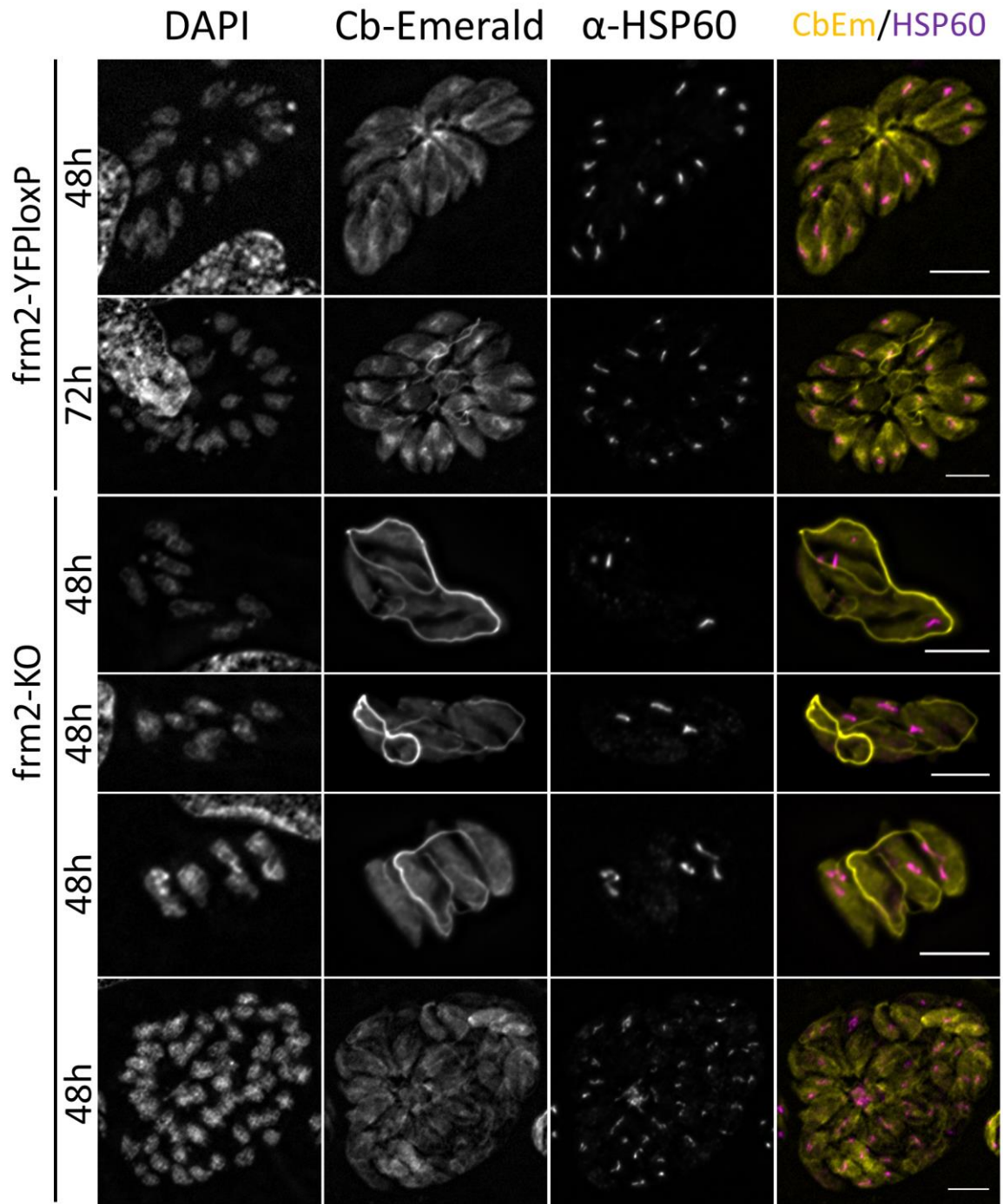


Figure 5-9: Transient expression of the actin-chromobody-emerald (Cb-Emerald/CbEm) in DiCre-frm2-YFPloxP and DiCre-frm2-KO parasites

Parasites were transiently transfected with the Cb-Emerald plasmid. Subsequently, the samples were grown with or without 50nM Rapamycin and fixed after 48h or 72h with 4%PFA. Apicoplasts were stained with α -HSP60 by IFA. Nuclei were stained with DAPI. The figure shows representative images. Scale bars are 5 μ m.

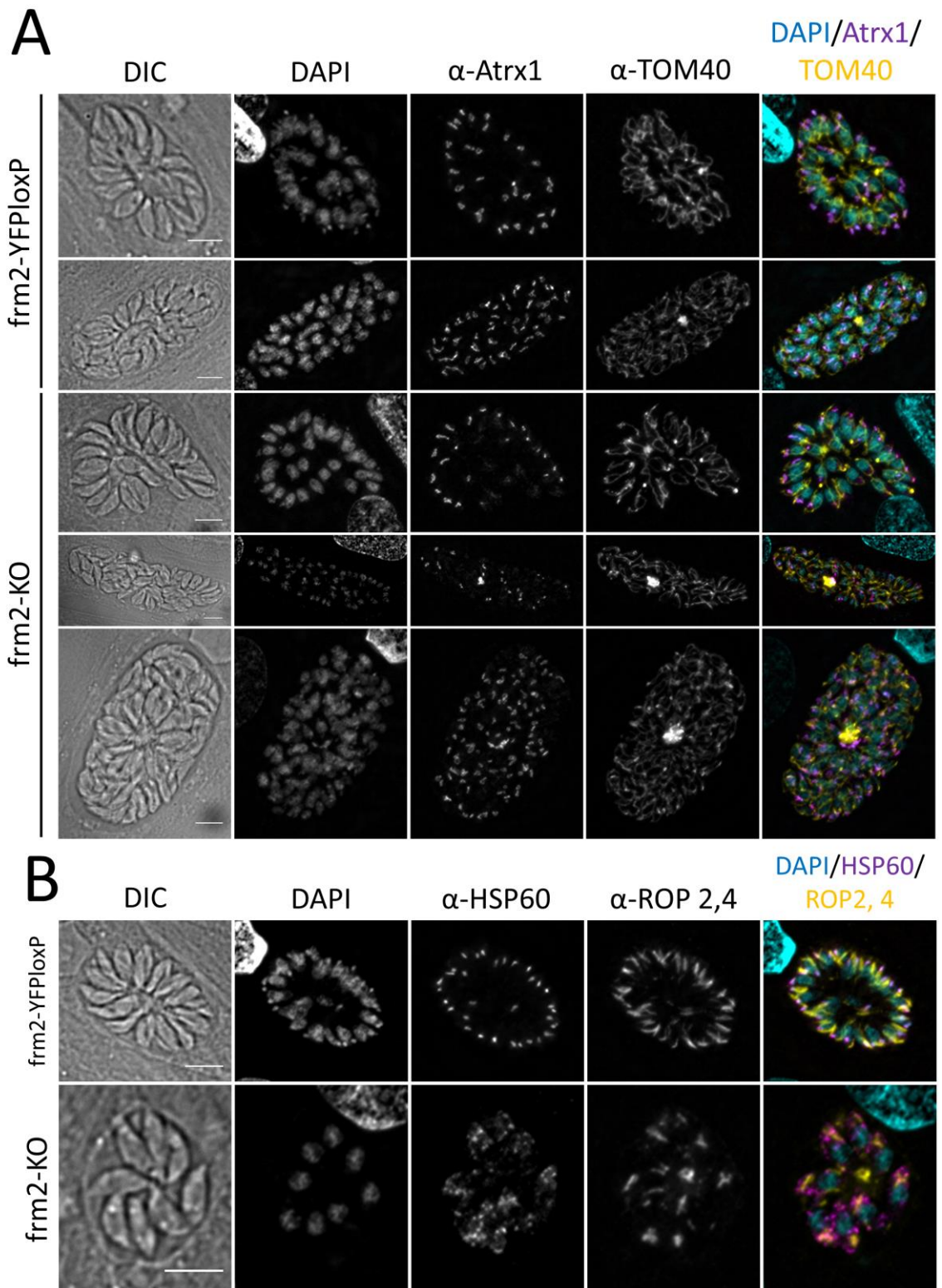


Figure 5-10: IFA depicting the effect of *Tgformin2* depletion with the DiCre system on morphology and positioning of mitochondria and rhoptries

(A) and (B) Parasites were grown with or without 50nM Rapamycin for 48h and fixed with 4%PFA. Apicoplasts were stained with α -HSP60 or α -Atrx1 by IFA. Rhoptries were visualized with α -Rop2,4. Mitochondria were stained with α -TOM40. Nuclei were stained with DAPI. The figure shows representative images. Scale bars are 5 μ m.

5.3 The role of the apicoplast in maintenance of actin dynamics

Bioinformatic studies performed by Dr Jonathan Wilkes at the Wellcome Centre for Integrative Parasitology (Glasgow, UK) revealed that *TgFormin2* contains a PTEN-C2-like domain (Stortz et al. 2019). The PTEN-C2 domain was reported to be involved in membrane recruitment (Das, Dixon, and Cho 2003). Interestingly, the PTEN domain mediates localisation of formin homology 5 (FH5) to the chloroplast in rice (Zhang et al. 2011). Since most *TgFormin2* appeared to be in contact with the apicoplast (**Figure 5-8**), I hypothesised that the apicoplast might act as an anchoring point for *TgFormin2*. This would mean that the apicoplast would not only be important for correct *TgFormin2* localisation, but, indirectly, also for maintaining the cAC. I argued that the role of the apicoplast in *TgFormin2* recruitment and cAC maintenance could easily be addressed by depleting the apicoplast from parasites.

To deplete *Toxoplasma* parasites of the apicoplast, the gene *TgdrpA* was disrupted with the split-Cas9 system. *TgDrpA* had been described previously as critical for the apicoplast segregation process by mediating apicoplast fission (van Dooren et al. 2009). Conditional expression of a dominant negative *TgDrpA* mutant rendered the parasites unable to segregate their apicoplasts. This resulted in apicoplast loss in parasites during intracellular growth. I argued that the disruption of *TgdrpA* presented a reliable tool for assessing the impact of the apicoplast loss on the cAC anterior to the nucleus.

For this purpose, I introduced the *drpA*sgrRNA into the RHsCas9-CbEm parental strain to generate the line RHsCas9-CbEm-*drpA*sgrRNA. Integration of the *drpA*sgrRNA was confirmed by analytical PCR (**Figure 5-2 A**). Disruption of *TgDrpA* via split-Cas9 resulted in parasites devoid of the apicoplast (**Figure 5-11**). In addition, apicoplasts appeared elongated, most likely due to the lack of apicoplast fission in the absence of functional *TgDrpA* (van Dooren et al. 2009). Interestingly, parasites lacking an apicoplast still displayed the cAC anterior to the nucleus showing that the apicoplast is not essential for cAC maintenance. Conditional disruption of *TgFormin2* function via the split-Cas9 or the DiCre system caused the cAC to disappear (**Figure 5-3 and Figure 5-8**), suggesting that there are no compensatory functions for maintaining the cAC in *Toxoplasma*.

Hence, the presence of the cAC indirectly suggests correct *TgFormin2* localisation and function in the absence of an apicoplast. It was recently reported that *TgFormin2* co-localises with the Golgi apparatus in non-dividing parasites and that depletion of the apicoplast does not impact *TgFormin2* localisation (Tosetti et al. 2019). These findings make an exclusive role for the apicoplast in *TgFormin2* recruitment in non-dividing parasites highly unlikely.

The function of the PTEN-C2 domain remains to be elucidated. One could speculate that the PTEN-C2-like domain mediates *TgFormin2* localisation and traffic to the apical region of the parasites independent from the apicoplast. I am further hypothesising that this domain might be involved in re-located *TgFormin2* to the edges of the dividing apicoplast (Tosetti et al. 2019). Further investigation is required to determine the biological relevance of the PTEN-C2-like domain.

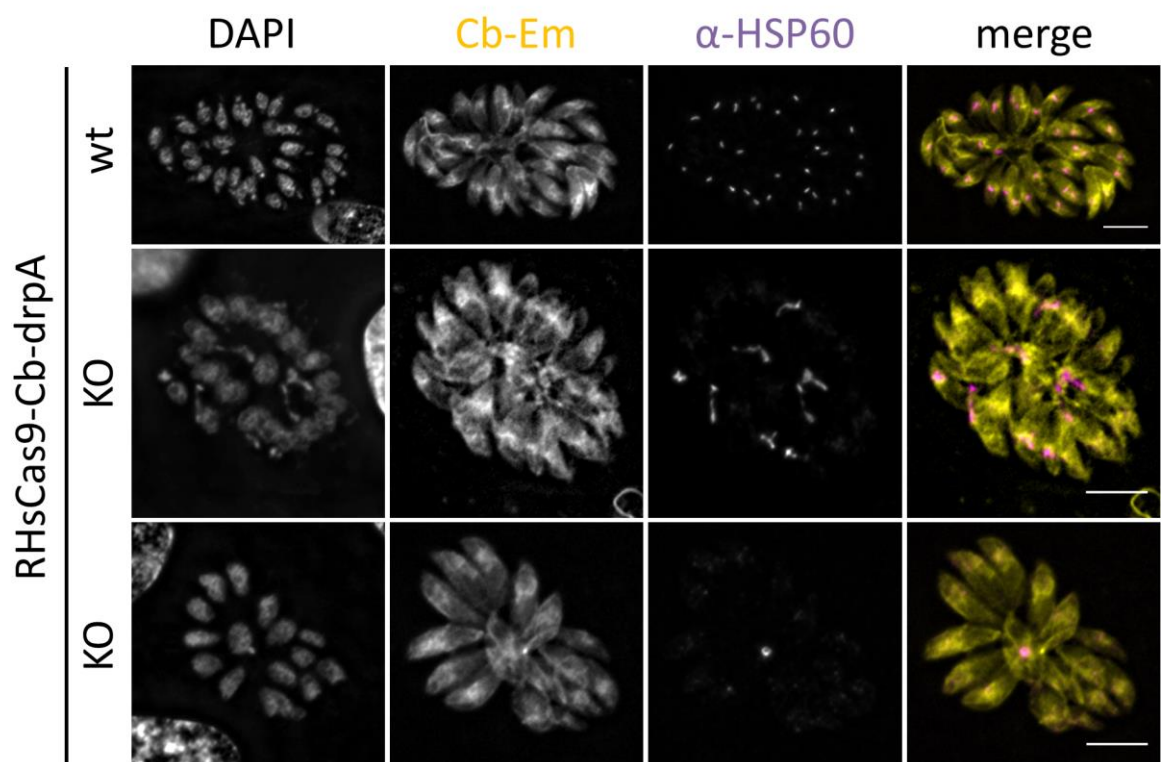


Figure 5-11: Disruption of *TgDrpA* in RHsplit-Cas9 parasites expressing actin-chromobody-Emerald (Cb-Em or Cb)

IFA depicts the effect of *TgDrpA* (RHsCas9-Cb-DrpA) disruption on the actin network (Cb-Emerald) and apicoplast segregation (HSP60). To achieve gene disruption (KO), parasites were incubated with 50nM rapamycin for 1h. Parasites were fixed after 48h with 4%PFA. Apicoplasts were stained with α -HSP60 by IFA. Nuclei were stained with DAPI. The figure shows representative images. Scale bars are 5 μ m.

5.4 The effect of the cytosolic actin centre on overall actin dynamics in intracellular *Toxoplasma*

Two independent systems identified *TgFormin2* as nucleation factor critical for maintaining the cytosolic actin centre (cAC) anterior to the nucleus. Upon loss *TgFormin2* function, the cAC, but not the intravacuolar filaments, is lost in intracellular parasites (**Figure 5-3 and Figure 5-9**). This phenotype was described by IFA and confirmed by time-averaged local intensity profiling (**Figure 5-12 and Appendix Figure 7-4**) (**Supplement Movie V4**).

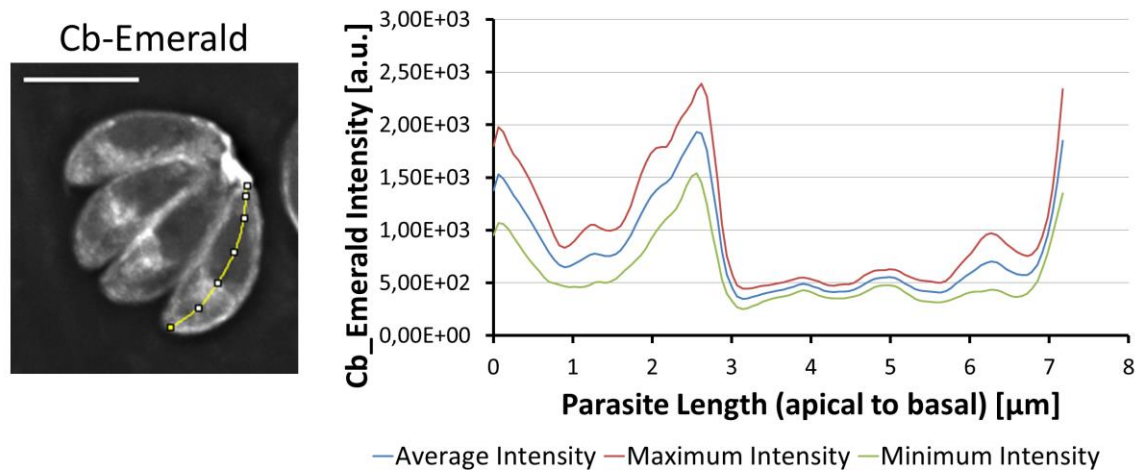
To analyse the effect of cAC loss on actin distribution and dynamics within parasites, I performed live microscopy on RHsCas9-CbEm-*formin2*-wt and RHsCas9-CbEm-*formin2*-KO parasites. Non-treated RHsCas9-CbEm-*formin2*-wt parasites displayed a highly dynamic cytosolic actin centre (cAC) that interacted with the parasite periphery (**Figure 5-13**) (**Supplement Movie V4**). Collapsed t-stack images and skeletonisation analysis confirmed that actin accumulated at four accumulation sites: the two poles, the cytosolic actin centre (cAC) anterior to the nucleus and the parasite periphery (**Figure 5-14**) (**Supplement Movie V4**). Upon *Tgformin2* disruption, parasites lost the cAC (**Figure 5-14**) (**Supplement Movie V4**). In addition the actin signal in the periphery appeared strongly reduced. Actin polymerisation outside the parasite bodies, i.e. the residual body was not affected. Actin accumulation was still detectable at the apical tip in some parasites.

Kymograph analysis in *formin2*-wt parasites showed particle trajectories to the apical and basal pole indicating bi-directional actin flow along the periphery (**Figure 5-15 and Appendix Figure 7-5**) (**Supplement Movie V4**). Kymographs of RH-sCas9-CbEm-*formin2*-KO parasites appeared overall more diffuse, although some tracks could still be observed. This is most likely due to residual actin in the periphery and perhaps due to actin polymerisation mediated by *TgFormin1* located at the apical tip (Jacot et al. 2016).

In summary, these data indicate that the *TgFormin2*-mediated cytosolic actin centre (cAC) majorly contributes to actin distribution and dynamics within intracellular parasites. Upon cAC loss, actin abundance was highly reduced in the parasite periphery. Peripheral actin flow also appeared affected, with

kymographs showing less clear trajectories. This strongly indicates that the highly dynamic cAC does indeed fuel lateral, bi-directional actin flow in intracellular *Toxoplasma*. In conclusion, actin nucleation mediated by *TgFormin2* appears to be required for the maintenance of intracellular actin dynamics.

A RH-sCas9-formin2-wt (movie 04)



B RH-sCas9-formin2-KO (movie 04)

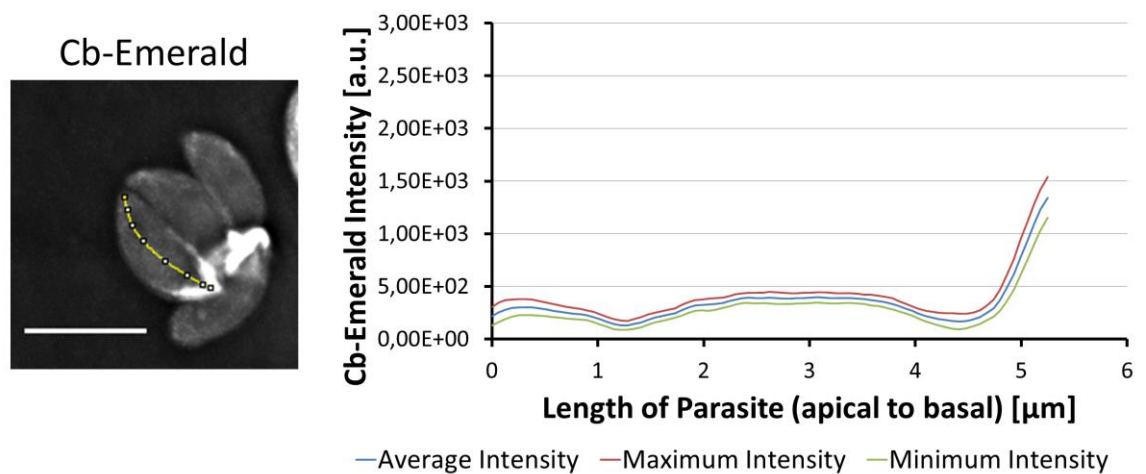


Figure 5-12: Actin distribution in intracellular RHsCas9-CbEm-formin2 wt and KO parasites along the middle axis

(A) and (B) Time-averaged intensity profiling along the parasites middle axis in RHsCas9-CbEm-formin2-wt and RHsCas9-CbEm-formin2-KO parasites. Parasites were incubated with or without 50nM rapamycin for 1h. After a growth period of 72h, cultures were mechanically lysed and incubated on a fresh host cell monolayer for another 24h prior to live microscopy. At least 10 independent movies were produced and analysed for each condition. Movies are depicted as images representing collapsed t-stacks. Intensity profiles depict Cb-Emerald intensity along the measured axis (yellow line) over the entire duration of the movie. The figure shows representative images. Scale bars are 5μm. Please see also **Appendix Figure 7-4** and **Supplement Movie V4**.

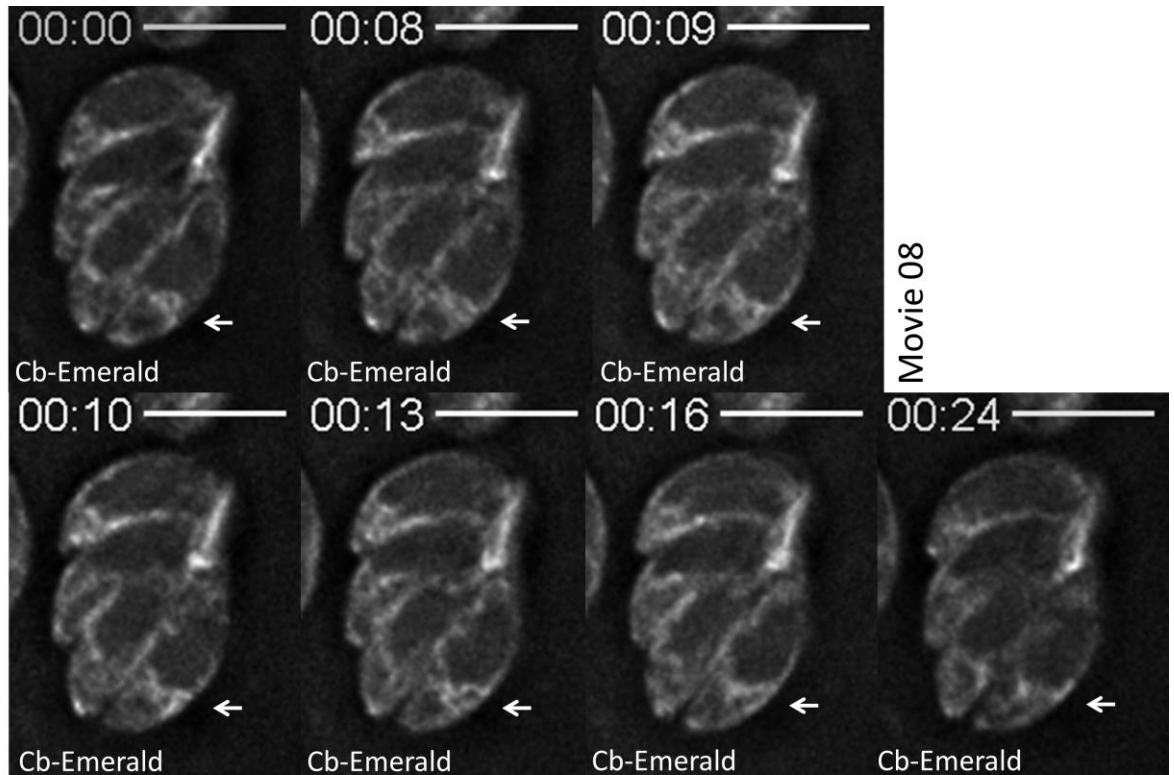


Figure 5-13: Live microscopy analysis investigating the interaction of the cytoplasmic actin pool and peripheral actin in the RHsCas9-CbEm-formin2-wt line

Parasites were grown for 72h. Cultures were then mechanically lysed and incubated on a fresh host cell monolayer for another 24h prior to live microscopy. Images depict the contact of the cytoplasmic actin pool with peripheral actin (white arrows). At least 10 independent movies were produced and analysed. The figure shows representative images. Time is depicted as mm:ss. Scale bars are 5 μ m. Please see also **Supplement Movie V4**.

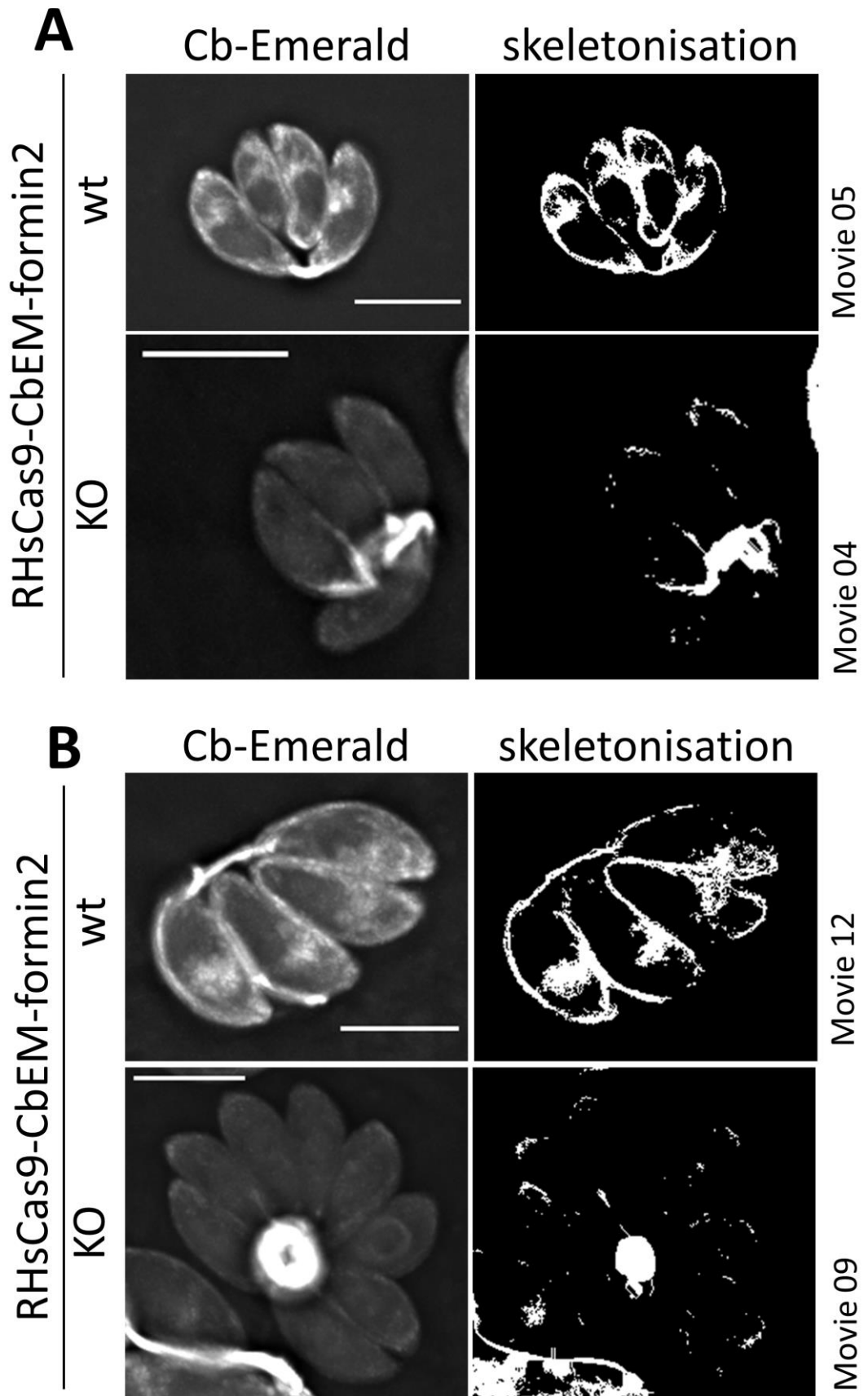


Figure 5-14: Skeletonisation analysis investigating actin distribution in RHsCas9-CbEm-formin2-wt and RHsCas9-CbEm-formin2-KO parasites

(A) and (B) RHsCas9-CbEm-formin2-wt parasites were cultured under normal conditions. RHsCas9-CbEm-formin2-KO parasites were treated with 50nM rapamycin for 1h. After a growth period of 72h, cultures were mechanically lysed and incubated on a fresh host cell monolayer for another 24h prior to live microscopy. Movies are shown with their respective skeletonisation analyses. Movies are depicted as collapsed t-stacks. At least 10 independent movies were produced and analysed for each depicted condition. The figure shows representative movies and skeletonisation. Scale bars are 5 μ m. Please see also **Supplement Movie V4**.

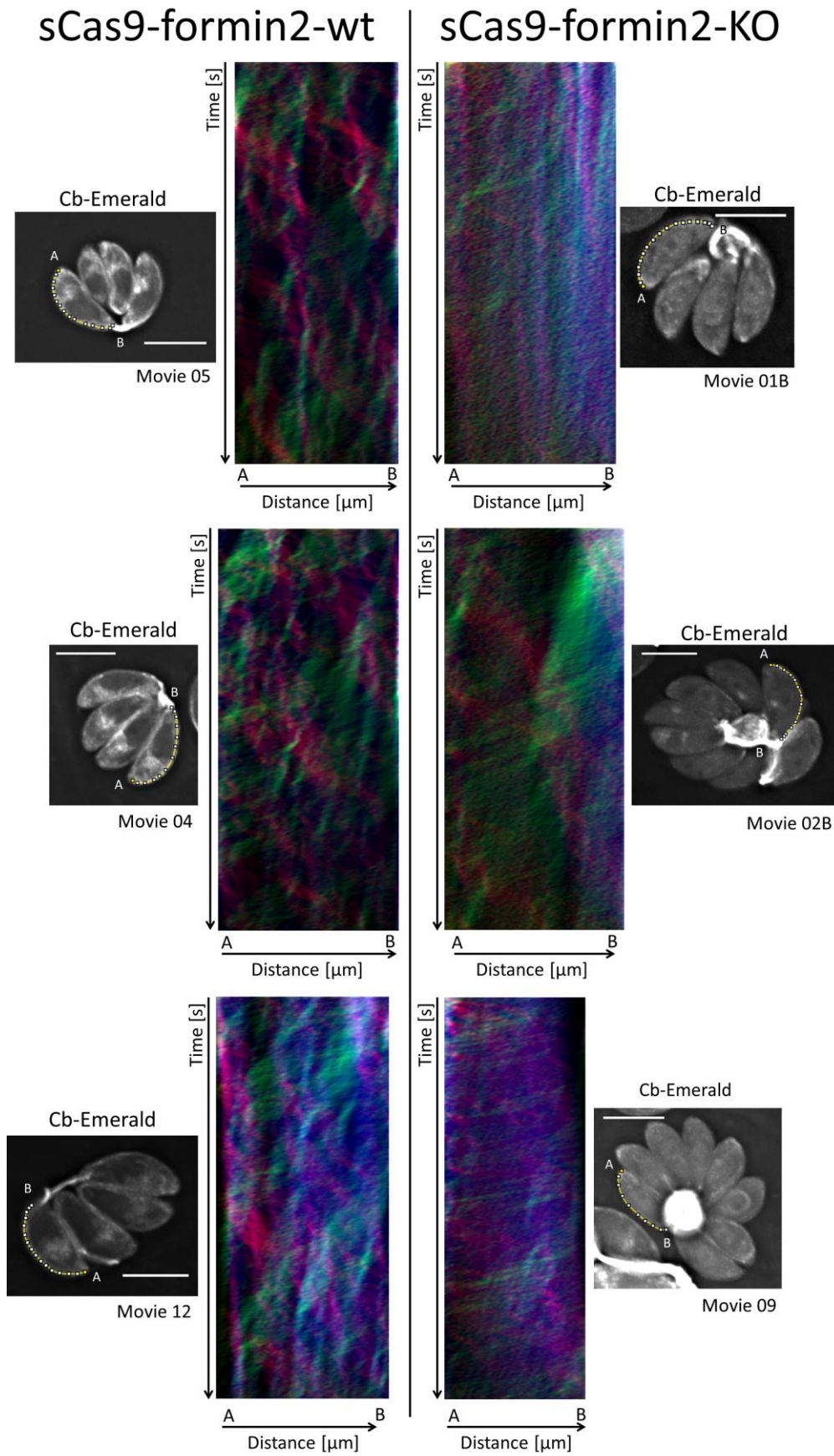


Figure 5-15: Kymograph analysis of peripheral actin flow in intracellular RHsCas9-CbEm-formin2-wt and KO parasites

Particle movement alongside the periphery is depicted via three colour-coded kymographs. Red tracks represent particles moving to the basal end, green tracks show particle flow to the apical end and blue depicts static particles. The yellow line represents the area of kymograph measurement. Particle movement was measured from the apical (A) to the basal pole (B). Parasites were incubated with or without 50nM rapamycin for 1h. After a growth period of 72h, cultures were mechanically lysed and incubated on a fresh host cell monolayer for another 24h prior to live microscopy. Images represent videos as collapsed t-stacks. At least 10 independent movies were produced and analysed for each depicted condition. The figure shows representative kymographs. Scale bars are 5µm. Please see also **Appendix Figure 7-5** and **Supplement Movie V4**.

5.5 Summary, conclusions and on-going work

In this chapter, I addressed *TgFormin2* localisation and function within the *Toxoplasma* actin network. *TgFormin2* was important for apicoplast inheritance and positioning as well as the maintenance of the cytosolic actin centre (cAC) anterior to the nucleus. The cAC appeared critical for overall actin distribution and flow in intracellular parasites, indicating that actin dynamics within intracellular parasites pre-dominantly depend on *TgFormin2*-driven actin nucleation.

Most recently, during writing of this thesis, Tosetti and co-workers published their investigation of the three actin nucleation factors in *Toxoplasma*, namely *TgFormin1*, 2 and 3 (Tosetti et al. 2019). According to this study, *TgFormin3* localises to the basal pole and the residual body mediating actin nucleation outside the parasite body during intracellular growth. Actin nucleation by *TgFormin1* does not majorly contribute to intracellular actin dynamics. Instead, *TgFormin1* was reported to be critical for motility, invasion and egress of extracellular parasites. Results presented by Tosetti and colleagues regarding *TgFormin2* stand in strong agreement with data presented here. It can be concluded that *TgFormins* fulfil non-overlapping roles during different stages of the asexual lytic cycle in *Toxoplasma*.

TgFormin1-mediated actin nucleation was described to be critical for maintaining actin flow in extracellular parasites (Tosetti et al. 2019). According to live microscopy studies of moving and non-moving extracellular parasites, actin appears to accumulate at the basal end of the parasite, indicating actin flow from the apical to the basal pole. Tosetti and co-workers suggest that actin

translocation to the basal pole happens along the parasite periphery (Tosetti et al. 2019). This peripheral flow seems to be MyosinA-dependent and, thus, to be mediated by the actomyosin system (Tosetti et al. 2019). Data presented here provide experimental evidence that the parasite periphery represents a site of increased actin abundance during intracellular growth. Actin flow appears bi-directional alongside the periphery in intracellular parasites and is fuelled by TgFormin2-mediated actin polymerisation in the cytosolic region anterior to the nucleus. It remains to be elucidated whether intracellular actin flow happens in a MyosinA-dependent fashion.

During the process of the submitting this thesis, Hunt and co-workers reported TgCAP to be critical for maintaining the cAC (Hunt et al. 2019). This finding potentially indicates an interaction between TgCAP and TgFormin2. In *Plasmodium*, PfCAP was found to be capable of exchanging ADP to ATP on rabbit actin monomers *in vitro* (Makkonen et al. 2013). Exploring the nature of the potential interaction between TgCAP and TgFormin2 presents an exciting opportunity for future research efforts.

Previously, actin polymerisation in *Toxoplasma* had been proposed to occur in an isodesmic fashion (Skillman et al. 2013). The model was applied to explain the previously reported presence of short and unstable actin filaments in *Toxoplasma* (Sahoo et al. 2006). Both studies were based on *in vitro* experiments with recombinant *Toxoplasma* actin. The model was also used to explain the limited set of actin nucleation factors (Baum et al. 2006), most prominently the lack of the Arps2/3 complex (Gordon and Sibley 2005), as the isodesmic model suggested nucleation-independent actin polymerisation (Skillman et al. 2013).

The recent observation of a filamentous actin network *in vivo* (Periz et al. 2017) was the first direct experimental evidence to indicate the presence of actin factors that would allow for the formation of long filamentous actin structures in *Toxoplasma*. Data presented here and by others (Tosetti et al. 2019) clearly show that actin nucleation factors play a critical role in maintaining actin structures and dynamics *in vivo*. In combination, these data sets strongly indicate that *Toxoplasma* actin polymerisation relies heavily on actin nucleation factors. This raises the question about the relevance of the isodesmic polymerisation model (Skillman et al. 2013) for actin dynamics *in vivo*. It is

important to note that data presented here do not directly disprove the isodesmic model for actin polymerisation. However, the functional requirement for such a unique polymerisation mechanism for eukaryotic actin still needs to be defined *in vivo*.

The split-Cas9 system was capable of accurately describing the features unique to *TgFormin2* loss of function. This was clearly demonstrated by the reproduction of the phenotypic characteristics with the DiCre system (this study) and with a clonal *Tgformin2* knock-out line (Tosetti et al. 2019). Upon rapamycin induction, the split-Cas9 system achieved a higher rate of *Tgformin2* loss of function (68% (± 6.6)) than the DiCre system (35.7% (± 3.8)). I am speculating that the long DNA sequence between the two loxP sites (ca. 19,000bps) might act as a physical hindrance to Cre-recombinase functionality. The distance between the two loxP sites might be too large for the Cre-recombinase to act at its full potential. During the course of this thesis, numerous phenotypes were reproduced with the split-Cas9 system. In addition, the system was also capable of reliably investigating the biological novelty of the *Formin2* phenotype. I therefore propose this system as a reliable tool for the investigation of actin dynamics in intracellular *Toxoplasma*.

I reasoned that the split-Cas9 system was well suited for the purpose of screening for novel actin factors. The system can be exploited for phenotypic screening due to its inducible nature. Phenotypic screening capacity presents a novelty in *Toxoplasma* research since the use of constitutively expressed Cas9 can only be used for measuring overall parasite fitness (Sidik et al. 2016). I was therefore eager to initiate a medium throughput phenotypical screening approach for novel apicomplexan actin factors. At the same time, this approach also aimed at addressing the impact on apicoplast replication. Apicoplast replication is linked to actin dynamics (Andenmatten et al. 2013; Jacot, Daher, and Soldati-Favre 2013; Haase et al. 2015; Whitelaw et al. 2017) and could therefore act as valuable indicator for overall actin function within the parasite.

For this purpose, I designed a library consisting of sgRNAs targeting about 320 apicomplexan-specific genes in total. The selected genes did not code for any signal peptide since I suspected actin binding proteins to be cytosolic. The screen was performed by Janessa Grech and Dr Elena Jimenez-Ruiz at the LMU

Munich (Germany). About 20 gene candidates were identified with a potential role in apicoplast biology and/or actin network dynamics. Careful validation of these candidates is subject to on-going research at the moment.

6 Discussion

Actin is a highly abundant structural protein in eukaryotes that is critical for several cellular processes, including cytokinesis, cargo trafficking and cellular motility (Baum et al. 2006; Pollard and Cooper 2009). In *Toxoplasma* biology, the investigation of actin dynamics and functions presents a major research focus. Actin plays a key function in parasite egress, motility and invasion (Dobrowolski and Sibley 1996; Drewry and Sibley 2015; Egarter et al. 2014; Whitelaw et al. 2017). Actin was also reported to be involved in apicoplast inheritance (Andenmatten et al. 2013; Whitelaw et al. 2017) and dense granule trafficking (Heaslip, Nelson, and Warshaw 2016; Whitelaw et al. 2017). Overall, actin is critical for the completion of the lytic cycle and, thus, parasite survival (Andenmatten et al. 2013; Egarter et al. 2014). Of relevance, despite numerous functions of actin during the lytic cycle, intracellular morphology and replication rate in culture appear to be largely unaffected by the lack of actin (Egarter et al. 2014; Periz et al. 2017). Noteworthy, depletion of *TgACT1* results in asynchronous replication (Periz et al. 2017).

Recently, actin structures were successfully visualised by exploiting actin-chromobodies in *Toxoplasma*, revealing an extensive actin network within the parasitophorous vacuole (PV) (Periz et al. 2017). This network connects individual parasites with each other and appears important for vesicle trafficking between individual parasites within the PV (Periz et al. 2017). In addition, highly dynamic actin structures accumulate anterior to the nucleus in individual parasites (Periz et al. 2017). This thesis aimed at exploiting actin visualisation to investigate actin dynamics *in vivo* in unprecedented detail. For this purpose, the actin-chromobody was combined with the split-Cas9 technology (Zetsche, Volz, and Zhang 2015) to enable rapid gene disruption in *Toxoplasma*.

In this study, I established the split-Cas9 system as a conditional tool for gene disruption in *Toxoplasma* (refer to chapters 3, 4 and 5). Despite the appearance of DNA damage-related phenotypes immediately after split-Cas9 activation, the system is capable of efficiently disrupting genes of interest. However, the gene-specific phenotype must be distinguishable from the unspecific DNA damage phenotype to avoid misinterpretation of results. Gene-specific phenotypes were reproduced for a variety of genes, including *Tggap40* (Harding et al. 2016)

(chapter 3), *Tgmec17* (Varberg et al. 2016) (chapter 3) and *TgdrpA* (van Dooren et al. 2009) (chapter 5). Importantly, combination of the split-Cas9 system with the actin-chromobody technology reproduced the previously reported actin network phenotypes for the genes *Tgactin1* and *Tgadf* (Periz et al. 2017) (chapter 4). Furthermore, *Tgadf* gene disruption strongly indicated that TgADF presents an important factor in the disassembly of the intravacuolar F-actin filaments prior to parasite egress from the host cell.

The actin-chromobody enabled live microscopy and kymograph analysis investigating actin dynamics in intracellular parasites. By doing so, I re-defined four actin accumulation sites in intracellular *Toxoplasma* parasites: the apical and basal end, the cytosolic region anterior to the nucleus (cAC) and the periphery (chapter 4). These actin polymerisation centres appeared to be connected by bi-directional actin flow alongside the parasite periphery. The split-Cas9 system revealed TgFormin2 as critical for maintaining the cAC (chapter 5). Since cAc loss severely affected actin distribution and peripheral actin flow, I concluded that actin dynamics within intracellular parasites predominantly depend on TgFormin2-driven actin nucleation. Furthermore, TgFormin2 appeared to be important for apicoplast inheritance and positioning (chapter 5). The split-Cas9-mediated TgFormin2 phenotype was confirmed by excising the *Tgformin2* gene with the DiCre system. Results for TgFormin2 obtained in this study stand in strong agreement with observations made by Tosetti and co-workers (Tosetti et al. 2019).

6.1 Application of CRISPR/Cas9 strategies in *Toxoplasma*

The type II CRISPR/Cas9 system was successfully applied for genome editing in various organisms, including human cells (Jinek et al. 2013; Mali et al. 2013), woody plants (Fan et al. 2015), beetles (Gilles, Schinko, and Averof 2015) and rabbits (Yan et al. 2014). CRISPR/Cas9 has also positively impacted genome modification efforts in trypanosomatids (Lander and Chiurillo 2019). In *Toxoplasma*, CRISPR/Cas9 was shown to be effective for single target gene disruption and site-specific insertions (Shen et al. 2014; Sidik et al. 2014). Nevertheless, phenotypic analysis based on CRISPR/Cas9 faces challenges in *Toxoplasma*.

Several studies reported that prolonged or constitutive Cas9 expression can negatively impact *Toxoplasma* morphology and/or fitness (Serpeloni et al. 2016; Sidik et al. 2016; Markus et al. 2019). This challenge was overcome by expressing Cas9 together with a sgRNA (Sidik et al. 2016). It was argued that Cas9 toxicity is caused by endogenous RNA mediating Cas9 activity (Sidik et al. 2016) and/or by secondary non-targeted Cas9 nuclease activity in the absence of any sgRNA (Markus et al. 2019). It was suggested that co-expression of a sgRNA might sequester Cas9 enzymes, thus preventing undesired nuclease activity (Markus et al. 2019). Interestingly, in contrast to the conditional ddFKBP-Cas9 system (Serpeloni et al. 2016), prolonged split-Cas9 activation did not result in aberrant parasite morphology. Most likely, this is because of the reduced efficiency of split-Cas9 in comparison to the wild-type Cas9 enzyme (Zetsche, Volz, and Zhang 2015). Despite its reduced efficiency, the split-Cas9 system still achieved high gene disruption rates of over 95% in induced populations. Potentially, less efficient Cas9 variants could be constitutively expressed in *Toxoplasma* without the need for a decoy sgRNA.

A previous report indicates a negative impact of transiently transfected Cas9-sgRNA plasmid on parasite fitness as measured by plaque assay immediately after transfection (Sidik et al. 2014). The effect was observed in RH parasites and, to a greater extent, in RH Δ ku80 parasites. Sidik and co-workers hypothesised that DNA damage caused by Cas9 could be responsible for this decrease in fitness, especially in the RH Δ ku80 strain. Data presented here shows that DNA damage presents a universal outcome of Cas9 activity and strongly impacts parasite and nuclear morphology. Therefore, in agreement with the hypothesis proposed by Sidik and co-workers (Sidik et al. 2014), I conclude that the repair of the Cas9-mediated DSB presents a bottleneck for parasite recovery (**Figure 6-1**).

Because of this, my data urge caution when phenotypic analysis is performed immediately after Cas9 activity. For instance, it was suggested that *TgMec17* is important for parasite replication based on transient Cas9 experiments (Varberg et al. 2016). However, the proposed impact of *TgMec17* depletion on nuclear replication was only reproducible with the split-Cas9 system, but not with the DiCre system. I am therefore proposing that replication defect is not *TgMec17*

specific, but rather represents the effect of Cas9-mediated DNA damage in the 1st lytic cycle of parasites.

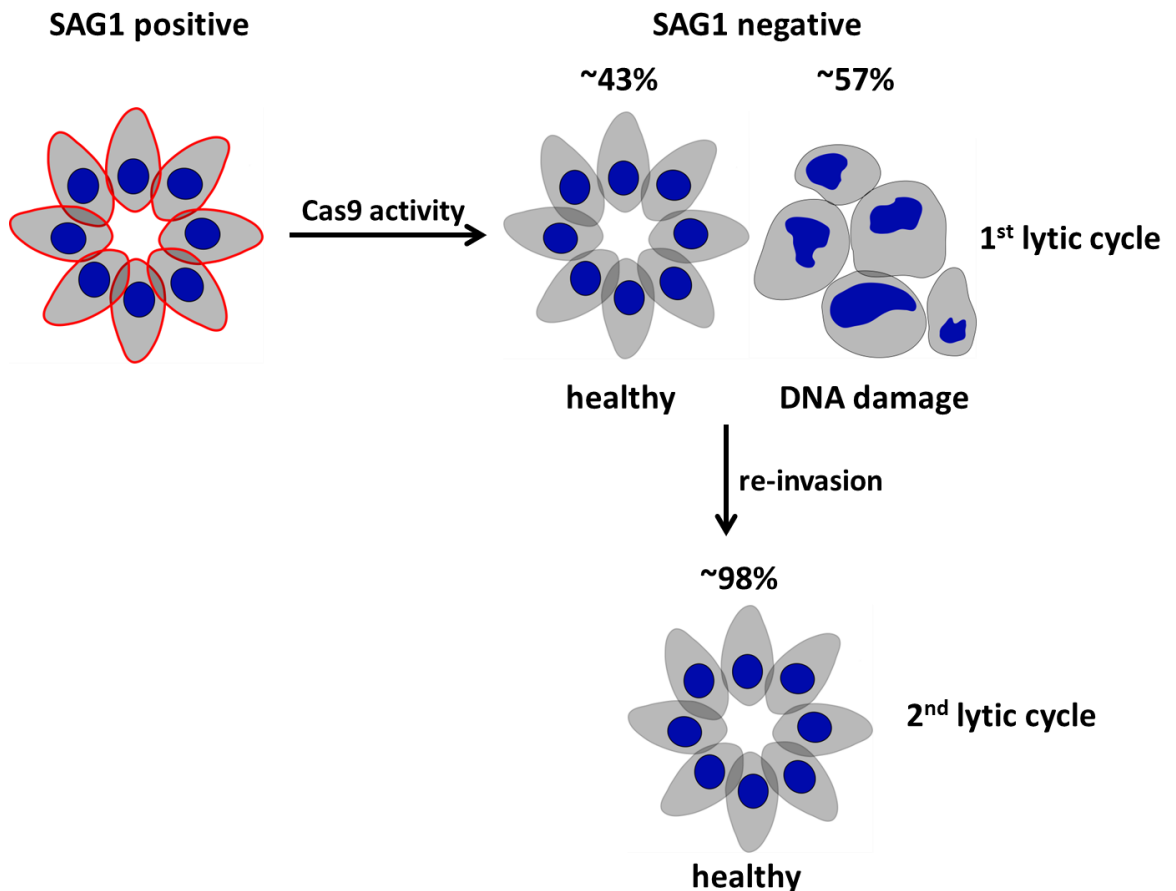


Figure 6-1: Schematic depiction of the DNA damage bottleneck that a *Toxoplasma* population has to overcome after Cas9 activity

Cas9-mediated double-stranded DNA breaks cause a DNA damage phenotype within the 1st lytic cycle after Cas9 activity. The DNA damage phenotype is lost in the 2nd lytic cycle, most likely due to the incapability of DNA damage parasites to re-invade. The schematic exemplarily depicts the results obtained for the *Tgsag1* gene during this study. Parasites expressing *TgSAG1* on their surface are outlined in red. Parasites lacking *TgSAG1* are shown without red outline.

Independent disruptions of the same gene usually produced similar levels of DNA damage abundance. Interestingly, however, the overall abundance of DNA damage within the 1st generation of a population can vary strongly when different genes are targeted by Cas9. For example, disruption of *sag1* caused a DNA phenotype in 55.67% (± 3.79) of parasites, while the number for *actin1* disruption was only 30% (± 2.65). Potentially, different genomic loci are more accessible to the DNA repair machinery. Transcriptional pressure might also

impact the rate of successful DSB repair. Whether these speculation hold true, however, remains to be elucidated.

In mammalian cells, the usual DNA repair outcome after Cas9-mediated DNA cleavage was reported to be insertions or deletions (indels) of maximal 20bp (Koike-Yusa et al. 2014; Tan et al. 2015; van Overbeek et al. 2016). However, Kosicki and co-workers showed that large deletions ranging from 250bp to 6kb can occur after Cas9 mediated DNA cleavage (Kosicki, Tomberg, and Bradley 2018). The indels observed for the targeted genes in my study (*Tgsag1*, *Tgmec17*, *Tgactin1*, *Tgadf* and *Tgformin2*) support previous reports in mammalian cells. While most indels are short insertions or deletions, Cas9-mediated cleavage of the *formin2* gene resulted in a large deletion (over 150bp) at the targeted locus. My findings stand also in agreement with previous reports in *Toxoplasma*. While smaller indels seem to appear more frequently in this organism (Shen et al. 2014; Sidik et al. 2014; Serpeloni et al. 2016), larger insertions over 100bp have been reported (Sidik et al. 2014). Overall, it would appear that *Toxoplasma* tends to show similar DNA repair outcomes to mammalian cells.

In the context of CRISPR/Cas9-mediated genome targeting in mammalian cells, it has been reported that a variety of additional on-target DNA modifications, including inversions, can occur outside the cut site (Kosicki, Tomberg, and Bradley 2018). It would therefore appear that the CRISPR/Cas9 system has the potential to cause substantial genome rearrangements with unpredictable impact on the organism. Whether this is also true for *Toxoplasma* remains unclear. However, due to the similar DNA repair behaviour so far, it seems likely that similar events could also occur. In addition to the DNA damage phenotype, this possibility presents another reason to evaluate phenotypes thoroughly when applying CRISPR/Cas9.

Nevertheless, I argue that a conditional CRISPR/Cas9 system might be more robust with regards to proper phenotype depiction than, for example, clonal lines. In an induced split-Cas9 *Toxoplasma* population, different genomic modifications (indels) will be responsible for target gene disruption in different parasites. Since large genome rearrangements do not present the majority of DNA repair events (Kosicki, Tomberg, and Bradley 2018), truthful phenotypic

description should be possible by quantitative analysis of the entire induced population. A high induction rate as described for the split-Cas9 system is certainly beneficial in this endeavour.

At this point it should be mentioned that target sites in the human genome appear to be repaired in a non-random fashion (van Overbeek et al. 2016; Chakrabarti et al. 2019). This means that certain type of indels preferentially occur at a given target site after DNA repair. A large scale study investigating over 1,000 target sites in the human genome, however, reported that not all target sites display highly preferred indels (Chakrabarti et al. 2019). While some target sites appear to possess one preferred sequence alteration, other sites lack a clear preference with DNA repair resulting in various indels. Target sites of the induced split-Cas9 populations for the genes *Tgadf*, *Tgactin1* and *Tgformin2* showed different indels after gene disruption. I therefore propose that these populations should display their respective phenotype due to a variety of indels making the phenotypic analyses more robust. For *Tgmec17* and *Tgsag1*, several gRNAs were applied for target gene disruption. This presents another way to increase the number of indels and minimize the chance of incorrect phenotypic analysis due to on-target genome rearrangements.

The CRISPR/Cas9 technology enables genome wide screens in mammalian cells (Shalem et al. 2014; Wang et al. 2014; Jiang et al. 2019; Korkmaz et al. 2019). In *Toxoplasma*, a genome-wide CRISPR/Cas9 screen identified novel fitness-conferring genes (Sidik et al. 2016; Sidik, Huet, and Lourido 2018). The relevance of this screen for the overall scientific advancement in apicomplexan biology cannot be overstated. Nevertheless, the application of a constitutively expressed Cas9 enzyme allowed only for the assessment of overall parasite fitness. This leaves phenotypic screens to be achieved in the future. Due to its conditional nature, the split-Cas9 system is generally well suited for such an approach. While the underlying Cas9-mediated DNA damage limits its application, I argue that the split-Cas9 system is capable of supporting a phenotypic screen for novel actin factors.

First of all, research strongly indicates that *Tgactin1*, although critical for completion of the lytic life cycle, is not essential for intracellular growth and replication (Andenmatten et al. 2013; Egarter et al. 2014; Periz et al. 2017;

Whitelaw et al. 2017). In agreement with this, detrimental effects on nuclear integrity or parasite morphology, as described here for the DNA damage phenotype, have not been reported. The same is true for the actin depolymerisation factor (*TgADF*) (Mehta and Sibley 2011; Haase et al. 2015; Periz et al. 2017).

Secondly, this thesis shows that the split-Cas9 system was able to reproduce previously published actin phenotypes with the actin-chromobody for the genes *Tgactin1* and *Tgadf* (Periz et al. 2017). In addition, the split-Cas9 enabled phenotypic description resulting from the disruption of the *Tgformin2* gene. The validity of the described characteristics was confirmed by DiCre system (Andenmatten et al. 2013) and by an independent study (Tosetti et al. 2019). It should also be mentioned that the various actin phenotypes are easily distinguished, indicating that Cas9 activity does not interfere with the true nature of the phenotype. A medium-throughput screen is on-going at the moment, aiming at identifying novel actin binding proteins.

In summary, split-Cas9 extends the molecular toolbox that researchers have at their disposal for exploring *Toxoplasma* biology. Since the successful repair of Cas9-mediated DSB presents a significant obstacle, some parasites display a DNA damage phenotype after split-Cas9 activation. This limits the potential applications for this system. For instance, the system is not suitable for investigating nuclear or cellular replication. However, other biological questions addressing actin and apicoplast biology can be addressed applying this technology. In this context, vacuoles displaying an obvious DNA damage phenotype can easily be excluded from the analysis. Although the split-Cas9 system can be utilised for targeted gene characterisation approaches, I am hypothesising that the technique is most powerful in the context of phenotypic screening.

Due to the Cas9 mode of action, DSBs within genome cannot be avoided when aiming at gene control on the genetic level. One alternative approach, however, that would circumvent the challenges caused by DNA damage in *Toxoplasma* is the use of RNA-cleaving CRISPR/Cas systems. RNA cleavage would control gene expression on the transcriptional level. Type II CRISPR/Cas9 system from *Streptococcus pyogenes* can be programmed to target and cleave ssRNA

(O'Connell et al. 2014). It can also be exploited to target RNA nucleases to RNA molecules (Batra et al. 2017). In addition, Cas9 enzymes from other species were reported to target RNA as well as type III and VI CRISPR/Cas systems (Wang et al. 2019).

In the type VI CRISPR/Cas13a system, a single crRNA is sufficient to promote Cas13a-mediated ssRNA cleavage (Abudayyeh et al. 2016). However, Abudayyeh and colleagues observed collateral cleavage of standby RNAs upon Cas13a-mediated target RNA cleavage. It was suggested that this phenomenon is responsible for the observed growth rate inhibition in bacteria expressing RFP, Cas13a and a RFP-targeting crRNA (Abudayyeh et al. 2016). Intriguingly, when Cas13a was expressed in mammalian and plant cells for targeted transcript knockdown, no signs of collateral RNA cleavage were observed (Abudayyeh et al. 2017). Collateral RNA cleavage was also reported for Cas13b (Smargon et al. 2017) and Cas13d nucleases (Konermann et al. 2018).

The fact that Cas13 can be targeted to RNA molecules by only one crRNA (Abudayyeh et al. 2016) should make expression of all necessary components achievable in *Toxoplasma*. Of course, the potential for collateral RNA cleavage would have to be addressed carefully. Nevertheless, exploiting CRISPR/Cas system for transcriptome modification in *Toxoplasma* presents an exciting outlook.

6.2 Actin dynamics in *Toxoplasma*

Visualisation of the *in vivo* actin network in *Toxoplasma* (Periz et al. 2017) can be considered a milestone in apicomplexan biology. Initial experiments performed by Periz and colleagues revealed that individual parasites are connected by a filamentous actin network. Vesicular trafficking between individual parasites within the PV was proposed to occur along actin filaments (Periz et al. 2017). The actin network appears dynamic with intravacuolar filaments being dis- and reassembled during parasite replication (Periz et al. 2017). In addition, highly dynamic actin structures accumulate anterior to the nucleus in individual parasites (Periz et al. 2017).

Time-lapse microscopy was used in this thesis to further define actin dynamics in intracellular parasites. Actin accumulates at the apical and basal end of the parasite, the cytosolic region anterior to the nucleus and the periphery. Intriguingly, the cytosolic actin centre (cAC) anterior to the nucleus is highly dynamic and frequently interacts with peripheral actin. Overall, actin accumulation sites seem to be connected by bi-directional actin flow along the parasite periphery, as shown by kymograph analysis. I would therefore argue that intracellular parasites possess a dynamically connected actin network that spans their whole body (**Figure 6-2**). While filamentous actin structures enable vesicle trafficking between individual parasites (Periz et al. 2017), the intracellular actin network might mediate cargo transport within parasites.

For instance, dense granule trafficking was reported to rely on actin and *TgMyoF* (Heaslip, Nelson, and Warshaw 2016; Whitelaw et al. 2017). Unsurprisingly, the distribution pattern of *TgMyoF* in intracellular parasites (Jacot, Daher, and Soldati-Favre 2013; Tosetti et al. 2019) appears similar to the actin distribution described by Periz et al. (Periz et al. 2017) and this thesis. *TgMyoF* is present in the same region as the cytosolic actin centre (cAC), localising to the area of the apicoplast and *TgFormin2* (Jacot, Daher, and Soldati-Favre 2013; Tosetti et al. 2019). In addition, *TgMyoF* can be found in the parasite periphery (Jacot, Daher, and Soldati-Favre 2013; Tosetti et al. 2019).

Peripheral, bi-directional actin flow was also observed in resting extracellular parasites (Del Rosario et al. 2019). Interestingly, this actin flow did not depend on *MyoA*, a core component of the acto-myosin motor complex (Fréna, Dubremetz, et al. 2017). Whether bi-directional actin flow in intracellular parasites is *MyoA* independent remains to be seen. Other myosins could be responsible for peripheral actin translocation in intra- and extracellular parasites. *TgMyoG* was reported to localise to the parasite periphery (Fréna, Jacot, et al. 2017), while *TgMyoL* showed a ubiquitous distribution throughout the cytoplasm (Fréna, Jacot, et al. 2017). Hence, both myosins could represent reasonable candidates for maintaining the actin flow. Due to its similar distribution pattern to actin (Jacot, Daher, and Soldati-Favre 2013; Tosetti et al. 2019), the same is true for *TgMyoF*. Interestingly, actin translocation appears *MyoA* dependent upon calcium stimulation (Del Rosario et al. 2019; Tosetti et al. 2019). This might indicate that different signalling pathways in *Toxoplasma*

exploit different cellular factors to mediate actin translocation. In addition, the reportedly fast turnover of apicomplexan filaments (Sahoo et al. 2006; Skillman et al. 2011; Kumpula et al. 2017, 2019) might also contribute to directed actin translocation.

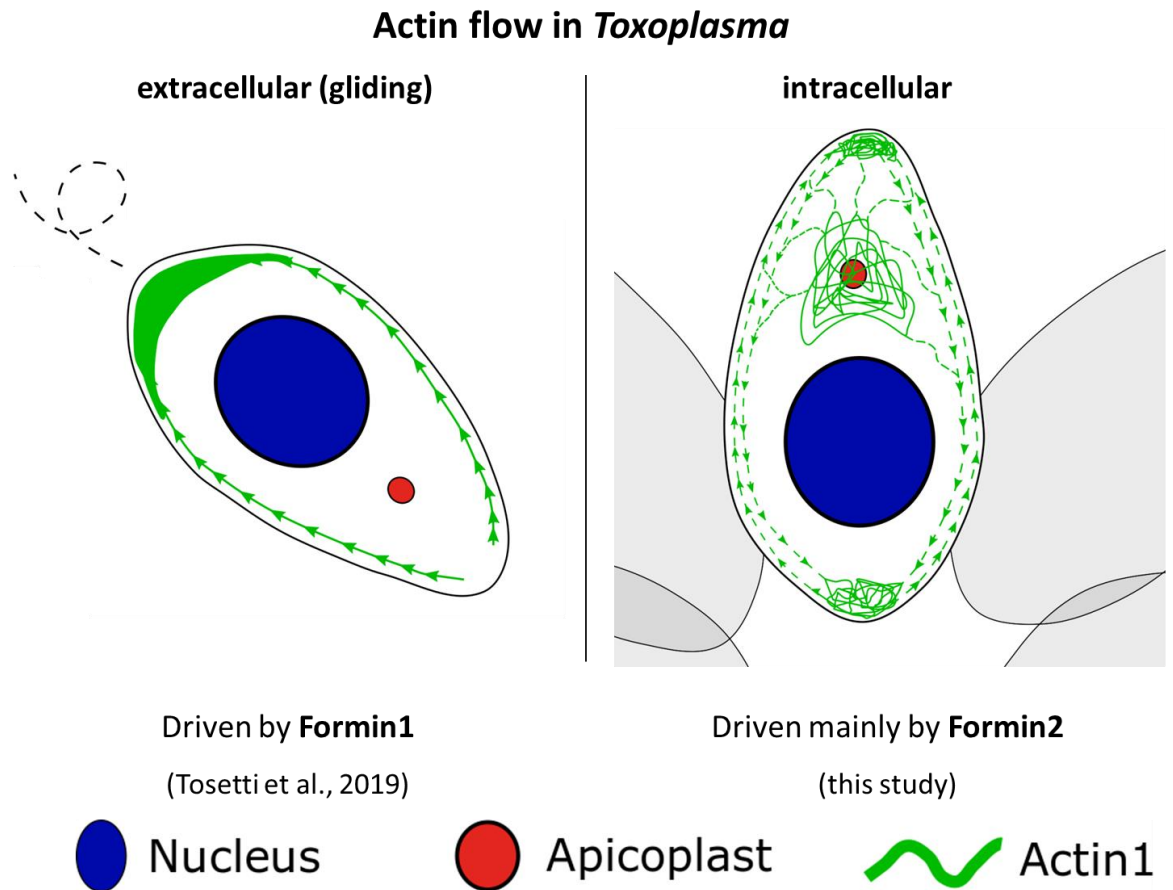


Figure 6-2: Schematic depicting a model for actin flow in extracellular (gliding) and intracellular *Toxoplasma* parasites

Actin accumulates at the basal pole of extracellular parasites due to a *TgFormin1*-mediated actin flow. In intracellular parasites, the cytosolic actin centre (cAC) anterior to the nucleus fuels the bi-directional actin flow. *TgFormins2* promotes cAC dynamics and is, thus, mainly responsible for maintaining actin dynamics in individual, intracellular parasites. Actin accumulation at the apical and basal pole in intracellular parasites is most likely supported by the other *TgFormins*. *TgFormin1* and 3 were found to localise to the apical and the basal pole, respectively. Reprinted from eLife (Stortz et al. 2019) under the Creative Commons Attribution 4.0 International License.

6.3 *In vivo* Functions of Formins in *Toxoplasma*

In vivo actin dynamics differ substantially from what can be observed *in vitro* (Pollard 2016). To efficiently control all aspects of actin assembly and disassembly, eukaryotic cells exploit a vast number of actin binding proteins (ABPs) (Pollard 2016). Processes that are heavily controlled by ABPs include *de novo* actin filament synthesis and actin treadmilling. In comparison to other eukaryotes, apicomplexan parasites encode for a limited set of ABPs (Baum et al. 2006). Strikingly, Formins are the only known actin nucleators in *Toxoplasma* and *Plasmodium* as spire (Baum et al. 2006) and the Arp2/3 complex (Gordon and Sibley 2005) are absent.

This thesis and a recent report by Tosetti and colleagues (Tosetti et al. 2019) elucidate the non-overlapping functions of *Tg*Formins *in vivo*. Strikingly, actin flow appears to depend on different Formins in extracellular and intracellular *Toxoplasma* parasites (**Figure 6-2**). Actin translocation to the basal end was reported to power motility in extracellular parasites and depends on *Tg*Formin1 (Tosetti et al. 2019). In intracellular parasites, however, peripheral actin flow and overall actin distribution within individual parasites appear to be mainly mediated by *Tg*Formin2 as described in this thesis. A similar function was reported for *Pf*Formin2 in intracellular *Plasmodium falciparum* blood stages (Stortz et al. 2019). Actin structures within the PV, but outside individual parasites, rely on *Tg*Formin3 (Tosetti et al. 2019).

Noteworthy, it was reported that resting extracellular parasites depict similar actin distribution to intracellular parasites, including bi-directional actin flow in the periphery (Del Rosario et al. 2019). Gliding motility appears to promote and require rearrangements of overall actin flow in a *MyoA*-dependent fashion (Del Rosario et al. 2019; Tosetti et al. 2019). This is supported by two independent studies that observed actin accumulation at the poles in extracellular parasites upon motility induction (Del Rosario et al. 2019; Tosetti et al. 2019).

In summary, *Tg*Formin2 and 3 act mainly during intracellular growth, while *Tg*Formin1 is crucial for gliding in extracellular parasites. I am hypothesising that *Toxoplasma* employs distinct mechanisms when directing actin flow during a resting or moving state. The exact molecular nature of these mechanisms, especially for intracellular parasites, will be the focus of future studies.

Proper actin dynamics are crucial for apicoplast replication and inheritance in *Toxoplasma* as depletion of actin causes apicoplast loss (Andenmatten et al. 2013; Whitelaw et al. 2017). The ABPs *TgFormin2* (Jacot, Daher, and Soldati-Favre 2013; Tosetti et al. 2019), *TgADF* (Jacot, Daher, and Soldati-Favre 2013; Haase et al. 2015) and *TgProfilin* (Jacot, Daher, and Soldati-Favre 2013) are critical for apicoplast segregation as they maintain actin dynamics. It was suggested that *TgMyoF* and *TgFormin2* act together to mediate proper apicoplast inheritance (Tosetti et al. 2019). A comparative study investigating the role of Formin2 in apicoplast inheritance in *Toxoplasma* and *Plasmodium* proposed that MyoF pulls the replicating apicoplast into the newly forming daughter cells along Formin2-mediated actin cables (Stortz et al. 2019).

Interestingly, *TgFormin2* knock-out lines are viable in culture (Tosetti et al. 2019). In *TgFormin2* knock-out populations, about 40% of parasites show normal apicoplast segregation while 60% of vacuoles show at least partial apicoplast loss (Tosetti et al. 2019). I made highly similar observations when excising *TgFormin2* conditionally via the DiCre system. Unsurprisingly, about 90% of parasites lacking the cAC after split-Cas9-mediated *Tgformin2* disruption showed impaired apicoplast inheritance with up to 75% of vacuoles showing apicoplasts mislocalised to the residual body. This solidifies the current understanding that apicoplast segregation and correct positioning depends on *TgFormin2*-mediated actin polymerisation. As mentioned above, the importance of actin dynamics on apicoplast inheritance is well documented in *Toxoplasma* (Andenmatten et al. 2013; Jacot, Daher, and Soldati-Favre 2013; Haase et al. 2015; Whitelaw et al. 2017). Nevertheless, the massive and most prominent accumulation of apicoplast material in the residual body presents a characteristic feature of the *TgFormin2* phenotype. As of now, it remains unclear when and how the apicoplast mislocalise to the residual body during parasite replication. Potentially, the lack of *TgFormin2*-promoted actin filaments renders the parasites unable to pull the apicoplast into the newly forming daughter cells via *TgMyoF*. As a result, apicoplasts accumulate outside of the parasite, i.e. the residual body. Live microscopy investigating parasite and apicoplast replication in *TgFormin2* depleted parasites (over several rounds of replication) should present a suitable method to address this question in the future.

In parasites lacking the apicoplast, the cAC was still present indicating a normal localisation and function of *TgFormin2*. This hypothesis is supported by findings showing localisation of *TgFormin2* to the apical region of parasites lacking the apicoplast (Tosetti et al. 2019). Furthermore, Tosetti and colleagues reported co-localisation of *TgFormin2* and the Golgi apparatus. Collectively, these observations might indicate anchorage of *TgFormin2* to the Golgi apparatus or to both, the apicoplast and the Golgi apparatus. Based on IFA data presented by Tosetti and co-workers, it might be reasonable to assume that the close proximity of *TgFormin2* and the apicoplast in non-dividing parasites could be the result of the close proximity between the Golgi and the apicoplast. Further experiments will be required to fully determine the nature of *TgFormin2* localisation in dividing and non-dividing parasites.

Based on the results from *in vitro* sedimentation assays, actin polymerisation was proposed to occur in an isodesmic fashion with actin polymerisation occurring independently from a critical concentration in *Toxoplasma* (Skillman et al. 2013). According to this model, actin assembly and disassembly happen at the same rate. Thus, the kinetically unfavourable actin nucleation prior to filament elongation would not present a rate limiting step. It was argued by Skillman and colleagues that F-actin formation could therefore happen independently from nucleation-promoting factors. In addition, the model was applied to explain the previously reported presence of short and unstable actin filaments in *Toxoplasma* (Sahoo et al. 2006).

Kumpula and co-workers challenged the reliability of actin sedimentation assays for analysing apicomplexan actin kinetics (Kumpula et al. 2017). They argued that the short length of apicomplexan actin oligomers could prevent their sedimentation. Pyrene fluorescence assays suggested kinetics for *PfACT1* similar to canonical actin with F-actin formation depending on nucleation (Kumpula et al. 2017). Of relevance, the same study revealed that *PfACT1* has a higher depolymerisation rate than canonical actin. Subsequently, crystallography studies revealed that unique structural features in the *PfACT1* molecule promote filament destabilisation and, eventually, depolymerisation (Kumpula et al. 2019). For instance, within the *PfACT1* molecule, the interaction between the A-loop and the *Plasmodium*-specific residue Lys270 enables a conformational stage that promotes actin filament fragmentation (Kumpula et al. 2019). Collectively,

these data indicate that the instability of apicomplexan F-actin can be explained by structural features not found in canonical actin.

Originally, the isodesmic model was believed to offer an explanation for the limited set of actin nucleation factors (Baum et al. 2006), most prominently the lack of the Arp2/3 complex (Gordon and Sibley 2005). However, findings presented by myself and Tosetti et al. (Tosetti et al. 2019) clearly show the critical function of *Tg*Formins in maintaining actin dynamics. Very similar observations have been made in *Plasmodium* (Stortz et al. 2019). Collectively, these data support canonical actin kinetics depending on nucleation in the apicomplexan *Plasmodium* and *Toxoplasma* parasites. At this point of time, all *in vitro* and *in vivo* observations can be explained by the canonical understanding of actin dynamics. Although the isodesmic model (Skillman et al. 2013) has not been disproven directly, it does not offer exclusive explanations for any of the published actin-related phenotypes *in vivo* (Periz et al. 2017; Whitelaw et al. 2017; Del Rosario et al. 2019; Stortz et al. 2019; Tosetti et al. 2019).

6.4 *In vivo* Functions of *Tg*ADF in *Toxoplasma*

Periz and colleagues presented time-lapse microscopy depicting rapid disassembly of intravacuolar actin filaments prior to parasite egress in a calcium dependent manner (Periz et al. 2017). Follow-up experiments performed here indicated that the actin depolymerisation factor (*Tg*ADF) is important for intravacuolar filament disassembly prior to parasite egress.

*Tg*ADF displays a ubiquitous distribution throughout the parasite cytoplasm (Allen et al. 1997; Mehta and Sibley 2011; Haase et al. 2015). The inducible nature of the filament disassembly prior to egress (Periz et al. 2017) might suggest a signalling cascade as underlying activation mechanism. This would require a controlled activation of *Tg*ADF activity to enable rapid and site-specific actin filament disassembly. In other organisms, ADF activity depends on its phosphorylation status (Mizuno 2013). ADF activity is inhibited by LIM kinase-dependent phosphorylation (Arber et al. 1998; Yang et al. 1998). The SSH phosphatase can mediate ADF dephosphorylation, thus leading to its re-activation (Niwa et al. 2002). I therefore speculate that a calcium-dependent

pathway might exist that mediates *Tg*ADF activation prior to egress by modulating the enzyme's phosphorylation status. Studies with *Tg*ADF phosphorylation mutants might be able to provide clarification about the exact underlying mechanism.

Interestingly, *in vitro* sedimentation assays with rabbit actin suggested that *Tg*ADF does not stably associate with F-actin (Mehta and Sibley 2010). In the same study, *Tg*ADF also displayed a weaker severing activity than the canonical yeast cofilin and appeared to prevent F-actin assembly mainly by sequestering monomeric G-actin. Of relevance, the severing activity was measured on rabbit actin for both enzymes. The observation that *Tg*ADF appears responsible for the rapid breakdown of already existing filaments *in vivo* would suggest that *Tg*ADF-mediated filament severing has relevance for actin dynamics. It was proposed that amino acid residues on the *Toxoplasma* actin monomer surface differ from conventional actin and that these differences contribute to filament instability (Sahoo et al. 2006; Skillman et al. 2011). Potentially, the weaker severing activity of *Tg*ADF is sufficient to mediate filament breakdown due to the more unstable nature of *Toxoplasma* F-actin. The intravacuolar network was also reported to dis- and reassemble when intracellular parasites replicate (Periz et al. 2017). It is reasonable to hypothesize that *Tg*ADF might also be involved in mediating the network disassembly during replication.

Noteworthy, filament disassembly is not an essential requirement for successful parasite egress. Potentially, the disassembly process might serve the purpose of recycling actin by reintroducing monomeric actin to the cytosolic actin pool. Actin was shown to be critical for parasite egress (Egarter et al. 2014; Whitelaw et al. 2017). Therefore, increasing the overall actin concentration within the parasite might benefit successful egress. Overall, experiments performed on *Tg*ADF and *Tg*Formin2 emphasize that the actin-chromobody technology (Periz et al. 2017) is a powerful tool for investigating relevant actin processes *in vivo*.

6.5 Outlook on *Tg*Profilin function and concluding remarks

This study sets a solid foundation for future projects exploring actin kinetics in *Toxoplasma*. Unsurprisingly, *Tg*Formin2 and *Tg*ADF appear to be key players in maintaining actin dynamics in *Toxoplasma*. The *in vivo* function of *Tg*Profilin within the actin network, however, still requires investigation. *In vitro* assays suggest fundamental differences in the mode of action between *Toxoplasma* and yeast Profilin. *Tg*Profilin inhibits *Tg*Formin-mediated actin polymerisation (Skillman et al. 2012) while yeast Profilin enhances Formin-mediated F-actin assembly (Sagot et al. 2002). In yeast, Profilin is required for Formin-mediated formation of actin cables *in vitro* (Evangelista et al. 2002).

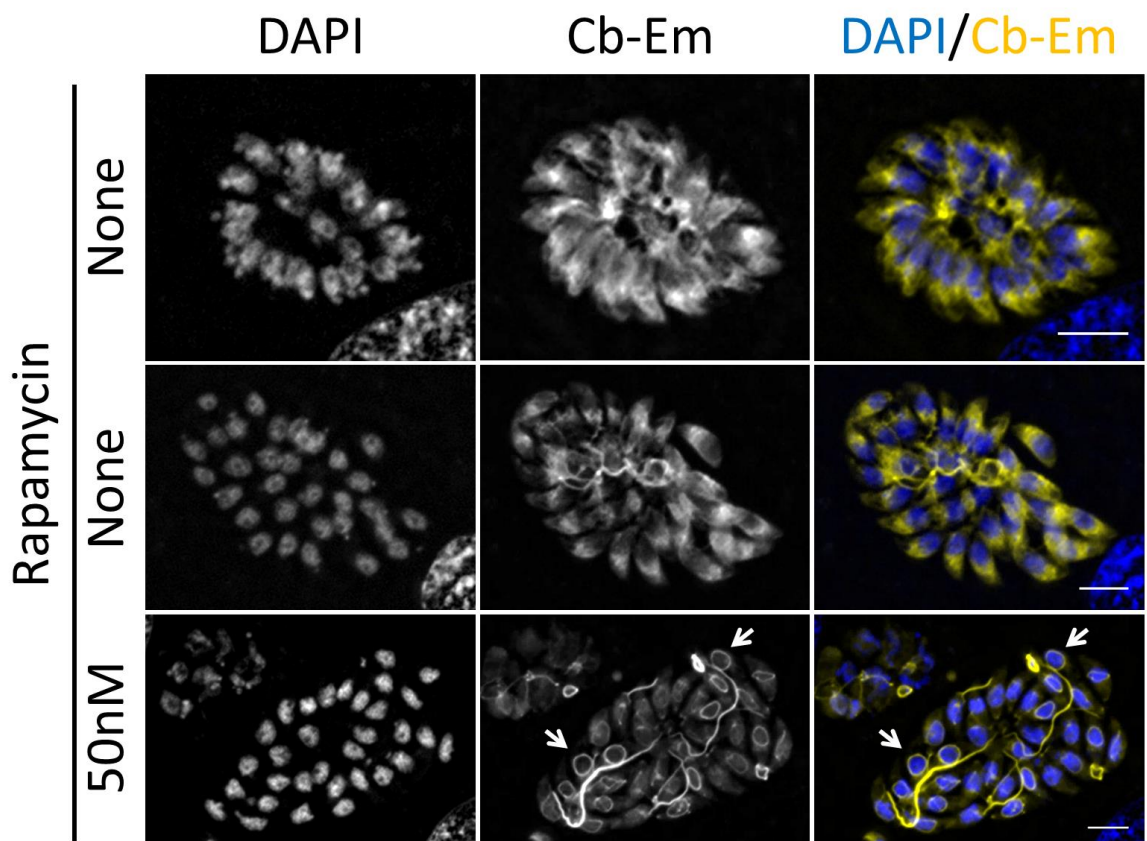


Figure 6-3: Disruption of *Tg*Profilin in RHsplit-Cas9 parasites expressing actin-chromobody-Emerald (Cb-Em or Cb)

IFA depicts the effect of *Tgprofilin* (RHsCas9-Cb-Profilin) disruption on the actin network (Cb-Emerald). To achieve gene disruption, parasites were incubated with 50nM rapamycin for 1h. Parasites were fixed after 48h with 4%PFA. The figure shows representative images. Scale bars are 5 μ m. White arrows exemplarily indicate circular actin structures. Analytical PCR was performed to confirm the integration of the profilin-sgRNA-plasmid into the parasite genome (Figure 5-2).

Preliminary data suggest that split-Cas9-mediated *Tgprofilin* disruption does not abolish *TgFormin*-mediated actin polymerisation in *Toxoplasma* (Figure 6-3). It would seem that intravacuolar filaments can appear more prominent after *TgProfilin* disruption. In addition, some parasites show circular actin structures that appear predominantly around the nucleus. Collectively, appearance of more prominent actin structures could suggest that the loss of *TgProfilin* increases actin polymerisation. Circular actin structures around the nucleus might represent increased *TgFormin2*-mediated actin polymerisation abolishing the dynamic nature of the cAC anterior to the nucleus. These *in vivo* observations would support a role for *TgProfilin* in actin sequestering as proposed *in vitro* by Skillman and colleagues (Skillman et al. 2012). *TgProfilin* might regulate actin filament formation by limiting the G-actin pool available for filament assembly. Future experiments will be performed to validate these preliminary findings and to further characterise *TgProfilin* function *in vivo*.

In conclusion, the actin-chromobody technology initiated a new era of actin research in apicomplexan parasites. With the obstacle of actin visualisation overcome in *Toxoplasma* (Periz et al. 2017) and *Plasmodium* (Stortz et al. 2019), actin studies *in vivo* now present an exciting opportunity to expand our knowledge on this abundant structural protein. The first steps were made in this endeavour by investigating the *in vivo* functions of Formins in apicomplexans (Stortz et al. 2019; Tosetti et al. 2019) and *TgCAP* in *Toxoplasma* (Hunt et al. 2019). Moreover, novel functions for actin during host cell invasion (Del Rosario et al. 2019) and organelle recycling during intracellular replication (Periz et al. 2019). To identify novel ABPs in *Toxoplasma*, screening approaches exploiting the split-Cas9 system are currently on-going in the Meissner laboratory (LMU Munich).

The data presented in this thesis significantly contributed to our understanding of actin dynamics in *Toxoplasma*. Kymograph analysis gave detailed insights into overall actin dynamics in intracellular parasites. Furthermore, the ABPs *TgADF* and *TgFormin2* were investigated for their function within the actin network *in vivo*. The split-Cas9 system will allow for phenotypic screening to further unravel the mechanics underlying actin dynamics in *Toxoplasma*.

7 Appendix

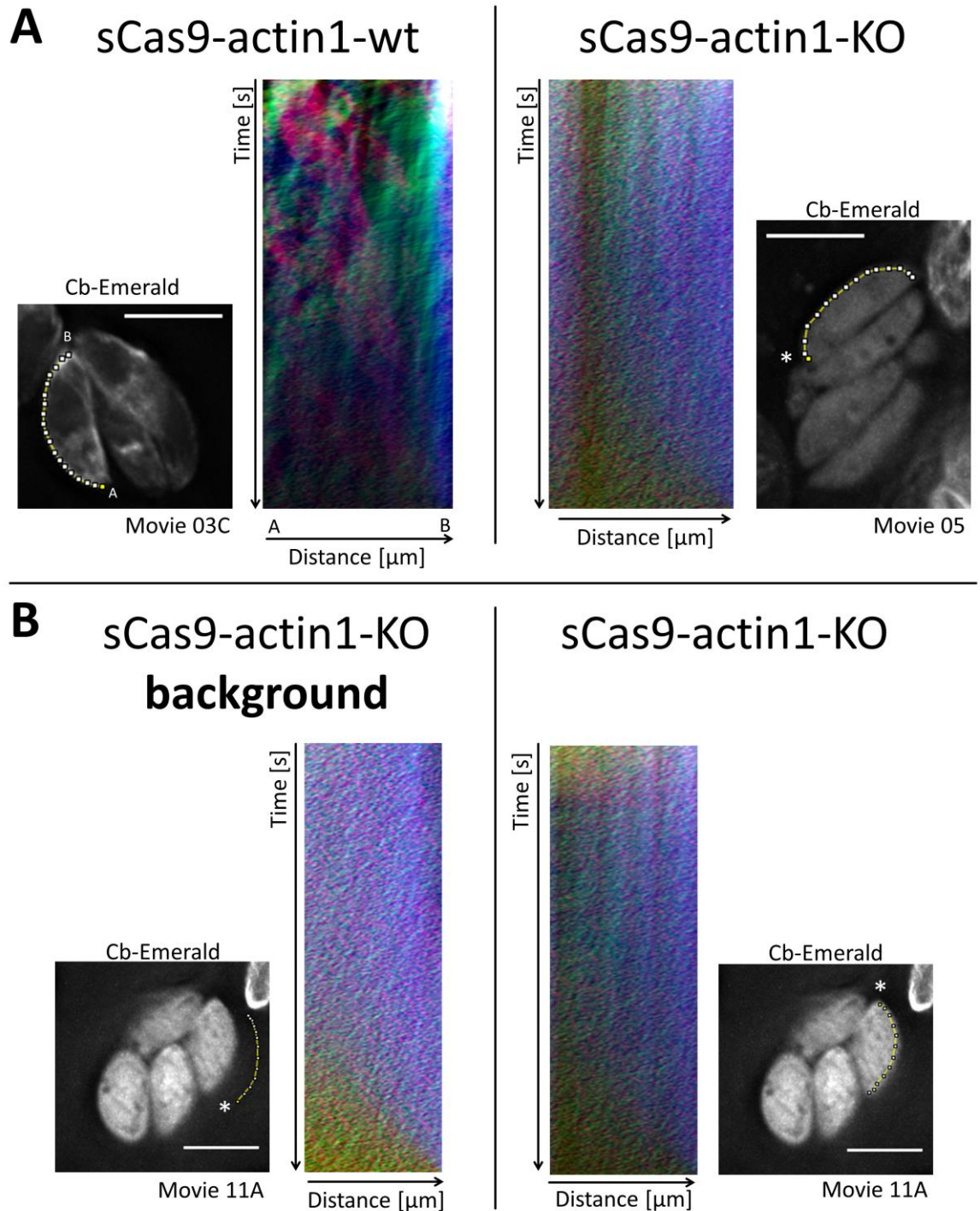


Figure 7-1: Kymograph analysis of peripheral actin flow in intracellular RHsCas9-CbEm-actin1-wt and KO parasites

(A) Kymograph analysis RHsCas9-CbEm-actin1-wt (sCas9-actin1-wt) and RHsCas9-CbEm-actin1-KO (sCas9-actin1-KO). (B) Kymograph analysis RHsCas9-CbEm-actin1-KO (sCas9-actin1-KO) and movie background. Particle movement alongside the periphery or the movie background is depicted via three colour-coded kymographs. Red tracks represent particles moving to the basal end, green tracks show particle flow to the apical end and blue depicts static particles. The yellow line represents the area of kymograph

measurement. Particle movement was measured from the apical (A) to the basal pole (B). As polarity is difficult to define for sCas9-actin1-KO parasites, the start point of the flow measurement is indicated with an asterisk. The same is true for the background measurement. Parasites were incubated with or without 50nM rapamycin for 1h. After a growth period of 72h, cultures were mechanically lysed and incubated on a fresh host cell monolayer for another 24h prior to live microscopy. Images represent videos as collapsed t-stacks. At least 5 independent movies were produced and analysed for each depicted condition. The figure shows representative kymographs. Scale bars are 5 μ m. Please see also **Figure 4-12** and **Supplement Movie V2**. Please note that live microscopy for the RHsCas9-CbEm-actin strain was performed by Dr Mario Del Rosario.

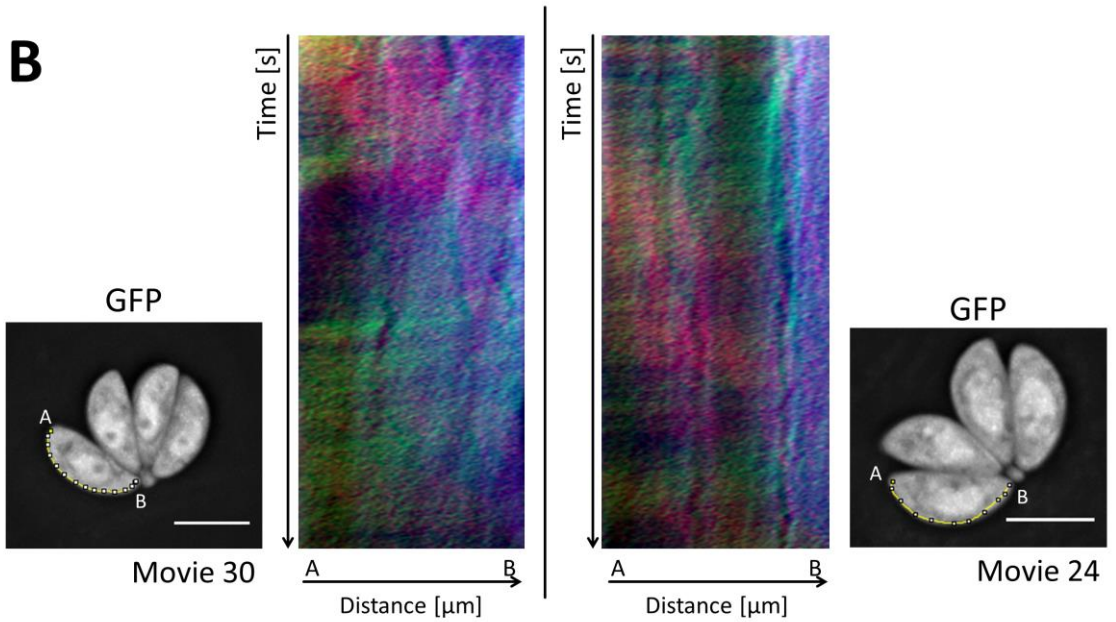
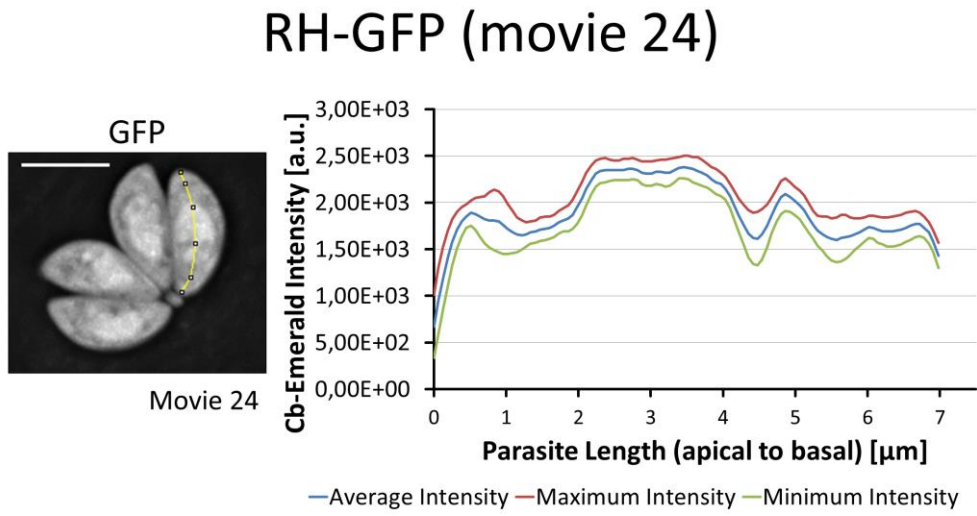
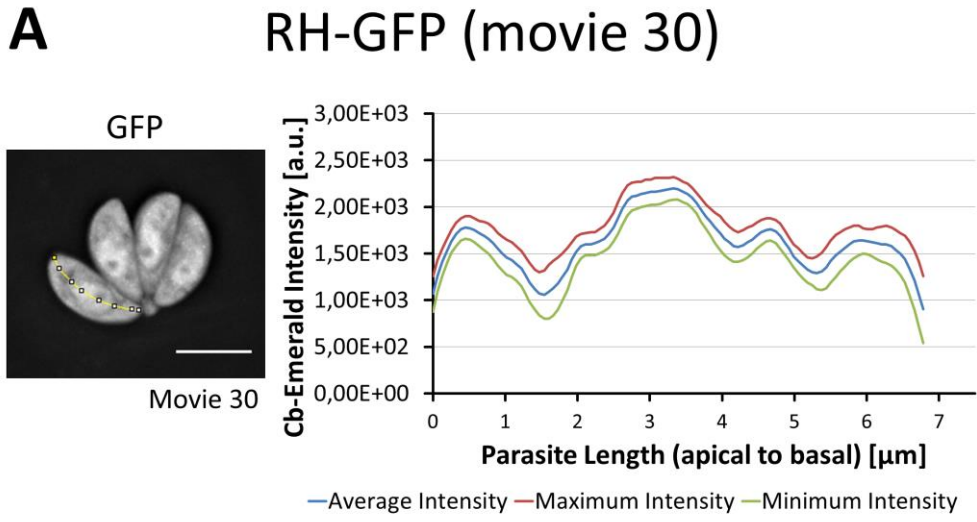
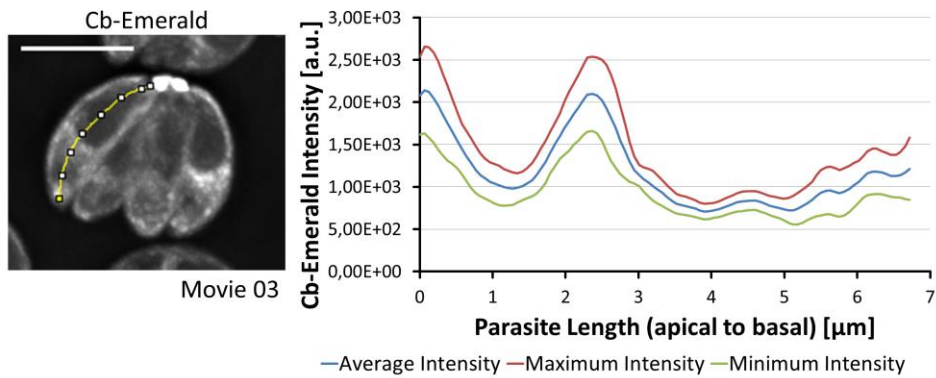


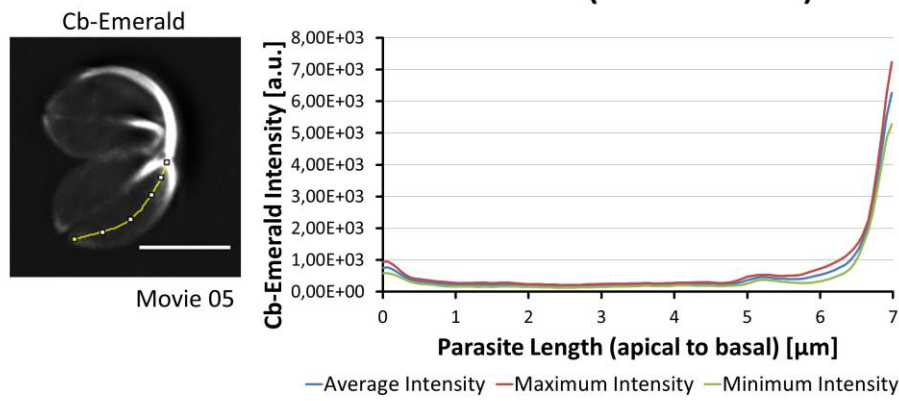
Figure 7-2: Actin distribution and kymograph analysis in intracellular RH-GFP parasites

Figure 7-2 continued: (A) Time-averaged intensity profiling along the parasites middle axis in RH-GFP parasites. Intensity profiles depict Cb-Emerald intensity along the measured axis (yellow line) over the entire duration of the movie. **(B)** Particle movement alongside the periphery is depicted via three colour-coded kymographs. Red tracks represent particles moving to the basal end, green tracks show particle flow to the apical end and blue depicts static particles. The yellow line represents the area of kymograph measurement. Particle movement was measured from the apical (A) to the basal pole (B). For all analyses, RH-GFP parasites were grown for 24h prior to live microscopy. At least 10 independent movies were produced and analysed for each condition. Movies are depicted as images representing collapsed t-stacks. The figure shows representative images. Scale bars are 5 μ m. Please see also **Figure 4-8** and **Figure 4-12** and **Supplement Movie V3**.

A RHsCas9-CbEm-*adf*-wt (movie 03)



RHsCas9-CbEm-*adf*-KO (movie 05)



B

RHsCas9-CbEm-*adf*-wt (movie 03)

RHsCas9-CbEm-*adf*-KO (movie 05)

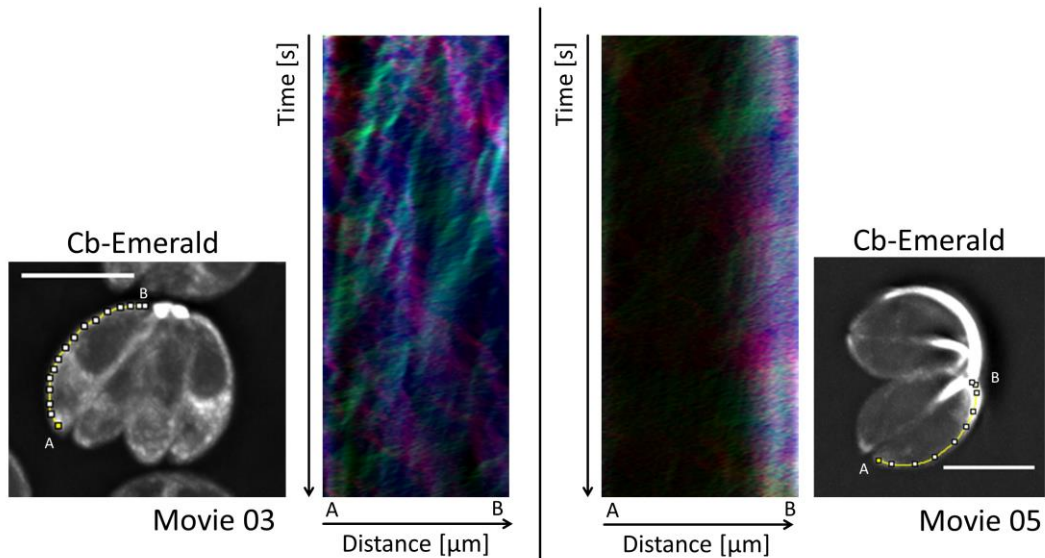


Figure 7-3: Actin distribution and kymograph analysis in intracellular RHsCas9-CbEm-*adf* wt and KO parasites

(A) Time-averaged intensity profiling along the parasites middle axis in RHsCas9-CbEm-*adf*-wt and RHsCas9-CbEm-*adf*-KO parasites. Intensity profiles depict Cb-Emerald intensity along the measured axis (yellow line) over the entire duration of the movie. (B) Particle movement alongside the periphery is depicted via three colour-coded

kymographs. Red tracks represent particles moving to the basal end, green tracks show particle flow to the apical end and blue depicts static particles. The yellow line represents the area of kymograph measurement. Particle movement was measured from the apical (A) to the basal pole (B). For all analyses, parasites were incubated with or without 50nM rapamycin for 1h. After a growth period of 72h, cultures were mechanically lysed and incubated on a fresh host cell monolayer for another 24h prior to live microscopy. At least 10 independent movies were produced and analysed for each condition. Movies are depicted as images representing collapsed t-stacks. The figure shows representative images. Scale bars are 5 μ m. Please see also **Figure 4-9** and **Figure 4-12** and **Supplement Movie V1**.

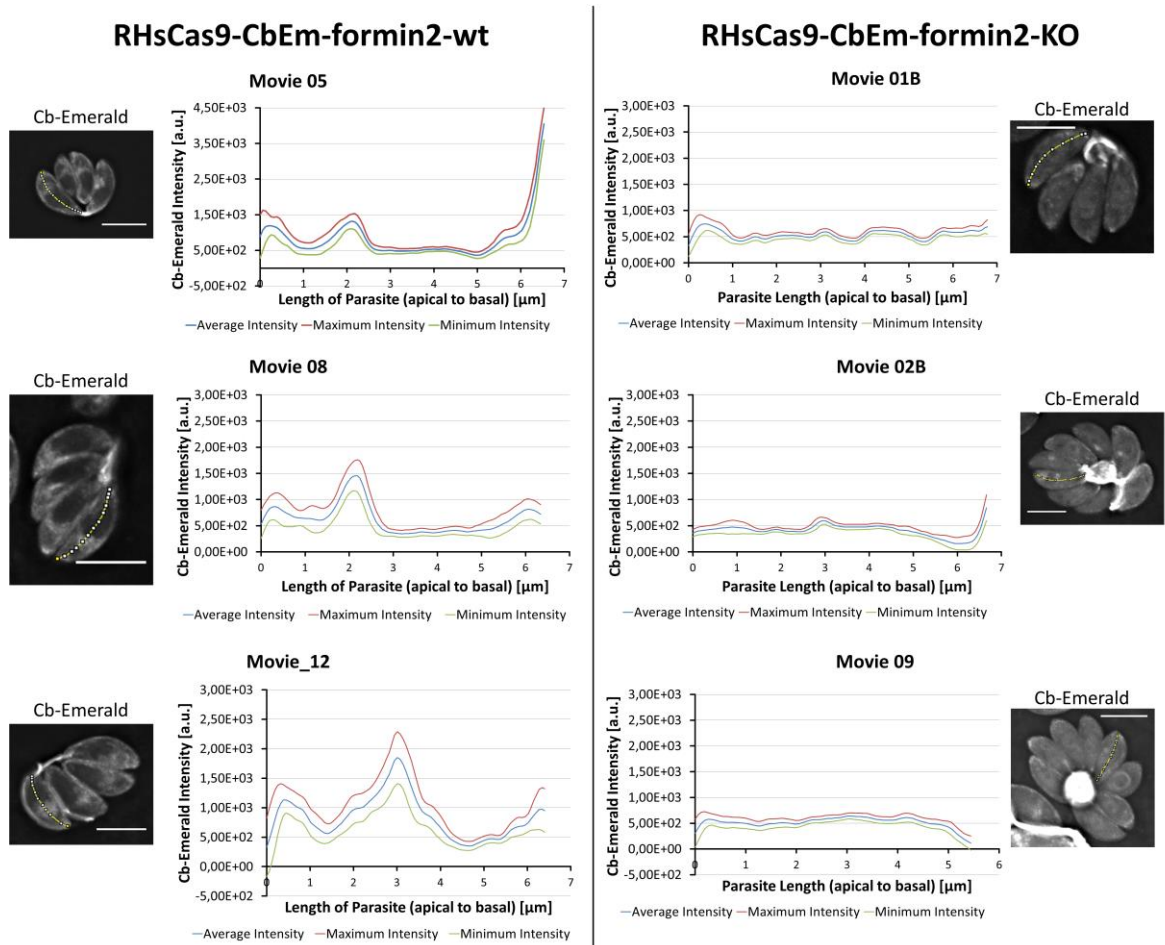


Figure 7-4: Actin distribution in intracellular RHsCas9-CbEm-formin2 wt and KO parasites along the middle axis

(A) and (B) Time-averaged intensity profiling along the parasites middle axis in RHsCas9-CbEm-formin2-wt and RHsCas9-CbEm-formin2-KO parasites. Parasites were incubated with or without 50nM rapamycin for 1h. After a growth period of 72h, cultures were mechanically lysed and incubated on a fresh host cell monolayer for another 24h prior to live microscopy. At least 10 independent movies were produced and analysed for each condition. Movies are depicted as images representing collapsed t-stacks. Intensity profiles depict Cb-Emerald intensity along the measured axis (yellow line) over the entire duration of the movie. The figure shows representative images. Scale bars are 5 μ m. Please see also **Figure 5-12** and **Supplement Movie V4**.

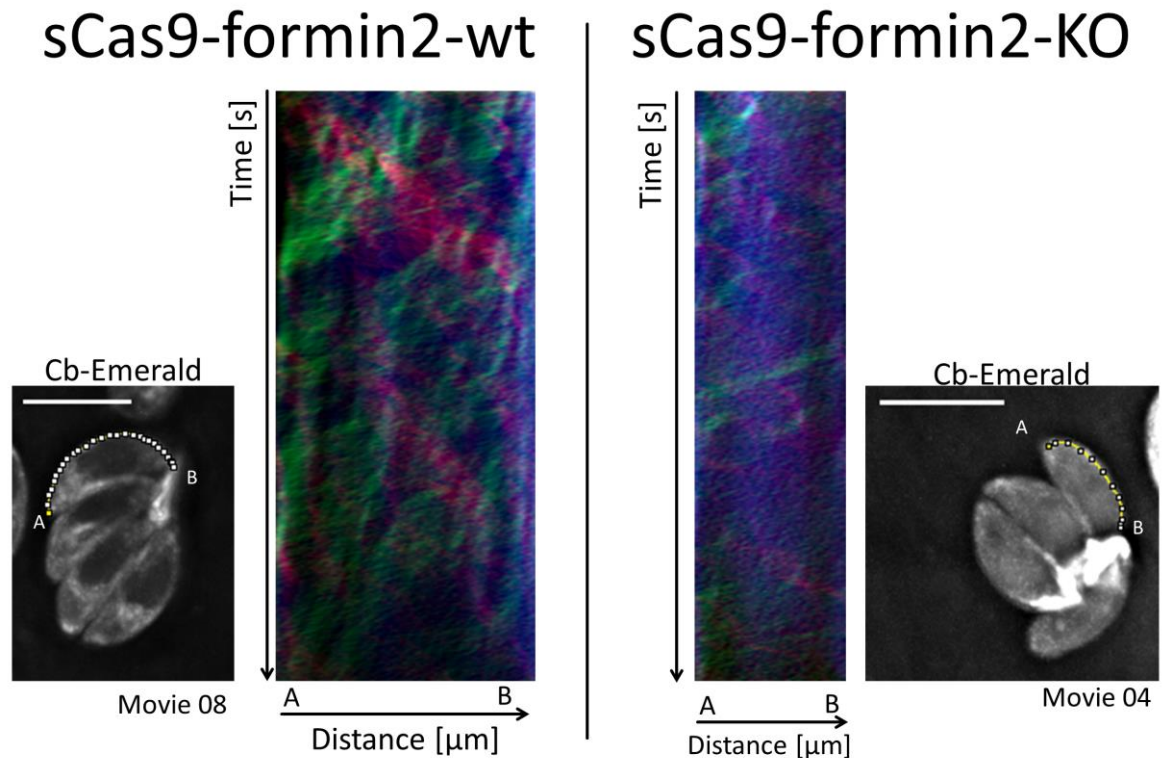


Figure 7-5: Kymograph analysis of peripheral actin flow in intracellular RHsCas9-CbEm-formin2-wt and KO parasites

Particle movement alongside the periphery is depicted via three colour-coded kymographs. Red tracks represent particles moving to the basal end, green tracks show particle flow to the apical end and blue depicts static particles. The yellow line represents the area of kymograph measurement. Particle movement was measured from the apical (A) to the basal pole (B). Parasites were incubated with or without 50nM rapamycin for 1h. After a growth period of 72h, cultures were mechanically lysed and incubated on a fresh host cell monolayer for another 24h prior to live microscopy. Images represent videos as collapsed t-stacks. At least 10 independent movies were produced and analysed for each depicted condition. The figure shows representative kymographs. Scale bars are 5 μ m. Please see also **Figure 5-15** and **Supplement Movie V4**.

The top rows show the predicted DNA sequence in case of in-frame tag positioning for the lines formin2-HA (A) and DiCre-formin2-YFPloxP (B). The bottom row depicts the actual DNA sequence present in the two lines. Noteworthy, the nucleotide substitution in the linker sequence of the formin2-HA line (A) does not change the amino acid sequence. Colour coding: yellow: linker sequence, red: stop codon, orange: loxP sequence, green: 3xHA tag (A) or YFP tag (B), blue: *Tgformin2* sequence. Sequencing was performed by Eurofins (GATC services, LightRun Tubes). Please note that preparations for sequencing were performed by Dr Mirko Singer.

8 Bibliography

- Abudayyeh, Omar O., Jonathan S. Gootenberg, Patrick Essletzbichler, Shuo Han, Julia Joung, Joseph J. Belanto, Vanessa Verdine, et al. 2017. "RNA Targeting with CRISPR-Cas13." *Nature* 550: 280-84. <https://doi.org/10.1038/nature24049>.
- Abudayyeh, Omar O., Jonathan S. Gootenberg, Silvana Konermann, Julia Joung, Ian M. Slaymaker, David B.T. Cox, Sergey Shmakov, et al. 2016. "C2c2 Is a Single-Component Programmable RNA-Guided RNA-Targeting CRISPR Effector." *Science* 353 (6299): aaf5573. <https://doi.org/10.1126/science.aaf5573>.
- Adl, Sina M., David Bass, Christopher E. Lane, Julius Lukeš, Conrad L. Schoch, Alexey Smirnov, Sabine Agatha, et al. 2019. "Revisions to the Classification, Nomenclature, and Diversity of Eukaryotes." *Journal of Eukaryotic Microbiology* 66 (1): 4-119. <https://doi.org/10.1111/jeu.12691>.
- Adl, Sina M., Brian S. Leander, Alastair G. B. Simpson, John M. Archibald, O. Roger. Anderson, David Bass, Samuel S. Bowser, et al. 2007. "Diversity, Nomenclature, and Taxonomy of Protists." *Systematic Biology* 56 (4): 684-89. <https://doi.org/10.1080/10635150701494127>.
- Adl, Sina M., Alastair G.B. Simpson, Christopher E. Lane, Julius Lukeš, David Bass, Samuel S. Bowser, Matthew W. Brown, et al. 2012. "The Revised Classification of Eukaryotes." *Journal of Eukaryotic Microbiology* 59 (5): 429-93. <https://doi.org/10.1111/j.1550-7408.2012.00644.x>.
- Akella, Jyothi S, Dorota Wloga, Jihyun Kim, Natalia G Starostina, Sally Lyons-, Naomi S Morrissette, Scott T Dougan, and Edward T Kipreos. 2010. "MEC-17 Is an α -Tubulin Acetyltransferase." *Nature* 467 (7312): 218-22. <https://doi.org/10.1038/nature09324>.
- Allen, M. Leah, Janice M. Dobrowolski, Hayyah Muller, L. David Sibley, and Tag E. Mansour. 1997. "Cloning and Characterization of Actin Depolymerizing Factor from *Toxoplasma Gondii*." *Molecular and Biochemical Parasitology*

88: 43-52. [https://doi.org/10.1016/S0166-6851\(97\)00069-8](https://doi.org/10.1016/S0166-6851(97)00069-8).

- Andenmatten, Nicole, Saskia Egarter, Allison J Jackson, Nicolas Jullien, Jean-Paul Herman, and Markus Meissner. 2013. "Conditional Genome Engineering in *Toxoplasma Gondii* Uncovers Alternative Invasion Mechanisms." *Nature Methods* 10 (2): 125-27. <https://doi.org/10.1038/nmeth.2301>.
- Anderson-White, Brooke R., F. Douglas Ivey, Katherine Cheng, Tomasz Szatanek, Alexander Lorestani, Con J. Beckers, David J.P. Ferguson, Nivedita Sahoo, and Marc Jan Gubbels. 2011. "A Family of Intermediate Filament-like Proteins Is Sequentially Assembled into the Cytoskeleton of *Toxoplasma Gondii*." *Cellular Microbiology* 13 (1): 18-31. <https://doi.org/10.1111/j.1462-5822.2010.01514.x>.
- Arber, Silvia, Freda A. Barbayannis, Hartwig Hanser, Corinna Schneider, Clement A. Stanyon, Ora Bernard, and Pico Caroni. 1998. "Regulation of Actin Dynamics through Phosphorylation of Cofilin by LIM-Kinase." *Nature* 393 (6687): 805-9. <https://doi.org/10.1038/31729>.
- Armstrong, Christopher M., and Daniel E. Goldberg. 2007. "An FKBP Destabilization Domain Modulates Protein Levels in *Plasmodium Falciparum*." *Nature Methods* 4 (12): 1007-9. <https://doi.org/10.1038/nmeth1132>.
- Attias, Marcia, Kildare Miranda, and Wanderley De Souza. 2019. "Development and Fate of the Residual Body of *Toxoplasma Gondii*." *Experimental Parasitology* 196: 1-11. <https://doi.org/10.1016/j.exppara.2018.11.004>.
- Banaszynski, Laura A., Ling-chun Chen, Lystranne A. Maynard-Smith, A. G. Lisa Ooi, and Thomas J. Wandless. 2006. "A Rapid, Reversible, and Tunable Method to Regulate Protein Function in Living Cells Using Synthetic Small Molecules." *Cell* 126 (5): 995-1004. <https://doi.org/10.1016/j.cell.2006.07.025>.
- Bargieri, Daniel Y., Nicole Andenmatten, Vanessa Lagal, Sabine Thiberge, Jamie A. Whitelaw, Isabelle Tardieux, Markus Meissner, and Robert Ménard. 2013.

“Apical Membrane Antigen 1 Mediates Apicomplexan Parasite Attachment but Is Dispensable for Host Cell Invasion.” *Nature Communications* 4: 2552. <https://doi.org/10.1038/ncomms3552>.

Batra, Ranjan, David A. Nelles, Elaine Pirie, Steven M. Blue, Ryan J. Marina, Harrison Wang, Isaac A. Chaim, et al. 2017. “Elimination of Toxic Microsatellite Repeat Expansion RNA by RNA-Targeting Cas9.” *Cell* 170 (5): 899-912.e10. <https://doi.org/10.1016/j.cell.2017.07.010>.

Baum, Jake, Anthony T Papenfuss, Buzz Baum, Terence P Speed, and Alan F Cowman. 2006. “Regulation of Apicomplexan Actin-Based Motility.” *Nature Reviews Microbiology* 4: 621-28. <https://doi.org/10.1038/nrmicro1465>.

Bellenchi, Gian Carlo, Christine B. Gurniak, Emerald Perlas, Silvia Middei, Martine Ammassari-Teule, and Walter Witke. 2007. “N-Cofilin Is Associated with Neuronal Migration Disorders and Cell Cycle Control in the Cerebral Cortex.” *Genes and Development* 21: 2347-57. <https://doi.org/10.1101/gad.434307>.

Belli, Sabina I., Nicholas C. Smith, and David J.P. Ferguson. 2006. “The Coccidian Oocyst: A Tough Nut to Crack!” *Trends in Parasitology* 22 (9): 416-23. <https://doi.org/10.1016/j.pt.2006.07.004>.

Besteiro, Sébastien, Jean François Dubremetz, and Maryse Lebrun. 2011. “The Moving Junction of Apicomplexan Parasites: A Key Structure for Invasion.” *Cellular Microbiology* 13 (6): 797-805. <https://doi.org/10.1111/j.1462-5822.2011.01597.x>.

Besteiro, Sébastien, Adeline Michelin, Joël Poncet, Jean François Dubremetz, and Maryse Lebrun. 2009. “Export of a *Toxoplasma Gondii* Rhoptry Neck Protein Complex at the Host Cell Membrane to Form the Moving Junction during Invasion.” *PLoS Pathogens* 5 (2): e1000309. <https://doi.org/10.1371/journal.ppat.1000309>.

Black, Michael, Frank Seeber, Dominique Soldati, Kami Kim, and John C. Boothroyd. 1995. “Restriction Enzyme-Mediated Integration Elevates

Transformation Frequency and Enables Co-Transfection of *Toxoplasma Gondii*.” *Molecular and Biochemical Parasitology* 74 (1): 55-63.

[https://doi.org/10.1016/0166-6851\(95\)02483-2](https://doi.org/10.1016/0166-6851(95)02483-2).

Black, Michael W, and John C Boothroyd. 2000. “Lytic Cycle of *Toxoplasma Gondii*.” *Microbiology and Molecular Biology Reviews* 64 (3): 607-23.

<https://doi.org/10.1128/MMBR.64.3.607-623.2000>.Updated.

Blader, Ira J., Bradley I. Coleman, Chun-Ti Chen, and Marc-Jan Gubbels. 2015.

“Lytic Cycle of *Toxoplasma Gondii* : 15 Years Later.” *Annual Review of Microbiology* 69: 463-85. <https://doi.org/10.1146/annurev-micro-091014-104100>.

Bougdour, Alexandre, Eric Durandau, Marie Pierre Brenier-Pinchart, Philippe Ortet, Mohamed Barakat, Sylvie Kieffer, Aurélie Curt-Varesano, et al. 2013.

“Host Cell Subversion by *Toxoplasma* GRA16, an Exported Dense Granule Protein That Targets the Host Cell Nucleus and Alters Gene Expression.” *Cell Host and Microbe* 13 (4): 489-500.

<https://doi.org/10.1016/j.chom.2013.03.002>.

Braun, Laurence, Marie-Pierre Brenier-Pinchart, Manickam Yogavel, Aurélie Curt-

Varesano, Rose-Laurence Curt-Bertini, Tahir Hussain, Sylvie Kieffer-Jaquinod, et al. 2013. “ A *Toxoplasma* Dense Granule Protein, GRA24, Modulates the Early Immune Response to Infection by Promoting a Direct and Sustained Host P38 MAPK Activation .” *The Journal of Experimental Medicine* 210 (10): 2071-86. <https://doi.org/10.1084/jem.20130103>.

Breitsprecher, Dennis, Richa Jaiswal, Jeffrey P. Bombardier, Christopher J.

Gould, Jeff Gelles, and Bruce L. Goode. 2012. “Rocket Launcher Mechanism of Collaborative Actin Assembly Defined by Single-Molecule Imaging.”

Science 336 (6085): 1164-68. <https://doi.org/10.1126/science.1218062>.

Brown, Kevin, Shaojun Long, and L. David Sibley. 2018. “Conditional Knockdown

of Proteins Using Auxin-Inducible Degron (AID) Fusions in *Toxoplasma Gondii*.” *Bio-Protocol* 8 (4): e2728.

<https://doi.org/10.21769/bioprotoc.2728>.

- Brown, Kevin M., Shaojun Long, and L. David Sibley. 2017. "Plasma Membrane Association by N-Acylation Governs PKG Function in *Toxoplasma Gondii*." *MBio* 8: e00375-17. <https://doi.org/10.1128/mBio.00375-17>.
- Bullen, Hayley E., Hugo Bisio, and Dominique Soldati-Favre. 2019. "The Triumvirate of Signaling Molecules Controlling *Toxoplasma* Microneme Exocytosis: Cyclic GMP, Calcium, and Phosphatidic Acid." *PLOS Pathogens* 15 (5): e1007670. <https://doi.org/10.1371/journal.ppat.1007670>.
- Bullen, Hayley E., Yonggen Jia, Yoshiki Yamaro-Botté, Hugo Bisio, Ou Zhang, Natacha Klages Jemelin, Jean Baptiste Marq, Vern Carruthers, Cyrille Y. Botté, and Dominique Soldati-Favre. 2016. "Phosphatidic Acid-Mediated Signaling Regulates Microneme Secretion in *Toxoplasma*." *Cell Host and Microbe* 19 (3): 349-60. <https://doi.org/10.1016/j.chom.2016.02.006>.
- Burki, Fabien, Kamran Shalchian-Tabrizi, Marianne Minge, Åsmund Skjæveland, Sergey I. Nikolaev, Kjetill S. Jakobsen, and Jan Pawlowski. 2007. "Phylogenomics Reshuffles the Eukaryotic Supergroups." *PLoS ONE* 2 (8): 1-6. <https://doi.org/10.1371/journal.pone.0000790>.
- Cai, Xiaomin, A. Lorraine Fuller, Larry R. McDougald, and Guan Zhu. 2003. "Apicoplast Genome of the Coccidian *Eimeria Tenella*." *Gene* 321 (1-2): 39-46. <https://doi.org/10.1016/j.gene.2003.08.008>.
- Carrier, Marie-France, Valérie Laurent, Jérôme Santolini, Ronald Melki, Dominique Didry, Gui-xian Xia, Yan Hong, Nam-Hai Chua, and Dominique Pantaloni. 1997. "Actin Depolymerizing Factor (ADF/Cofilin) Enhances the Rate of Filament Turnover: Implication in Actin-Based Motility." *The Journal of Cell Biology* 136 (6): 1307-22. <https://doi.org/10.1083/jcb.136.6.1307>.
- Carlsson, L., L. E. Nyström, I. Sundkvist, F. Markey, and U. Lindberg. 1977. "Actin Polymerizability Is Influenced by Profilin, a Low Molecular Weight Protein in Non-Muscle Cells." *Journal of Molecular Biology* 115: 465-83. [https://doi.org/10.1016/0022-2836\(77\)90166-8](https://doi.org/10.1016/0022-2836(77)90166-8).
- Castrillon, D H, and S A Wasserman. 1994. "Diaphanous Is Required for

Cytokinesis in *Drosophila* and Shares Domains of Similarity with the Products of the Limb Deformity Gene.” *Development* 120 (12): 3367-77.

<http://www.ncbi.nlm.nih.gov/pubmed/7821209>.

Chakrabarti, Anob M., Tristan Henser-Brownhill, Josep Monserrat, Anna R.

Poetsch, Nicholas M. Luscombe, and Paola Scaffidi. 2019. “Target-Specific Precision of CRISPR-Mediated Genome Editing.” *Molecular Cell* 73 (4): 699-713.e6. <https://doi.org/10.1016/j.molcel.2018.11.031>.

Chen, Allan L., Elliot W. Kim, Justin Y. Toh, Ajay A. Vashisht, Andrew Q.

Rashoff, Christina Van, Amy S. Huang, et al. 2015. “Novel Components of the Toxoplasma Inner Membrane Complex Revealed by BioID.” *MBio* 6 (1): e02357-14. <https://doi.org/10.1128/mBio.02357-14>.

Chen, Allan L., Andy S. Moon, Hannah N. Bell, Amy S. Huang, Ajay A. Vashisht,

Justin Y. Toh, Andrew H. Lin, et al. 2017. “Novel Insights into the Composition and Function of the Toxoplasma IMC Sutures.” *Cellular Microbiology* 19: e12678. <https://doi.org/10.1111/cmi.12678>.

Chen, C.-T., and M.-J. Gubbels. 2013. “The Toxoplasma Gondii Centrosome Is

the Platform for Internal Daughter Budding as Revealed by a Nek1 Kinase Mutant.” *Journal of Cell Science* 126 (15): 3344-55.

<https://doi.org/10.1242/jcs.123364>.

Clough, Barbara, and Eva Maria Frickel. 2017. “The Toxoplasma Parasitophorous

Vacuole: An Evolving Host-Parasite Frontier.” *Trends in Parasitology* 33 (6): 473-88. <https://doi.org/10.1016/j.pt.2017.02.007>.

Cong, Le, F Ann Ran, David Cox, Shuailiang Lin, Robert Barretto, Naomi Habib,

Patrick D. Hsu, et al. 2013. “Multiplex Genome Engineering Using CRISPR/Cas Systems.” *Science* 339 (6121): 819-23.

<https://doi.org/10.1126/science.1231143>.

Cooke, Roger. 1975. “The Role of the Bound Nucleotide in the Polymerization of

Actin.” *Biochemistry* 14 (14): 3250-56.

<https://doi.org/10.1021/bi00685a035>.

- Coppin, Alexandra, Jean Stéphane Varré, Luc Lienard, David Dauvillée, Yann Guérardel, Marie Odile Soyer-Gobillard, Alain Buléon, Steven Ball, and Stanislas Tomavo. 2005. "Evolution of Plant-like Crystalline Storage Polysaccharide in the Protozoan Parasite *Toxoplasma Gondii* Argues for a Red Alga Ancestry." *Journal of Molecular Evolution* 60 (2): 257-67.
<https://doi.org/10.1007/s00239-004-0185-6>.
- Courtemanche, Naomi. 2018. "Mechanisms of Formin-Mediated Actin Assembly and Dynamics." *Biophysical Reviews* 10: 1553-69.
<https://doi.org/10.1007/s12551-018-0468-6>.
- Critchlow, Susan E., and Stephen P. Jackson. 1998. "DNA End-Joining: From Yeast to Man." *Trends in Biochemical Sciences* 23 (10): 394-98.
[https://doi.org/10.1016/S0968-0004\(98\)01284-5](https://doi.org/10.1016/S0968-0004(98)01284-5).
- Daher, Wassim, Natacha Klages, Marie-France Carlier, and Dominique Soldati-Favre. 2012. "Molecular Characterization of *Toxoplasma Gondii* Formin 3, an Actin Nucleator Dispensable for Tachyzoite Growth and Motility." *Eukaryotic Cell* 11 (3): 343-52. <https://doi.org/10.1128/ec.05192-11>.
- Daher, Wassim, Fabienne Plattner, Marie-France Carlier, and Dominique Soldati-Favre. 2010. "Concerted Action of Two Formins in Gliding Motility and Host Cell Invasion by *Toxoplasma Gondii*." *PLoS Pathogens* 6 (10): e1001132.
<https://doi.org/10.1371/journal.ppat.1001132>.
- Darvill, Nick, David J. Dubois, Sarah L. Rouse, Pierre Mehdi Hammoudi, Tom Blake, Stefi Benjamin, Bing Liu, Dominique Soldati-Favre, and Steve Matthews. 2018. "Structural Basis of Phosphatidic Acid Sensing by APH in Apicomplexan Parasites." *Structure* 26 (8): 1059-71.
<https://doi.org/10.1016/j.str.2018.05.001>.
- Das, S., J. E. Dixon, and W. Cho. 2003. "Membrane-Binding and Activation Mechanism of PTEN." *Proceedings of the National Academy of Sciences of the United States of America* 100 (13): 7491-96.
<https://doi.org/10.1073/pnas.0932835100>.

- Deeks, Michael J., and Patrick J. Hussey. 2005. "Arp2/3 and SCAR: Plants Move to the Fore." *Nature Reviews Molecular Cell Biology* 6: 954-64. <https://doi.org/10.1038/nrm1765>.
- Dhanasekaran, Shanmugham, Nagasuma R. Chandra, B. K. Chandrasekhar Sagar, Pundi N. Rangarajan, and Govindarajan Padmanaban. 2004. "δ-Aminolevulinic Acid Dehydratase from Plasmodium Falciparum ." *Journal of Biological Chemistry* 279 (8): 6934-42. <https://doi.org/10.1074/jbc.m311409200>.
- Dobrowolski, Janice M., Ingrid R. Niesman, and L. David Sibley. 1997. "Actin in the Parasite Toxoplasma Gondii Is Encoded by a Single Copy Gene, Act1 and Exists Primarily in a Globular Form." *Cell Motility and the Cytoskeleton* 37 (3): 253-62. [https://doi.org/10.1002/\(SICI\)1097-0169\(1997\)37:3<253::AID-CM7>3.0.CO;2-7](https://doi.org/10.1002/(SICI)1097-0169(1997)37:3<253::AID-CM7>3.0.CO;2-7).
- Dobrowolski, Janice M., and L. David Sibley. 1996. "Toxoplasma Invasion of Mammalian Cells Is Powered by the Actin Cytoskeleton of the Parasite." *Cell* 84 (6): 933-39. [https://doi.org/10.1016/s0092-8674\(00\)81071-5](https://doi.org/10.1016/s0092-8674(00)81071-5).
- Dominguez, Roberto, and Kenneth C Holmes. 2011. "Actin Structure and Function." *Annual Review of Biophysics* 40 (3): 169-86. <https://doi.org/10.1146/annurev-biophys-042910-155359>.
- Donahue, Carolyn G., Vern B. Carruthers, Stacey D. Gilk, and Gary E. Ward. 2000. "The Toxoplasma Homolog of Plasmodium Apical Membrane Antigen-1 (AMA-1) Is a Microneme Protein Secreted in Response to Elevated Intracellular Calcium Levels." *Molecular and Biochemical Parasitology* 111 (1): 15-30. [https://doi.org/10.1016/S0166-6851\(00\)00289-9](https://doi.org/10.1016/S0166-6851(00)00289-9).
- Donald, R. G., and D. S. Roos. 1993. "Stable Molecular Transformation of Toxoplasma Gondii: A Selectable Dihydrofolate Reductase-Thymidylate Synthase Marker Based on Drug-Resistance Mutations in Malaria." *Proceedings of the National Academy of Sciences of the United States of America* 90 (24): 11703-7. <https://doi.org/10.1073/pnas.90.24.11703>.

- Donald, Robert G. K., Darrick Carter, Buddy Ullman, and David S. Roos. 1996. "Insertional Tagging, Cloning, and Expression of the *Toxoplasma Gondii* Hypoxanthine-Xanthine-Guanine Phosphoribosyltransferase Gene." *Journal of Biological Chemistry* 271 (24): 14010-19. <https://doi.org/10.1074/jbc.271.24.14010>.
- Dooren, Giel G. van, Sarah B. Reiff, Cveta Tomova, Markus Meissner, Bruno M. Humbel, and Boris Striepen. 2009. "A Novel Dynamin-Related Protein Has Been Recruited for Apicoplast Fission in *Toxoplasma Gondii*." *Current Biology* 19 (4): 267-76. <https://doi.org/10.1016/j.cub.2008.12.048>.
- Dooren, Giel G. van, and Boris Striepen. 2013. "The Algal Past and Parasite Present of the Apicoplast." *Annual Review of Microbiology* 67 (1): 271-89. <https://doi.org/10.1146/annurev-micro-092412-155741>.
- Doudna, Jennifer A., and Emmanuelle Charpentier. 2014. "The New Frontier of Genome Engineering with CRISPR-Cas9." *Science* 346 (6213): 1258096. <https://doi.org/10.1126/science.1258096>.
- Drewry, Lisa L., and L. David Sibley. 2015. "Toxoplasma Actin Is Required for Efficient Host Cell Invasion." *MBio* 6 (3): e00557-15. <https://doi.org/10.1128/mBio.00557-15>.
- Dubey, J. P. 2006. "Comparative Infectivity of Oocysts and Bradyzoites of *Toxoplasma Gondii* for Intermediate (Mice) and Definitive (Cats) Hosts." *Veterinary Parasitology* 140 (1-2): 69-75. <https://doi.org/10.1016/j.vetpar.2006.03.018>.
- Dubey, J. P., and J. K. Frenkel. 1976. "Feline Toxoplasmosis from Acutely Infected Mice and the Development of *Toxoplasma* Cysts." *The Journal of Protozoology* 23 (4): 537-46. <https://doi.org/10.1111/j.1550-7408.1976.tb03836.x>.
- Dubey, J. P., D. S. Lindsay, and C. A. Speer. 1998. "Structures of *Toxoplasma Gondii* Tachyzoites, Bradyzoites, and Sporozoites and Biology and Development of Tissue Cysts." *Clinical Microbiology Reviews* 11 (2): 267-99.

<https://doi.org/10.1128/CMR.11.2.267>.

- Dubey, J.P. 1998. "Toxoplasma Gondii Oocyst Survival under Defined Temperatures." *The Journal of Parasitology* 84 (4): 862-65.
[https://doi.org/DOI: 10.2307/3284606](https://doi.org/DOI:10.2307/3284606).
- Dubey, Rashmi, Brooke Harrison, Sriveny Dangoudoubiyam, Giulia Bandini, Katherine Cheng, Aziz Kosber, Carolina Agop-Nersesian, et al. 2017. "Differential Roles for Inner Membrane Complex Proteins across Toxoplasma Gondii and Sarcocystis Neurona Development." *MSphere* 2 (5): e00409-17.
<https://doi.org/10.1128/mSphere.00409-17>.
- Dumetre, A., J. P. Dubey, D. J. P. Ferguson, P. Bongrand, N. Azas, and P.-H. Puech. 2013. "Mechanics of the Toxoplasma Gondii Oocyst Wall." *Proceedings of the National Academy of Sciences of the United States of America* 110 (28): 11535-40. <https://doi.org/10.1073/pnas.1308425110>.
- Edwards, Marc, Adam Zwolak, Dorothy A. Schafer, David Sept, Roberto Dominguez, and John A. Cooper. 2014. "Capping Protein Regulators Fine-Tune Actin Assembly Dynamics." *Nature Reviews Molecular Cell Biology* 15 (10): 677-89. <https://doi.org/10.1038/nrm3869>.
- Egarter, Saskia, Nicole Andenmatten, Allison J. Jackson, Jamie A. Whitelaw, Gurman Pall, Jennifer Ann Black, David J P Ferguson, Isabelle Tardieux, Alex Mogilner, and Markus Meissner. 2014. "The Toxoplasma Acto-MyoA Motor Complex Is Important but Not Essential for Gliding Motility and Host Cell Invasion." *PLoS ONE* 9 (3): e91819.
<https://doi.org/10.1371/journal.pone.0091819>.
- Endo, T., K. K. Sethi, and G. Piekarski. 1982. "Toxoplasma Gondii: Calcium Ionophore A23187-Mediated Exit of Trophozoites from Infected Murine Macrophages." *Experimental Parasitology* 53 (2): 179-88.
[https://doi.org/10.1016/0014-4894\(82\)90059-5](https://doi.org/10.1016/0014-4894(82)90059-5).
- Evangelista, M., Sally Zigmund, and Charles Boone. 2003. "Formins: Signaling Effectors for Assembly and Polarization of Actin Filaments." *Journal of Cell*

Science 116 (13): 2603-11. <https://doi.org/10.1242/jcs.00611>.

Evangelista, Marie, Kelly Blundell, Mark S. Longtine, Clinton J. Chow, Neil Adames, John R. Pringle, Matthias Peter, and Charles Boone. 1997. "Bni1p, a Yeast Formin Linking Cdc42p and the Actin Cytoskeleton During Polarized Morphogenesis." *Science* 276 (5309): 118-122. <https://doi.org/10.1126/science.276.5309.118>.

Evangelista, Marie, David Pruyne, David C. Amberg, Charles Boone, and Anthony Bretscher. 2002. "Formins Direct Arp2/3-Independent Actin Filament Assembly to Polarize Cell Growth in Yeast." *Nature Cell Biology* 4: 32-41. <https://doi.org/10.1038/ncb718>.

Fan, Di, Tingting Liu, Chaofeng Li, Bo Jiao, Shuang Li, Yishu Hou, and Keming Luo. 2015. "Efficient CRISPR/Cas9-Mediated Targeted Mutagenesis in Populus in the First Generation." *Scientific Reports* 5: 12217. <https://doi.org/10.1038/srep12217>.

Fang, Jianmin, Norma Marchesini, and Silvia N. J. Moreno. 2006. "A Toxoplasma Gondii Phosphoinositide Phospholipase C (Tg PI-PLC) with High Affinity for Phosphatidylinositol." *Biochemical Journal* 394 (2): 417-25. <https://doi.org/10.1042/bj20051393>.

Feierbach, Becket, and Fred Chang. 2001. "Roles of the Fission Yeast Formin For3p in Cell Polarity, Actin Cable Formation and Symmetric Cell Division." *Current Biology* 11 (21): 1656-65. [https://doi.org/10.1016/S0960-9822\(01\)00525-5](https://doi.org/10.1016/S0960-9822(01)00525-5).

Ferguson, D. J.P., W. M. Hutchison, and J. CHR Siim. 1975. "The Ultrastructural Development of the Macrogamete and Formation of the Oocyst Wall of Toxoplasma Gondii." *Acta Pathologica Microbiologica Scandinavica Section B Microbiology* 83 B (5): 491-505. <https://doi.org/10.1111/j.1699-0463.1975.tb00130.x>.

Fox, Barbara A., Jessica G. Ristuccia, Jason P. Gigley, and David J. Bzik. 2009. "Efficient Gene Replacements in Toxoplasma Gondii Strains Deficient for

Nonhomologous End Joining.” *Eukaryotic Cell* 8 (4): 520-29.
<https://doi.org/10.1128/ec.00357-08>.

Frénal, Karine, Jean-François Dubremetz, Maryse Lebrun, and Dominique Soldati-Favre. 2017. “Gliding Motility Powers Invasion and Egress in Apicomplexa.” *Nature Reviews Microbiology* 15 (11): 645-60.
<https://doi.org/10.1038/nrmicro.2017.86>.

Frénal, Karine, Damien Jacot, Pierre Mehdi Hammoudi, Arnault Graindorge, Bohumil MacO, and Dominique Soldati-Favre. 2017. “Myosin-Dependent Cell-Cell Communication Controls Synchronicity of Division in Acute and Chronic Stages of *Toxoplasma Gondii*.” *Nature Communications* 8: 15710.
<https://doi.org/10.1038/ncomms15710>.

Frénal, Karine, Valérie Polonais, Jean Baptiste Marq, Rolf Stratmann, Julien Limenitakis, and Dominique Soldati-Favre. 2010. “Functional Dissection of the Apicomplexan Glideosome Molecular Architecture.” *Cell Host and Microbe* 8 (4): 343-57. <https://doi.org/10.1016/j.chom.2010.09.002>.

Frenkel, J.K., J.P. Dubey, and N.L. Miller. 1970. “*Toxoplasma Gondii* in Cats: Fecal Stages Identified as Coccidian Oocysts.” *Science* 167 (3919): 893-96.
<https://doi.org/10.1126/science.167.3919.893>.

Frenkel, J.K., A. Ruiz, and M. Chinchilla. 1975. “Soil Survival of *Toxoplasma* Oocysts in Kansas and Costa Rica.” *The American Journal of Tropical Medicine and Hygiene* 24 (3): 439-43.
<https://doi.org/10.4269/ajtmh.1975.24.439>.

Fujii, Takashi, Atsuko H. Iwane, Toshio Yanagida, and Keiichi Namba. 2010. “Direct Visualization of Secondary Structures of F-Actin by Electron Cryomicroscopy.” *Nature* 467: 724-28.
<https://doi.org/10.1038/nature09372>.

Funes, Soledad, Edgar Davidson, Adrián Reyes-Prieto, Susana Magallón, Pascal Herion, Michael P. King, and Diego González-Halphen. 2002. “A Green Algal Apicoplast Ancestor.” *Science* 298 (5601): 2155.

<https://doi.org/10.1126/science.1076003>.

Gaji, Rajshekhar Y., Derrick E. Johnson, Moritz Treeck, Mu Wang, Andy Hudmon, and Gustavo Arrizabalaga. 2015. "Phosphorylation of a Myosin Motor by TgCDPK3 Facilitates Rapid Initiation of Motility during Toxoplasma Gondii Egress." *PLoS Pathogens* 11 (11): e1005268.

<https://doi.org/10.1371/journal.ppat.1005268>.

Gajria, Bindu, Amit Bahl, John Brestelli, Jennifer Dommer, Steve Fischer, Xin Gao, Mark Heiges, et al. 2008. "ToxoDB: An Integrated Toxoplasma Gondii Database Resource." *Nucleic Acids Research* 36 (Database issue): D553-56. <https://doi.org/10.1093/nar/gkm981>.

Garrison, Erin, Moritz Treeck, Emma Ehret, Heidi Butz, Tamila Garbuz, Benji P. Oswald, Matt Settles, John Boothroyd, and Gustavo Arrizabalaga. 2012. "A Forward Genetic Screen Reveals That Calcium-Dependent Protein Kinase 3 Regulates Egress in Toxoplasma." *PLoS Pathogens* 8 (11): e1003049.

<https://doi.org/10.1371/journal.ppat.1003049>.

Gasiunas, Giedrius, Rodolphe Barrangou, Philippe Horvath, and Virginijus Siksnys. 2012. "Cas9-CrRNA Ribonucleoprotein Complex Mediates Specific DNA Cleavage for Adaptive Immunity in Bacteria." *Proceedings of the National Academy of Sciences of the United States of America* 109 (39): E2579-86. <https://doi.org/10.1073/pnas.1208507109>.

Gaskins, Elizabeth, Stacey Gilk, Nicolette DeVore, Tara Mann, Gary Ward, and Con Beckers. 2004. "Identification of the Membrane Receptor of a Class XIV Myosin in Toxoplasma Gondii." *Journal of Cell Biology* 165 (3): 383-93.

<https://doi.org/10.1083/jcb.200311137>.

Genova, Bruno Martorelli Di, Sarah K. Wilson, J. P. Dubey, and Laura J. Knoll. 2019. "Intestinal Delta-6-Desaturase Activity Determines Host Range for Toxoplasma Sexual Reproduction." *PLoS Biology* 17 (8): e3000364.

<https://doi.org/10.1371/journal.pbio.3000364>.

Gilles, Anna F., Johannes B. Schinko, and Michalis Averof. 2015. "Efficient

CRISPR-Mediated Gene Targeting and Transgene Replacement in the Beetle *Tribolium Castaneum*.” *Development* 142 (16): 2832-39.

<https://doi.org/10.1242/dev.125054>.

Giovannini, Donatella, Stephan Späth, Céline Lacroix, Audrey Perazzi, Daniel Bargieri, Vanessa Lagal, Camille Lebugle, et al. 2011. “Independent Roles of Apical Membrane Antigen 1 and Rhoptry Neck Proteins during Host Cell Invasion by Apicomplexa.” *Cell Host and Microbe* 10 (6): 591-602.
<https://doi.org/10.1016/j.chom.2011.10.012>.

Gisselberg, Jolyn E., Teegan A. Dellibovi-Ragheb, Krista A. Matthews, Gundula Bosch, and Sean T. Prigge. 2013. “The Suf Iron-Sulfur Cluster Synthesis Pathway Is Required for Apicoplast Maintenance in Malaria Parasites.” *PLoS Pathogens* 9 (9): e1003655. <https://doi.org/10.1371/journal.ppat.1003655>.

Gold, Daniel A., Aaron D. Kaplan, Agnieszka Lis, Glenna C.L. Bett, Emily E. Rosowski, Kimberly M. Cirelli, Alexandre Bougdour, et al. 2015. “The Toxoplasma Dense Granule Proteins GRA17 and GRA23 Mediate the Movement of Small Molecules between the Host and the Parasitophorous Vacuole.” *Cell Host and Microbe* 17 (5): 642-52.
<https://doi.org/10.1016/j.chom.2015.04.003>.

Goldberg, Daniel E., and Paul A. Sigala. 2017. “Plasmodium Heme Biosynthesis: To Be or Not to Be Essential?” *PLOS Pathogens* 13 (9): e1006511.
<https://doi.org/10.1371/journal.ppat.1006511>.

Goldman, Morris, Russel K. Carver, and Alexander J. Sulzer. 1958. “Reproduction of *Toxoplasma Gondii* by Internal Budding.” *The Journal of Parasitology* 44 (2): 161-71. <https://doi.org/10.2307/3274692>.

Goode, Bruce L., and Michael J. Eck. 2007. “Mechanism and Function of Formins in the Control of Actin Assembly.” *Annual Review of Biochemistry* 76: 593-627. <https://doi.org/10.1146/annurev.biochem.75.103004.142647>.

Gordon, Jennifer L, and L David Sibley. 2005. “Comparative Genome Analysis Reveals a Conserved Family of Actin-like Proteins in Apicomplexan

Parasites.” *BMC Genomics* 6: 179. <https://doi.org/10.1186/1471-2164-6-179>.

Gorski, Stanislaw A., Jörg Vogel, and Jennifer A. Doudna. 2017. “RNA-Based Recognition and Targeting: Sowing the Seeds of Specificity.” *Nature Reviews Molecular Cell Biology* 18 (4): 215-28. <https://doi.org/10.1038/nrm.2016.174>.

Gould, Kathleen L, and Laura M Machesky. 1999. “The Arp2/3 Complex: A Multifunctional Actin Organizer.” *Current Opinion in Cell Biology* 11: 117-21. [https://doi.org/10.1016/s0955-0674\(99\)80014-3](https://doi.org/10.1016/s0955-0674(99)80014-3).

Graceffa, Philip, and Roberto Dominguez. 2003. “Crystal Structure of Monomeric Actin in the ATP State: Structural Basis of Nucleotide-Dependent Actin Dynamics.” *Journal of Biological Chemistry* 278 (36): 34172-80. <https://doi.org/10.1074/jbc.M303689200>.

Gras, Simon, Allison Jackson, Stuart Woods, Gurman Pall, Jamie Whitelaw, Jacqueline M. Leung, Gary E. Ward, Craig W. Roberts, and Markus Meissner. 2017. “Parasites Lacking the Micronemal Protein MIC2 Are Deficient in Surface Attachment and Host Cell Egress, but Remain Virulent in Vivo.” *Wellcome Open Research* 2: 32. <https://doi.org/10.12688/wellcomeopenres.11594.2>.

Gras, Simon, Elena Jimenez-Ruiz, Christen M. Klinger, Katja Schneider, Andreas Klingl, Leandro Lemgruber, and Markus Meissner. 2019. “An Endocytic-Secretory Cycle Participates in *Toxoplasma Gondii* in Motility.” *PLOS Biology* 17 (6): e3000060. <https://doi.org/10.1371/journal.pbio.3000060>.

Gubbels, Marc Jan, Marnix Wieffer, and Boris Striepen. 2004. “Fluorescent Protein Tagging in *Toxoplasma Gondii*: Identification of a Novel Inner Membrane Complex Component Conserved among Apicomplexa.” *Molecular and Biochemical Parasitology* 137: 99-110. <https://doi.org/10.1016/j.molbiopara.2004.05.007>.

Guérin, Amandine, Hiba El Hajj, Diana Penarete-Vargas, Sébastien Besteiro, and

- Maryse Lebrun. 2017. "RON4L1 Is a New Member of the Moving Junction Complex in *Toxoplasma Gondii*." *Scientific Reports* 7 (1): 17907. <https://doi.org/10.1038/s41598-017-18010-9>.
- Gupta, C. M., S. Thiyagarajan, and A. A. Sahasrabudde. 2015. "Unconventional Actins and Actin-Binding Proteins in Human Protozoan Parasites." *International Journal for Parasitology* 45 (7): 435-47. <https://doi.org/10.1016/j.ijpara.2015.01.011>.
- Gurniak, Christine B., Emerald Perlas, and Walter Witke. 2005. "The Actin Depolymerizing Factor N-Cofilin Is Essential for Neural Tube Morphogenesis and Neural Crest Cell Migration." *Developmental Biology* 278: 231-41. <https://doi.org/10.1016/j.ydbio.2004.11.010>.
- Haase, Silvia, Dennis Zimmermann, Maya A. Olshina, Mark Wilkinson, Fabio Fisher, Yan Hong Tan, Rebecca J. Stewart, et al. 2015. "Disassembly Activity of Actin-Depolymerizing Factor (ADF) Is Associated with Distinct Cellular Processes in Apicomplexan Parasites." *Molecular Biology of the Cell* 26 (17): 3001-12. <https://doi.org/10.1091/mbc.e14-10-1427>.
- Hakansson, S., H. Morisaki, J. Heuser, and L. D. Sibley. 1999. "Time-Lapse Video Microscopy of Gliding Motility in *Toxoplasma Gondii* Reveals a Novel, Biphasic Mechanism of Cell Locomotion." *Molecular Biology of the Cell* 10 (11): 3539-47. <https://doi.org/10.1091/mbc.10.11.3539>.
- Hamers-Casterman, C, T Atarhouch, S Muyldermans, G Robinson, C Hamers, E B Songa, N Bendahman, and R Hamers. 1993. "Naturally Occurring Antibodies Devoid of Light Chains." *Nature* 363 (6428): 446-48. <https://doi.org/10.1038/363446a0>.
- Hanson, Jean, and J. Lowy. 1963. "The Structure of F-Actin and of Actin Filaments Isolated from Muscle." *Journal of Molecular Biology* 6 (1): 46-60. [https://doi.org/10.1016/S0022-2836\(63\)80081-9](https://doi.org/10.1016/S0022-2836(63)80081-9).
- Harding, Clare R., Saskia Egarter, Matthew Gow, Elena Jiménez-Ruiz, David J. P. Ferguson, and Markus Meissner. 2016. "Gliding Associated Proteins Play

Essential Roles during the Formation of the Inner Membrane Complex of *Toxoplasma Gondii*.” *PLoS Pathogens* 12 (2): e1005403.

<https://doi.org/10.1371/journal.ppat.1005403>.

Harding, Clare R., and Markus Meissner. 2014. “The Inner Membrane Complex through Development of *Toxoplasma Gondii* and *Plasmodium*.” *Cellular Microbiology* 16 (5): 632-41. <https://doi.org/10.1111/cmi.12285>.

Harris, Elizabeth S., Fang Li, and Henry N. Higgs. 2004. “The Mouse Formin, FRL α , Slows Actin Filament Barbed End Elongation, Competes with Capping Protein, Accelerates Polymerization from Monomers, and Severs Filaments.” *Journal of Biological Chemistry* 279 (19): 20076-87.

<https://doi.org/10.1074/jbc.M312718200>.

Hartenian, Ella, and John G. Doench. 2015. “Genetic Screens and Functional Genomics Using CRISPR/Cas9 Technology.” *FEBS Journal* 282 (8): 1383-93.

<https://doi.org/10.1111/febs.13248>.

Hartmann, Jan, Ke Hu, Cynthia Y. He, Laurence Pelletier, David S. Roos, and Graham Warren. 2006. “Golgi and Centrosome Cycles in *Toxoplasma Gondii*.” *Molecular and Biochemical Parasitology* 145 (1): 125-27.

<https://doi.org/10.1016/j.molbiopara.2005.09.015>.

He, Cynthia Y., Michael K. Shaw, Charles H. Pletcher, Boris Striepen, Lewis G. Tilney, and David S. Roos. 2001. “A Plastid Segregation Defect in the Protozoan Parasite *Toxoplasma Gondii*.” *EMBO Journal* 20 (3): 330-39.

<https://doi.org/10.1093/emboj/20.3.330>.

Heaslip, Aoife T., Shane R. Nelson, and David M. Warshaw. 2016. “Dense Granule Trafficking in *Toxoplasma Gondii* Requires a Unique Class 27 Myosin and Actin Filaments.” *Molecular Biology of the Cell* 27 (13): 2080-89.

<https://doi.org/10.1091/mbc.e15-12-0824>.

Hehl, Adrian B., Christine Lekutis, Michael E. Grigg, Peter J. Bradley, Jean François Dubremetz, Eduardo Ortega-Barria, and John C. Boothroyd. 2000. “*Toxoplasma Gondii* Homologue of *Plasmodium* Apical Membrane Antigen 1

Is Involved in Invasion of Host Cells.” *Infection and Immunity* 68 (12): 7078-86. <https://doi.org/10.1128/IAI.68.12.7078-7086.2000>.

Herm-Götz, Angelika, Carolina Agop-Nersesian, Sylvia Münter, Joshua S. Grimley, Thomas J. Wandless, Friedrich Frischknecht, and Markus Meissner. 2007. “Rapid Control of Protein Level in the Apicomplexan *Toxoplasma Gondii*.” *Nature Methods* 4 (12): 1003-5. <https://doi.org/10.1038/nmeth1134>.

Herm-Götz, Angelika, Stefan Weiss, Rolf Stratmann, Setsuko Fujita-Becker, Christine Ruff, Edgar Meyhöfer, Thierry Soldati, Dietmar J. Manstein, Michael A. Geeves, and Dominique Soldati. 2002. “*Toxoplasma Gondii* Myosin A and Its Light Chain: A Fast, Single-Headed, plus-End-Directed Motor.” *EMBO Journal* 21 (9): 2149-58. <https://doi.org/10.1093/emboj/21.9.2149>.

Hu, Ke, Jeff Johnson, Laurence Florens, Martin Fraunholz, Sapna Suravajjala, Camille DiLullo, John Yates, David S. Roos, and John M. Murray. 2006. “Cytoskeletal Components of an Invasion Machine - the Apical Complex of *Toxoplasma Gondii*.” *PLoS Pathogens* 2 (2): e13. <https://doi.org/10.1371/journal.ppat.0020013>.

Hu, Ke, Tara Mann, Boris Striepen, Con J.M. Beckers, David S. Roos, and John M. Murray. 2002. “Daughter Cell Assembly in the Protozoan Parasite *Toxoplasma Gondii*.” *Molecular Biology of the Cell* 13 (2): 593-606. <https://doi.org/10.1091/mbc.01-06-0309>.

Hu, Ke, David S. Roos, and John M. Murray. 2002. “A Novel Polymer of Tubulin Forms the Conoid of *Toxoplasma Gondii*.” *Journal of Cell Biology* 156 (6): 1039-50. <https://doi.org/10.1083/jcb.200112086>.

Hunt, Alex, Matthew Robert Geoffrey Russell, Jeanette Wagener, Robyn Kent, Romain Carmeille, Christopher J. Peddie, Lucy Collinson, Aoife Heaslip, Gary E. Ward, and Moritz Treeck. 2019. “Differential Requirements for Cyclase-Associated Protein (CAP) in Actin-Dependent Processes of *Toxoplasma Gondii*.” *ELife* 8: e50598. <https://doi.org/10.7554/elife.50598>.

Hunter, Christopher a., and L. David Sibley. 2012. “Modulation of Innate

Immunity by *Toxoplasma Gondii* Virulence Effectors.” *Nature Reviews Microbiology* 10 (11): 766-78. <https://doi.org/10.1038/nrmicro2858>.

Huynh, My-Hang, and Vern B. Carruthers. 2009. “Tagging of Endogenous Genes in a *Toxoplasma Gondii* Strain Lacking Ku80.” *Eukaryotic Cell* 8 (4): 530-39. <https://doi.org/10.1128/EC.00358-08>.

Huynh, My Hang, and Vern B. Carruthers. 2006. “*Toxoplasma* MIC2 Is a Major Determinant of Invasion and Virulence.” *PLoS Pathogens* 2 (8): e84. <https://doi.org/10.1371/journal.ppat.0020084>.

Ignatev, Alexander, Saligram Prabhakar Bhargav, Juha Vahokoski, Petri Kursula, and Inari Kursula. 2012. “The Lasso Segment Is Required for Functional Dimerization of the Plasmodium Formin 1 FH2 Domain.” *PLoS ONE* 7 (3): e33586. <https://doi.org/10.1371/journal.pone.0033586>.

Ikeda, Sakae, Leslie A. Cunningham, Dawnalyn Boggess, Craig D. Hobson, John P. Sundberg, Jürgen K. Naggert, Richard S. Smith, and Patsy M. Nishina. 2003. “Aberrant Actin Cytoskeleton Leads to Accelerated Proliferation of Corneal Epithelial Cells in Mice Deficient for Destrin (Actin Depolymerizing Factor).” *Human Molecular Genetics* 12 (9): 1029-36. <https://doi.org/10.1093/hmg/ddg112>.

Imamura, Hiroshi, Kazuma Tanaka, Taro Hihara, Masato Umikawa, Takashi Kamei, Kazuo Takahashi, Tomo Sasaki, and Yoshimi Takai. 1997. “Bni1p and Bnr1p: Downstream Targets of the Rho Family Small G-Proteins Which Interact with Profilin and Regulate Actin Cytoskeleton in *Saccharomyces Cerevisiae*.” *EMBO Journal* 16 (10): 2745-55. <https://doi.org/10.1093/emboj/16.10.2745>.

Ingouff, Mathieu, Jonathan N. Fitz Gerald, Christophe Guérin, Hélène Robert, Mikael Blom Sørensen, Daniel Van Damme, Danny Geelen, Laurent Blanchoin, and Frédéric Berger. 2005. “Plant Formin AtFH5 Is an Evolutionarily Conserved Actin Nucleator Involved in Cytokinesis.” *Nature Cell Biology* 7 (4): 374-80. <https://doi.org/10.1038/ncb1238>.

- Ishino, Yoshizumi, Hideo Shinagawa, Kozo Makino, Mitsuko Amemura, and Atsuo Nakata. 1987. "Nucleotide Sequence of the *lap* Gene, Responsible for Alkaline Phosphatase Isozyme Conversion in *Escherichia Coli*, and Identification of the Gene Product." *Journal of Bacteriology* 169 (12): 5429-33. <https://doi.org/10.1128/jb.169.12.5429-5433.1987>.
- Jacot, Damien, Wassim Daher, and Dominique Soldati-Favre. 2013. "Toxoplasma Gondii Myosin F, an Essential Motor for Centrosomes Positioning and Apicoplast Inheritance." *The EMBO Journal* 32 (12): 1702-16. <https://doi.org/10.1038/emboj.2013.113>.
- Jacot, Damien, Nicolò Tosetti, Isa Pires, Jessica Stock, Arnault Graindorge, Yu Fu Hung, Huijong Han, Rita Tewari, Inari Kursula, and Dominique Soldati-Favre. 2016. "An Apicomplexan Actin-Binding Protein Serves as a Connector and Lipid Sensor to Coordinate Motility and Invasion." *Cell Host and Microbe* 20 (6): 731-43. <https://doi.org/10.1016/j.chom.2016.10.020>.
- Janouskovec, Jan, Ales Horák, Miroslav Oborník, Julius Lukes, and Patrick J Keeling. 2010. "A Common Red Algal Origin of the Apicomplexan, Dinoflagellate, and Heterokont Plastids." *Proceedings of the National Academy of Sciences of the United States of America* 107 (24): 10949-54. <https://doi.org/10.1073/pnas.1003335107>.
- Jansen, Ruud, Jan D. A. Van Embden, Wim Gaastra, and Leo M. Schouls. 2002. "Identification of Genes That Are Associated with DNA Repeats in Prokaryotes." *Molecular Microbiology* 43 (6): 1565-75. <https://doi.org/10.1046/j.1365-2958.2002.02839.x>.
- Jiang, Chang, Stephen J. Trudeau, Taek-Chin Cheong, Rui Guo, Mingxiang Teng, Liang Wei Wang, Zhonghao Wang, et al. 2019. "CRISPR/Cas9 Screens Reveal Multiple Layers of B Cell CD40 Regulation." *Cell Reports* 28 (5): 1307-1322.e8. <https://doi.org/10.1016/j.celrep.2019.06.079>.
- Jiang, Fuguo, and Jennifer A. Doudna. 2017. "CRISPR-Cas9 Structures and Mechanisms." *Annual Review of Biophysics* 46: 505-29. <https://doi.org/10.1146/annurev-biophys-062215-010822>.

- Jiang, Fuguo, Kaihong Zhou, Linlin Ma, Saskia Gressel, and Jennifer A. Doudna. 2015. "A Cas9-Guide RNA Complex Preorganized for Target DNA Recognition." *Science* 348 (6242): 1477-81. <https://doi.org/10.1126/science.aab1452>.
- Jiang, Wenyan, David Bikard, David Cox, Feng Zhang, and Luciano A. Marraffini. 2013. "RNA-Guided Editing of Bacterial Genomes Using CRISPR-Cas Systems." *Nature Biotechnology* 31 (3): 233-39. <https://doi.org/10.1038/nbt.2508>.
- Jiménez-Ruiz, Elena, Eleanor H. Wong, Gurman S. Pall, and Markus Meissner. 2014. "Advantages and Disadvantages of Conditional Systems for Characterization of Essential Genes in *Toxoplasma Gondii*." *Parasitology* 141 (11): 1390-98. <https://doi.org/10.1017/S0031182014000559>.
- Jinek, Martin, Krzysztof Chylinski, Ines Fonfara, Michael Hauer, Jennifer A. Doudna, and Emmanuelle Charpentier. 2012. "A Programmable Dual-RNA-Guided DNA Endonuclease in Adaptive Bacterial Immunity." *Science* 337 (6096): 816-21. <https://doi.org/10.1126/science.1225829>.
- Jinek, Martin, Alexandra East, Aaron Cheng, Steven Lin, Enbo Ma, and Jennifer Doudna. 2013. "RNA-Programmed Genome Editing in Human Cells." *ELife* 2: e00471. <https://doi.org/10.7554/eLife.00471>.
- Joiner, Keith A., and David S. Roos. 2002. "Secretory Traffic in the Eukaryotic Parasite *Toxoplasma Gondii*: Less Is More." *Journal of Cell Biology* 157 (4): 557-63. <https://doi.org/10.1083/jcb.200112144>.
- Jomaa, Hassan, Jochen Wiesner, Silke Sanderbrand, Boran Altincicek, Claus Weidemeyer, Martin Hintz, Ivana Türbachova, et al. 1999. "Inhibitors of the Nonmevalonate Pathway of Isoprenoid Biosynthesis as Antimalarial Drugs." *Science* 285 (5433): 1573-76. <https://doi.org/10.1126/science.285.5433.1573>.
- Jullien, Nicolas, Isabelle Goddard, Samia Selmi-Ruby, Jean Luc Fina, Harold Cremer, and Jean Paul Herman. 2007. "Conditional Transgenesis Using

Dimerizable Cre (DiCre).” *PLoS ONE* 2 (12): e1355.
<https://doi.org/10.1371/journal.pone.0001355>.

Jullien, Nicolas, Francois Sampieri, Alain Enjalbert, and Jean-Paul Herman. 2003. “Regulation of Cre Recombinase by Ligand-Induced Complementation of Inactive Fragments.” *Nucleic Acids Research* 31 (21): e131.
<https://doi.org/10.1093/nar/gng131>.

Kabsch, Wolfgang, Hans Georg Mannherz, Dietrich Suck, Emil F Pai, and Kenneth C Holmes. 1990. “Atomic Structure of the Actin: DNase I Complex.” *Nature* 347: 37-44. <https://doi.org/10.1038/347037a0>.

Kafsack, Björn F. C., Janethe D. O. Pena, Isabelle Coppens, Sandeep Ravindran, John C. Boothroyd, and Vern B. Carruthers. 2009. “Rapid Membrane Disruption by a Perforin-Like Protein Facilitates Parasite Exit from Host Cells.” *Reform and Revolt in the City of Dreaming Spires* 323 (5913): 530-33. <https://doi.org/10.1126/science.1165740>.

Kan-o, Meikun, Ryu Takeya, Takaya Abe, Naoyuki Kitajima, Motohiro Nishida, Ryuji Tominaga, Hitoshi Kurose, and Hideki Sumimoto. 2012. “Mammalian Formin Fhod3 Plays an Essential Role in Cardiogenesis by Organizing Myofibrillogenesis.” *Biology Open* 1: 889-96.
<https://doi.org/10.1242/bio.20121370>.

Kanellos, Georgios, Jing Zhou, Hitesh Patel, Rachel A. Ridgway, David Huels, Christine B. Gurniak, Emma Sandilands, et al. 2015. “ADF and Cofilin1 Control Actin Stress Fibers, Nuclear Integrity, and Cell Survival.” *Cell Reports* 13: 1949-64. <https://doi.org/10.1016/j.celrep.2015.10.056>.

Katris, Nicholas J., Giel G. van Dooren, Paul J. McMillan, Eric Hanssen, Leann Tilley, and Ross F. Waller. 2014. “The Apical Complex Provides a Regulated Gateway for Secretion of Invasion Factors in Toxoplasma.” *PLoS Pathogens* 10 (4): e1004074. <https://doi.org/10.1371/journal.ppat.1004074>.

Kennedy, Kit, Simon A. Cobbold, Eric Hanssen, Jakob Birnbaum, Natalie J. Spillman, Emma McHugh, Hannah Brown, et al. 2019. “Delayed Death in the

Malaria Parasite Plasmodium Falciparum Is Caused by Disruption of Prenylation-Dependent Intracellular Trafficking.” *PLOS Biology* 17 (7): e3000376. <https://doi.org/10.1371/journal.pbio.3000376>.

- Kim, Kami, and John C. Boothroyd. 1995. “Toxoplasma Gondii: Stable Complementation of Sag1 (P30) Mutants Using SAG1 Transfection and Fluorescence-Activated Cell Sorting.” *Experimental Parasitology* 80 (1): 46-53. <https://doi.org/10.1006/expr.1995.1006>.
- Kissinger, Jessica C., Bindu Gajria, Li Li, Ian T. Paulsen, and David S. Roos. 2003. “ToxoDB: Accessing the Toxoplasma Gondii Genome.” *Nucleic Acids Research* 31 (1): 234-36. <https://doi.org/10.1093/nar/gkg072>.
- Kohler, S., S Köhler, C F Delwiche, P W Denny, L G Tilney, P Webster, R J Wilson, J D Palmer, and D S Roos. 1997. “A Plastid of Probable Green Algal Origin in Apicomplexan Parasites.” *Science* 275 (5305): 1485-89. <https://doi.org/10.1126/science.275.5305.1485>.
- Koike-Yusa, Hiroko, Yilong Li, E-Pien Tan, Martin Del Castillo Velasco-Herrera, and Kosuke Yusa. 2014. “Genome-Wide Recessive Genetic Screening in Mammalian Cells with a Lentiviral CRISPR-Guide RNA Library.” *Nature Biotechnology* 32 (3): 267-73. <https://doi.org/10.1038/nbt.2800>.
- Konermann, Silvana, Peter Lotfy, Nicholas J. Brideau, Jennifer Oki, Maxim N. Shokhirev, and Patrick D. Hsu. 2018. “Transcriptome Engineering with RNA-Targeting Type VI-D CRISPR Effectors.” *Cell* 173 (3): 665-676.e14. <https://doi.org/10.1016/j.cell.2018.02.033>.
- Korkmaz, Gozde, Zohar Manber, Rui Lopes, Stefan Prekovic, Karianne Schuurman, Yongsoo Kim, Hans Teunissen, et al. 2019. “A CRISPR-Cas9 Screen Identifies Essential CTCF Anchor Sites for Estrogen Receptor-Driven Breast Cancer Cell Proliferation.” *Nucleic Acids Research* 47 (18): 9557-72. <https://doi.org/10.1093/nar/gkz675>.
- Korn, Edward D., Marie-France Carlier, and Dominique Pantaloni. 1987. “Actin Polymerization and ATP Hydrolysis.” *Science* 238 (4827): 638-44.

<https://doi.org/10.1126/science.3672117>.

- Kosicki, Michael, Kärt Tomberg, and Allan Bradley. 2018. "Repair of Double-Strand Breaks Induced by CRISPR-Cas9 Leads to Large Deletions and Complex Rearrangements." *Nature Biotechnology* 36 (8): 765-771.
<https://doi.org/10.1038/nbt.4192>.
- Kovar, David R., Elizabeth S. Harris, Rachel Mahaffy, Henry N. Higgs, and Thomas D. Pollard. 2006. "Control of the Assembly of ATP- and ADP-Actin by Formins and Profilin." *Cell* 124: 423-35. <https://doi.org/10.1016/j.cell.2005.11.038>.
- Kreidenweiss, Andrea, Annika V. Hopkins, and Benjamin Mordmüller. 2013. "2A and the Auxin-Based Degron System Facilitate Control of Protein Levels in Plasmodium Falciparum." *PLoS ONE* 8 (11): e78661.
<https://doi.org/10.1371/journal.pone.0078661>.
- Kucera, Kaury, A. Alicia Koblansky, Lauren P. Saunders, Kendra B. Frederick, Enrique M. De La Cruz, Sankar Ghosh, and Yorgo Modis. 2010. "Structure-Based Analysis of Toxoplasma Gondii Profilin: A Parasite-Specific Motif Is Required for Recognition by Toll-Like Receptor 11." *Journal of Molecular Biology* 403 (4): 616-29. <https://doi.org/10.1016/j.jmb.2010.09.022>.
- Kumar, Bijay, Sushma Chaubey, Priyanka Shah, Aiman Tanveer, Manish Charan, Mohammad Imran Siddiqi, and Saman Habib. 2011. "Interaction between Sulphur Mobilisation Proteins SufB and SufC: Evidence for an Iron-Sulphur Cluster Biogenesis Pathway in the Apicoplast of Plasmodium Falciparum." *International Journal for Parasitology* 41 (9): 991-99.
<https://doi.org/10.1016/j.ijpara.2011.05.006>.
- Kumpula, Esa-Pekka, Andrea J. Lopez, Leila Tajedin, Huijong Han, and Inari Kursula. 2019. "Atomic View into Plasmodium Actin Polymerization, ATP Hydrolysis, and Fragmentation." *PLOS Biology* 17 (6): e3000315.
<https://doi.org/10.1371/journal.pbio.3000315>.
- Kumpula, Esa-Pekka, Isa Pires, Devaki Lasiwa, Henni Piirainen, Ulrich Bergmann, Juha Vahokoski, and Inari Kursula. 2017. "Apicomplexan Actin

Polymerization Depends on Nucleation.” *Scientific Reports* 7: 12137.
<https://doi.org/10.1038/s41598-017-11330-w>.

Lacombe, Alice, Andrew E. Maclean, Jana Ovciarikova, Julie Tottey, Alexander Mühleip, Paula Fernandes, and Lilach Sheiner. 2019. “Identification of the *Toxoplasma Gondii* Mitochondrial Ribosome, and Characterisation of a Protein Essential for Mitochondrial Translation.” *Molecular Microbiology* 112 (4): 1235-52. <https://doi.org/10.1111/mmi.14357>.

Lamarque, Mauld, Sébastien Besteiro, Julien Papoin, Magali Roques, Brigitte Vulliez-Le Normand, Juliette Morlon-Guyot, Jean François Dubremetz, et al. 2011. “The RON2-AMA1 Interaction Is a Critical Step in Moving Junction-Dependent Invasion by Apicomplexan Parasites.” *PLoS Pathogens* 7 (2): e1001276. <https://doi.org/10.1371/journal.ppat.1001276>.

Lamarque, Mauld H., Magali Roques, Marie Kong-Hap, Michelle L. Tonkin, George Rugarabamu, Jean Baptiste Marq, Diana M. Penarete-Vargas, Martin J. Boulanger, Dominique Soldati-Favre, and Maryse Lebrun. 2014. “Plasticity and Redundancy among AMA-RON Pairs Ensure Host Cell Entry of *Toxoplasma* Parasites.” *Nature Communications* 5: 4098.
<https://doi.org/10.1038/ncomms5098>.

Lander, Noelia, and Miguel A. Chiurillo. 2019. “State-of-the-Art CRISPR/Cas9 Technology for Genome Editing in Trypanosomatids.” *Journal of Eukaryotic Microbiology* 66 (6): 981-91. <https://doi.org/10.1111/jeu.12747>.

Lappalainen, Pekka, and David G Drubin. 1997. “Cofilin Promotes Rapid Actin Filament Turnover in Vivo.” *Nature* 388: 78-82.
<https://doi.org/10.1038/40418>.

Lekutis, C, D J Ferguson, M E Grigg, M Camps, and J C Boothroyd. 2001. “Surface Antigens of *Toxoplasma Gondii*: Variations on a Theme.” *International Journal for Parasitology* 31: 1285-92. [https://doi.org/10.1016/S0020-7519\(01\)00261-2](https://doi.org/10.1016/S0020-7519(01)00261-2).

Leung, Jacqueline M., Mark A. Rould, Christoph Konradt, Christopher A. Hunter,

and Gary E. Ward. 2014. "Disruption of TgPHIL1 Alters Specific Parameters of *Toxoplasma Gondii* Motility Measured in a Quantitative, Three-Dimensional Live Motility Assay." *PLoS ONE* 9 (1): e85763. <https://doi.org/10.1371/journal.pone.0085763>.

LEVINE, N. D., J. O. CORLISS, F. E.G. COX, G. DEROUX, J. GRAIN, B. M. HONIGBERG, G. F. LEEDALE, et al. 1980. "A Newly Revised Classification of the Protozoa." *The Journal of Protozoology* 27 (1): 37-58. <https://doi.org/10.1111/j.1550-7408.1980.tb04228.x>.

Leyser, Ottoline. 2018. "Auxin Signaling." *Plant Physiology* 176: 465-79. <https://doi.org/10.1104/pp.17.00765>.

Long, Shaojun, Bryan Anthony, Lisa L. Drewry, and L. David Sibley. 2017. "A Conserved Ankyrin Repeat-Containing Protein Regulates Conoid Stability, Motility and Cell Invasion in *Toxoplasma Gondii*." *Nature Communications* 8: 2236. <https://doi.org/10.1038/s41467-017-02341-2>.

Long, Shaojun, Kevin M. Brown, Lisa L. Drewry, Bryan Anthony, Isabelle Q.H. Phan, and L. David Sibley. 2017. "Calmodulin-like Proteins Localized to the Conoid Regulate Motility and Cell Invasion by *Toxoplasma Gondii*." *PLoS Pathogens* 13 (5): e1006379. <https://doi.org/10.1371/journal.ppat.1006379>.

Lourido, Sebastian, Joel Shuman, Chao Zhang, Kevan M Shokat, Raymond Hui, and L. David Sibley. 2010. "Calcium-Dependent Protein Kinase 1 Is an Essential Regulator of Exocytosis in *Toxoplasma*." *Nature* 465 (7296): 359-62. <https://doi.org/10.1038/nature09022>.

Lourido, Sebastian, Keliang Tang, and L. David Sibley. 2012. "Distinct Signalling Pathways Control *Toxoplasma* Egress and Host-Cell Invasion." *EMBO Journal* 31 (24): 4524-34. <https://doi.org/10.1038/emboj.2012.299>.

Lovett, Jennie L., Norma Marchesini, Silvia N.J. Moreno, and L. David Sibley. 2002. "Toxoplasma Gondii Microneme Secretion Involves Intracellular Ca²⁺ Release from Inositol 1,4,5-Triphosphate (IP₃)/Ryanodine-Sensitive Stores." *Journal of Biological Chemistry* 277 (29): 25870-76.

<https://doi.org/10.1074/jbc.M202553200>.

Luft, Benjamin J., and Jack S. Remington. 1992. "Toxoplasmic Encephalitis in AIDS." *Clinical Infectious Diseases* 15 (2): 211-22.

<https://doi.org/10.1093/clinids/15.2.211>.

Machesky, Laura M, Simon J Atkinson, Christophe Ampe, Joel Vandekerckhove, and Thomas D Pollard. 1994. "Purification of a Cortical Complex Containing Two Unconventional Actins from *Acanthamoeba* by Affinity Chromatography on Profilin-Agarose." *Journal of Cell Biology* 127 (1): 107-15.

<https://doi.org/10.1083/jcb.127.1.107>.

Makarova, Kira S., Daniel H. Haft, Rodolphe Barrangou, Stan J. J. Brouns, Emmanuelle Charpentier, Philippe Horvath, Sylvain Moineau, et al. 2011. "Evolution and Classification of the CRISPR-Cas Systems." *Nature Reviews Microbiology* 9 (6): 467-77. <https://doi.org/10.1038/nrmicro2577>.

Makarova, Kira S., Yuri I. Wolf, and Eugene V. Koonin. 2018. "Classification and Nomenclature of CRISPR-Cas Systems: Where from Here?" *The CRISPR Journal* 1 (5): 325-36. <https://doi.org/10.1089/crispr.2018.0033>.

Makkonen, Maarit, Enni Bertling, Natalia A. Chebotareva, Jake Baum, and Pekka Lappalainen. 2013. "Mammalian and Malaria Parasite Cyclase-Associated Proteins Catalyze Nucleotide Exchange on G-Actin through a Conserved Mechanism." *Journal of Biological Chemistry* 288 (2): 984-94.

<https://doi.org/10.1074/jbc.M112.435719>.

Mali, Prashant, Luhan Yang, Kevin M. Esvelt, John Aach, Marc Guell, James E. DiCarlo, Julie E. Norville, and George M. Church. 2013. "RNA-Guided Human Genome Engineering via Cas9." *Science* 339 (6121): 823-26.

<https://doi.org/10.1126/science.1232033>.

Mangeol, P., B. Prevo, and E. J. G. Peterman. 2016. "KymographClear and KymographDirect: Two Tools for the Automated Quantitative Analysis of Molecular and Cellular Dynamics Using Kymographs." *Molecular Biology of the Cell* 27 (12): 1948-57. <https://doi.org/10.1091/mbc.e15-06-0404>.

- Mann, Tara, and Con Beckers. 2001. "Characterization of the Subpellicular Network, a Filamentous Membrane Skeletal Component in the Parasite *Toxoplasma Gondii*." *Molecular & Biochemical Parasitology* 115: 257-68. [https://doi.org/10.1016/S0166-6851\(01\)00289-4](https://doi.org/10.1016/S0166-6851(01)00289-4).
- Markus, Benedikt M., George W. Bell, Hernan A. Lorenzi, and Sebastian Lourido. 2019. "Optimizing Systems for Cas9 Expression in *Toxoplasma Gondii*." *MSphere* 4: e00386-19. <https://doi.org/10.1128/msphere.00386-19>.
- McCoy, James M., Lachlan Whitehead, Giel G. van Dooren, and Christopher J. Tonkin. 2012. "TgCDPK3 Regulates Calcium-Dependent Egress of *Toxoplasma Gondii* from Host Cells." *PLoS Pathogens* 8 (12): e1003066. <https://doi.org/10.1371/journal.ppat.1003066>.
- McFadden, G. I., M. E. Reith, J. Munholland, and N. Lang-Unnasch. 1996. "Plastid in Human Parasites." *Nature* 381 (6582): 482. <https://doi.org/10.1038/381482a0>.
- McFadden, Geoffrey Ian, and Ellen Yeh. 2017. "The Apicoplast: Now You See It, Now You Don't." *International Journal for Parasitology* 47 (2-3): 137-44. <https://doi.org/10.1016/j.ijpara.2016.08.005>.
- Mehta, Simren, and L. David Sibley. 2010. "Toxoplasma Gondii Actin Depolymerizing Factor Acts Primarily to Sequester G-Actin." *Journal of Biological Chemistry* 285 (9): 6835-47. <https://doi.org/10.1074/jbc.M109.068155>.
- Mehta, Simren, and L David Sibley. 2011. "Actin Depolymerizing Factor Controls Actin Turnover and Gliding Motility in *Toxoplasma Gondii*." *Molecular Biology of the Cell* 22 (8): 1290-99. <https://doi.org/10.1091/mbc.E10-12-0939>.
- Meissner, Markus, Manuela S. Breinich, Paul R. Gilson, and Brendan S. Crabb. 2007. "Molecular Genetic Tools in *Toxoplasma* and *Plasmodium*: Achievements and Future Needs." *Current Opinion in Microbiology* 10 (4): 349-56. <https://doi.org/10.1016/j.mib.2007.07.006>.

- Meissner, Markus, Dirk Schlüter, and Dominique Soldati. 2002. "Role of Toxoplasma Gondii Myosin A in Powering Parasite Gliding and Host Cell Invasion." *Science* 298 (5594): 837-40. <https://doi.org/10.1126/science.1074553>.
- Melak, Michael, Matthias Plessner, and Robert Grosse. 2017. "Actin Visualization at a Glance." *Journal of Cell Science* 130: 525-30. <https://doi.org/10.1242/jcs.189068>.
- Mercier, Corinne, and Marie France Cesbron-Delauw. 2015. "Toxoplasma Secretory Granules: One Population or More?" *Trends in Parasitology* 31 (2): 60-71. <https://doi.org/10.1016/j.pt.2014.12.002>.
- Mital, Jeffrey, Markus Meissner, Dominique Soldati, and Gary E Ward. 2005. "Conditional Expression of Toxoplasma Gondii Apical Membrane Antigen-1 (TgAMA1) Demonstrates That TgAMA1 Plays a Critical Role in Host Cell Invasion." *Molecular Biology of the Cell* 16 (9): 4341-49. <https://doi.org/10.1091/mbc.E05-04-0281>.
- Mizuno, Kensaku. 2013. "Signaling Mechanisms and Functional Roles of Cofilin Phosphorylation and Dephosphorylation." *Cellular Signalling* 25 (2): 457-69. <https://doi.org/10.1016/j.cellsig.2012.11.001>.
- Mondragon, R, and E Frixione. 1996. "Ca(2+)-Dependence of Conoid Extrusion in Toxoplasma Gondii Tachyzoites." *The Journal of Eukaryotic Microbiology* 43 (2): 120-27. <https://doi.org/10.1111/j.1550-7408.1996.tb04491.x>.
- Montaville, Pierre, Antoine Jégou, Julien Pernier, Christel Compper, Bérengère Guichard, Binyam Mogessie, Melina Schuh, Guillaume Romet-Lemonne, and Marie-France Carlier. 2014. "Spire and Formin 2 Synergize and Antagonize in Regulating Actin Assembly in Meiosis by a Ping-Pong Mechanism." *PLoS Biology* 12 (2): e1001795. <https://doi.org/10.1371/journal.pbio.1001795>.
- Moon, Anne, and David G. Drubin. 1995. "The ADF/Cofilin Proteins: Stimulus-Responsive Modulators of Actin Dynamics." *Molecular Biology of the Cell* 6: 1423-31. <https://doi.org/10.1091/mbc.6.11.1423>.

- Moore, Robert B., Miroslav Oborník, Jan Janouškovec, Tomáš Chrudimský, Marie Vancová, David H. Green, Simon W. Wright, et al. 2008. "A Photosynthetic Alveolate Closely Related to Apicomplexan Parasites." *Nature* 451 (7181): 959-63. <https://doi.org/10.1038/nature06635>.
- Mordue, Dana G, Naishadh Desai, Michael Dustin, and L David Sibley. 1999. "Invasion by *Toxoplasma Gondii* Establishes a Moving Junction That Selectively Excludes Host Cell Plasma Membrane Proteins on the Basis of Their Membrane Anchoring." *J. Exp. Med* 190 (12): 1783-92. <https://doi.org/10.1084/jem.190.12.1783>.
- Morrisette, Naomi. 2015. "Targeting *Toxoplasma* Tubules: Tubulin, Microtubules, and Associated Proteins in a Human Pathogen." *Eukaryotic Cell* 14: 2-12. <https://doi.org/10.1128/ec.00225-14>.
- Morrisette, Naomi S, and L David Sibley. 2002. "Cytoskeleton of Apicomplexan Parasites." *Microbiology and Molecular Biology Reviews* 66 (1): 21-38. <https://doi.org/10.1128/mnbr.66.1.21-38.2002>.
- Moseley, J. B., Isabelle Sagot, Amity L. Manning, Yingwu Xu, Michael J. Eck, David Pellman, and Bruce L. Goode. 2004. "A Conserved Mechanism for Bni1- and MDia1-Induced Actin Assembly and Dual Regulation of Bni1 by Bud6 and Profilin." *Molecular Biology of the Cell* 15: 896-907. <https://doi.org/10.1091/mbc.e03-08-0621>.
- Moudy, Robin, Timothy J. Manning, and Con J. Beckers. 2001. "The Loss of Cytoplasmic Potassium upon Host Cell Breakdown Triggers Egress of *Toxoplasma Gondii*." *Journal of Biological Chemistry* 276 (44): 41492-501. <https://doi.org/10.1074/jbc.M106154200>.
- Moura, Lenildo De, Lilian Maria Garcia Bahia-Oliveira, Marcelo Y. Wada, Jeffrey L. Jones, Suely H. Tuboi, Eduardo H. Carmo, Walter Massa Ramalho, et al. 2006. "Waterborne Toxoplasmosis, Brazil, from Field to Gene." *Emerging Infectious Diseases* 12 (2): 326-29. <https://doi.org/10.3201/eid1202.041115>.
- Mullins, R. Dyche, John A. Heuser, and Thomas D. Pollard. 1998. "The

Interaction of Arp2/3 Complex with Actin: Nucleation, High Affinity Pointed End Capping, and Formation of Branching Networks of Filaments.”

Proceedings of the National Academy of Sciences of the United States of America 95: 6181-86. <https://doi.org/10.1073/pnas.95.11.6181>.

Mullins, R. D., D. C. Diche, W. F. Stafford, and T. D. Pollard. 1997. “Structure, Subunit Topology, and Actin-Binding Activity of the Arp2/3 Complex from *Acanthamoeba*.” *Journal of Cell Biology* 136 (2): 331-43. <https://doi.org/10.1083/jcb.136.2.331>.

Muniz-Hernández, S., M. González Del Carmen, M. Mondragon, C. Mercier, M. F. Cesbron, S. L. Mondragón-González, S. González, and R. Mondragón. 2011. “Contribution of the Residual Body in the Spatial Organization of *Toxoplasma Gondii* Tachyzoites within the Parasitophorous Vacuole.” *Journal of Biomedicine and Biotechnology* 2011: 473983. <https://doi.org/10.1155/2011/473983>.

Murakami, Kenji, Takuo Yasunaga, Taro Q.P. Noguchi, Yuki Gomibuchi, Kien X. Ngo, Taro Q.P. Uyeda, and Takeyuki Wakabayashi. 2010. “Structural Basis for Actin Assembly, Activation of ATP Hydrolysis, and Delayed Phosphate Release.” *Cell* 143: 275-87. <https://doi.org/10.1016/j.cell.2010.09.034>.

Nagaraj, Viswanathan Arun, Rajavel Arumugam, Nagasuma R. Chandra, Dasari Prasad, Pundi N. Rangarajan, and Govindarajan Padmanaban. 2009. “Localisation of *Plasmodium Falciparum* Uroporphyrinogen III Decarboxylase of the Heme-Biosynthetic Pathway in the Apicoplast and Characterisation of Its Catalytic Properties.” *International Journal for Parasitology* 39 (5): 559-68. <https://doi.org/10.1016/j.ijpara.2008.10.011>.

Nagaraj, Viswanathan Arun, Rajavel Arumugam, Bulusu Gopalakrishnan, Yeleswarapu Sri Jyothsna, Pundi N. Rangarajan, and Govindarajan Padmanaban. 2008. “Unique Properties of *Plasmodium Falciparum* Porphobilinogen Deaminase.” *Journal of Biological Chemistry* 283 (1): 437-44. <https://doi.org/10.1074/jbc.M706861200>.

Nagy, Andras. 2000. “Cre Recombinase: The Universal Reagent for Genome

Tailoring.” *Genesis* 26 (2): 99-109. [https://doi.org/10.1002/\(SICI\)1526-968X\(200002\)26:2<99::AID-GENE1>3.0.CO;2-B](https://doi.org/10.1002/(SICI)1526-968X(200002)26:2<99::AID-GENE1>3.0.CO;2-B).

Nair, Sethu C., Carrie F. Brooks, Christopher D. Goodman, Angelika Sturm, Geoffrey I. McFadden, Sandeep Sundriyal, Justin L. Anglin, Yongcheng Song, Silvia N.J. Moreno, and Boris Striepen. 2011. “Apicoplast Isoprenoid Precursor Synthesis and the Molecular Basis of Fosmidomycin Resistance in *Toxoplasma Gondii*.” *The Journal of Experimental Medicine* 208 (7): 1547-59. <https://doi.org/10.1084/jem.201100392095c>.

Nichols, Barbara A., Mary Louise Chiappino, and G. Richard O’Connor. 1983. “Secretion from the Rhoptries of *Toxoplasma Gondii* during Host-Cell Invasion.” *Journal of Ultrastructure Research* 83 (1): 85-98. [https://doi.org/10.1016/S0022-5320\(83\)90067-9](https://doi.org/10.1016/S0022-5320(83)90067-9).

Nichols, Barbara A, and Mary Louise Chiappino. 1987. “Cytoskeleton of *Toxoplasma Gondii*.” *The Journal of Protozoology* 34 (2): 217-26. <http://www.ncbi.nlm.nih.gov/pubmed/3585817>.

Nihongaki, Yuta, Fuun Kawano, Takahiro Nakajima, and Moritoshi Sato. 2015. “Photoactivatable CRISPR-Cas9 for Optogenetic Genome Editing.” *Nature Biotechnology* 33: 755-760. <https://doi.org/10.1038/nbt.3245>.

Nishi, M., K. Hu, J. M. Murray, and D. S. Roos. 2008. “Organellar Dynamics during the Cell Cycle of *Toxoplasma Gondii*.” *Journal of Cell Science* 121 (9): 1559-68. <https://doi.org/10.1242/jcs.021089>.

Nishida, Eisuke, Shohei Maekawa, and Hikoichi Sakai. 1984. “Cofilin, a Protein in Porcine Brain That Binds to Actin Filaments and Inhibits Their Interactions with Myosin and Tropomyosin.” *Biochemistry* 23: 5307-13. <https://doi.org/10.1021/bi00317a032>.

Nishimura, Kohei, Tatsuo Fukagawa, Haruhiko Takisawa, Tatsuo Kakimoto, and Masato Kanemaki. 2009. “An Auxin-Based Degron System for the Rapid Depletion of Proteins in Nonplant Cells.” *Nature Methods* 6 (12): 917-22. <https://doi.org/10.1038/nmeth.1401>.

- Niwa, Ryusuke, Kyoko Nagata-Ohashi, Masatoshi Takeichi, Kensaku Mizuno, and Tadashi Uemura. 2002. "Control of Actin Reorganization by Slingshot, a Family of Phosphatases That Dephosphorylate ADF/Cofilin." *Cell* 108 (2): 233-46. [https://doi.org/10.1016/S0092-8674\(01\)00638-9](https://doi.org/10.1016/S0092-8674(01)00638-9).
- O'Connell, Mitchell R., Benjamin L. Oakes, Samuel H Sternberg, Alexandra East-Seletsky, Matias Kaplan, and Jennifer A. Doudna. 2014. "Programmable RNA Recognition and Cleavage by CRISPR/Cas9." *Nature* 516: 263-66. <https://doi.org/10.1038/nature13769>.
- Olshina, Maya A., Hella Baumann, Keith R. Willison, and Jake Baum. 2016. "Plasmodium Actin Is Incompletely Folded by Heterologous Protein-Folding Machinery and Likely Requires the Native Plasmodium Chaperonin Complex to Enter a Mature Functional State." *FASEB Journal* 30 (1): 405-16. <https://doi.org/10.1096/fj.15-276618>.
- Otomo, Takanori, Diana R Tomchick, Chinatsu Otomo, Sanjay C Panchal, Mischa Machius, and Michael K Rosen. 2005. "Structural Basis of Actin Filament Nucleation and Processive Capping by a Formin Homology 2 Domain." *Nature* 433 (7025): 488-94. <https://doi.org/10.1038/nature03251>.
- Otterbein, L. R., P. Graceffa, and R. Dominguez. 2001. "The Crystal Structure of Uncomplexed Actin in the ADP State." *Science* 293 (5530): 708-11. <https://doi.org/10.1126/science.1059700>.
- Ouologuem, Dinkorma T., and David S. Roos. 2014. "Dynamics of the Toxoplasma Gondii Inner Membrane Complex." *Journal of Cell Science* 127: 3320-30. <https://doi.org/10.1242/jcs.147736>.
- Overbeek, Megan van, Daniel Capurso, Matthew M. Carter, Matthew S. Thompson, Elizabeth Frias, Carsten Russ, John S. Reece-Hoyes, et al. 2016. "DNA Repair Profiling Reveals Nonrandom Outcomes at Cas9-Mediated Breaks." *Molecular Cell* 63 (4): 633-46. <https://doi.org/10.1016/j.molcel.2016.06.037>.
- Paing, May M., and Niraj H. Tolia. 2014. "Multimeric Assembly of Host-Pathogen

- Adhesion Complexes Involved in Apicomplexan Invasion.” *PLoS Pathogens* 10 (6): e1004120. <https://doi.org/10.1371/journal.ppat.1004120>.
- Pantaloni, Dominique, and Marie-France Carlier. 1993. “How Profilin Promotes Actin Filament Assembly in the Presence of Thymosin B4.” *Cell* 75: 1007-14. [https://doi.org/10.1016/0092-8674\(93\)90544-Z](https://doi.org/10.1016/0092-8674(93)90544-Z).
- Panza, P., J. Maier, C. Schmees, U. Rothbauer, and C. Sollner. 2015. “Live Imaging of Endogenous Protein Dynamics in Zebrafish Using Chromobodies.” *Development* 142 (10): 1879-84. <https://doi.org/10.1242/dev.118943>.
- Paul, Aditya S., and Thomas D. Pollard. 2009. “Review of the Mechanism of Processive Actin Filament Elongation by Formins.” *Cell Motility and the Cytoskeleton* 66 (8): 606-17. <https://doi.org/10.1002/cm.20379>.
- Peng, Duo, and Rick Tarleton. 2015. “EuPaGDT: A Web Tool Tailored to Design CRISPR Guide RNAs for Eukaryotic Pathogens.” *Microbial Genomics* 1 (4): e000033. <https://doi.org/10.1099/mgen.0.000033>.
- Periz, Javier, Mario Del Rosario, Alexandra McStea, Simon Gras, Colin Loney, Lin Wang, Marisa L. Martin-Fernandez, and Markus Meissner. 2019. “A Highly Dynamic F-Actin Network Regulates Transport and Recycling of Micronemes in *Toxoplasma Gondii* Vacuoles.” *Nature Communications* 10: 4183. <https://doi.org/10.1038/s41467-019-12136-2>.
- Periz, Javier, Jamie Whitelaw, Clare Harding, Simon Gras, Mario Igor Del Rosario Minina, Fernanda Latorre-Barragan, Leandro Lemgruber, et al. 2017. “*Toxoplasma Gondii* F-Actin Forms an Extensive Filamentous Network Required for Material Exchange and Parasite Maturation.” *ELife* 6: e24119. <https://doi.org/10.7554/eLife.24119>.
- Philip, Nisha, and Andrew P. Waters. 2015. “Conditional Degradation of *Plasmodium* Calcineurin Reveals Functions in Parasite Colonization of Both Host and Vector.” *Cell Host and Microbe* 18 (1): 122-31. <https://doi.org/10.1016/j.chom.2015.05.018>.

- Pino, Paco, Sarah Sebastian, Eunbin Arin Kim, Erin Bush, Mathieu Brochet, Katrin Volkmann, Elyse Kozlowski, Manuel Llinás, Oliver Billker, and Dominique Soldati-Favre. 2012. "A Tetracycline-Repressible Transactivator System to Study Essential Genes in Malaria Parasites." *Cell Host and Microbe* 12 (6): 824-34. <https://doi.org/10.1016/j.chom.2012.10.016>.
- Plattner, Fabienne, Felix Yarovinsky, Stephane Romero, Dominique Didry, Marie France Carlier, Alan Sher, and Dominique Soldati-Favre. 2008. "Toxoplasma Profilin Is Essential for Host Cell Invasion and TLR11-Dependent Induction of an Interleukin-12 Response." *Cell Host and Microbe* 3 (2): 77-87. <https://doi.org/10.1016/j.chom.2008.01.001>.
- Plessner, Matthias, Michael Melak, Pilar Chinchilla, Christian Baarlink, and Robert Grosse. 2015. "Nuclear F-Actin Formation and Reorganization upon Cell Spreading." *Journal of Biological Chemistry* 290 (18): 11209-16. <https://doi.org/10.1074/jbc.M114.627166>.
- Pollard, Thomas D. 2007. "Regulation of Actin Filament Assembly by Arp2/3 Complex and Formins." *Annual Review of Biophysics and Biomolecular Structure* 36: 451-77. <https://doi.org/10.1146/annurev.biophys.35.040405.101936>.
- Pollard, Thomas D. 2016. "Actin and Actin-Binding Proteins." *Cold Spring Harbor Perspectives in Biology* 8 (8): a018226. <https://doi.org/10.1101/cshperspect.a018226>.
- Pollard, Thomas D., and Christopher C. Beltzner. 2002. "Structure and Function of the Arp2/3 Complex." *Current Opinion in Structural Biology* 12 (6): 768-74. [https://doi.org/10.1016/S0959-440X\(02\)00396-2](https://doi.org/10.1016/S0959-440X(02)00396-2).
- Pollard, Thomas D., and Gary G. Borisy. 2003. "Cellular Motility Driven by Assembly and Disassembly of Actin Filaments." *Cell* 112: 453-65. [https://doi.org/10.1016/S0092-8674\(03\)00120-X](https://doi.org/10.1016/S0092-8674(03)00120-X).
- Pollard, Thomas D. 1984. "Polymerization of ADP-Actin." *Journal of Cell Biology* 99 (3): 769-77. <https://doi.org/10.1083/jcb.99.3.769>.

- Pollard, Thomas D, Laurent Blanchoin, and R Dyche Mullins. 2000. "Molecular Mechanisms Controlling Actin Filament Dynamics in Nonmuscle Cells." *Annual Review of Biophysics and Biomolecular Structure* 29: 545-76.
<https://doi.org/10.1146/annurev.biophys.29.1.545>.
- Pollard, Thomas D, and John A Cooper. 2009. "Actin, a Central Player in Cell Shape and Movement." *Science* 326 (5957): 1208-12.
<https://doi.org/10.1126/science.1175862>.
- Pospich, Sabrina, Esa-Pekka Kumpula, Julian von der Ecken, Juha Vahokoski, Inari Kursula, and Stefan Raunser. 2017. "Near-Atomic Structure of Jasplakinolide-Stabilized Malaria Parasite F-Actin Reveals the Structural Basis of Filament Instability." *Proceedings of the National Academy of Sciences of the United States of America* 114 (40): 10636-41.
<https://doi.org/10.1073/pnas.1707506114>.
- Pring, Martin, Marie Evangelista, Charles Boone, Changsong Yang, and Sally H. Zigmond. 2003. "Mechanism of Formin-Induced Nucleation of Actin Filaments." *Biochemistry* 42 (2): 486-96.
<https://doi.org/10.1021/bi026520j>.
- Pruyne, David, Marie Evangelista, Changsong Yang, Erfei Bi, Sally Zigmond, Anthony Bretscher, and Charles Boone. 2002. "Role of Formins in Actin Assembly: Nucleation and Barbed-End Association." *Science* 297 (5581): 612-15. <https://doi.org/10.1126/science.1072309>.
- Pszenny, Viviana, Karen Ehrenman, Julia D. Romano, Andrea Kennard, Aric Schultz, David S. Roos, Michael E. Grigg, Vern B. Carruthers, and Isabelle Coppens. 2016. "A Lipolytic Lecithin:Cholesterol Acyltransferase Secreted by Toxoplasma Facilitates Parasite Replication and Egress." *Journal of Biological Chemistry* 291 (8): 3725-46.
<https://doi.org/10.1074/jbc.M115.671974>.
- Quinlan, Margot E., John E. Heuser, Eugen Kerkhoff, and R. Dyche Mullins. 2005. "Drosophila Spire Is an Actin Nucleation Factor." *Nature* 433 (7024): 382-88.
<https://doi.org/10.1038/nature03241>.

- Quinlan, Margot E., Susanne Hilgert, Anaid Bedrossian, R. Dyché Mullins, and Eugen Kerkhoff. 2007. "Regulatory Interactions between Two Actin Nucleators, Spire and Cappuccino." *Journal of Cell Biology* 179 (1): 117-28. <https://doi.org/10.1083/jcb.200706196>.
- Radke, Jay R, Michael N Guerini, Maria Jerome, and Michael W White. 2003. "A Change in the Premitotic Period of the Cell Cycle Is Associated with Bradyzoite Differentiation in *Toxoplasma Gondii*." *Molecular and Biochemical Parasitology* 131 (2): 119-27. [https://doi.org/10.1016/S0166-6851\(03\)00198-1](https://doi.org/10.1016/S0166-6851(03)00198-1).
- Ramakrishnan, Srinivasan, Melissa D. Docampo, James I. MacRae, François M. Pujol, Carrie F. Brooks, Giel G. Van Dooren, J. Kalervo Hiltunen, Alexander J. Kastaniotis, Malcolm J. McConville, and Boris Striepen. 2012. "Apicoplast and Endoplasmic Reticulum Cooperate in Fatty Acid Biosynthesis in Apicomplexan Parasite *Toxoplasma Gondii*." *Journal of Biological Chemistry* 287 (7): 4957-71. <https://doi.org/10.1074/jbc.M111.310144>.
- Riedl, Julia, Alvaro H. Crevenna, Kai Kessenbrock, Jerry Haochen Yu, Dorothee Neukirchen, Michal Bista, Frank Bradke, et al. 2008. "Lifeact: A Versatile Marker to Visualize F-Actin." *Nature Methods* 5 (7): 605-7. <https://doi.org/10.1038/nmeth.1220>.
- Rivers, J. P., A. J. Sinclair, and M. A. Crawford. 1975. "Inability of the Cat to Desaturate Essential Fatty Acids." *Nature* 258: 171-73. <https://doi.org/10.1038/258171a0>.
- Robert-Gangneux, Florence, and Marie-Laure Dardé. 2012. "Epidemiology of and Diagnostic Strategies for Toxoplasmosis." *Clinical Microbiology Reviews* 25 (2): 264-96. <https://doi.org/10.1128/CMR.05013-11>.
- Rocchetti, Alessandra, Chris Hawes, and Verena Kriechbaumer. 2014. "Fluorescent Labelling of the Actin Cytoskeleton in Plants Using a Cameloid Antibody." *Plant Methods* 10 (1): 12. <https://doi.org/10.1186/1746-4811-10-12>.

- Romero, Stéphane, Christophe Le Clainche, Dominique Didry, Coumaran Egile, Dominique Pantaloni, and Marie-France Carlier. 2004. "Formin Is a Processive Motor That Requires Profilin to Accelerate Actin Assembly and Associated ATP Hydrolysis." *Cell* 119: 419-29. <https://doi.org/10.1016/j.cell.2004.09.039>.
- Roos, David S., and Maria E. Fichera. 1997. "A Plastid Organelle as a Drug Target in Apicomplexan Parasites." *Nature* 390 (6658): 407-9. <https://doi.org/10.1038/37132>.
- Rosario, Mario Del, Javier Periz, Georgios Pavlou, Oliver Lyth, Fernanda Latorre-Barragan, Sujaan Das, Gurman S. Pall, et al. 2019. "Apicomplexan F-Actin Is Required for Efficient Nuclear Entry during Host Cell Invasion." *EMBO Reports*, e48896. <https://doi.org/10.15252/embr.201948896>.
- Rouiller, Isabelle, Xiao-Ping Xu, Kurt J. Amann, Coumaran Egile, Stephan Nickell, Daniela Nicastro, Rong Li, Thomas D. Pollard, Niels Volkmann, and Dorit Hanein. 2008. "The Structural Basis of Actin Filament Branching by the Arp2/3 Complex." *Journal of Cell Biology* 180 (5): 887-95. <https://doi.org/10.1083/jcb.200709092>.
- Ruggiero, Michael A., Dennis P. Gordon, Thomas M. Orrell, Nicolas Bailly, Thierry Bourgoin, Richard C. Brusca, Thomas Cavalier-Smith, Michael D. Guiry, and Paul M. Kirk. 2015. "A Higher Level Classification of All Living Organisms." *PLoS ONE* 10 (4): e0119248. <https://doi.org/10.1371/journal.pone.0119248>.
- Sagot, Isabelle, Saskia K. Klee, and David Pellman. 2002. "Yeast Formins Regulate Cell Polarity by Controlling the Assembly of Actin Cables." *Nature Cell Biology* 4: 42-50. <https://doi.org/10.1038/nc719>.
- Sagot, Isabelle, Avital A. Rodal, James Moseley, Bruce L. Goode, and David Pellman. 2002. "An Actin Nucleation Mechanism Mediated by Bni1 and Profilin." *Nature Cell Biology* 4: 626-31. <https://doi.org/10.1038/ncb834>.
- Sahoo, Nivedita, Wandy Beatty, John Heuser, David Sept, and L. David Sibley. 2006. "Unusual Kinetic and Structural Properties Control Rapid Assembly and

Turnover of Actin in the Parasite *Toxoplasma Gondii*.” *Molecular Biology of the Cell* 17: 895-906. <https://doi.org/10.1091/mbc.e05-06-0512>.

Sapranaukas, Rimantas, Giedrius Gasiunas, Christophe Fremaux, Rodolphe Barrangou, Philippe Horvath, and Virginijus Siksnys. 2011. “The *Streptococcus Thermophilus* CRISPR/Cas System Provides Immunity in *Escherichia Coli*.” *Nucleic Acids Research* 39 (21): 9275-82. <https://doi.org/10.1093/nar/gkr606>.

Sato, Shigeharu, Barbara Clough, Leighton Coates, and R. J.M. Wilson. 2004. “Enzymes for Heme Biosynthesis Are Found in Both the Mitochondrion and Plastid of the Malaria Parasite *Plasmodium Falciparum*.” *Protist* 155 (1): 117-25. <https://doi.org/10.1078/1434461000169>.

Schindelin, Johannes, Ignacio Arganda-Carreras, Erwin Frise, Verena Kaynig, Mark Longair, Tobias Pietzsch, Stephan Preibisch, et al. 2012. “Fiji: An Open-Source Platform for Biological-Image Analysis.” *Nature Methods* 9 (7): 676-82. <https://doi.org/10.1038/nmeth.2019>.

Schmelas, Carolin, and Dirk Grimm. 2018. “Split Cas9, Not Hairs – Advancing the Therapeutic Index of CRISPR Technology.” *Biotechnology Journal* 13 (9): e1700432. <https://doi.org/10.1002/biot.201700432>.

Schmitz, Stephan, Munira Grainger, Steven Howell, Lesley J. Calder, Martina Gaeb, Jennifer C. Pinder, Anthony A. Holder, and Claudia Veigel. 2005. “Malaria Parasite Actin Filaments Are Very Short.” *Journal of Molecular Biology* 349: 113-25. <https://doi.org/10.1016/j.jmb.2005.03.056>.

Schneider, C. A., W. S. Rasband, and K. W. Eliceiri. 2012. “NIH Image to ImageJ: 25 Years of Image Analysis HHS Public Access.” *Nature Methods* 9 (7): 671-75. <https://doi.org/10.1038/nmeth.2089>.

Schüler, Herwig, Ann-Kristin Mueller, and Kai Matuschewski. 2005. “Unusual Properties of *Plasmodium Falciparum* Actin: New Insights into Microfilament Dynamics of Apicomplexan Parasites.” *FEBS Letters* 579: 655-60. <https://doi.org/10.1016/j.febslet.2004.12.037>.

- Schultz, Aric J., and Vern B. Carruthers. 2018. "Toxoplasma Gondii LCAT Primarily Contributes to Tachyzoite Egress." *MSphere* 3: e00073-18. <https://doi.org/10.1128/mspheredirect.00073-18>.
- Schwab, J. C., C. J. Beckers, and K. A. Joiner. 1994. "The Parasitophorous Vacuole Membrane Surrounding Intracellular Toxoplasma Gondii Functions as a Molecular Sieve." *Proceedings of the National Academy of Sciences of the United States of America* 91 (2): 509-13. <https://doi.org/10.1073/pnas.91.2.509>.
- Selden, Lynn A., Henry J. Kinosian, James E. Estes, and Lewis C. Gershman. 1999. "Impact of Profilin on Actin-Bound Nucleotide Exchange and Actin Polymerization Dynamics." *Biochemistry* 38 (9): 2769-78. <https://doi.org/10.1021/bi981543c>.
- Sept, David, and J. Andrew McCammon. 2001. "Thermodynamics and Kinetics of Actin Filament Nucleation." *Biophysical Journal* 81: 667-74. [https://doi.org/10.1016/S0006-3495\(01\)75731-1](https://doi.org/10.1016/S0006-3495(01)75731-1).
- Serpeloni, Mariana, Elena Jiménez-Ruiz, Newton Medeiros Vidal, Constanze Kroeber, Nicole Andenmatten, Leandro Lemgruber, Patricia Mörking, Gurman S. Pall, Markus Meissner, and Andréa R. Ávila. 2016. "UAP56 Is a Conserved Crucial Component of a Divergent mRNA Export Pathway in Toxoplasma Gondii." *Molecular Microbiology* 102 (4): 672-89. <https://doi.org/10.1111/mmi.13485>.
- Shalem, Ophir, E. Neville Sanjana, Ella Hartenian, Xi Shi, David A. Scott, Tarjei S. Mikkelsen, Dirk Heckl, et al. 2014. "Genome-Scale CRISPR-Cas9 Knockout Screening in Human Cells." *Science* 343 (6166): 84-87. <https://doi.org/10.1126/science.1247005>.
- Sheffield, Harley G, and Marjorie L Melton. 1968. "The Fine Structure and Reproduction of Toxoplasma Gondii." *The Journal of Parasitology* 54 (2): 209-26. <https://doi.org/10.2307/3276925>.
- Sheiner, Lilach, Jessica L. Demerly, Nicole Poulsen, Wandy L. Beatty, Olivier

- Lucas, Michael S. Behnke, Michael W. White, and Boris Striepen. 2011. "A Systematic Screen to Discover and Analyze Apicoplast Proteins Identifies a Conserved and Essential Protein Import Factor." *PLoS Pathogens* 7 (12): e1002392. <https://doi.org/10.1371/journal.ppat.1002392>.
- Shen, Bang, Kevin M. Brown, Tobie D. Lee, and L. David Sibley. 2014. "Efficient Gene Disruption in Diverse Strains of *Toxoplasma Gondii* Using CRISPR/CAS9." *MBio* 5 (3): e01114-14. <https://doi.org/10.1128/mBio.01114-14>.
- Shida, Toshinobu, Juan G Cueva, Zhenjie Xu, Miriam B Goodman, and Maxence V Nachury. 2010. "The Major Alpha-Tubulin K40 Acetyltransferase AlphaTAT1 Promotes Rapid Ciliogenesis and Efficient Mechanosensation." *Proceedings of the National Academy of Sciences of the United States of America* 107 (50): 21517-22. <https://doi.org/10.1073/pnas.1013728107>.
- Sidik, Saima M., Caroline G. Hackett, Fanny Tran, Nicholas J. Westwood, and Sebastian Lourido. 2014. "Efficient Genome Engineering of *Toxoplasma Gondii* Using CRISPR/Cas9." *PLoS ONE* 9 (6): e100450. <https://doi.org/10.1371/journal.pone.0100450>.
- Sidik, Saima M., Diego Huet, Suresh M. Ganesan, My Hang Huynh, Tim Wang, Armiyaw S. Nasamu, Prathapan Thiru, et al. 2016. "A Genome-Wide CRISPR Screen in *Toxoplasma* Identifies Essential Apicomplexan Genes." *Cell* 166 (6): 1423-1435.e12. <https://doi.org/10.1016/j.cell.2016.08.019>.
- Sidik, Saima M, Diego Huet, and Sebastian Lourido. 2018. "CRISPR-Cas9-Based Genome-Wide Screening of *Toxoplasma Gondii*." *Nature Protocols* 13 (1): 307-23. <https://doi.org/10.1038/nprot.2017.131>.
- Sinclair, A. J., J. G. McLean, and E. A. Monger. 1979. "Metabolism of Linoleic Acid in the Cat." *Lipids* 14 (11): 932-36. <https://doi.org/10.1007/BF02533508>.
- Skillman, Kristen M., Wassim Daher, I. Christopher, Dominique Soldati-Favre, and L. David Sibley. 2012. "Toxoplasma Gondii Profilin Acts Primarily to

Sequester G-Actin While Formins Efficiently Nucleate Actin Filament Formation in Vitro.” *Biochemistry* 51 (12): 2486-95.

<https://doi.org/10.1021/bi201704y>.

Skillman, Kristen M., Karthikeyan Diraviyam, Asis Khan, Keliang Tang, David Sept, and L. David Sibley. 2011. “Evolutionarily Divergent, Unstable Filamentous Actin Is Essential for Gliding Motility in Apicomplexan Parasites.” *PLoS Pathogens* 7 (10): e1002280.

<https://doi.org/10.1371/journal.ppat.1002280>.

Skillman, Kristen M, Christopher I Ma, Daved H Fremont, Karthikeyan Diraviyam, John a Cooper, David Sept, and L David Sibley. 2013. “The Unusual Dynamics of Parasite Actin Result from Isodesmic Polymerization.” *Nature Communications* 4: 2285. <https://doi.org/10.1038/ncomms3285>.

Smargon, Aaron A., David B.T. Cox, Neena K. Pyzocha, Kaijie Zheng, Ian M. Slaymaker, Jonathan S. Gootenberg, Omar A. Abudayyeh, et al. 2017. “Cas13b Is a Type VI-B CRISPR-Associated RNA-Guided RNase Differentially Regulated by Accessory Proteins Csx27 and Csx28.” *Molecular Cell* 65 (4): 618-630.e7. <https://doi.org/10.1016/j.molcel.2016.12.023>.

Soosairajah, Juliana, Sankar Maiti, O’Neil Wiggan, Patrick Sarmiere, Nathalie Moussi, Boris Sarcevic, Rashmi Sampath, James R. Bamburg, and Ora Bernard. 2005. “Interplay between Components of a Novel LIM Kinase-Slingshot Phosphatase Complex Regulates Cofilin.” *EMBO Journal* 24 (3): 473-86. <https://doi.org/10.1038/sj.emboj.7600543>.

Speer, C. A., S. Clark, and J. P. Dubey. 1998. “Ultrastructure of the Oocysts , Sporocysts , and Sporozoites of Toxoplasma Gondii.” *The Journal of Parasitology* 84 (3): 505-12. <https://doi.org/10.2307/3284713>.

Sternberg, Samuel H., Sy Redding, Martin Jinek, Eric C. Greene, and Jennifer A. Doudna. 2014. “DNA Interrogation by the CRISPR RNA-Guided Endonuclease Cas9.” *Nature* 507 (7490): 62-67. <https://doi.org/10.1038/nature13011>.

Stortz, Johannes Felix, Mario del Rosario, Mirko Singer, Jonathan M. Wilkes,

Markus Meissner, and Sujaan Das. 2019. "Formin-2 Drives Polymerisation of Actin Filaments Enabling Segregation of Apicoplasts and Cytokinesis in *Plasmodium Falciparum*." *ELife* 8: e49030.

<https://doi.org/10.7554/eLife.49030>.

Striepen, Boris, Michael J. Crawford, Michael K. Shaw, Lewis G. Tilney, Frank Seeber, and David S. Roos. 2000. "The Plastid of *Toxoplasma Gondii* Is Divided by Association with the Centrosomes." *Journal of Cell Biology* 151 (7): 1423-34. <https://doi.org/10.1083/jcb.151.7.1423>.

Su, C., D. Evans, R. H. Cole, J. C. Kissinger, J. W. Ajioka, and L. D. Sibley. 2003. "Recent Expansion of *Toxoplasma* through Enhanced Oral Transmission." *Science* 299 (5605): 414-16. <https://doi.org/10.1126/science.1078035>.

Suraneni, Praveen, Boris Rubinstein, Jay R. Unruh, Michael Durnin, Dorit Hanein, and Rong Li. 2012. "The Arp2/3 Complex Is Required for Lamellipodia Extension and Directional Fibroblast Cell Migration." *Journal of Cell Biology* 197 (2): 239-51. <https://doi.org/10.1083/jcb.201112113>.

Suss-Toby, E, J Zimmerberg, and G E Ward. 1996. "Toxoplasma Invasion: The Parasitophorous Vacuole Is Formed from Host Cell Plasma Membrane and Pinches off via a Fission Pore." *Proceedings of the National Academy of Sciences of the United States of America* 93 (16): 8413-18. <https://doi.org/10.1073/pnas.93.16.8413>.

Suvorova, Elena S., Maria Francia, Boris Striepen, and Michael W. White. 2015. "A Novel Bipartite Centrosome Coordinates the Apicomplexan Cell Cycle." *PLoS Biology* 13 (3): e1002093. <https://doi.org/10.1371/journal.pbio.1002093>.

Tan, E-Pien, Yilong Li, Martin Del Castillo Velasco-Herrera, Kosuke Yusa, and Allan Bradley. 2015. "Off-Target Assessment of CRISPR-Cas9 Guiding RNAs in Human IPS and Mouse ES Cells." *Genesis* 53 (2): 225-36. <https://doi.org/10.1002/dvg.22835>.

Tardieux, Isabelle. 2017. "Actin Nanobodies Uncover the Mystery of Actin

Filament Dynamics in *Toxoplasma Gondii*.” *Trends in Parasitology* 33 (8): 579-81. <https://doi.org/10.1016/j.pt.2017.06.007>.

Teale, William D., Ivan A. Paponov, and Klaus Palme. 2006. “Auxin in Action: Signalling, Transport and the Control of Plant Growth and Development.” *Nature Reviews Molecular Cell Biology* 7: 847-859. <https://doi.org/10.1038/nrm2020>.

Thompson, Morgan E., Ernest G. Heimsath, Timothy J. Gauvin, Henry N. Higgs, and F. Jon Kull. 2013. “FMNL3 FH2-Actin Structure Gives Insight into Formin-Mediated Actin Nucleation and Elongation.” *Nature Structural and Molecular Biology* 20 (1): 111-18. <https://doi.org/10.1038/nsmb.2462>.

Tolliday, Nicola, Lynn VerPlank, and Rong Li. 2002. “Rho1 Directs Formin-Mediated Actin Ring Assembly during Budding Yeast Cytokinesis.” *Current Biology* 12 (21): 1864-70. [https://doi.org/10.1016/S0960-9822\(02\)01238-1](https://doi.org/10.1016/S0960-9822(02)01238-1).

Torrey, E. Fuller, and Robert H. Yolken. 2013. “*Toxoplasma* Oocysts as a Public Health Problem.” *Trends in Parasitology* 29 (8): 380-84. <https://doi.org/10.1016/j.pt.2013.06.001>.

Tosetti, Nicolò, Nicolas Dos Santos Pacheco, Dominique Soldati-Favre, and Damien Jacot. 2019. “Three F-Actin Assembly Centers Regulate Organelle Inheritance, Cell-Cell Communication and Motility in *Toxoplasma Gondii*.” *ELife* 8: e42669. <https://doi.org/10.7554/elife.42669>.

Tran, Johnson Q., Jessica C. de Leon, Catherine Li, My Hang Huynh, Wandy Beatty, and Naomi S. Morrissette. 2010. “RNG1 Is a Late Marker of the Apical Polar Ring in *Toxoplasma Gondii*.” *Cytoskeleton* 67: 586-98. <https://doi.org/10.1002/cm.20469>.

Truong, Dong Jiunn Jeffery, Karin Kühner, Ralf Kühn, Stanislas Werfel, Stefan Engelhardt, Wolfgang Wurst, and Oskar Ortiz. 2015. “Development of an Intein-Mediated Split-Cas9 System for Gene Therapy.” *Nucleic Acids Research* 43 (13): 6450-58. <https://doi.org/10.1093/nar/gkv601>.

- Tyebji, Shiraz, Simona Seizova, Anthony J. Hannan, and Christopher J. Tonkin. 2019. "Toxoplasmosis: A Pathway to Neuropsychiatric Disorders." *Neuroscience and Biobehavioral Reviews* 96: 72-92. <https://doi.org/10.1016/j.neubiorev.2018.11.012>.
- Ushijima, Tomoki, Noriko Fujimoto, Sho Matsuyama, Meikun Kan-o, Hiroshi Kiyonari, Go Shioi, Yohko Kage, Sho Yamasaki, Ryu Takeya, and Hideki Sumimoto. 2018. "The Actin-Organizing Formin Protein Fhod3 Is Required for Postnatal Development and Functional Maintenance of the Adult Heart in Mice." *Journal of Biological Chemistry* 293 (1): 148-62. <https://doi.org/10.1074/jbc.M117.813931>.
- Vahokoski, Juha, Saligram Prabhakar Bhargav, Ambroise Desfosses, Maria Andreadaki, Esa-Pekka Kumpula, Silvia Muñico Martinez, Alexander Ignatev, et al. 2014. "Structural Differences Explain Diverse Functions of Plasmodium Actins." *PLoS Pathogens* 10 (4): e1004091. <https://doi.org/10.1371/journal.ppat.1004091>.
- Varberg, Joseph M., Leah R. Padgett, Gustavo Arrizabalaga, and William J. Sullivan Jr. 2016. "TgATAT-Mediated-Tubulin Acetylation Is Required for Division of the Protozoan Parasite Toxoplasma Gondii." *MSphere* 1 (1): e00088-15. <https://doi.org/10.1128/mSphere.00088-15>.
- Volkman, Niels, Kurt J. Amann, Svetla Stoilova-McPhie, Coumaran Egile, Dirk C. Winter, Larnele Hazelwood, John E. Heuser, Rong Li, Thomas D. Pollard, and Dorit Hanein. 2001. "Structure of Arp2/3 Complex in Its Activated State and in Actin Filament Branch Junctions." *Science* 293 (5539): 2456-59. <https://doi.org/10.1126/science.1063025>.
- Waller, R F, P J Keeling, R G Donald, B Striepen, E Handman, N Lang-Unnasch, A F Cowman, G S Besra, D S Roos, and G I McFadden. 1998. "Nuclear-Encoded Proteins Target to the Plastid in Toxoplasma Gondii and Plasmodium Falciparum." *Proceedings of the National Academy of Sciences of the United States of America* 95: 12352-57. <https://doi.org/10.1073/pnas.95.21.12352>.

- Waller, Ross F., and Patrick J. Keeling. 2006. "Alveolate and Chlorophycean Mitochondrial Cox2 Genes Split Twice Independently." *Gene* 383: 33-37. <https://doi.org/10.1016/j.gene.2006.07.003>.
- Waller, Ross F, Patrick J Keeling, Giel G van Dooren, and Geoffrey I McFadden. 2003. "Comment on 'A Green Algal Apicophast Ancestor.'" *Science* 301 (5629): 49. <https://doi.org/10.1126/science.1083647>.
- Wang, Fei, Lianrong Wang, Xuan Zou, Suling Duan, Zhiqiang Li, Zixin Deng, Jie Luo, Sang Yup Lee, and Shi Chen. 2019. "Advances in CRISPR-Cas Systems for RNA Targeting, Tracking and Editing." *Biotechnology Advances* 37 (5): 708-29. <https://doi.org/10.1016/j.biotechadv.2019.03.016>.
- Wang, Tim, Jenny J. Wei, David M. Sabatini, and Eric S. Lander. 2014. "Genetic Screens in Human Cells Using the CRISPR-Cas9 System." *Science* 343 (6166): 80-84. <https://doi.org/10.1126/science.1246981>.
- Wasserman, Steven. 1998. "FH Proteins as Cytoskeletal Organizers." *Trends in Cell Biology* 8 (3): 111-15. [https://doi.org/10.1016/S0962-8924\(97\)01217-8](https://doi.org/10.1016/S0962-8924(97)01217-8).
- Watts, Elizabeth, Yihua Zhao, Animesh Dhara, Becca Eller, Abhijit Patwardhan, and Anthony P. Sinai. 2015. "Novel Approaches Reveal That Toxoplasma Gondii Bradyzoites within Tissue Cysts Are Dynamic and Replicating Entities In Vivo." *MBio* 6 (5): e01155-15. <https://doi.org/10.1128/mbio.01155-15>.
- Welch, Matthew D., Angela H. DePace, Suzie Verma, Akihiro Iwamatsu, and Timothy J. Mitchison. 1997. "The Human Arp2/3 Complex Is Composed of Evolutionarily Conserved Subunits and Is Localized to Cellular Regions of Dynamic Actin Filament Assembly." *The Journal of Cell Biology* 138 (2): 375-84. <https://doi.org/10.1083/jcb.138.2.375>.
- Welch, Matthew D., Akihiro Iwamatsu, and Timothy J. Mitchison. 1997. "Actin Polymerization Is Induced by Arp2/3 Protein Complex at the Surface of *Listeria Monocytogenes*." *Nature* 385: 265-69. <https://doi.org/10.1038/385265a0>.

- Werk, R. 1985. "How Does *Toxoplasma Gondii* Enter Host Cells?" *Reviews of Infectious Diseases* 7 (4): 449-57. <https://doi.org/10.1093/clinids/7.4.449>.
- White, Michael W., Jay R. Radke, and Joshua B. Radke. 2014. "Toxoplasma Development - Turn the Switch on or Off?" *Cellular Microbiology* 16 (4): 466-72. <https://doi.org/10.1111/cmi.12267>.
- Whitelaw, Jamie A., Fernanda Latorre-Barragan, Simon Gras, Gurman S. Pall, Jacqueline M. Leung, Aoife Heaslip, Saskia Egarter, et al. 2017. "Surface Attachment, Promoted by the Actomyosin System of *Toxoplasma Gondii* Is Important for Efficient Gliding Motility and Invasion." *BMC Biology* 15 (1). <https://doi.org/10.1186/s12915-016-0343-5>.
- Williamson, Donald H., Malcolm J. Gardner, Peter Preiser, Daphne J. Moore, Kaveri Rangachari, and Robert J M Wilson. 1994. "The Evolutionary Origin of the 35 Kb Circular DNA of *Plasmodium Falciparum*: New Evidence Supports a Possible Rhodophyte Ancestry." *Molecular & General Genetics* 243 (2): 249-52. <https://doi.org/10.1007/BF00280323>.
- Wilson, Iain. 1993. "Plastids Better Red than Dead." *Nature* 366 (6456): 638. <https://doi.org/10.1038/366638a0>.
- Wilson, R. J.M. (Iain), Paul W. Denny, Peter R. Preiser, Kaveri Rangachari, Kate Roberts, Anjana Roy, Andrea Whyte, et al. 1996. "Complete Gene Map of the Plastid-like DNA of the Malaria Parasite *Plasmodium Falciparum*." *Journal of Molecular Biology* 261 (2): 155-72. <https://doi.org/10.1006/jmbi.1996.0449>.
- Wioland, Hugo, Berengere Guichard, Yosuke Senju, Sarah Myram, Pekka Lappalainen, Antoine Jégou, and Guillaume Romet-Lemonne. 2017. "ADF/Cofilin Accelerates Actin Dynamics by Severing Filaments and Promoting Their Depolymerization at Both Ends." *Current Biology* 27: 1956-67. <https://doi.org/10.1016/j.cub.2017.05.048>.
- Woychik, Richard P, Richard L Maas, Rolf Zeller, Thomas F Vogt, and Philip Leder. 1990. "'Formins': Proteins Deduced from the Alternative Transcripts

of the Limb Deformity Gene.” *Nature* 346: 850-53.

<https://doi.org/10.1038/346850a0>.

Wright, Addison V, Samuel H Sternberg, David W Taylor, Brett T Staahl, Jorge A Bardales, Jack E Kornfeld, and Jennifer A Doudna. 2015. “Rational Design of a Split-Cas9 Enzyme Complex.” *Proceedings of the National Academy of Sciences of the United States of America* 112 (10): 2984-89.

<https://doi.org/10.1073/pnas.1501698112>.

Xu, Yingwu, James B. Moseley, Isabelle Sagot, Florence Poy, David Pellman, Bruce L. Goode, and Michael J. Eck. 2004. “Crystal Structures of a Formin Homology-2 Domain Reveal a Tethered Dimer Architecture.” *Cell* 116 (5): 711-23.

[https://doi.org/10.1016/S0092-8674\(04\)00210-7](https://doi.org/10.1016/S0092-8674(04)00210-7).

Yadav, Rahul, Prem Prakash Pathak, Vaibhav Kumar Shukla, Anupam Jain, Shubhra Srivastava, Sarita Tripathi, S.V.S.R. Krishna Pulavarti, Simren Mehta, L. David Sibley, and Ashish Arora. 2011. “Solution Structure and Dynamics of ADF from *Toxoplasma Gondii*.” *Journal of Structural Biology* 176: 97-111.

<https://doi.org/10.1016/j.jsb.2011.07.011>.

Yan, Quanmei, Qunjun Zhang, Huaqiang Yang, Qingjian Zou, Chengcheng Tang, Nana Fan, and Liangxue Lai. 2014. “Generation of Multi-Gene Knockout Rabbits Using the Cas9/GRNA System.” *Cell Regeneration* 3: 12.

<https://doi.org/10.1186/2045-9769-3-12>.

Yang, Neng, Osamu Higuchi, Kazumasa Ohashi, Kyoko Nagata, Atsushi Wada, Kenji Kangawa, Eisuke Nishida, and Kensaku Mizuno. 1998. “Cofilin Phosphorylation by LIM-Kinase 1 and Its Role in Rac-Mediated Actin Reorganization.” *Nature* 393 (6687): 809-12.

<https://doi.org/10.1038/31735>.

Yeh, Ellen, and Joseph L. DeRisi. 2011. “Chemical Rescue of Malaria Parasites Lacking an Apicoplast Defines Organelle Function in Blood-Stage *Plasmodium Falciparum*.” *PLoS Biology* 9 (8): e1001138.

<https://doi.org/10.1371/journal.pbio.1001138>.

- Yeoh, Sharon, Brian Pope, Hans G. Mannherz, and Alan Weeds. 2002. "Determining the Differences in Actin Binding by Human ADF and Cofilin." *Journal of Molecular Biology* 315: 911-25. <https://doi.org/10.1006/jmbi.2001.5280>.
- Yilmaz, Salih M, and Sewell H. Hopkins. 1972. "Effects of Different Conditions on Duration of Infectivity of Toxoplasma Gondii Oocysts." *The Journal of Parasitology* 58 (5): 938-39. <https://doi.org/10.2307/3286589>.
- Yonezawa, N., E. Nishida, and H. Sakai. 1985. "PH Control of Actin Polymerization by Cofilin." *Journal of Biological Chemistry* 260 (27): 14410-12.
- Zetsche, Bernd, Sara E Volz, and Feng Zhang. 2015. "A Split-Cas9 Architecture for Inducible Genome Editing and Transcription Modulation." *Nature Biotechnology* 33: 139-42. <https://doi.org/10.1038/nbt.3149>.
- Zhang, Sha, Chang Liu, Jiaojiao Wang, Zhanhong Ren, Christopher J J. Staiger, and Haiyun Ren. 2016. "A Processive Arabidopsis Formin Modulates Actin Filament Dynamics in Association with Profilin." *Molecular Plant* 9: 900-910. <https://doi.org/10.1016/j.molp.2016.03.006>.
- Zhang, Zheng, Yi Zhang, Hexin Tan, Ying Wang, Gang Li, Wanqi Liang, Zheng Yuan, Jianping Hu, Haiyun Ren, and Dabing Zhang. 2011. "RICE MORPHOLOGY DETERMINANT Encodes the Type II Formin FH5 and Regulates Rice Morphogenesis ." *The Plant Cell* 23 (2): 681-700. <https://doi.org/10.1105/tpc.110.081349>.
- Zhou, Wenyuan, and Alexander Deiters. 2016. "Conditional Control of CRISPR/Cas9 Function." *Angewandte Chemie - International Edition* 55: 5394-99. <https://doi.org/10.1002/anie.201511441>.
- Zigmond, Sally H., Marie Evangelists, Charles Boone, Changsong Yang, Arvin C. Dar, Frank Sicheri, Joe Forkey, and Martin Pring. 2003. "Formin Leaky Cap Allows Elongation in the Presence of Tight Capping Proteins." *Current Biology* 13: 1820-23. <https://doi.org/10.1016/j.cub.2003.09.057>.

